Preparation, Characterization and Properties of Fluorinated and Non-fluorinated Copolymers of Cyanate Esters

Zhao Lei

School of Materials Science & Engineering

A thesis submitted to the Nanyang Technological University
in fulfilment of the requirement for the degree of
degree of Doctor of Philosophy

2007

ACKNOWLEDGEMENTS

I would like to express my deepest gratitude to my supervisor, Associate Professor Hu Xiao, for his invaluable advice and guidance. His vision has always inspired me to find solutions to problems. He also created many opportunities for me to improve my research abilities.

I would like to express my gratitude to Ass/P Li Guoyuan, A/P Li Lin, Dr Que Wenxiu and Dr Yu Shuzhu for the useful discussions, suggestions and helps in this work. I would like to thank Ass/P Kantisara Pita from School of Electrical and Electronics Engineering for allocating me to use the equipments in Photonic Lab. I would like to thank all the technicians in Photonic Lab for their assistance. I am also grateful to the technicians in MSE Laboratories for their helpfulness and unfailing technical support, See-Toh Swee Sing, Joyce Ng and Wu Shucheng in Polymer Lab, Sng Jing Li and Sandy Leong in Microelectronics materials Lab, Patrick Lai and Yan Yong Kwang in Surface Engineering Lab, Irene Heng in Electron Microscopy & X-ray Diffraction Lab, and Tan Kek Koon in Computer Facilities Lab.

I would like to thank all my friends in NTU for their friendships.

Last but not the least, I would like to thank my parents, brothers, and my wife for their continuing love and support.

ABSTRACT

Cyanate ester resins or polycyanurates are of a class of promising high performance thermosetting polymers, which possess highly desirable chemical and physical properties for various applications. However, the functional properties of polycyanurates such as dielectric and optical properties have not been studied systematically. The preparation and characterization of dielectric and optical polycyanurate thin films is a new and interesting research area and has new potential applications.

As a part of this research work, optical quality thin films of polycyanurate homopolymers and copolymers have been prepared through optimizing the polymerization conditions, spin coating parameters and thermal curing procedures. Polycyanurates and their thin films were characterized by FTIR (Fourier-Transform Infrared), DSC (Differential Scanning Calorimetry), TGA (Thermogravimetric Analysis), AFM (Atomic Force Microscope), DEA (Dielectric Analysis), Prism Coupler, and Nano-indentation. In addition, new curing kinetics models for aromatic and aliphatic polycyanurates were established.

The dielectric studies of the polycyanurate homopolymers and copolymers revealed that the heterogeneity of the polymer can be quantified using the Cole-Cole plot based on the DEA data. This method is a sensitive way of comparing heterogeneity in polymer systems, and such subtle differences in heterogeneity may not be detectable using conventional techniques such as DSC.

The study on the optical properties of polycyanurate thin films showed that the composition and heterogeneity have strong effects on optical properties such as refractive index and propagation loss. Through copolymerization of four cyanate monomers with different compositions, the refractive index of the polycyanurate thin films can be controlled in a broad range between 1.44 to 1.61 and the propagation loss is between 0.86 to 1.82 dB/cm.

Based on the basic thermodynamic consideration, the dependence of glass transition temperature on the composition and conversion of polycyanurate homopolymers and copolymers were investigated. The relationship among the glass transition temperature, composition and conversion of the polycyanurate homopolymers and copolymers was established.

The study of nanoindentation of the polycyanurate thin films revealed that there was a linear relationship between the hardness and glass transition temperature.

Based on isothermal DSC studying on the curing kinetics of polycyanurates, a variable 'n' nth order kinetics model was proposed for aliphatic cyanate ester (DFCy), which has more accurate and reasonable prediction of the experimental data than the frequently used fixed 'n' kinetics model. A WLF-type kinetics model with temperature dependent reaction order was also established for the curing reaction of uncatalyzed aromatic cyanate ester (BACy).

TABLE OF CONTENTS

CHAPTER 4 PREPARATION OF POLYCYANURATE THIN FILMS

CHAPTER 5 DIELECTRIC PROPERTIES AND HETEROGENEITY OF POLYCYANURATE HOMOPOLYMERS AND COPOLYMERS

CHAPTER 6 OPTICAL PROPERTIES OF POLYCYANURATE THIN FILMS

CHAPTER 7 THERMAL AND MECHANICAL PROPERTIES OF POLYCYANURATE THIN FILMS

LIST OF FIGURES

LIST OF TABLES

CHAPTER 1

INTRODUCTION

1.1 Background and Motivations

Cyanate ester resins (CE) or polycyanurates are of a class of high performance thermosetting polymers with a high glass transition temperature, low dielectric constant and loss factor, good adhesion on different substrates, excellent resistance against most common solvents, and remarkable mechanical properties [1-5]. Furthermore, their properties can be further adjusted and improved by changing the backbone structure and by blending or copolymerizing with other polycyanurate resins or other thermosetting and thermoplastic polymer systems according to the specific requirements [6-20]. Although currently polycyanurates are mainly used in aerospace structural composites [21-24] and printed circuit board industries [25,26] and these applications mainly concern their mechanical and dielectric properties of the bulk materials, new interests in optical or photonic [27-33], thin films [34-38] and nanocomposite applications [39,40] have evolved recently and they are expected to enthuse researchers for a long period of time in the future.

The characterizations and structure-property relationships of cyanate ester resins as bulk materials have been extensively studied. It was found that the unusual low dielectric constant, low moisture absorption, high thermal stability and epoxy-like processability of cyanate ester resins were mainly attributed to their unique symmetrical triazine network structure that formed via a cyclotrimerization during the curing process [1-3]. Various cyanate ester monomers with different backbone structures have been synthesized and

reported. Some are commercially available, making it convenient to choose suitable materials to meet specific application requirements [41-50]. Furthermore, polycyanurate resins are expected to exhibit low optical loss and tunable refractive index due to their high free volume, low polarity, high purity and various backbone structures, in addition to their other amazing properties such as high thermal stability, good adhesive to substrate and low dielectric constant. polycyanurates would have great possibility for new applications in photonic or optical interconnections and devices [27-33]. However, so far the studies on the optical properties of cyanate ester resins such as refractive index, propagation loss, thermo-optical coefficient, birefringence and luminescence are still in elementary stages.

The modifications of polycyanurates have attracted many research attentions. Extensive researches in blending cyanate ester monomers with conventional and high performance thermoplastics or thermosetting resins has led to the generation of key information on morphological features and toughening mechanisms, to the extent that even simulation of morphology and property has now become possible [6-8]. In recent years, blending cyanate ester resin with epoxy (EP) and bismaleimide (BMI) resins has attracted a lot of research attentions and has achieved commercial success [9-19]. While the CE/BMI blend is now known to form an interpenetrating network (IPN) [15-17], the reaction mechanism with epoxy is still intriguing [9,13,14]. Recently, preliminary investigations of the CE/clay nanocomposites have been reported [39,40]. The copolymerization of different cyanate ester monomers are also very interesting since it does not change the unique symmetrical triazine network structure of polycyanurate, which may have many advantages in modifying or adjusting the optical properties of polycyanurate resins including controlling the refractive index and reducing the optical loss. However, the reported work on polycyanurate copolymers so far has mainly focused on improving the

process-ability or enhancing the thermal stability [1,20]. On the other hand, it is well known that the compatibility or miscibility have great influence on the final properties of a polymer blend. The degree of miscibility of the components is an important factor in determining the properties of the system through micromorphology. Miscibility in multi-component polymeric systems, particularly in binary polymer blends, has been extensively studied both experimentally, using a variety of experimental techniques, and theoretically. However, the cyanate ester copolymers are macroscopically homogeneous and the heterogeneity may not be detectable by using the commonly employed thermal or mechanical analysis techniques. Such subtle heterogeneity may not significantly influence the mechanical properties of the polymer, but it has very important effects on the dielectric or optical properties. Therefore, it is meaningful and challengeable to establish the relationship between the properties and heterogeneity of the macroscopically homogeneous polycyanurate polymers.

Polymeric thin films of few microns are widely used in electronic and photonic applications. It has been reported that polycyanurate thin films can be prepared by spin coating [27,28,34-37], dip coating [29] or by the evaporation method [38]. However, most of the reported works on polycyanurate thin films have tried to understand the adhesion mechanism of polycyanurate on different substrates and the optical properties of polycyanurate thin film were not concerned in most cases. The work reported on optical quality polycyanurate thin film is only at the initial stage [27-29]. Therefore it is meaningful to study the refractive index, birefringence and propagation loss of polycyanurate thin films, find out the effects of backbone structures, compositions and heterogeneity on the optical properties of polycyanurates.

It is also imperative to study the kinetics aspects of curing reaction of cyanate ester resins, as they drive the complex changes in morphology and structure of the polymer during its processing operations. Understanding the kinetic aspects is helpful in controlling the curing process to design suitable processing parameters and achieve optimum properties of the cured polymers. The reaction kinetics of aromatic cyanate ester resins with added catalysts have attracted much research attention and different techniques based on Differential Scanning Calorimetry (DSC) [51-55], Fourier-Transform Infrared (FTIR) [56-58], and Dielectric Analysis (DEA) [59] have been employed to study the curing reaction. It is generally accepted that the curing behavior of polycyanurates is dominated by chemical control firstly at the early curing stage and then followed by diffusion control at the later curing stage [60, 61]. An n th-order kinetics was proposed to model the catalyzed reaction of aromatic cyanate esters in the chemical controlled regime. However, such a model with a fixed reaction order may not be accurate for thermosetting curing systems such as cyanate ester resins, because the model assume that the functional groups have equal reactivity during the entire curing process, which may not be valid. Therefore, a variable 'n' is more appropriate. On the other hand, although the catalyzed aromatic cyanate ester reaction are more beneficial in practice than the uncatalyzed systems for aerospace or electronic material applications, as regard to optical and dielectric properties, uncatalyzed systems are more preferred. However, there are only a few reports on the reaction kinetics of uncatalyzed aromatic cyanate ester systems, especially scanty reports for the aliphatic cyanate ester curing system.

The emerging importance of cyanate ester systems can be understood from the increasing research interest as well as their potential applications. It is very significance to carry out systematic studies on the preparation, characterizations of modified cyanate ester thin

films, understand their curing behavior well and explore new promising applications for this class of high performance functional thermosetting polymer.

1.2 Objectives and Scope of this Research

The main objective of this study is to characterize the properties, especially the dielectric, optical and thermal properties, of polycyanurate and modified polycyanurate thin films, understand the factors affecting these properties, put efforts on controlling or improving these properties and leading to some new potential applications. In order to obtain modified polycyanurate thin films with desired optical, dielectric, thermal and mechanical properties, four kinds of cyanate ester monomers with different molecular structures were carefully chosen, and the fundamental aspects on the prepolymerization, preparation of thin film, characterizations, and curing reaction kinetics of modified cyanate ester resin were studied in detail. This study will focus on four important topics: (1) preparation of polycyanurate thin films; (2) characterization of polycyanurates and their thin films; (3) modification of cyanate ester resins; and (4) curing kinetics of cyanate ester resins.

1.2.1 Preparation of Polycyanurate Thin Films

Preparation of polycyanurate thin films includes three main steps, prepolymerization of cyanate ester monomer, spin coating and thermal curing. Synthesis of cyanate ester prepolymers is very crucial for the preparation of polycyanurate thin films using the spin coating method. Therefore the prepolymerization of cyanate ester resin was studied and the optimum conditions for the prepolymerization were settled down according to the experiments. Degrees of prepolymerization of the cyanate ester prepolymers were measured by both DSC and FTIR methods. TGA characterization was also carried out for cyanate ester prepolymers. Then polycyanurate thin films were prepared by spin coating

followed by thermal curing. The influences of the processing parameters: solution concentration, spin speed and spin time, were investigated and discussed. The surface morphology of the thin films was studied using SEM and AFM.

1.2.2 Characterization of Polycyanurates and Their Thin Films

The characterizations of cyanate ester monomer were carried out by employing Differential Scanning Calorimeter (DSC) and Fourier-Transform Infrared (FTIR) spectroscopy. The glass transition temperatures of the partial cured and fully cured polycyanurates were measured by DSC. The surface morphology of polycyanurate thin films was characterized by SEM and AFM. Optical absorptions of polycyanurate thin films in the middle infrared region (400-4000 cm^{-1}) were characterized by FTIR spectroscopy. The refractive indices (both TE and TM mode), birefringence and thicknesses of polycyanurate homopolymer and copolymer thin films were measured by Prism Coupling technique. The optical propagation losses of the polycyanurate thin films were also measured by the prism coupler system using the moving optical fiber method. The mechanical properties of the polycyanurate thin films including hardness and modulus were measured by nano-indentator.

The emphasis was mainly put on understanding the structure/property relationship of polycyanurates and modified polycyanurates, understanding the effects of processing, curing and the chemical structure of cyanate ester on the dielectric, optical, thermal, and mechanical properties of polycyanurates and their thin films, especially by studying the effects of different backbone structures, compositions and heterogeneity of polycyanurates on the dielectric and optical properties.

1.2.3 Modification of Cyanate Ester Resins

In order to control the dielectric and optical properties of polycyanurates, modified polycyanurates were prepared by copolymerizing common cyanate ester with fluorinated cyanate ester or monofunctional cyanate ester. The objective is to investigate the effects of the modification on the dielectric, optical, thermal and mechanical properties.

1.2.4 Curing Kinetics of Cyanate Ester Resins

Studying the curing kinetics is imperative as it is helpful in controlling the curing process, designing appropriate processing parameters and achieving optimized properties of the curing polymers. The thermal curing reactions of uncatalyzed aromatic and aliphatic cyanate ester resins were monitored by isothermal DSC method. Kinetics parameters including reaction constant, activation energy, pre-exponential factor, and reaction order were calculated, and the kinetics model was proposed. The objective is to establish working models which can predict the experimental data accurately for the entire curing conversions of polycyanurates, including both the chemical and diffusion controlled regions.

1.3 Major Contributions of the Thesis

- Based on extensive experiments, optical quality polycyanurate thin films with thickness from hundreds of nanometers to several microns were prepared. Furthermore, the thickness of the polycyanurate thin films can be precisely controlled by adjusting the prepolymerization conditions and the spin coating parameters.
- Various characterization techniques have been utilized to evaluate the dielectric, optical, thermal, mechanical and surface morphology properties of the modified polycyanurate thin films. The factors that influence these properties are discussed.

- Based on the DEA data, the heterogeneities of different polycyanurate homopolymers and copolymers were successfully characterized and quantified by employing the Cole-Cole equation. This is the first time such a method is used for polymer/polymer systems, and it is a sensitive way of comparing heterogeneity in polymer systems even though such subtle differences in heterogeneity may not be detectable using conventional techniques such as DSC.
- A new variable 'n' nth order curing kinetics model is proposed for the first time in this work. This new model predicts the experimental reaction processing more accurately than the traditional fixed 'n' nth order model. the variable 'n' kinetics model should be useful for other thermosetting systems which follow the nth order kinetics in general.
- A temperature dependent reaction order kinetics model was proposed for the autocatalytic reaction of uncatalyzed aromatic cyanate ester. The new autocatalytic kinetics has predicted the experimental data more accurately. This new model should be used for accurate modeling of curing reactions of thermosets following autocatalytic kinetics.

1.4 Organization of the Thesis

This thesis contains ten chapters. Chapter 1 introduces the background, the objectives and the scope of this research. The major contributions of the work are also provided in this chapter. A review of literatures about the studying of cyanate ester resins published in recent years is given in Chapter 2. Chapter 3 describes the research methodology and experimental procedures. Chapter 4 presents the preparation of polycyanurate thin films. Chapter 5 and Chapter 6 discuss the dielectric and optical properties of polycyanurate thin films respectively. The thermal properties and mechanical properties of polycyanurate thin films are presented in Chapter 7. The study of thermal curing kinetics of aliphatic and

aromatic cyanate ester resins is discussed in Chapter 8 and Chapter 9. Chapter 10 summaries the whole thesis and gives recommendations for the future work.

CHAPTER 2

LITERATURE REVIEW

2.1 Introduction to Cyanate Ester Resins

Cyanate ester resins (CE) or polycyanurates are defined as the three dimensional networks of oxygen linked triazine (or cyanurate) units which are formed via cyclotrimerization of aliphatic or aromatic monomers containing reactive ring-forming cyanate ester functional groups ($-O-C\equiv N$) [1,2]. In literature, the monomers are generally named 'cyanate ester', while the cured resins are alternately named 'polycyanurates' or 'triazine resins'. However, both the monomer and cured resin can also be named 'cyanate ester'. Chemically the monomers of this family of thermosetting resins are esters of phenols and cyanic acids and may be represented by the general structure model illustrated in Figure 2.1 [1-3]. There are also few cyanate ester monomers that can not be represented by the general structure shown in Figure 2.1, and some of them are presented in Table 2.1.

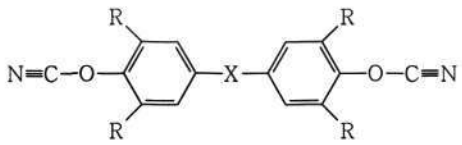

Figure 2.1 General chemical structure model for cyanate ester monomers

Where R may be a range of functional groups, e.g., hydrogen atoms, methyl or allyl group and the bridging group X may be simply an isopropylidenyl moiety or an extended aromatic or cycloaliphatic backbone

Difunctional or multifunctional CE monomers can undergo polycyclotrimerization to form a heterocyclic ring (triazine or cyanurate) network structure either thermally or by

transition metal complexes catalysts in the presence of an active hydrogen co-catalyst such as nonylphenol [1-5]. As shown in Figure 2.2.

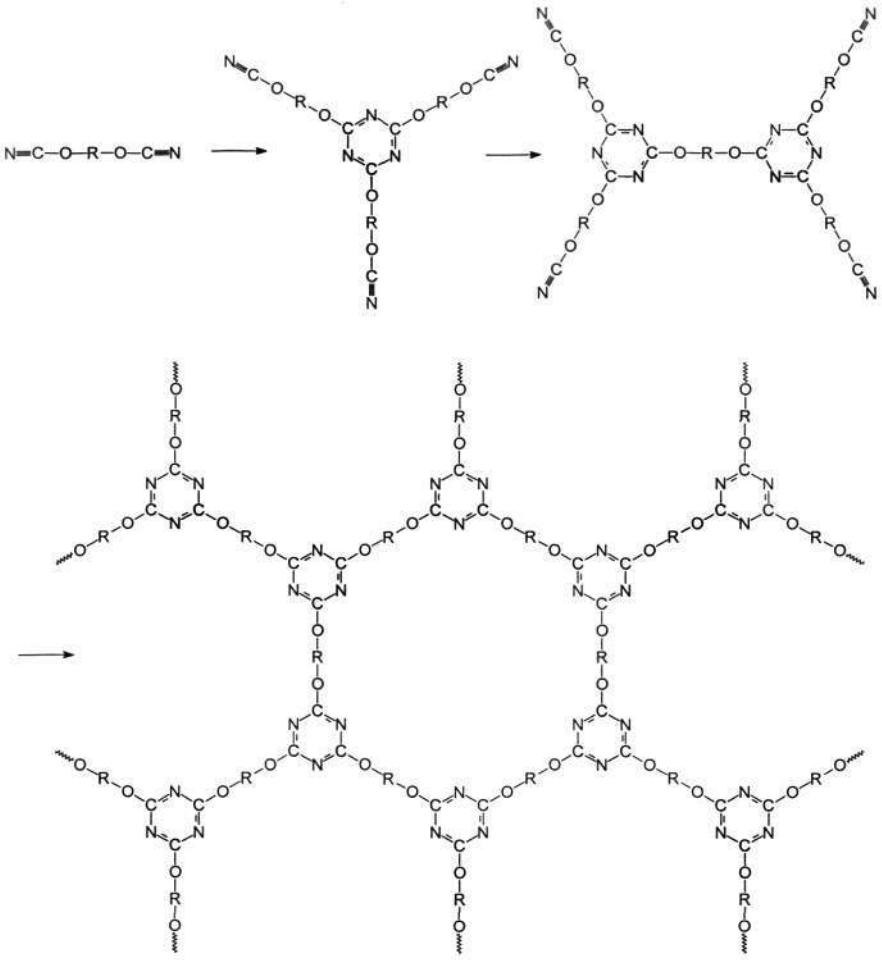

Figure 2.2 Polycyclotrimerization of a difunctional cyanate ester

Three difunctional CE molecules react to form a triazine or cyanurate. The resulting triazine has three free reactive $-OCN$ groups, therefore it can react further with monomers and form pentamers, heptamers and higher oligomers until finally a highly branched three dimensional network is built. The triazine-rings are the trifunctional connections of this network. The trimerization process appears to proceed in a stepwise manner and n values of 3, 5, 7, 9, etc. can be readily identified by GPC or LC separation methods [1]. At sufficiently high temperatures and with appropriate reaction time an almost complete transformation of the cyanate-groups can be obtained. The

polymerization of CE reaction has a great advantage, that no gaseous or liquid byproducts are formed during the reaction.

The cured CE resins (polycyanurate or polytriazine) possess many attractive physical, electrical, thermal and processing properties for several applications, e.g., aerospace structural composites [21-24], electronics [25-26] and adhesive [34,62]. These properties can be further tuned by changing the backbone structure and by blending or copolymerizing with other polymer systems or other CEs with different backbone structures. Some kinds of commonly used CE monomers are listed in Table 2.1 along with their key physical properties of homopolymers.

A variety of CEs with tailorable physical-chemical properties have been synthesized by appropriate selection of the precursor phenol. The physical characteristics like melting point and processing window, dielectric characteristics, environmental stability, and thermo-mechanical characteristics largely depend on the backbone structure. In addition to the bisphenol-based CEs, other types like CEs bearing elements such as sulfur [43], phosphorus [44], silicon [45], liquid crystalline CE [46,47] and polymers with pedant cyanate ester groups [48,49] have been synthesized and reported, too. For example, among the CE monomers listed in Table 2.1, AroCy B-10 (BACy) is the most interesting one in research and it has been commercialized and commonly used in printed circuit board (PCB) and aerospace structure composites [21-26]. BACy has a bisphenol A backbone structure and can be processed much like epoxy resins for many applications. AroCy F-10 (BFCy) is a fluorinated Bisphenol A CE resin, in which the aliphatic hydrogen atoms of BACy are replaced by fluorine atoms and expected to have a lower dielectric constant, water absorption and optical loss. The cumylphenol cyanate ester is a mono-functional polymer, and although it can not be used singly, it can be copolymerized

with other cyanate esters to modify properties through changing the crosslink density of the copolymer system.

Table 2.1 Structures of cyanate esters and their monomer and homopolymer properties

Structure of cyanate ester (Monomer)	Trade name /supplier	Melt. Pt. (°C)	Tg (°C)	H_2O absorption (%)	ε (1 MHz)
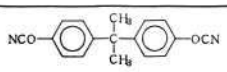	AroCy B-10/Ciba-Geigy BT-2000/Mitsubishi Lonsa	79	289	2.5	2.91
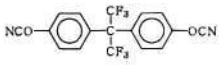	AroCy F-10/Ciba-Geigy	87	270	1.8	2.66
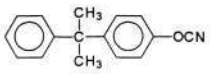	8889/Oakwood	-	-	-	-
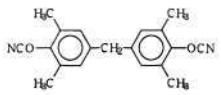	AroCy M-10/Ciba-Geigy	106	252	1.4	2.75
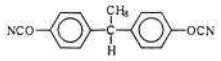	AroCy L-10/Ciba-Geigy	29	258	2.4	2.98
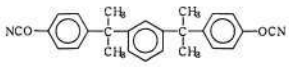	XU-366/Ciba-Geigy RTX-366	68	192	0.7	2.64
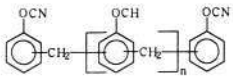	Primaset PT-30/Lonsa XU-371/Ciba-Geigy	Semi-solid	350	3.8	3.08
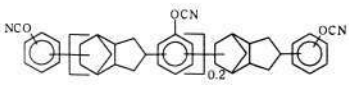	XU-71787/Dow Chemical	Semi-solid	244	1.4	2.80
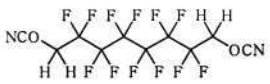	5933/Oakwood	108	92	0.12	2.29

Melt. Pt.: *melting point*; Tg: *glass transition temperature*; ε: *dielectric constant*

Although the majority of the publications concerns polycyanurates with aromatic backbones, a few aliphatic polycyanurates are also reported. A series of cyanate ester monomers containing fluoromethylene bridges in their backbone have been synthesized and characterized [41-42]. The oligomers can be represented by the general formula

$NCOCH_2(CF_2)_nCH_2OCN$, where n=3, 4, 6, 8 or 10. Their melting points vary from –8 °C to 181 °C depending on the number of fluoromethylene bridges in the backbone and the glass transition temperature (Tg) of the cured resin is in the range of 84-101 °C, significantly lower than that of most aromatic polycyanurates. The dielectric constant (2.3-2.6) of the cured resin is the lowest among polycyanurates and the moisture absorption (0.68-1.67) is lower than that of cured BACy. The low-density polymers have critical surface tension of 23-40 dyn/cm and refractive indices are in the range 1.382-1.447. These were achieved without any penalty on thermal stability. Among the series, the 1,6-dicyanatohexafluoromethylene (DFCy) exhibited optimum properties. The authors proposed [42] a structure for the network comprising macrocyclic rings containing triazine, generating a lot of free volume and thereby contributing to the low dielectric constant and low refractive indices and optical loss. The structure of the fluoromethylene polycyanurate network is shown in Figure 2.3. It is a promising potential polymer system for photonic and relative applications.

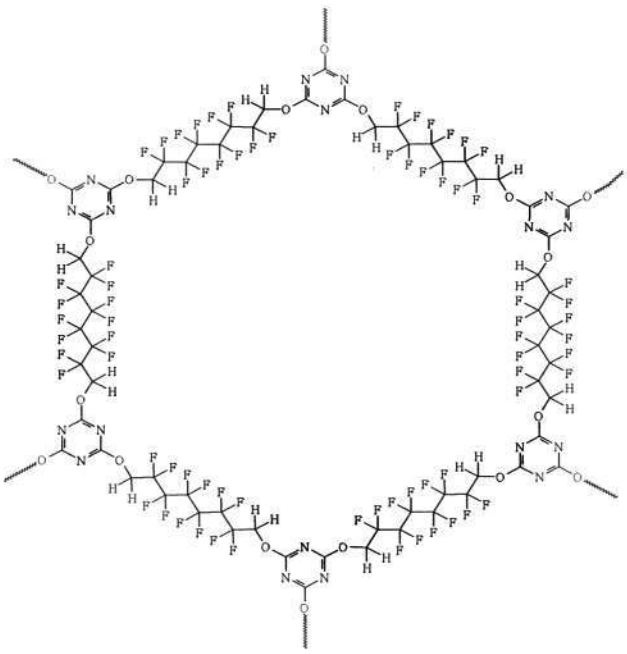

Figure 2.3 Fluoromethylene polycyanurate network

Presently, the bulk of polycyanurate resins is consumed by the aerospace structural composites and high-speed electronics industry, mainly for composites and printed circuit

board (PCB). However, polycyanurates are not only suitable for high performance resin matrix composites, but also suitable for optical or other functional applications. It is believed that this thermosetting resin system with its many useful features is poised to find more positions in specific applications such as dielectric thin film, optical and photonic materials. The emerging importance of polycyanurate systems can be understood from the increasing research interests in this area, evident in terms of a rapid increasing of publications and patents. There are various review articles devoted to various aspects of polycyanurates [1-5].

2.2 Curing of Cyanate Ester Resins

Cyanate ester resins are remarkable in that they polymerize via a cyclotrimerization to form a triazine network with a high degree of efficiency. Study on the mechanism and kinetics of curing of cyanate ester resins can also be found [51-61,63-65]. In practice, cyanate ester resins are usually cured by a transition metal carboxylate, or chelate catalyst, in the presence of a hydrogen donor such as nonylphenol. The transition metals used include acetyl acetones of Cr, Fe, Co, Ni, Cu, Zn [52,53,65], and dibutyl tin dilaurate (DBTDL) [52]. The co-catalyst used usually is nonylphenol. It has been reported that soluble transition metal cations are of the order of 10^3 times more effective at promoting rapid gelation than the active hydrogen accelerators, but that after the gel-point, this trend is reversed and active hydrogen compounds are better than transition metals at achieving high degrees of conversion [2]. The effectiveness of the transition metal acetyl acetonates was found to be, $Cu^{2+} = Co^{2+} > Zn^{2+} > Mn^{2+} > Fe^{3+} > Al^{3+}$ [44]. Although the technology based on CE resin has developed greatly, the very basic information on its cure mechanism remain disputed [1]. It is generally accepted that the cyanate cure take place through cyclotrimerization to form the polycyanurate, but the detailed mechanism of the reaction is uncertain and a matter of some speculation. With added transition metal

catalysts, one possible mechanism is that the reaction occurs via the gathering of cyanate ester by transition metal and is co-catalyzed by active hydrogen as shown in Figure 2.4 [63], but there is no evidence reported for direct coordination between metal and cyanate functional groups resulting in a stable intermediate.

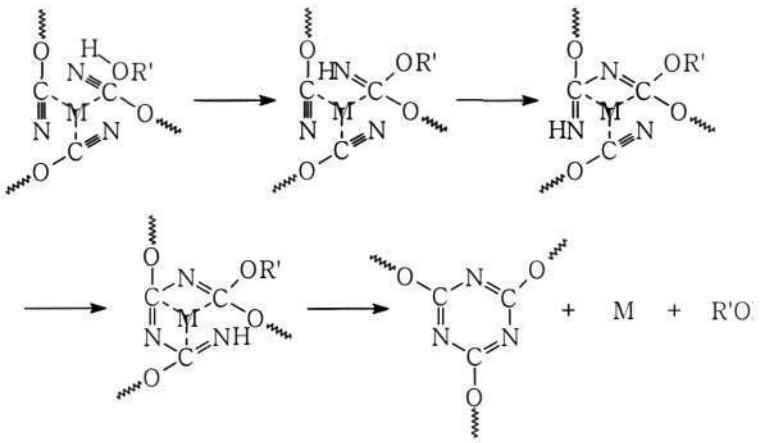

Figure 2.4 Catalyzed thermal trimerization of cyanate ester resin [63]

M: *metal cation*; R'OH: *compound with active hydrogen.*

It is usually accepted that completely purified cyanate monomer would not undergo any reaction when heated and a small amount of catalysts are needed to start the reaction [53]. However, cyanate ester monomers normally result from the condensation of phenols or diphenols with cyanogen halides. The parent diphenol and monosubstituted compounds are very difficult to be completely eliminated, therefore, they are often left as impurities in the commercial monomers [64]. It is reported that without added catalysts, the reaction is supposed to be catalyzed by these impurities, including moisture and residual phenol from the synthesis [63]. One possible mechanism of uncatalyzed cyanate ester system was reported by Grenier-Loustalot et al. [64]. They investigated the mechanism of polymerization of mono and dicyanates by HPLC and spectroscopic methods. Using HPLC/UV, secondary products like phenolic derivatives of the cyclic trimer and pentamer and carbamates could be detected. The authors proposed formation of dimer,

which could inhibit the polymerization and delay gelation. A reaction mechanism was proposed in Figure 2.5 [64].

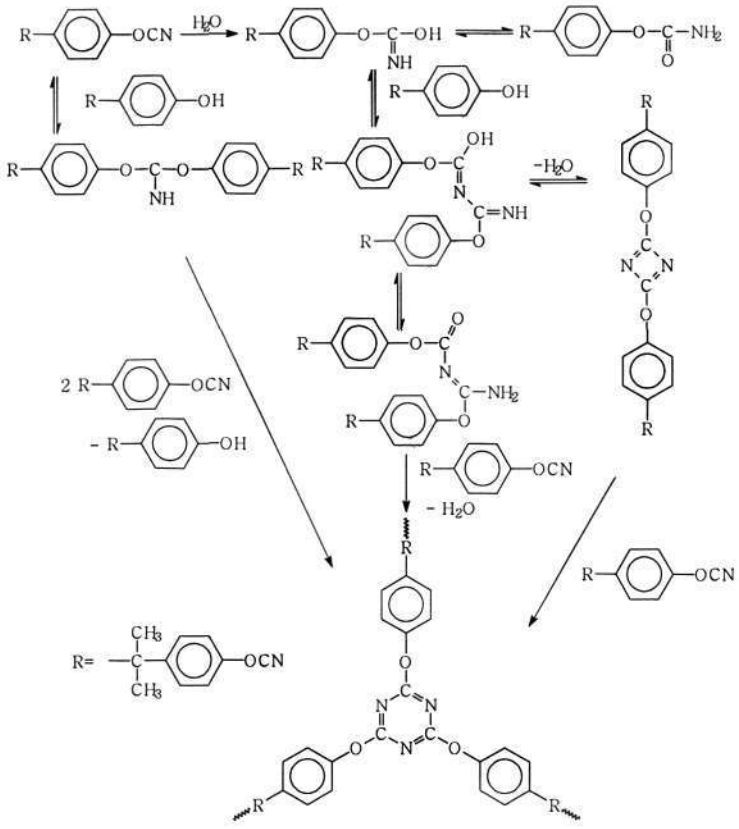

Figure 2.5 Proposed reaction mechanism for the polymerization of uncatalyzed cyanate ester resin [64]

The possibility of photo-curing of cyanate monomer by an organometallic compound is also reported by Liu and co-workers [51,66-67], the cyanate ester they used is BACy and the catalyst is tricarbonyl cyclopentadienyl manganese ($CpMn(CO)_3$). It is reported that the polymerization process includes two stages: initial UV irradiation and thermal curing. The irradiation of the photocatalysts for 15-120 seconds lowered the cure temperature of the network by over 100 °C. The reaction rate was described by a first order dependence on the active catalyst concentration and on the cyanate concentration. A mechanism (Figure 2.6) was proposed that it involved the photosubstitution of the carbonyls in the original catalyst by the cyanate functional groups during the irradiation stage and the formation of the active catalyst species at the thermal curing stage [51]. It provided a way

to prepare patternable polycyanurate thin films, which are often used in the fabrication of electronic components and optical devices.

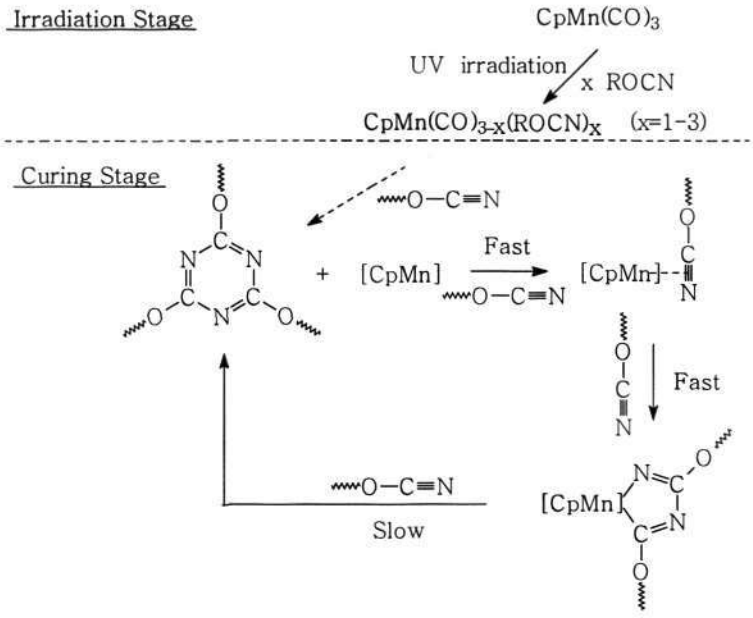

Figure 2.6 A proposed mechanism for the photocatalyzed polymerization of cyanate ester resin [51]

2.3 Properties of Polycyanurates

Traditionally, cyanate ester resins are used as the resin matrix for high performance composites for aerospace and electronic materials applications. Against the backdrops of other thermosetting polymers such as epoxy, polyimide, and bismaleimide resins, polycyanurates emerged as a new system with compromise properties of the above polymers. This new generation thermosetting resin encompasses the process-ability of EP resins, thermal characteristics of BMI resins, and the heat and fire resistance of phenolic resins. In the last decades, aromatic CEs have emerged as a new and unique class of high-performance thermosetting resins for use as prepreg matrices in both the aerospace and electronics industries [21-26]. A comparison of conventional high performance thermosetting matrix resins with CEs is given in Table 2.2 [2].

Table 2.2 Comparison of common high performance thermosetting polymer matrices [2]

Property	Epoxy	Phenolic	Toughened BMI	Polycyanurate
Density ($kg.m^{-3}$)x10^{-3}	1.20-1.25	1.24-1.32	1.20-1.30	1.10-1.35
Service temperature (°C)	Up to 180	200-250	~200	~200
Tensile modulus (GPa)	3.1-3.8	3.0-5.0	3.4-4.1	3.1-3.4
Dielectric constant (1 MHz)	3.8-4.5	4.3-5.4	3.4-3.7	2.7-3.2
Cure temperature (°C)	20-180	90-150	220-300	180-250
TGA onset (°C)	260-340	300-360	360-400	400-420

Depending on the backbone structures, the properties of polycyanurate are different, which provides a possibility to tune or adjust the properties for various applications by blending two or more different cyanate esters together. The traditional applications of polycyanurates utilize their excellent mechanical properties and they are mainly used as a class of high performance matrix for composites. However, except for good mechanical properties, polycyanurates also have promising tunable dielectric and optical properties and would find more positions in other potential new applications other than composites matrix. It can be predicted that there will be more and more researchers keeping watch on this area. Polycyanurate shows some outstanding properties for waveguide applications, for example high thermal stability, low optical loss in the telecommunication-windows in the wavelength regions around 1310 nm and 1550 nm, low birefringence, low dielectric constant, good adhesion properties on different substrates, excellent resistance against most common solvents and good mechanical properties [27-29]. Table 2.3 summarizes the distinctive features of polycyanurate resins. The characteristic properties of polycyanurate resins can be attributed to the common chemical features of monomer units and the cured cyanurate networks.

Table 2.3 Distinctive features of polycyanurates

Structure unit	Distinctive feature	Reference
Cyanate functionality	Easy to process, react with epoxy, blend with thermoplastics	[99]
Ring forming	High service temperature	[100]
-O- linkages	Toughness	[101]
Low crosslink density	Toughness	[101]
Low polarity	Low dielectric loss, low moisture absorption, low optical loss	[102]
High purity	Low dielectric loss, low corrosion potential, low optical loss	[103]
No –OH or –NH group	Low optical loss	[27]
Conjugate	Luminescence	[58]

The cured polycyanurate networks exhibit many attractive features. Relative to EP and BMI resins, polycyanurate resins are considerably more hydrophobic. This property is beneficial for polycyanurate to maintain high performance properties at high temperature, because high water uptake of a thermosetting significantly reduces heat resistance through plasticization, increase in dielectric constant and dielectric loss, and hydrolysis of chemical bonds. The ring-forming cyclotrimerization curing reaction creates a high concentration of aromatic rings linked by one atom of oxygen or carbon, which is responsible for the relatively high Tg, inherently low smoke generation and good flame retardancy. The relatively low crosslink density, high free volume due to oxygen links to triazine ring is responsible for its toughness, for example, higher strain energy release rate and tensile elongation. The network structure formed from the cyclotrimerization of cyanate esters indicates a symmetrical arrangement of electronegative oxygen and nitrogen atoms around electropositive carbons, resulting in short dipole moments and low energy storage in an electromagnetic field. While cyanate ester homopolymers contain an appreciable percentage of oxygen and nitrogen, their symmetrical arrangement and the resulting weak polarity are responsible for the low dielectric constant. The detailed properties of polycyanurate are introduced in the following sections.

2.3.1 Optical Properties of Polycyanurates

Polymer materials are being increasingly considered for optical applications [103-107] for their high thermo-optical coefficients, ease to fabrication, cost-effectiveness, and their compatibility with other materials. However, since extensive study of polymeric materials and devices operating at 1550 nm began just recently, few ideal materials have so for been made commercially available [103]. Therefore, fully exploiting the potentials of the polymer materials is of great urgent significance.

Polymers suitable for optical waveguide applications must have characteristics that increase a component's functionality and also have the physical characteristics to enable good manufacturability. They must have low propagation loss in a wide range around 1550 nm; be precisely adjustable and process-tolerant refractive index around 1.45; high glass transition temperature (ideally >200 °C); good processability (coating, adhesion, etching), low birefringence (ideally $<5\times10^{-5}$); low water uptake, and high chemical and environmental resistance [103].

2.3.1.1 Factors Influencing Optical Loss of Polymers

One of the most crucial issues regarding the applicability of polymeric materials is the optical propagation loss. The various mechanisms contributing to optical losses for polymers are basically similar to those for silica optical materials, but the relative magnitudes are different. Table 2.4 shows the loss factors for polymers [108].

The various factors contributing to optical loss in polymer waveguides can be divided in to intrinsic loss and extrinsic loss. Absorption losses include higher harmonics of molecular vibration in the IR region and electronic transitional absorption in the UV region. Scattering losses are mainly caused by so-called Rayleigh scattering. When

extrinsic scattering loss is under consideration, the absorption due to impurities and the scattering due to dust particles and microvoids can be reduced by designing appropriate waveguide fabrication apparatus. Scattering losses due to imperfections in the waveguide structure, such as surface fluctuations, mismatching of the interface, and birefringence due to the waveguide process, may be lowered by the development of a suitable fabricating technique. Losses attributable to extrinsic factors such as scattering due to imperfections in the waveguide structure and to contaminants and microvoids should be neglected. After optimum process conditions in waveguide fabrication have been achieved, the molecular vibrational absorption may be a major loss factor.

Table 2.4 Optical loss factors for polymers [108]

Intrinsic		Extrinsic	
Absorption	Scattering	Absorption	Scattering
Molecular vibration	Rayleigh scattering	Transition metals	Dust and microvoids
Electronic transition		Organic contaminants	Fluctuation of surface
			Orientational birefringence
			Interface imperfections

Molecular vibrations are the intrinsic loss factors in polymer optical waveguides. For the reduction of the optical loss in the critical region of 1550 nm it is strongly recommended to avoid absorbing molecular groups in the optical material system, especially OH and NH groups, which have strong absorption in the 1550 nm region. Cyanate esters are synthesized from phenols, therefore the absorption of OH group is of great concern. Figure 2.7 shows the dependence of the optical loss of different model compounds with different OH content (wt.%). There is a linear correlation between the optical loss and OH content [27]. The OH groups show a degree of absorption in the relevant wavelength

region, which is about two orders of magnitude higher than the one of the CH groups. Hence, in Figure 2.7 the CH vibration has little consequence.

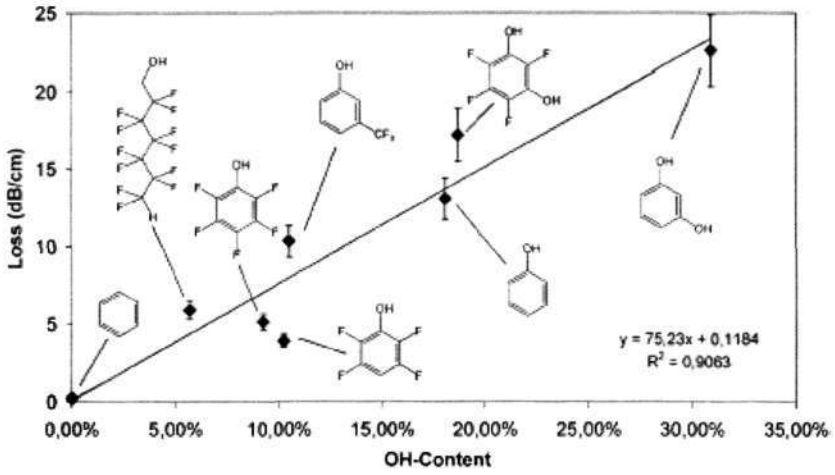

Figure 2.7 Optical losses versus OH content (wt.%) of different model compounds [27]

However, since almost all the polymers contain CH group, its contribution to the optical loss is also of particular interest in very low loss materials. Figure 2.8 shows the loss of OH and NH free model compounds versus their H content (wt.%). It shows a linear relationship with a coefficient of determination of 0.96.

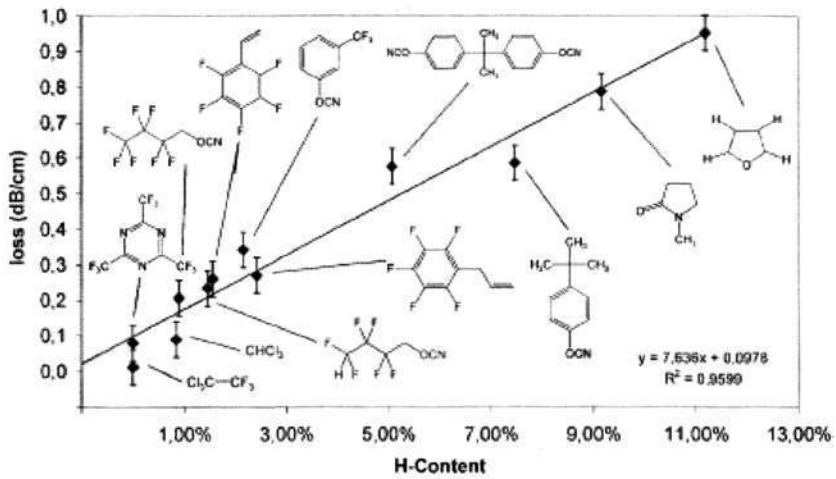

Figure 2.8 Optical losses versus H-content (wt.%) of different model compounds [27]

2.3.1.2 Reduction of Optical Loss

Reduction optical loss of the existing materials is an interesting research area. If polymer is to serve as optical transmission media, the attenuation loss in the 1550 nm region must be lowered. Because it is easy to avoid OH or NH group or other absorbing groups in the polymer structure, for most optical polymer, the large part of overall optical loss is contributed by the fundamental and overtone absorption of CH group, especially aliphatic CH group.

The theoretical fundamental frequency of molecular vibration can be established from the following equation [108]:

$$\nu = \frac{1}{2\pi c}\left(\frac{k}{\mu}\right)^{1/2}, \qquad \mu = \frac{m_1 \times m_2}{m_1 + m_2} \qquad \text{(Equation. 2.6)}$$

where ν is fundamental frequency, c is the velocity of light, k is the force constant, m_1 and m_2 are the atomic weights of diatomic atoms.

Hydrogen, being the lightest atom, causes the fundamental vibration of the CH bond to occur at wavelength of 3390 nm. Its high harmonic absorptions occur at approximate multiples of the fundamental frequency, and the intensities of such absorptions decrease by one order of magnitude with each harmonic. Table 2.5 gives the fundamental absorption (ν_1) and overtone absorptions (ν_n, n>1) of CH, CD, and CF bonds according to theoretical calculation [109]. The intensities of the absorptions are given in relation to the CH fundamental absorption.

Table 2.5 Positions and relative intensities of fundamental and overtone absorption of CH, CD, and CF bonds [109].

Absorption	C-H		C-D		C-F	
	λ(nm)	I_n/I_1^{C-H}	λ(nm)	I_n/I_1^{C-H}	λ(nm)	I_n/I_1^{C-H}
ν_1	3390	1.0	4484	0.4	8000	40
ν_2	1729	7.7×10^{-2}	2276	2.4×10^{-2}	4016	6.4×10^{-1}
ν_3	1176	6.8×10^{-3}	1541	1.6×10^{-3}	2688	1.2×10^{-2}
ν_4	901	7.2×10^{-4}	1174	1.3×10^{-4}	2024	2.5×10^{-4}
ν_5	736	9.1×10^{-5}	954	1.3×10^{-5}	1626	6.4×10^{-6}
ν_6	627	1.4×10^{-5}	808	1.5×10^{-6}	1361	1.9×10^{-7}
ν_7			704	1.9×10^{-7}	1171	6.4×10^{-9}
ν_8					1029	2.4×10^{-10}

It can be seen from Table 2.5 that the first overtone absorption of the CH bond at 1729 nm, which is quite near 1550 nm, will contribute to the overall optical loss of polymer in the 1550 nm region. If the hydrogen atoms are replaced by more massive atoms, the wavelengths of the fundamental vibration and subsequent harmonics would be shifted to longer wavelength regions. Therefore, the vibration absorption at 1550 nm is higher harmonic, the intensity of which is much lower, and then the optical loss become lower. Currently, deuterium (D) and halogen (fluorine, chlorine) are often used to replace hydrogen to reduce the optical loss of polymer [108,110-112].

To lower CH vibration absorption in polymer, deuterium was selected because it does not influence the original polymer characteristics, except with respect to molecular weight. Replacing the hydrogen in the polymer with deuterium results in a reduction of CH vibration absorption in the IR region, as well as its overtones in the near-IR to visible region. The fundamental vibration of the CD bond occurs at approximately 4484 nm, compared with 3390 nm for CH bond as shown in Table 2.5. By converting H to D,

fundamental frequencies for CD shift to a wavelength region 1.32 times higher than CH, The high harmonics for CD also appear in a higher wavelength region than those for CH. Therefore, vibration absorption in the IR region is expected to be further reduced. A commercial example of deuterated polymer is PMMA-d8 [108], which is a deuterated PMMA. Its optical loss is reduced about 40%.

Substitution of hydrogen atoms by fluorine atoms has opened the way to develop polymer materials with lower attenuation or loss [110-112]. If the CH atom pairs within a polymer were replaced by CF atom pairs, the increase in reduced mass would cause the fundamental absorptions to shift to a longer wavelength region than CD. This shift would allow the use of polymer waveguide at even longer wavelengths optical windows than were obtained with deuterium substitution. It is expected that with increasing substitution of fluorine atoms for hydrogen atoms, the intrinsic attenuation loss will approach that of a Rayleigh scattering contribution [108].

2.3.1.3 Optical Loss of Polycyanurates

The intrinsic optical advantage of CE is the absence of OH and NH groups, and even after the cyclotrimerization or curing none of these disturbing groups are present. But of course the polycyanurates contain CH groups; therefore one way to reduce the optical loss is to replace the hydrogen with fluorine. Figure 2.9 gives the optical loss of BACy monomer and hetptafluorobutylcyanate monomer measured by near-IR spectroscopy. The optical loss of the BACy monomer with no fluorine is about 0.58 dB/cm. The highly fluorinated (59.1 wt.%) heptafluorobutylcyanate with only two aliphatic CH groups shows only 0.21 dB/cm of optical loss. The BFCy (not shown in Figure 2.9), with 29.5 wt.% fluorine and eight aromatic CH groups has a reduced loss of about 0.48 dB/cm [27]. Table 2.6 gives the reported optical losses of some other polymers in order to compare with the optical

data of CE monomers. Through the comparison it is suggested that CEs possess lower optical loss, in addition to their other attractive properties such as high thermal stability, good adhesive to substrate and low dielectric constant, CEs would have great potential for new applications in photonics.

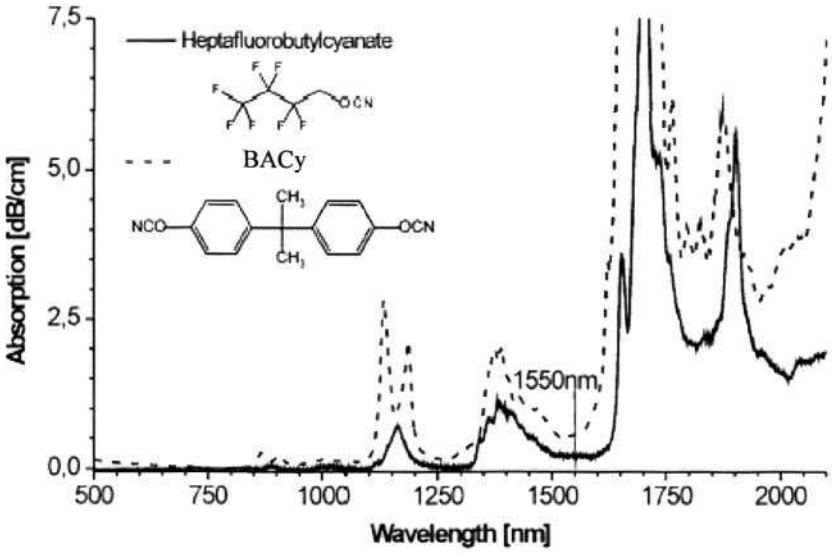

Figure 2.9 Near-IR spectra of cyanate ester monomers [27]

Table 2.6 Optical losses of some optical polymers

Polymer	Optical loss	Reference
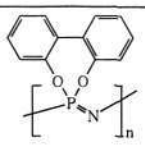 poly(2,2'-dioxybiphenil) phosphazene	10 dB/cm	[107]
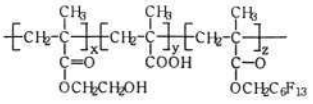 Fluorinated methacrylate polymer	2 dB/cm	[110]
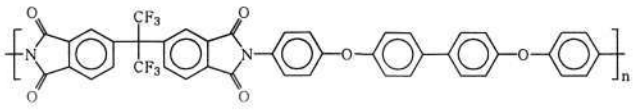 6FDA/APBP	2.9 dB/cm	[113]

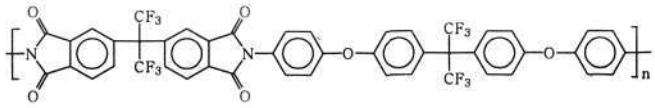 6FDA/BDAF	1.2 dB/cm	[113]

2.3.1.4 Refractive Index of Polycyanurates

One of the key features of organic polymers used in optical applications is the refractive index. Lenses, optical waveguides, and nonlinear optical devices are just three examples where this material parameter plays a key role in the system design. Several requirements should be met in optical devices fabrications. These are: the reproduction of an absolute refractive index; the realization of a defined refractive index; and the adjust range of the refractive index.

There are many internal and external factors influencing the refractive index. Such as the molecular chain arrangement, impurities, stress, etc. The polymerization of cyanate ester resin has many advantages in reproduction of refractive index. The cyanate ester reaction is a very clean reaction, that no byproducts, neither gaseous nor liquid are formed during the reaction, and the polycyanurate network has a well fixed symmetrical macromolecular structure.

Different atoms have different contributions to the refractive index. Figure 2.10 plotted the ratio of molar refraction RL (proportional to the induced dipole moment) to molar volume VL for different atoms present in organic polymers [114].

As one might expect, there is a broad range of values for each atom due to different binding structures and a varying chemical environment in different organic or inorganic compounds. However, it can be seen that fluorine and, to a smaller degree, oxygen lowers

the refractive index of a compound, whereas nitrogen, sulfur, and the heavier halogens have higher ratios and thus should not be present in a low refractive index polymer.

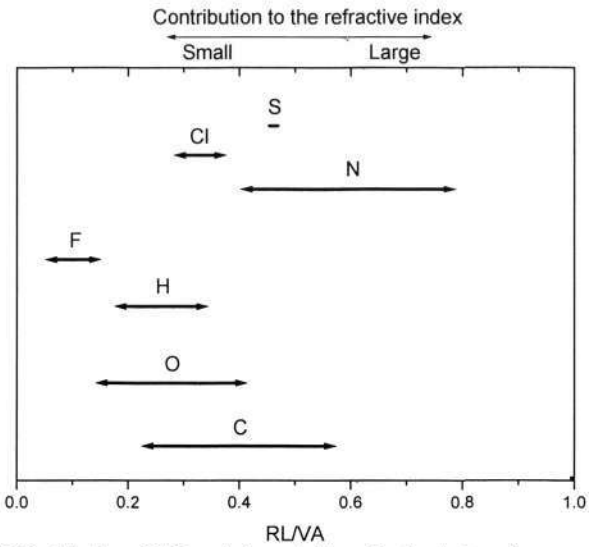

Figure 2.10 Contribution of different atoms to the refractive index of a compound [114]

The Lorenz-Lorentz equation offers the possibility to calculate the refractive index n_D of an unknown polymer, if its molar refractive RL and density ρ are known [114]:

$$\frac{n_D^2 - 1}{n_D^2 + 2}\frac{M_G}{\rho} = RL = \sum_{J=1}^{J} k_j R_j \qquad \text{(Equation 2.7)}$$

where n_D is the refractive index, M_G is the molecular weight of the repeating unit, ρ is the density (g/cm^3), RL is the molar refraction (cm^3/mol), k_j is the number of increments of the substructure j in the repeating unit, R_j is the molar refraction increment of substructure j (cm^3/mol), and J is the total number of individual substructures. According to equation 2.8 the molar refraction RL can be regarded as a sum of refraction increments R_j, each corresponding to a particular functional group within the polymer repeating unit. The increments of various polymer structures are given in Table 2.7 [114].

According to Equation 2.7 and Table 2.7, we can calculate the refractive index of several kinds of cyanate esters with different backbone structures. The calculated results for BACy, BFCy and DFCy homopolymers are 1.61, 1.54 and 1.37 respectively.

To obtain working optical components, not only the reproduction of an absolute refractive index is important but a predefined index must also be realized. The realization of a predefined refractive index is dependent on the adjust range and the reproducibility of refractive index. Generally, for an inorganic mono-modal optical waveguide, the index-contrast (controlled range of refractive index) is typically in the region around 0.01 depending on the design of the optical components and the dimensions of the device. For polycyanurate, it can be predicted that a broad adjust range of 1.4 to 1.6 can be achieved easily by copolymerization of cyanate esters with different backbone molecular structures. Some preliminary work has been done by researchers and it is reported that the refractive index in the range between 1.51 and 1.58 can be realized by using different polycyanurate copolymers [27].

Table 2.7 Increments of various polymer structures [114]

No.	increment	R_j	ΔR_j	V_j	ΔV_j	x	Δx
1	CF_3	6.149	± 0.66	40.274	± 2.78	0.153	± 0.020
2	CF_2CF_3	11.209	± 1.00	67.913	± 4.19	0.165	± 0.018
3	$CF(CF_3)_2$	15.782	± 1.18	93.013	± 4.94	0.170	± 0.016
4	$CH(CF_3)_2$	15.710	± 1.12	88.633	± 4.72	0.177	± 0.016
5	O(ether)	1.625	± 0.68	9.052	± 2.86	0.180	± 0.094
6	OCF_2O	8.311	± 1.22	45.743	± 5.11	0.182	± 0.033
7	OCF_2CF_2	11.747	± 1.25	64.331	± 5.27	0.183	± 0.025
8	CF_2	5.061	± 0.75	27.640	± 3.13	0.183	± 0.034
9	CF_2H	5.729	± 1.10	29.616	± 4.62	0.194	± 0.048
10	CO_3	6.266	± 1.07	31.608	± 4.50	0.198	± 0.044
11	$CO_2CH(CF_3)_2$	21.998	± 1.16	111.394	± 4.86	1.198	± 0.014
12	CCF_3	8.123	± 1.38	37.121	± 5.81	0.218	± 0.051
13	CH_3	5.901	± 0.59	25.798	± 2.50	0.229	± 0.032
14	OCH_2O	7.754	± 0.96	33.631	± 4.06	0.231	± 0.040
15	CO_2CH_3	12.189	± 0.66	48.559	± 2.77	0.251	± 0.020
16	CH_2CH_3	10.404	± 0.60	41.326	± 2.52	0.252	± 0.021
17	CN	6.477	± 0.74	24.445	± 3.12	0.265	± 0.046
18	CH_2O	6.312	± 0.40	23.648	± 1.68	0.270	± 0.025
19	CO_2	6.289	± 0.28	22.761	± 1.19	0.276	± 0.019

20	C_6F_5(arom)	27.181	± 0.94	97.648	± 3.93	0.278	± 0.015
21	CF	3.485	± 0.72	12.466	± 3.01	0.280	± 0.089
22	CHOH	5.851	± 0.69	20.288	± 2.90	0.288	± 0.054
23	CH_2	4.504	± 0.08	15.528	± 0.35	0.290	± 0.008
24	CHO	5.158	± 0.36	17.078	± 1.53	0.302	± 0.035
25	CHF	4.082	± 1.05	13.460	± 4.40	0.303	± 0.126
26	CCl_3	20.620	± 0.77	67.097	± 3.23	0.307	± 0.019
27	CFCl	10.450	± 1.01	33.022	± 4.26	0.317	± 0.051
28	CHCl	9.633	± 0.69	29.598	± 2.90	0.326	± 0.040
29	CCH_3	7.875	± 1.35	22.645	± 5.68	0.347	± 0.106
30	SO_2	9.630	± 1.23	27.713	± 5.15	0.348	± 0.078
31	C_6H_5(arom)	25.824	± 0.69	74.129	± 2.90	0.348	± 0.011
32	C=O	4.590	± 0.71	13.170	± 2.97	0.349	± 0.095
33	Br	10.116	± 1.02	28.843	± 4.27	0.351	± 0.063
34	C_6Cl_5(arom)	51.454	± 0.81	140.399	± 3.40	0.367	± 0.011
35	CCl_2	15.786	± 0.69	41.498	± 2.90	0.380	± 0.031
36	CONH	8.256	± 0.56	21.660	± 2.34	0.381	± 0.049
37	p-C_6H_4(arom)	25.235	± 0.38	65.912	± 1.61	0.383	± 0.011
38	CH	3.412	± 0.62	8.085	± 2.61	0.422	± 0.032
39	C_6H_3(arom)	24.785	± 1.04	53.710	± 4.37	0.462	± 0.042

2.3.2 Dielectric Properties of Polycyanurates

Dielectric properties including dielectric constant and loss factor are important parameters of polymer in various applications. Not only in designing dielectric matrix resins for advanced electronic circuitry, radomes, microwave antennas, and composites for aircraft with low radar observability, but also in fabricating optical components and devices, dielectric properties are of great significant. The intrinsic low dielectric constant of polycyanurate is due to its unique structure. Figure 2.11 shows the cyanurate network structure of BACy homopolymer.

Figure 2.11 indicates a symmetrical arrangement of electronegative oxygen and nitrogen atoms around electropositive carbon atoms in the polycyanurate structure. A high degree of polar symmetry tends to balance the pull of electrons, resulting in short dipole moment and low energy storage in an electromagnetic field [115]. While polycyanurate homopolymers contain appreciable percentages of oxygen and nitrogen (11% and 10%, respectively, for the polycyanurate of BACy), their symmetrical arrangement around a

central carbon atom and resulting weak polarity may explain the observed low dielectric loss. Another feature of polycyanurate contributing to its low dielectric loss is the absence of strong hydrogen bonds. The absence of proton donor groups in polycyanurate homopolymers precludes strong hydrogen bonds and further supports the observed low dielectric loss properties. Table 2.8 gives the dielectric constant (ε) and dissipation factor ($\tan\delta$) of some commercial polycyanurates and Figure 2.12 compares ε and $\tan\delta$ of several polycyanurate homopolymers with some other polymers [115]. Low loss values for the polycyanurate homopolymers reflect the structural features described before and approach the dielectric inertness of fluorocarbon and polyolefin thermoplastics. Polycyanurates offer the high Tg thermal properties of BMIs and can replace low polarity thermoplastics in applications where superior dimensional stability, mechanical properties and good adhesion performance are required.

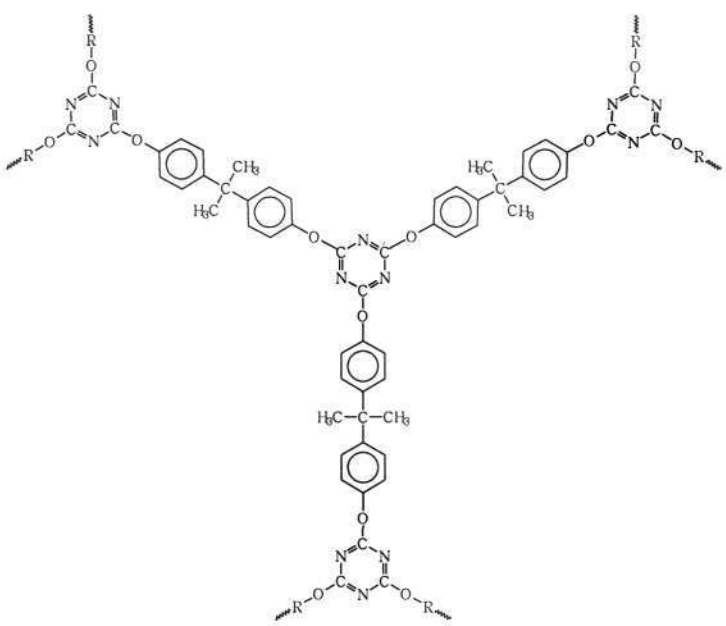

Figure 2.11 Polycyanurate structure formed by the cyclotrimerization of bisphenol A cyanate ester

Table 2.8 Dielectric loss properties of some commercial cyanate ester homopolymers [115]

Trade name	Homopolymer property			
	ε		$\tan\delta$ ($\times 10^{-3}$)	
	1 MHz	1 GHz	1 MHz	1 GHz
AroCy B-10	2.91	2.79	5	6
AroCy M-10	2.75	2.67	3	5
AroCy F-10	2.66	2.54	5	5
AroCy L-10	2.98	2.85	5	6
XU-366	2.64	2.53	1	2
XU-371	3.08	2.97	6	7
XU-71787	2.80	-	3	5

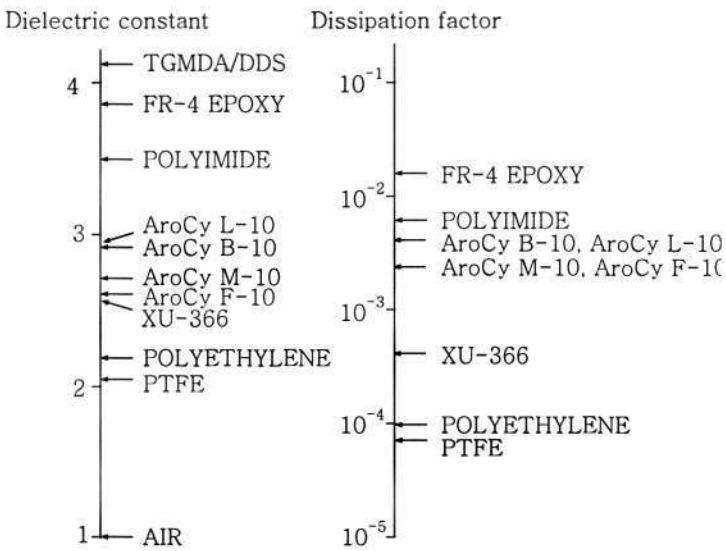

Figure 2.12 Dielectric constants and dissipation factors of CEs and some other polymers [115]
TGMDA/DDS: tetraglycidylmethylene dianiline cured with 4,4'-diaminodiphenyl sulfone;
FR-4 EPOXY: brominated epoxy cured with dicydiamide. PTFE: polytetrafluoroethylene

2.3.3 Thermal Stability of Polycyanurates

The thermal and thermal-oxidative stability of optical polymers are very important because they determine the upper service temperature and the environmental conditions under which they can be employed. As its most fundamental level, thermal stability of polymers is influenced by the strength of chemical bonds. In other words, the chemical structure of the polymer is of primary importance in respect to its stability [124,125]. The chemical composition is in itself a determining factor. Considering the comprehensive

study of thermal stabilities and degradation mechanisms of sets of polymers of closely related structure, the following generalizations can be drawn for a polymer to have high thermal stability can be drawn [126,127]:

- Only the strongest chemical bonds should be used.
- The structure should not allow easily for rearrangement.
- There should be a maximum use of resonance stabilization.
- All ring structures should have normal bond angles.
- Multiple bonds and aromatic rings should be utilized as much as possible.

It must be stressed that all these conditions really relate to a perfect structural unit in isolation. In practice there are interactions within and between molecules and seldom does a polymer have a perfect, idealized structure. In general, polymers with more aromatic rings and crosslinking structure are thermal stable and can be used in high temperature resistance applications. Table 2.9 presents some typical thermal properties of CE resins and some competitor resins. The data indicates that polycyanurate homopolymers exhibit a fine thermal stability. It is due to the aromatic nature of triazine ring that displays high thermal stability and thermally stable aromatic bisphenyl groups as bridge linking the triazine branch points. Figure 2.13 shows Tg versus strain capabilities of various thermosetting resin systems [1]. The relative position of the various systems indicates their comparative toughness and temperature endurance capabilities, and the dicyanates can be found to occupy a medium position.

Figure 2.14 shows TGA data between 300 °C and 900 °C for nine cyanate ester resins. Figure 2.15 shows the mass loss rate (derivative of the TGA) data for the PT-30 polycyanurate and the deconvolution of that data using an asymmetric double sigmoidal peak fit to isolate the individual mass loss processes that occur during heating. The data

reveal that the polycyanurates thermally decompose in two steps with the major mass event beginning at about 400 °C [129,130]. The monomer molecular structures of these CEs can be found in Table 2.1, except BPCCE, whose molecular structure is shown in Figure 2.14.

Table 2.9 Thermal properties of cyanate ester homopolymers and competitor resins [128]

Property		AroCy				XU-71787	TGMDA-DDS	BMI-MDA	BMI-DAB
		B-10	M-10	F-10	L-10				
HDT (°C)	Dry	254	242	243	249	-	232	270	266
	Wet	197	234	195	183	-	167	262	217
T_g (°C)	DMA	289	252	273	258	244	246	320	288
	TMA	257	244	270	259	223	210	297	263

TGMDA/DDS: tetraglycidylmethylene dianiline cured with 4,4'-diaminodiphenyl sulfone; BMI-MDA: bismaleimide cured with methylene dianiline; BMI-DAB: bismaleimide cured with 2,2'-bis(3-allyl-4-hydroxyphenol) isopropylidene.

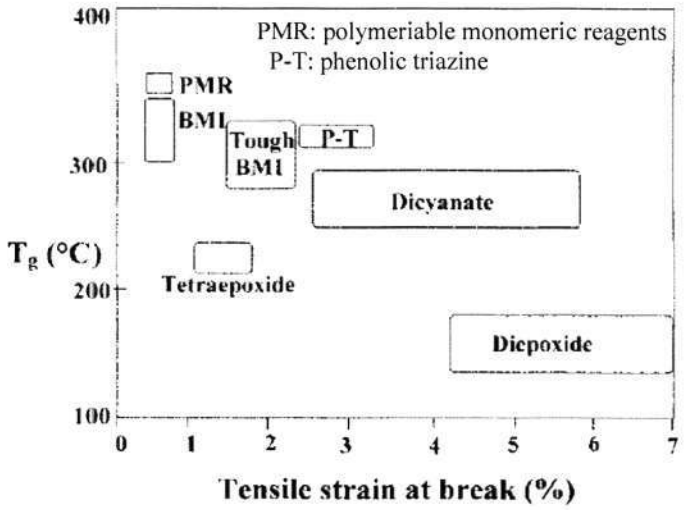

Figure 2.13 Service temperature and toughness of various thermosetting resins [1]

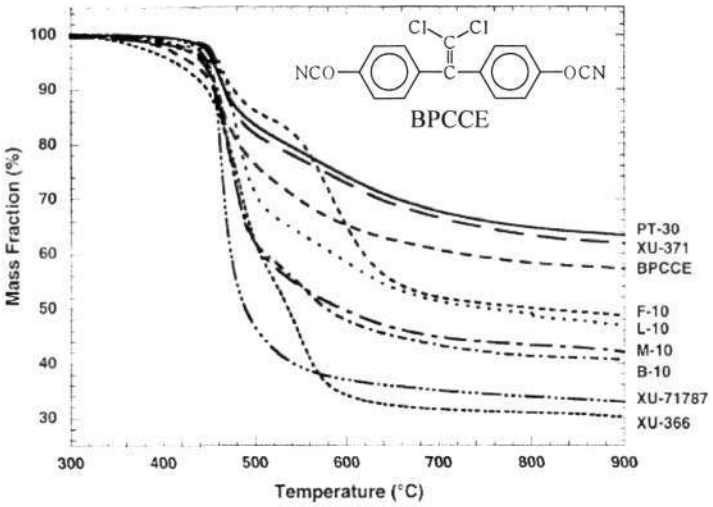

Figure 2.14 Thermogravimetric data of some polycyanurates [129]

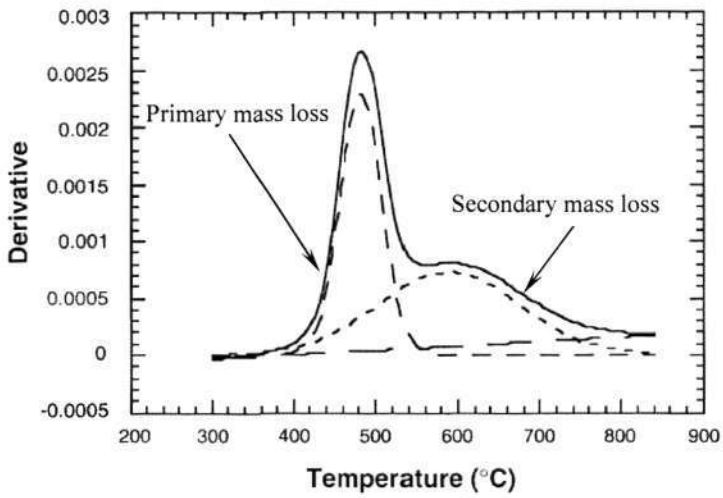

Figure 2.15 Mass loss rate versus temperature for PT-30 [129]

Table 2.10 shows the temperature at 5% weight loss, the temperature at maximum mass loss rate, the char yield at 900 °C, and the reported glass transition temperatures (Tg) [130]. The 5% weight loss temperature and the peak mass loss rate temperature are relatively insensitive to monomer chemical structure for the polycyanurates tested with average values of 448 ± 7 °C and 468 ± 8 °C respectively. The char yield is sensitive to the chemical structure of the monomer and increases with glass transition temperature and in rough proportion to the mole fraction of unsaturated carbon-carbon bonds.

Table 2.10 Thermal properties of polycyanurates [130]

Sample	T_g (°C)	5% weight loss temperature (°C)	Peak mass loss rate temperature (°C)	Char yield at 900°C (%)
XU-366	192	439	482	31
XU-71787	244	447	463	33
B-10	257	443	468	39
M-10	252	443	471	41
L-10	258	455	479	47
F-10	270	453	465	49
BPCCE	275	441	461	56
XU-371	350	454	461	62
PT-30	350	457	462	63

2.4 Modification of Polycyanurates

Despite their many attractive features, the search for further improvements in performance and reduction in cost of polycyanurate resins is never ending and a large number of studies have been devoted to matrix modification through blends and co-curing of these systems. polycyanurate resins have generated a lot of interest in high performance applications due to their attractive physical, dielectric, thermal, and mechanical characteristics. A large variety of cyanate ester momoners with different backbone structures and properties are available. This provides considerable scope for tailoring the properties of resin formulations. Polycyanurate resins are finding increasing use in the form of blends where their inherent low moisture absorption and low dielectric loss properties may be allied to other components such as EP or PI (BMI) resins. Depending on the nature of the component of the blend, co-reacted matrix or interpenetrating polymer networks can be produced.

Blends with other thermosetting resins including EP [9-14] and BMI [15-19] are very common and found in many commercial and patented resin formulations. However, although the CE/EP and CE/BMI blending systems show better processability and lower product costs, the desirable properties of polycyanurate such as high Tg, low dielectric constant and low optical loss are compromised in these modifying approaches. It is because the introduction of other polymers such as EP and BMI will destroy the symmetrical structure of polycyanurate, and in turn, greatly increase the dielectric loss and optical loss. It is recommended that not employing EP or BMI to modifying polycyanurate when dielectric and optical properties are concerned. Therefore, although the CE/EP and CE/BMI modified resin systems have attracted much attention, due to the above reason, these methods will not be adopted in this study.

A large variety of cyanate ester resins with different backbone structures and properties are commercially available, e.g., aromatic or aliphatic, monofunctional or multifunctional, and conjugate. It provides a new way to tailor the properties of resin formulations by blending different cyanate esters. Blending of different cyanate esters is advantageous since they are available in variety of liquid, semi-solid, solid and solution forms. It is worth noting that, since the oligomeric prepolymers are merely intermediates on the way to a full cure, blending different ratios of prepolymers and monomers of a particular cyanate ester will not affect the ultimate properties of the cured homopolymer. However, this may not hold true in blends with other CEs. Some CE blends possessing improved thermal and rheological properties have also been reported [20,131]. For example, Papathomas et. al. [20] reported the preparation of CE thermosetting resins by coreacting a fluorinated bisphenol A dicyanate (BFCy) monomer with a monofunctional CE (CPCy). Their objective in the study was to modify the BFCy system with reactive diluents of a nonpolar nature and produce matrix resins processable at FR-4 epoxylike conditions. By

introducing the monofunctional cyanate ester as a reactive diluent, the molar crosslink density of the resulting network was reduced. Highly branched triazine polymers resulted from this approach.

The modifying approach through blending of different cyanate esters has an obviously advantage in that it does not change the distinguish symmetrical triazine structure of CE resin, therefore, most of the properties contributed by this unique structure are expected to be reserved after the modification, which is greatly favorable in modifying the optical properties of polycyanurate including control the refractive index and reduce the optical loss. However, the reported work on CE/CE blends so far has mainly focused on improving the processability or enhancing the thermal stability. Therefore, more studies on the optical properties of CE/CE blends are necessary.

CHAPTER 3

EXPERIMENTAL

3.1 Materials

Four cyanate ester monomers were used in this work. 2,2'-Bis(4-cyanatophenyl)iso-propylidene (BACy), 2,2-Bis(4-cyanatophenyl)-1,1,1,3,3,3-hexafluoropropane (BFCy), 4-phenylphenol cyanate ester (CPCy) and 2,2,3,3,4,4,5,5,6,6,7,7-Dodecafluorooctanediol dicyanate ester (DFCy) were all purchased from Oakwood Products, Inc. West Columbia, SC. Their chemical structures are shown in Figure 3.1. The solvent used for spin coating is 1,1,1-trichloroethane (chloroform. Purity, 99.8%), from Aldrich.

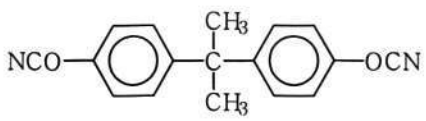

2,2'-Bis(4-cyanatophenyl)iso-propylidene (BACy)

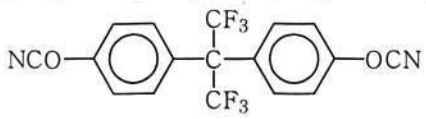

2,2-Bis(4-cyanatophenyl)-1,1,1,3,3,3-hexafluoropropane (BFCy)

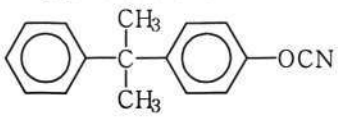

4-phenylphenol cyanate ester (CPCy)

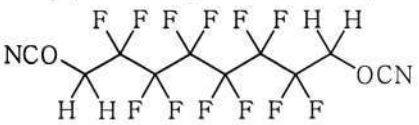

2,2,3,3,4,4,5,5,6,6,7,7-Dodecafluorooctanediol dicyanate ester (DFCy)

Figure 3.1 Chemical structures of cyanate ester monomers

3.2 Synthesis of Cyanate Ester Prepolymers

The prepolymers were prepared following the procedure is set out as below. Cyanate ester monomers was put into a 500 ml three-neck round bottom flask equipped with a gas inlet, gas outlet, thermometer and magnetic stirrer, heated to previous set temperature and hold at this temperature with stirring for 1 h to 8 h (the duration is depended on materials) in nitrogen atmosphere. Then the reaction was stopped rapidly by quenching the reaction in ice-water mixture prior to gelation. Careful control of prepolymerization conditions is critical in order to optimize the prepolymers for subsequent processing.

Sixteen polycyanurate prepolymers were prepared for spin coating. They are prepolymers of BACy, BFCy, DFCy homopolymers and BACy/BFCy (2:8, 4:6, 5:5, 6:4, 8:2 in molar ratio), BACy/DFCy (2:8, 4:6, 5:5, 6:4, 8:2 in molar ratio), BACy/CPCy (2:8, 4:6, 5:5 in molar ratio) copolymers.

3.3 Preparation of Polycyanurate Thin Films

The synthesized polycyanurate prepolymers were dissolved in chloroform and the solutions of different concentration 5-30 wt.% were filtered by using 0.2 μm PTFE syringe filter under cleanroom conditions. The solution is clear viscous and a light yellow color. Then the prepolymer solutions were spin-coated onto a substrate at various speeds ranging from 500 rpm to 3000 rpm for different durations from 5 s to 50 s. It should be noted that only one layer of the film was spun onto the substrate. The coated films were then thermal cured at different temperatures from 100 °C to 230 °C for a predetermined duration. The film thickness was controlled by changing the solution concentration, spin speed and spin time of the cyanate ester prepolymer solution. It should also be noted that cleaning of the substrate is important for proper adhesion of the films. Silicon (Si) and

microscope glass slide were used as substrates for different characterization purposes and they were ultrasonically cleaned in acetone and ethanol, rinsed with deionized water and blow dried with pure nitrogen blower.

3.4 Characterizations of Polycyanurates and Their Thin Films

3.4.1 Fourier-Transform Infrared (FTIR) Spectroscopy

FTIR spectroscopy is employed to study the chemical structure of polycyanurate resin and examine the curing of cyanate ester by monitoring the decrease of the cyanate-band in the IR spectrum in the wavenumber region around 2270 cm^{-1}. Infrared spectrums of monomers, prepolymers and cured cyanate ester resins were obtained by using a Perkin Elmer FT-2000 Fourier Transform Spectrometer in the range of 6500~400 cm^{-1} with 64 scans and a 2 cm^{-1} resolution step.

The samples for FTIR measurement were prepared by casting chloroform solutions of monomer or prepolymers onto silicon substrates. The coated films were placed on a hotplate at temperature 50 °C for about 30 min, then placed at room temperature in desiccator for over 24 hours in order to volatilize the residual solvent. And then the films were characterized or cured at different isothermal temperatures for different durations in nitrogen atmosphere before the characterization.

Silicon is one of possible substrates for IR spectroscopy which is often used in Attenuated Total Reflection (ATR) technique, but has not been used for transmittance measurements of polymers very frequently, because although silicon is transparent in the infrared spectral region above 1500 cm^{-1}, it has absorption in the wavenumber region below 1500 cm^{-1} (Figure 3.2), which is an important and interesting area for studying the structure or

reaction of polymers. However, for materials such as polycyanurate, the interesting wavenumber region of which is above 2000 cm^{-1}, using silicon as the FTIR substrate provides many advantages in comparison to other traditional FTIR window materials such as KBr. Silicon is not hygroscopic and is chemically inert, and resists thermal and mechanical shocks, scratching and fogging. In this study, the IR bands used to monitor the curing process are above 2000 cm^{-1} (more details will be discussed in Chapter 4), therefore, silicon wafer is chosen as the FTIR substrate.

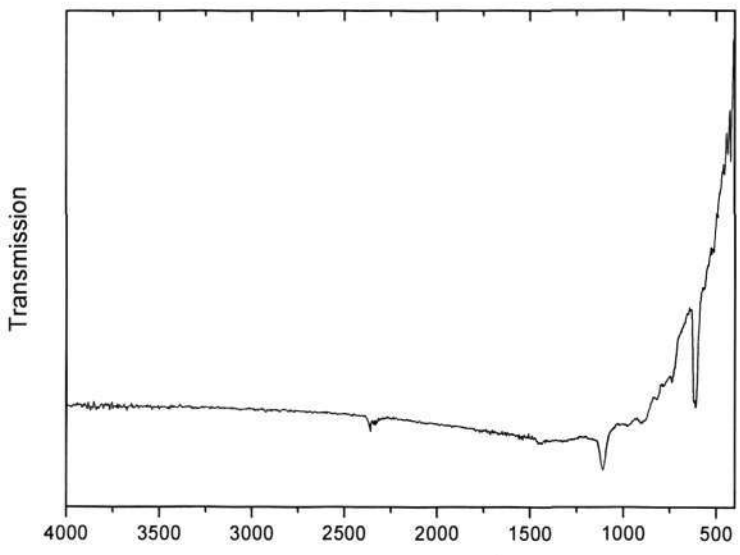

Figure 3.2 Infrared spectrum of silicon wafer

To monitor curing of polymer, a band that remains nearly constant throughout the treatment time is chosen as the reference band. The percentage conversion of resin, referred to as α in this thesis, is calculated using following equation:

$$\alpha = 1 - \left(\frac{I_{reactiveband}}{I_{referenceband}} \right)_{T,t} \Bigg/ \left(\frac{I_{reactiveband}}{I_{referenceband}} \right)_{T,t=0} \qquad \text{(Equation 3.1)}$$

where I is the intensity of vibration absorption peak, T is the temperature of isothermal cure, and t is the time of curing.

3.4.2 Differential Scanning Calorimetry (DSC) Analysis

In this experiment, a TA instrument DSC 2010 was used to analyze melting and chemical reaction behaviors of the BACy monomer, prepolymers and cured resins. Sample (around 5 mg) was hermetically sealed in aluminum pans for DSC analysis. Before the measurement, the temperature, baseline and heat flow calibrations were carried out by the recommended procedures using pure indium of melting point 156.4 °C and heat of fusion, $\Delta H_f = 6.80$ cal/g. The enthalpy of curing, ΔH was determined from the area under the exothermic peak and the sample mass.

The percentage conversion of prepolymers and partially cured polymers were determined by the following procedures. A DSC scan (ΔH_{TO}) of a pure uncured cyanate monomer with a heating rate of 5 °C/min was first obtained. Then the DSC scan (ΔH_f) of a prepolymer or a partially cured polymer was also obtained with the same heating rate of 5 °C /min. Nitrogen gas was used for purging at a flow rate of 60 cc/min in each scan. Curing conversion, α was calculated from Equation 3.2:

$$\alpha = \frac{\Delta H_{TO} - \Delta H_f}{\Delta H_{TO}} \qquad \text{(Equation 3.2)}$$

where ΔH_f is the enthalpy of the prepolymer or the partially cured polymer and ΔH_{TO}, the total enthalpy of reaction.

Curing study of the cyanate ester resin systems was also characterized by DSC using isothermal method. To avoid mass loss, hermetically sealed pan was used and the sample weight was measured before and after the experiment. To select suitable temperatures for the required isothermal experiments, a DSC scan with a heating rate of 10 °C/min was first obtained (An example is given in Figure 3.3). Temperatures above but near the onset of reaction were chosen. This method could avoid the improper choice of temperature,

which maybe too high or too low. Too low temperature would prolong unnecessarily the experimental time which might exceed the limit of instrument, whereas when the temperature is too high, the reaction time will be too short for detection by the equipment. Based on preliminary study and also for easier comparison, isothermal experiments were carried out at appropriate temperatures.

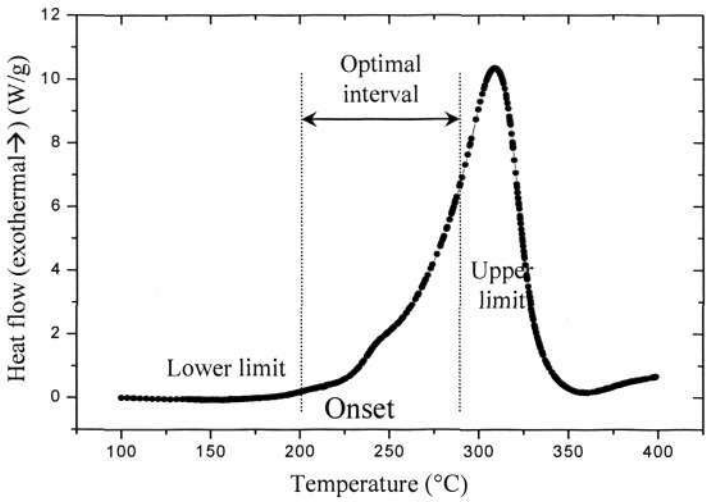

Figure 3.3 Isothermal curing temperatures selection rule

In an isothermal experiment, the sample pan was placed in the DSC cell at a temperature of 50 °C, and nitrogen gas was used for purging at a flow rate of 60 cc/min. After the system reached equilibrium, the temperature was raised to the isothermal curing temperature at a heating rate of 200 °C/min. This is to minimize unrecorded reaction heat during the initial heating before data collection was initiated. After hold at this isothermal temperature till there is no change in heat flow, the experiment is stopped. The conversion at time t, $\alpha(t)$, can be determined from the Equation:

$$\alpha(t) = \frac{\Delta H(t)}{\Delta H_{tot}} \qquad \text{(Equation 3.3)}$$

Where $\Delta H(t)$ are the enthalpies of the reaction at time t. For a given isothermal temperature, $\Delta H(t)$ is the accumulative heat of reaction up to curing time t and given by the area above the baseline and below the curve, as an example shown in Figure 3.4. The

baseline is a straight tangential line to the horizontal part of the isothermal DSC curing curve.

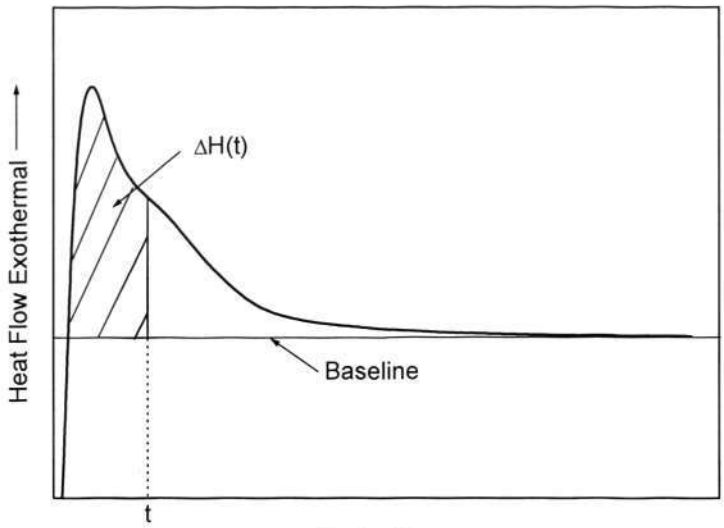

Figure 3.4 A typical isothermal DSC curing curve

3.4.3 Modulated Differential Scanning Calorimetry (MDSC)

MDSC was used to detect the glass transition temperatures of the polycyanurates. For a fully cured polycyanurate, it is difficult to measure its Tg using normal DSC, due to the high crosslink density nature of thermosetting resin, the Tg relaxation transition may not be sensitive to normal DSC. MDSC is a more accurate method to measure the Tg of this type of materials, because it can separate the reversing and non-reversing heat flow from the total heal flow. This provides an increased sensitivity.

The MDSC analyses were conducted using MDSC Model 2920, TA Instruments. The linear heating rate was 10 °C/min, the modulation condition was a period of 60 s with an amplitude of 1.592 °C (from the TA manual). All analyses were accomplished with the use of a nitrogen purge gas. Baseline calibration was carried out for the modulation condition, and temperature calibration was performed using pure indium.

3.4.4 Dielectric Analysis (DEA)

Dielectric analysis (DEA) measures the electric properties of a material as a function of time, temperature, and frequency. DEA measures two fundamental electric characteristics of materials: the capacitive (insulating) nature, which represents its ability to store electric charge; and the conductive nature, which represents its ability to transfer electric charge. Through DEA analysis, the dielectric constant, dielectric loss, and dielectric loss tangent of a material can be obtained.

A TA instruments DEA 2970 Dielectric Analyzer was used to measure the dielectric properties of the polycyanurate homopolymer and copolymer systems. The single surface sensor, also referred to as comb electrodes, contains an interdigitated array of excitation and response electrodes on a planar surface. The samples were melted and coated uniformly onto the sensors. The first run was conducted from room temperature to 300 °C at a heating rate of 2.5 °C/min and then furnace-cooled to room temperature. After the first curing run, the obtained sample was tested again from 75 °C to 300 °C at a heating rate of 5 °C/min. The dielectric constant (ε'), loss factor (ε'') were recorded at nine different frequencies, i.e., 1, 3, 10, 30, 100, 300, 1000, 3000, and 10,000 Hz. The DEA cell was purged with nitrogen adjusted to a flow rate of 500 ml/min throughout the experiment.

3.4.5 Measurements of Film Thickness and Refractive Index

The samples for film thickness and refractive index measurements were prepared by casting chloroform solutions of polycyanurate prepolymers onto silicon substrates. The coated films were placed on a hotplate at temperature 50 °C for about 30 min, then placed in a desiccator at room temperature for over 24 hours in order to volatilize the residual solvent. The films were then cured at different isothermal temperatures for different

durations in nitrogen atmosphere. A Metricon Model 2010 Prism Coupler (Metricon) was used to measure the thicknesses and refractive indices of the partially cured polycyanurate thin films. After the measurement, the percentage conversion of the partially cured cyanate ester was determined by FTIR.

The sample to be measured (Figure 3.5(a)) was brought into contact with the base of a prism by means of a pneumatically-operated coupling head, creating a small air gap between the film and the prism. A laser beam strikes the base of the prism and normally reflected light totally at the prism base onto a photodetector. At certain discrete values of the incident angle Θ, called mode angles, photons tunnel across the air gap into the film and enter into a guided optical propagation mode, causing a sharp drop in the intensity of light reaching the detector (Figure 3.5(b)).

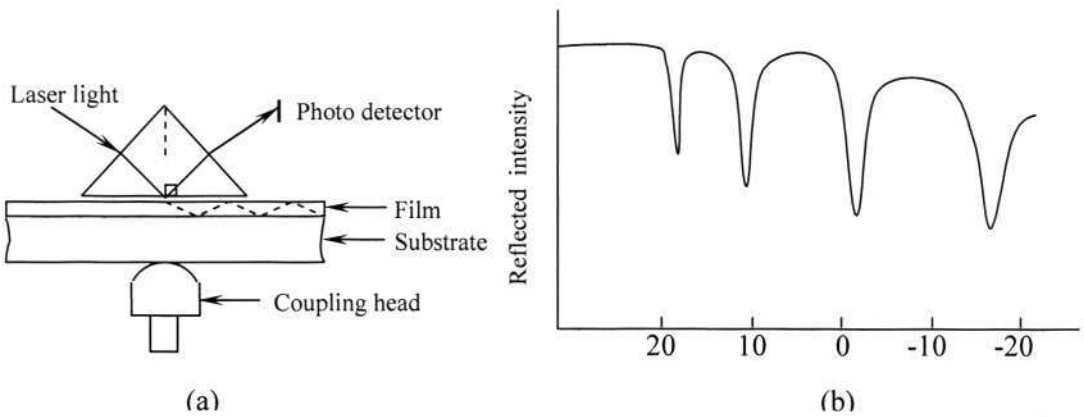

Figure 3.5 (a) Schematic of a prism coupler; (b) Intensity of reflected light vs. angle of incidence (Θ)

The angular location of the first mode determines film index, while the angular difference between the modes determines the thickness, allowing thickness and index to be measured completely independently. Measurements are made using a computer-driven rotary table which varies the incident angle Θ, and locates each of the film propagation modes. As soon as two of the mode angles are found, film thickness and index can be calculated. The entire measurement process is fully automated. The number of modes supported by a film of given index increases with film thickness. For most film/substrate

combinations, a thickness of 1000-2000 Å is required to support the first mode, while films in the one-micron range can support as many as four or five modes. If the film is thick enough to support two or more propagation modes (typically 3000- 4800 Å), the Model 2010 calculates thickness and index for each pair of modes, and displays the average and standard deviation of these multiple estimates.

3.4.6 Measurements of Optical Loss of Polycyanurate Thin Films

The measurements of optical loss of polycyanurate thin films use the moving optical fiber method. The sample used for the measurements of optical loss are polycyanurate thin films coated on silicon dioxide wafer, the wafer size is 2 cm ×5 cm. The wavelength measured is 1550 nm with InGaAs Detector (option 2010-WGL2).

The rotary table is first positioned so that the desired mode is excited and a propagating streak is obtained. The fiber is then driven by s stepper motor into close proximity to the prism at the start of the streak. The model 2010 loss preamplifier gain and offset controls are next adjusted to the signal level obtained from the streak. The fiber is then automatically scanned down the streak and the intensity versus distance profile is displayed on the PC monitor.

3.4.7 Thermal Mechanical Analysis (TMA)

A TA instrument TMA 2940 analyzer was employed in this study to investigate the thermal mechanical property of the cured resin systems. The average thickness of the specimens for TMA tests was 4.5 mm, and the diameter was 4.8 mm. The sample surfaces were smoothed using a Struers Rotopol-35 polishing machine to obtain parallel top and bottom surfaces. TMA measurement was performed from room temperature to

300 °C, the heating rate was set as 5 °C/min, and the mode chosen was standard expansion probe. The probe press was 0.01 N. Nitrogen was blown into the chamber at a rate of 50 cc/min.

3.4.8 Atomic Force Microscope (AFM)

The morphology of the surfaces of the polycyanurate thin films was studied by AFM. The AFM scanning was performed with a Scanning Probe Microscope (SPM) (Nanoscope III, Multimode from Digital Instruments, Santa Brabara, California) operating in tapping mode. The tapping AFM measurements were performed using standard silicon probes with a cantilever configuration of single beam and 225 mm of length, and with a tip of a nominal radius of curvature of 5–10 nm. Several specimens were scanned in different areas in order to analyse their morphologies. The images obtained were similar, thus demonstrating the reproducibility of the results.

3.4.9 Scanning Electron Microscopy (SEM)

The surface morphology of the polycyanurate thin film was examined using scanning electron microscopy (SEM) (Jeol MSM 5410). The samples were coated with a thin layer of gold before the SEM observation, and the SEM worked at 10 kV in this study.

3.4.10 Nanoindentation Analysis

The hardness and elastic modulus of the polycyanurate thin films were measured by using a TriboScope nanomechanical testing system. A Berkovich diamond tip was used as an indenter. During indentation, the indentation depth versus time and the load versus time were recored simultaneously and displayed as a standard Load/Depth curve. Hardness and the reduced modulus were determined from the unloading part of the force-depth curve.

CHAPTER 4

PREPARATION OF POLYCYANURATE THIN FILMS

4.1 Introduction

Polymer thin films are critical in many technological and industrial applications, such as optical coating, electronic packaging materials, dielectric coating, resist layers for lithography, sensor films, adhesion and lubrication. Polymer thin films of few microns are widely used in electronic, optical and adhesive applications [27-29,34-38]. Polycyanurate thin films have been prepared and reported by some research groups but most of the efforts have been made to understand the adhesion mechanisms of polycyanurate on different substrates. The work reported on optical quality polycyanurate thin film is only at the initial stage. Polycyanurate thin films can be prepared by spin coating method [27, 34-37], dip coating [29] or by evaporation method [38]. Polycyanurate thin films can be directly thermally deposited and cured at the surface of the substrate from the vapor of CE monomer, and this evaporation method has been used to prepare ultrathin film of several nanometers.

Spin coating is one of the simplest and the most commonly used techniques to prepare polymer thin films including polycyanurate thin films. The process involves simple fluid flow and evaporation behavior that generally give rather uniform coatings on wafers [138]. Spin coating is used for many applications where relatively flat substrates or objects are coated with thin layers of materials. The materials to be coated must be

dissolved or dispersed into a solvent and the solution is then deposited onto the surface and spun-off to leave a uniform layer for subsequent processing stages and ultimate use. The spin coating process can be broken down into several key stages: fluid dispense, spin-up, spin-off and finally evaporation dominated drying (Figure 4.1) [139].

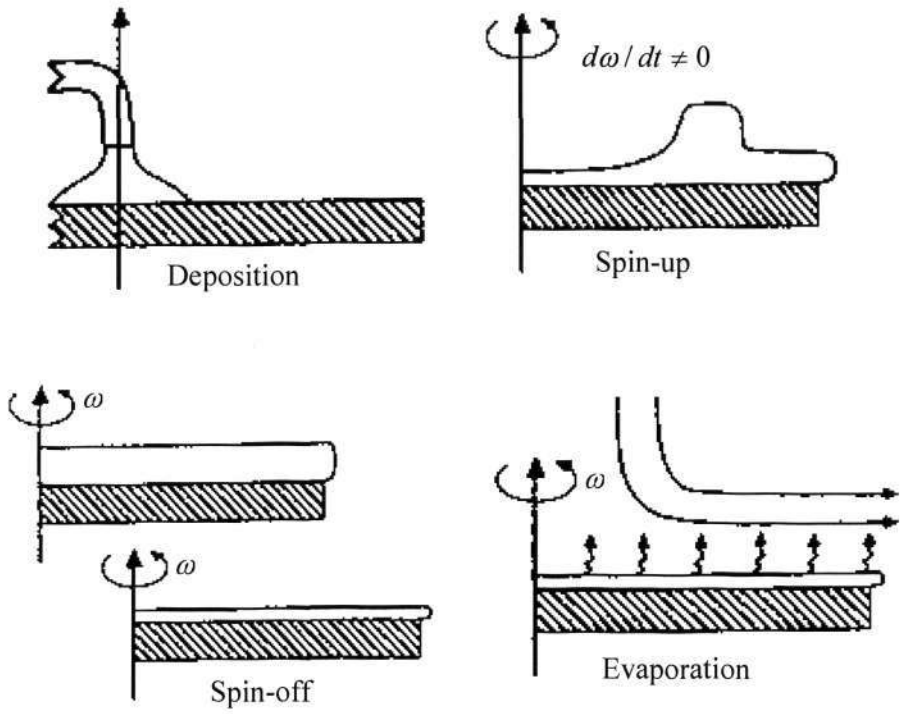

Figure 4.1 The key stages in spin coating processing

Optical quality thin films of a few microns thick can be obtained by spin coating method [140]. An advantage of spin coating is that a film of the polymer solution tends to become uniform in thickness during spin and, once uniform, tends to remain so provided that the viscosity is not shear dependent and does not vary over the substrate. This tendency arises due to the balance between the two main forces, i.e., centrifugal force, which drives flow radically outward, and viscous force (friction), which acts radially inward [141].

To prepare a desirable polycyanurate thin film by spin coating method comprising the steps of (1) synthesizing a polycyanurate prepolymer with appropriate conversion and

dissolving it in a solvent to prepare the precursor, (2) depositing a quantity of prepolymer solution on a substrate, (3) spinning the substrate to make a film of the triazine precursor, and (4) curing the prepolymer to form a cross-linked polymer. The film thickness can be controlled by adjusting the solution concentration and the spin coating parameters.

4.2 Prepolymerization of Cyanate Esters

Prepolymerization is a very useful formulating technique for developing resin systems that have specific rheological requirements. Prepolymers were usually synthesized for subsequent processing into various products for different applications. In this study, prepolymerization of cyanate ester monomers is crucial for the preparation of polycyanurate thin films. Several polycyanurate prepolymers were prepared for the spin coating process including homopolymers and copolymers. All of them are prepared following the similar procedures. The synthesized prepolymers were analyzed by TGA, DSC and FTIR techniques. The factors affecting the prepolymerization and the effects of processing parameters, such as solution concentration, spin speed and spin time, on the thin film deposition were investigated.

Cyanate ester monomer solution can also be directly used for spin coating. However, preliminary study shows that spin coating of cyanate ester monomer solution only gives spherule-like crystal at the surface of the substrate (Figure 4.2 (a)), and the coated monomer layer suffers from severe evaporation during the curing. Hence, it is not possible to obtain a uniform and dense film. Fortunately, when spin from a prepolymer solution, the polymer film becomes smooth and pin-hole free (Figure 4.2 (b)).

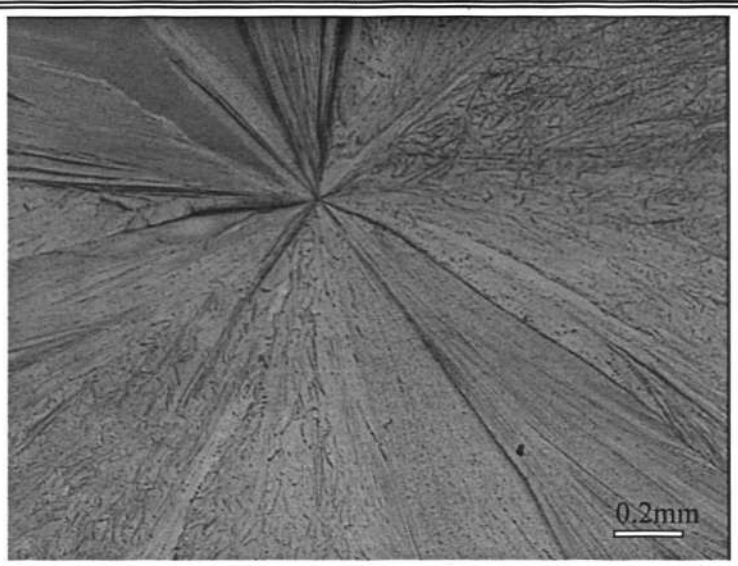

(a) Coated BACy monomer layer

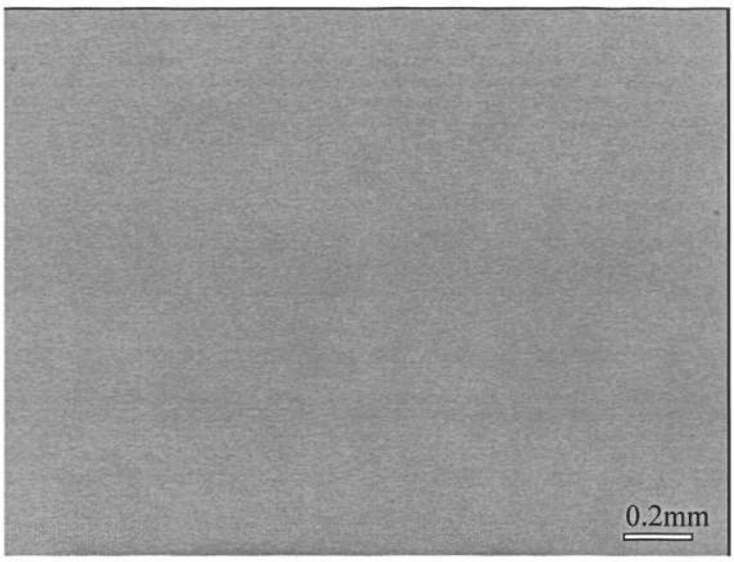

(b) coated BACy prepolymer layer

Figure 4.2 Comparison of POM graphs of spin-coated BACy monomer and prepolymer films

On the other hand, prepolymerization of cyanate ester monomers can also reduce the evaporation of monomer during thermal curing. This study finds that cyanate ester monomers are apt to evaporate when they are heated to a temperature above the melting point. Volatilization of cyanate ester monomers will make the subsequent thermal curing of thin film become difficult, because the volatilized cyanate ester monomer will no longer stay on the surface of the substrate, and leave some 'island' area. Hence the film

loses it uniformity. Prepolymerization can transfer the cyanate ester monomers to dimmers, trimers and higher oligomers with increased molecular weight and solution viscosity. Evaporation can then be suppressed effectively. The evaporation phenomenon can be monitored quantitatively by thermogravimetric analysis (TGA). Figure 4.3 shows the mass fraction and fractional mass loss rate versus temperature of BACy monomer.

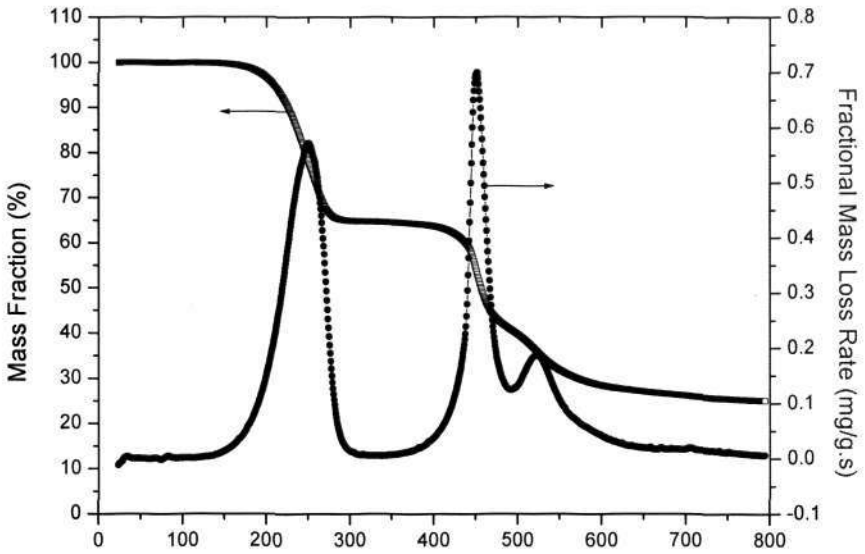

Figure 4.3 Thermogravimetric data of BACy monomer

In Figure 4.3, the mass loss rate curve shows three weight-loss peaks, the last two peaks at about 449 °C and 523 °C are attributed to the two-step thermal degradation of polycyanurate [130,131]. The first weight-loss peak between temperature 150 and 300 °C become weaker after prepolymerized and disappeared after fully cured, as shown in Figure 4.4 and Figure 4.5.

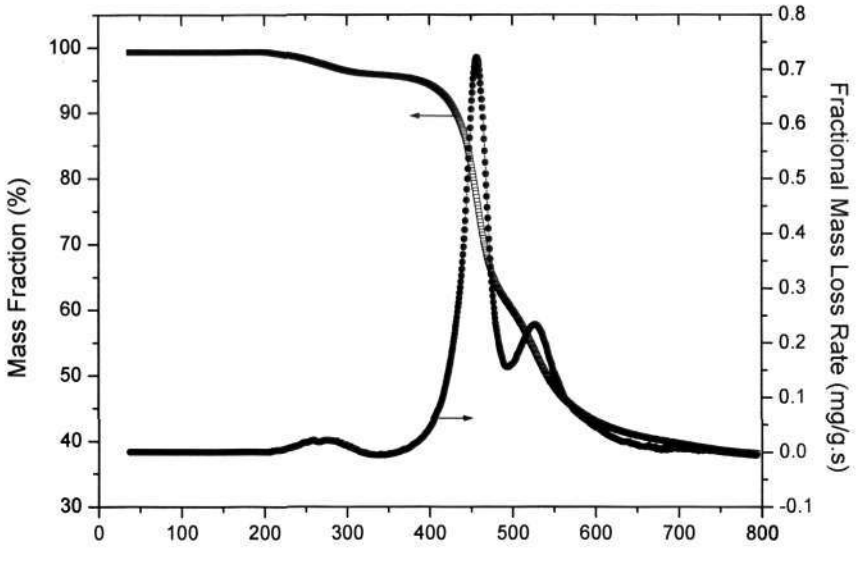

Figure 4.4 Thermogravimetric data of BACy prepolymer
(prepolymerized for 8 hrs @ 180 °C in nitrogen)

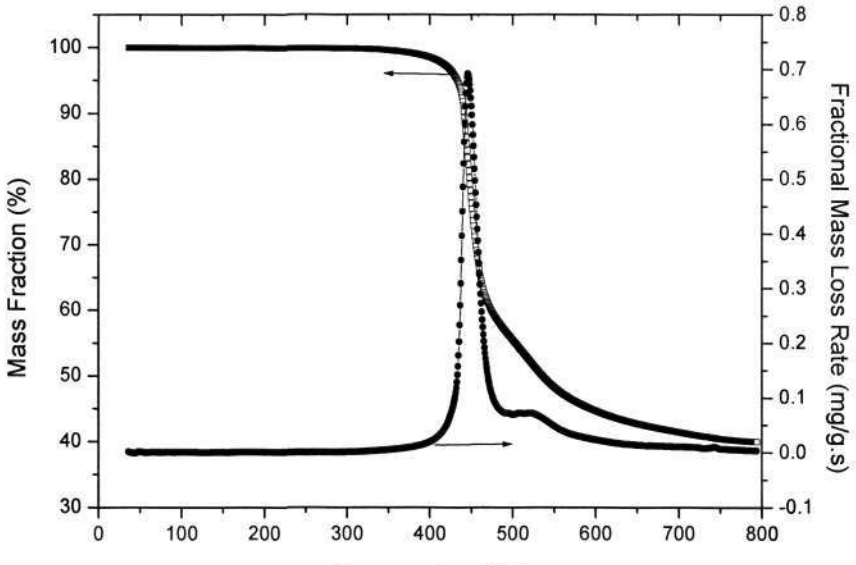

Figure 4.5 Thermogravimetric data of cured BACy resin
(Cured for 5 hrs @ 220 °C in nitrogen)

It suggests that the first weight-loss peaks in Figure 4.3 and Figure 4.4 are due to the evaporation of low molecular weight cyanate ester monomers since such a peak does not appear in the TGA curve of cured polycyanurate resin. The TGA data also indicate that prepolymerization can minimize the evaporation of cyanate ester. After BACy monomers

were prepolymerized in nitrogen atmosphere at 180 °C for about 8 hours, the mass loss due to evaporation was reduced to 3.96 wt.%, which is much lower than that of un-prepolymerized cyanate ester (35.18 wt.% evaporated). Unfortunately, even the evaporation of cyanate ester monomer was reduced to such a low level of 3.96 wt.%, it still may influence the quality of the cured cyanate ester films if they were not cured at an optimized conditions. By comparing the mass loss rate curves in Figure 4.3 and Figure 4.4, it can be seen that the initial evaporation shifts from 150 °C to 220 °C. This indicates that, if the films are cured at temperatures lower than 220 °C, the evaporation of the cyanate ester will be further reduced and high quality polycyanurate thin films can then be obtained.

To obtain optical quality spin coated polycyanurate thin films, evaporation of cyanate ester monomers or possible dimers must be prevented or at least minimized, and it seems that prepolymerization is an effective approach in this attempt. It should be noted that the prepolymerization conditions (temperature and time) must be careful controlled. The temperature chosen for prepolymerization process must not be too high or too low. Too low temperature not only would result in longer experimental time, but also would result in low degree of prepolymerization and subsequently result in poor quality of the polymer film. When the temperature is too high, the reaction time will be too short and the reaction will be difficult to control. Based on this consideration, Different Scanning Calorimetry (DSC) analysis was carried out to select the suitable temperature for prepolymerization of cyanate ester monomers. DSC curves of cyanate ester monomers were obtained at different heating rates. Figure 4.6 shows the DSC curves of BACy monomer at heating rate of 5, 10, 15 and 20 °C/min as an example. Table 4.1 presents the DSC data summerized from Figure 4.6.

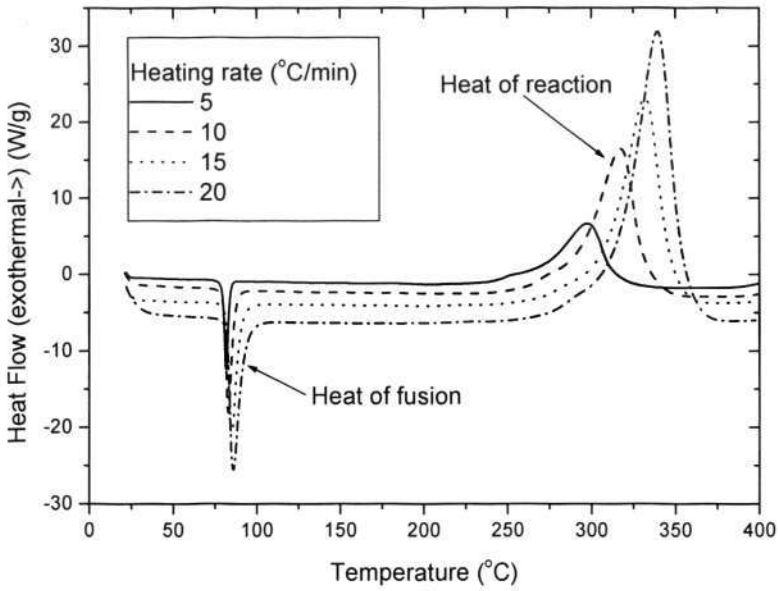

Figure 4.6 DSC curves of BACy monomer obtained at different heating rates

Table 4.1 DSC data of BACy monomer

Heat rate (°C/min)	Melting point (°C)	ΔH_{fusion} (J/g)	Curing temperature (°C)			ΔH_{cure} (J/g)
			Initial	Peak	End	
5	82.0	94.7	196.6	287.8	326.9	751.9
10	82.6	93.6	215.4	308.9	340.4	736.8
15	83.1	92.3	232.2	319.4	352.3	728.2
20	84.4	91.4	247.5	329.0	364.0	725.6

By plotting the intial curing temperatures versus heat rate, a linear relationship is found as shown in Figure 4.7. The interception at Y axis is 180.5 °C, which means that the initial reaction of BACy monomer at the heat rate of 0 °C would occur at 180.5 °C. Therefore, a temperature around 180.5 °C may be chosen as the minimum prepolymerization temperature for BACy. For a different cyanate ester, this temperature is also different. They are found to be 160 °C and 82 °C for BFCy and DFCy homopolymers respectively by following the similar DSC analysis procedures described above.

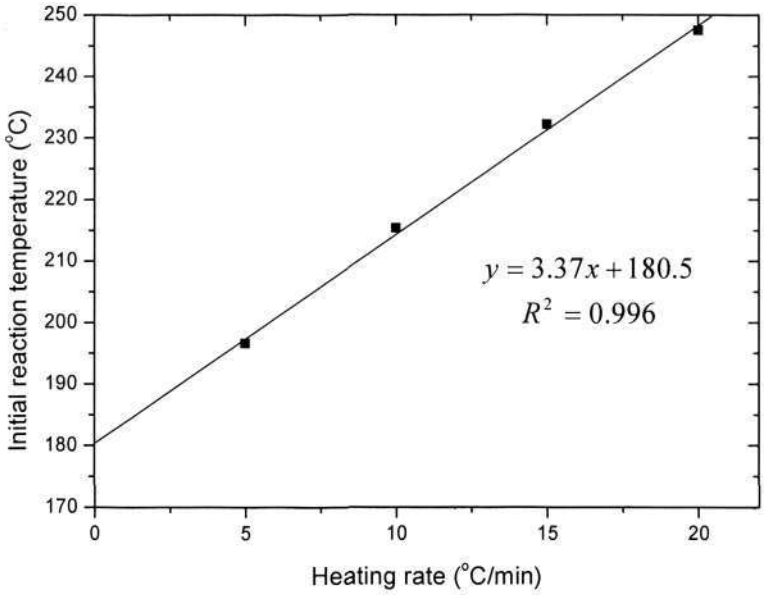

Figure 4.7 Plot of initial reaction temperature versus heating rate for BACy

Note prepolymerization is a very important step for preparing polycyanurate thin film using spin coating method, the prepolymerization conditions are further studied. The first important issue is to determine the prepolymerization temperature. Although the approximate prepolymerization temperature has been fixed, it is a theoretical value and need to be verified. Again BACy used as an example to study the influence of different conditions on the prepolymerization of cyanate ester. Three temperatures of 175 °C, 180 °C, and 190 °C were chosen for prepolymerization of BACy. The prepolymerization degrees at different reaction times were measured by DSC and FTIR (Table 4.2). It should be noted that once the prepolymerization was completed, the reaction was stopped rapidly by immersing the reaction flask into an ice-water bath. The reaction must be stopped immediately at the predetermined completion time for an accurate measurement of degree of prepolymerization. This is also important to prevent the incorrect assessment of solubility in the selected solvent, chloroform. The prepolymerization degree of the polymer was measured using the DSC and FTIR methods described in Chapter 3. The results from DSC method agree well with those obtained from FTIR method (Table 4.2).

For a better observation, the prepolymerization degrees in Table 4.2 were plotted against the prepolymerization times as shown in Figure 4.8.

Table 4.2 Degree of prepolymerization of BACy prepolymerized at different conditions

Time (min)	Prepolymerization degree (mol.%)					
	DSC			FTIR		
	175 °C	180 °C	190 °C	175 °C	180 °C	190 °C
60	8.9	23.7	28.0	10.1	22.9	28.0
120	12.2	32.5	37.6	12.6	31.3	36.4
180	14.1	37.7	42.2	13.3	38.5	43.7
240	15.3	41.0	47.3	15.0	41.0	47.9
300	16.0	42.7	52.0	16.8	41.5	51.4
360	16.3	43.6	54.0	16.3	44.8	53.1
420	16.5	44.2	54.3	16.5	44.2	56.1
480	16.6	44.5	54.8	17.0	44.1	57.5

Note: Prepolymers with conversions lower than 50% have good solubility in chloroform, while prepolymers with conversion higher than 50% can only partially dissolve or insoluble in chloroform.

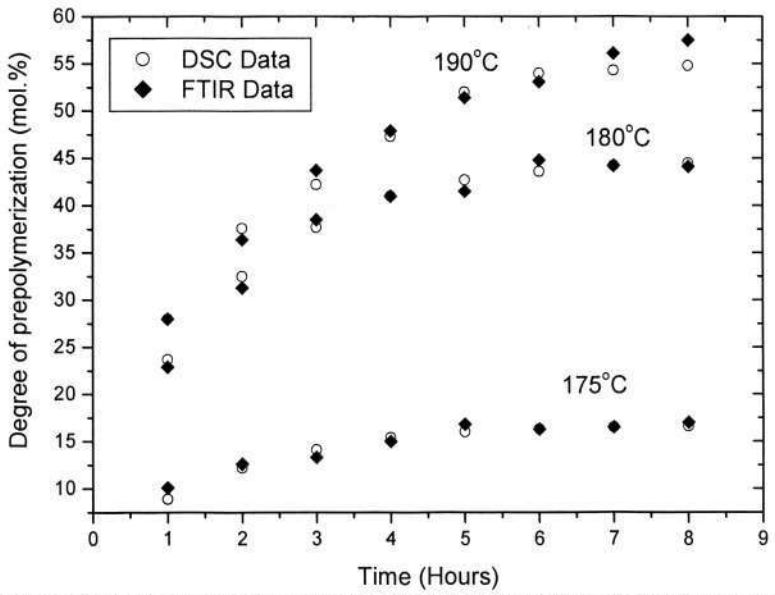

Figure 4.8 Plots of prepolymerization degree versus time at different temperatures

Figure 4.8 shows that when the prepolymer is synthesized at 175 °C, the reaction is too slow and the degree of prepolymerization is considerably lower (less than 20%) than those synthesized at higher temperatures (180 °C and 190 °C). Therefore, prepolymerization temperatures lower than 180 °C is not recommended, since it will prolong the experiment time unnecessarily. Although the prepolymerization of BACy can be carried out at a temperature higher than 180 °C with a shorter prepolymerization time, the reaction becomes too fast and it is more difficult to control the reaction before gelation occur. Moreover, a prepolymer with a well-predefined prepolymerization degree can hardly be obtained in this approach in practice. While in coating applications such as waveguide buildup, starting materials with predefined conversion and structure are needed so that the precise refractive index control can be reached [103]. Thus, for the prepolymerization of BACy homopolymer, 180 °C is a suitable condition in this case. The proper conditions for other polycyanurate systems are all determined following the similar procedures as described above.

It should be noted that the prepolymerization degrees of the cyanate ester prepolymers shown in Table 4.2 and Figure 4.8 obtained by DSC method were employing the method recommended by reference [52,142]. The total enthalpy of curing ΔH_{tot} of a pure uncured cyanate ester monomer was determined by a DSC scan using a heating rate of 5 °C/min. Then the enthalpy of curing ΔH_f of a prepolymer was also obtained using the same heating rate of 5 °C /min. Nitrogen gas was used for purging at a flow rate of 60 cc/min in each scan. Prepolymerization degree, α, was calculated from the following Equation [142]:

$$\alpha = \frac{\Delta H_{tot} - \Delta H_f}{\Delta H_{tot}} \qquad \text{(Equation 4.1)}$$

where ΔH_f is the enthalpy of the prepolymer and ΔH_{tot}, the total enthalpy of reaction of the monomer. Note that the true ΔH_{tot} for 100% curing may not be accurately obtained directly by experimental method, since the theoretical 100% conversion is difficult to achieve. However, in literature, it is generally accepted to take the enthalpy of reaction of the monomer at a heating rate of 5 °C/min or 10 °C/min as the total enthalpy of the curing reaction [52].

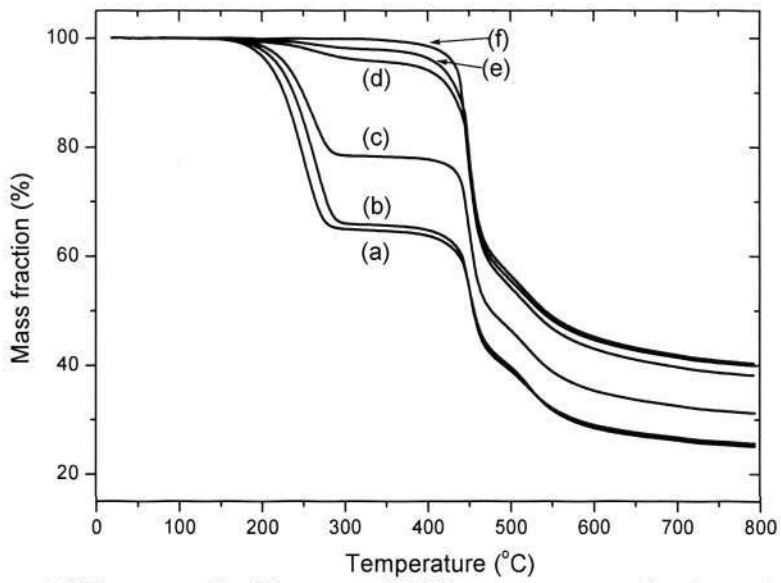

Figure 4.9 Thermogravimetric curves of BACy monomer, cured resin, and prepolymers (a) monomer (α=0), (b) 8hrs@175°C (α=16.6%), (c) 4hrs@180°C(α=41.0%), (d) 8hrs@180°C(α=44.5%), (e) 6hrs@190°C(α=54.3%), (f) 5hrs@220°C(α=80.0%).

Extensive experiments on the prepolymerization of cyanate ester show that it is necessary and crucial to keep the conversion of polycyanurate prepolymer at 44.0-47.0 mol.% to prevent evaporation during the thermal curing of the spin coated films and at the same time permit sufficient solubility in the selected solvent, chloroform. Figure 4.9 shows the TGA data of BACy monomer, cured resin, and some prepolymers. It can be seen that after prepolymerized at 180 °C for 8 hours, the evaporation of BACy monomer has been

reduced substantially. With selection of suitable spin coating and proper curing procedures, optical quality polycyanurate thin films can be obtained as a result.

4.3 Copolymerization of Cyanate Esters

It has been discussed in Chapter 2 that copolymerization of cyanate ester with different backbone structures is advantageous in controlling and modifying the properties of polycyanurates. The modifying approach through copolymerizing of different cyanate esters has an obvious advantage that it does not change the characteristic symmetrical triazine structure of polycyanurate resin. Therefore, most of the properties attributed to this unique structure are expected to remain after modification. This is favorable in modifying the optical properties of polycyanurate including tuning of the refractive index and reducing the optical loss, because no phase separation is expected via the copolymerization. In this research, three cyanate esters with fluorinated aromatic backbone structure (BFCy), fluorinated aliphatic backbone structure (DFCy), and monofunctional cyanate ester (CPCy) are copolymerized with bisphenol A cyanate ester (BACy) in order to control the optical, dielectric and other properties of the modified polycyanurate system.

In the fluorinated cyanate ester resin, the free volume is increased due to the relatively large volume of fluorine atoms relative to hydrogen atoms, which further led to lowering the refractive index [122,123]. In addition, the replacement of hydrogen atoms by fluorine atoms also can decrease local electron polarization, and hence lowering the refractive index. By adjusting the ratio of the non-fluorinated and fluorinated cyanate monomers, modified cyanate ester resin systems with different refractive indices and dielectric constants are obtained.

Monofunctional CE (CPCy) can also be used to copolymerize with dicyanate ester resin to control the free volume of the modified polymer, in turn to control the refractive index and dielectric constant of the modified resin. Because monofunctional cyanate ester only has one cyanate group, there will be more chain ends and intentionally created imperfections in the cured polycyanurate networks comparing to the homopolymer networks. Increasing amount of monofunctional cyanate ester monomer would result in an increase of the free volume and therefore a decrease of refractive index and dielectric constant. By adjusting the ratio of monofunctional cyanate ester and BACy, the free volume of the cured polycyanurate can be controlled, thus the refractive index and dielectric constant of the cured resins also can be controlled.

The copolymerization of cyanate esters follows the procedures of the prepolymerization of polycyanurate homopolymers as previous described. However it is important to verify the compatibility or reactivity between different cyanate esters. In this study, the compatibility between different cyanate esters is studied by DSC. Figures 4.10 to 4.12 show the DSC curves of cyanate ester copolymers of BACy/BFCy, BACy/DFCy and BACy/CPCy. The data summarized from Figures 4.10 to 4.12 are shown in Table 4.3.

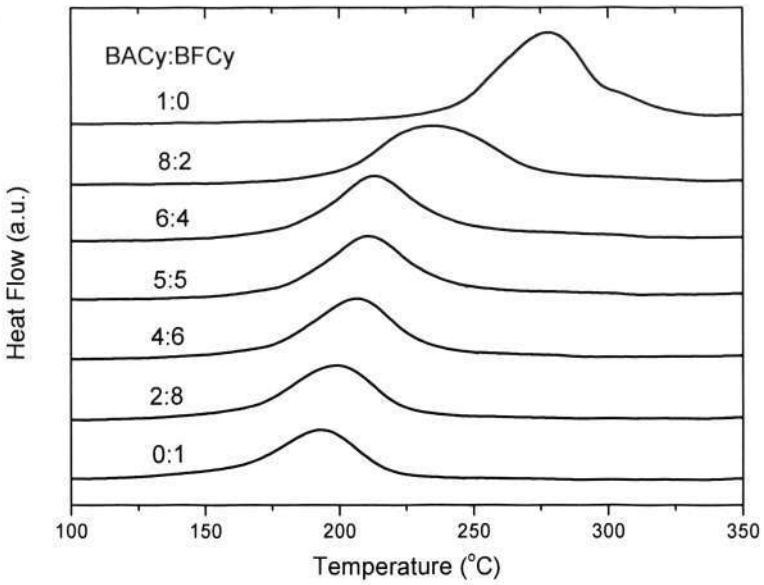

Figure 4.10 DSC curves of BACy/BFCy monomers and co-monomers at 5 °C/min

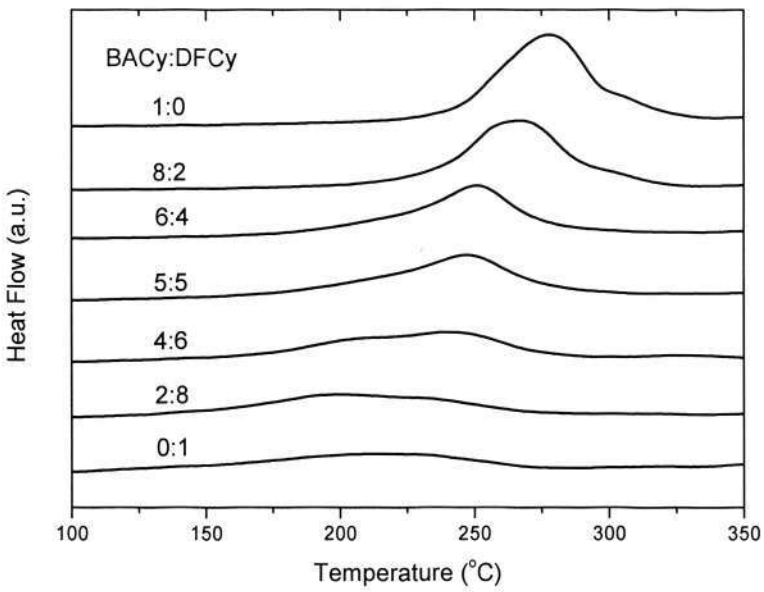

Figure 4.11 DSC curves of BACy/DFCy monomers and co-monomers at 5 °C/min

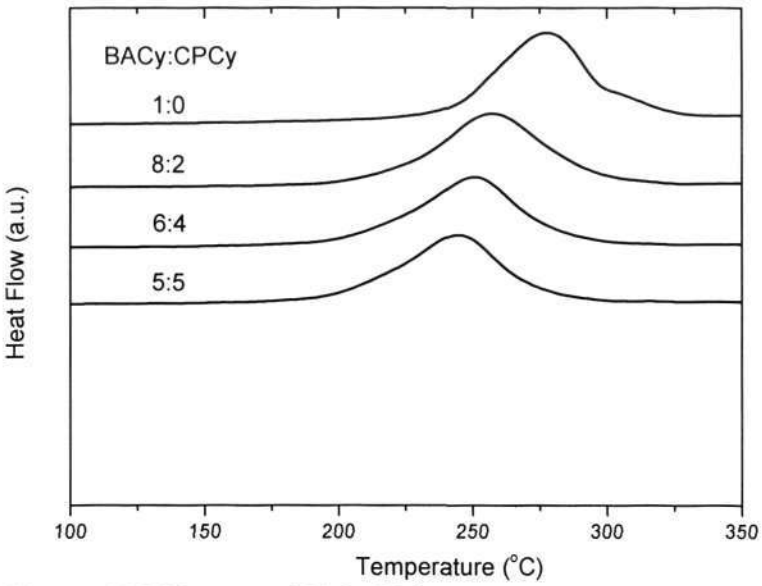

Figure 4.12 DSC curves of BACy/CPCy monomers and co-monomers at 5 °C/min

Table 4.3 Summary of DSC results of cyanate ester homopolymers and copolymers

Polycyanurates	T_{Peak}(°C)	Δ H(J/g)	Δ H(kJ/mol OCN)
BACy	277.7	807.1	112.2
BFCy	193.0	410.5	79.2
DFCy	215.1	309.5	63.8
CPCy	218.6	480.0	93.6
BACy/BFCy			
2:8	198.7	490.9	89.4
4:6	206.5	541.0	92.7
5:5	210.7	564.3	93.7
6:4	212.8	628.2	100.9
8:2	234.7	656.6	98.4
BACy/DFCy			
2:8	222.2	379.1	73.0
4:6	239.1	455.6	81.6
5:5	246.4	537.2	92.7
6:4	250.5	533.4	88.4
8:2	266.7	703.5	107.2
BACy/CPCy			
2:8	222.9	559.3	98.6
4:6	231.0	634.7	103.5
5:5	244.1	655.9	103.4
6:4	250.8	695.8	106.5
8:2	257.7	741.8	107.7

From Figures 4.10 to 4.12 and Table 4.3, it can be seen that the polymerization exotherm peaks and enthalpies of different cyanate ester monomers are different. The polymerization exotherm peak and enthalpy may serve as an indicator of reactivity, although it may not be so accurate for uncatalyzed thermal polymerization of polycyanurate because of the catalytic activity of very small quantities of impurities [1]. The polymerization enthalpy relates to the internal energy differences between monomer and polymer. The differences in the polymerization exotherm peak positions and enthalpies of different polycyanurates are probably caused by electron withdrawing effect of fluorine effect and steric effects [143,144]. From Figures 4.10 to 4.12, it can also be seen that most polycyanurate copolymers show single DSC curing exotherm, although the curing exotherm peak positions of the homopolymers are different. This indicates that two different cyanate ester monomers can be easily copolymerized at any molar ratio. The polymerization exotherm peaks and enthalpies of the copolymers are dependent on the compositions. However, it can be seen from Figure 4.11 that for certain BACy/DFCy copolymers, i.e., 4:6 and 2:8 systems, each showed an extra shoulder peak indicating the curing processing is not completely uniform. This may result in inhomogeneity in the cured copolymers. This in turn may influence the optical properties of the copolymers.

4.4 Preparation of Polycyanurate Thin Films by Spin Coating

The major processing parameters involved in spin coating are solution concentration, spin speed and spin time [138]. Take BACy as an example, the influence of these parameters on the preparation of polycyanurate thin films have been investigated using silicon wafers as substrate. It should be noted that the degree of prepolymerization also has a significant influence on the preparation of polycyanurate thin film, but for the reasons discussed in section 4.2, the conversion of the prepolymer is fixed as 44.5 mol.%.

4.4.1 Effect of Solution Concentration

In order to investigate the influence of solution concentration on the thickness of the thin film layer, a series of silicon wafers were coated with BACy prepolymer solutions of different concentrations varying from 5% to 30%, while the spin speed and spin time were fixed at 2500 rpms and 30 s respectively. The thicknesses of the coated films were then measured by using ae Metricon prism coupler and the results are listed in Table 4.4. The film thickness was plotted against the solution concentration as shown in Figure 4.13. All films were cured at 220 °C for 5 hours.

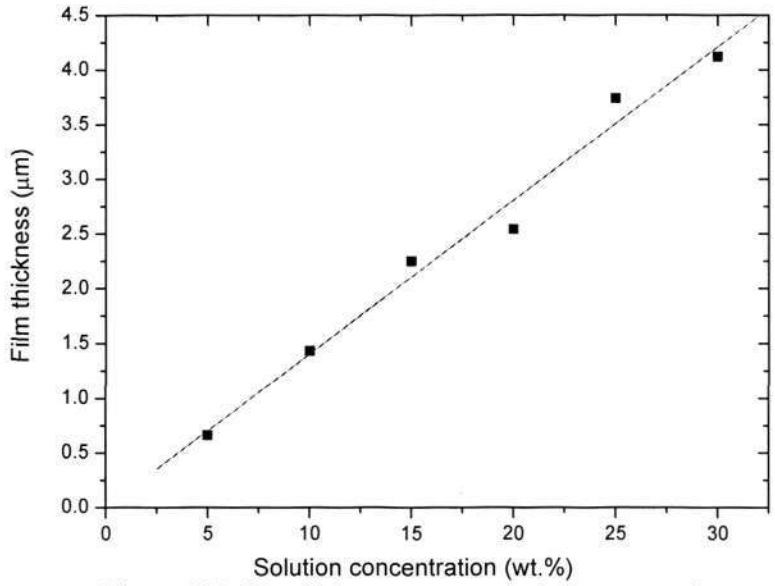

Figure 4.13 Film thickness versus solution concentration
Spin speed: 2500 rpm, spin time: 30 s

Table 4.4 Thicknesses of BACy thin films of different solution concentrations

(Spin speed: 2500 rpm, spin time: 30 s)

Solution concentration (wt.%)	5	10	15	20	25	30
Film thickness (μm)	0.66	1.43	2.25	2.54	3.74	4.12

Figure 4.13 suggests that there is a linear relationship between the film thickness and the solution concentration at a fixed spin speed and spin time. The film thinknesses are in the

range of 0.7 μm to 4.1 μm, which meet the requirement of dielectric and photonic applications in most cases. The film thickness can be controlled through varying the solution concentration, and the controlled range is much larger than that of spin coated sol-gel silica film that typically has a film thickness much less than 1.0 μm [145].

Another phenomenon was also noted that along with the increase of solution concentration, the uniformity of the thin film surface would become poorer when the concentration exceeds 30 wt.%. It is because that the increase of solution concentration results in the increase of viscosity, and makes the flow of the resin solution become difficult. The resin solution cannot spread evenly onto the substrate and this leads to defect on the thin film surface. In this case, to prepare optical quality BACy thin films, the solution concentration should be kept below 25 wt.%. A SEM micrograph of the film surface was shown in Figure 4.14. It can be seen from the picture that the film is smooth and pinhole free.

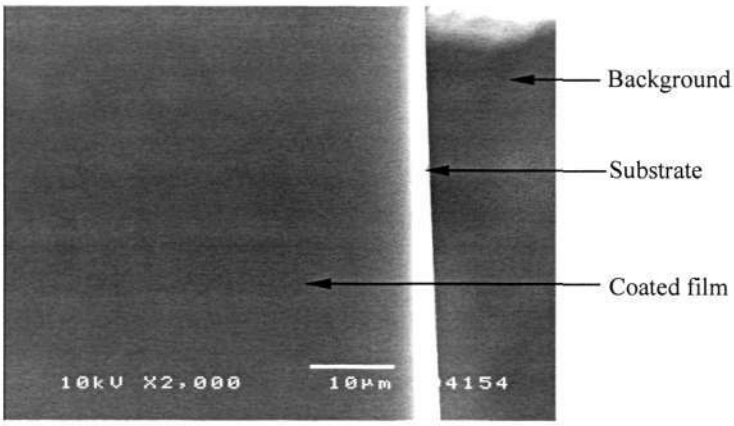

Figure 4.14 SEM graph of the film surface

(Solution concentration: 25 wt.%, spin speed: 2500 rpm, spin time: 30 s.)

Figures 4.15 and 4.16 show the AFM images of the polycyanurate thin films of prepolymer and cured polymers. The surface morphology of the polycyanurate thin films can be clearly observed. The roughness (RMS, root mean square) of the films is 0.7~1.0 nm.

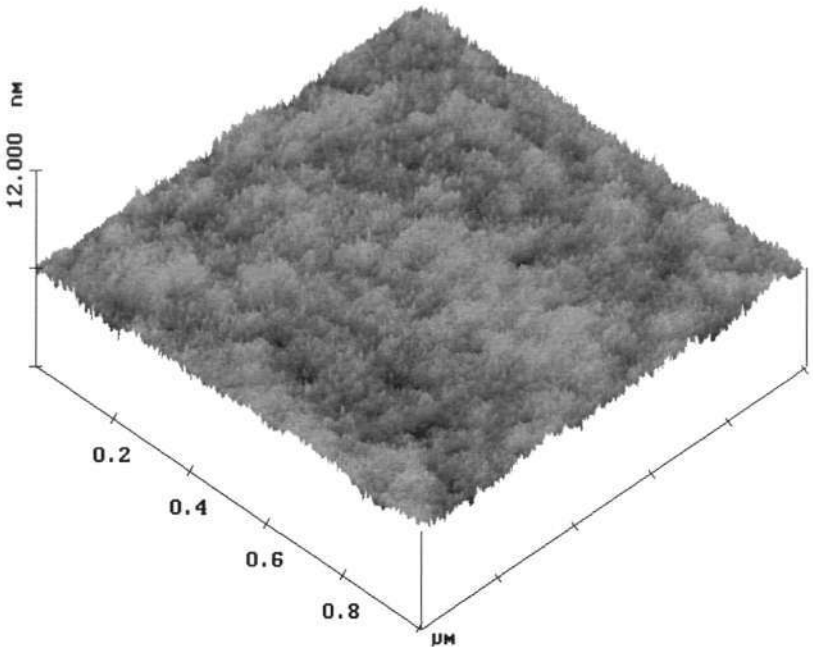

Figure 4.15 Surface morphology of polycyanurate thin film of prepolymer

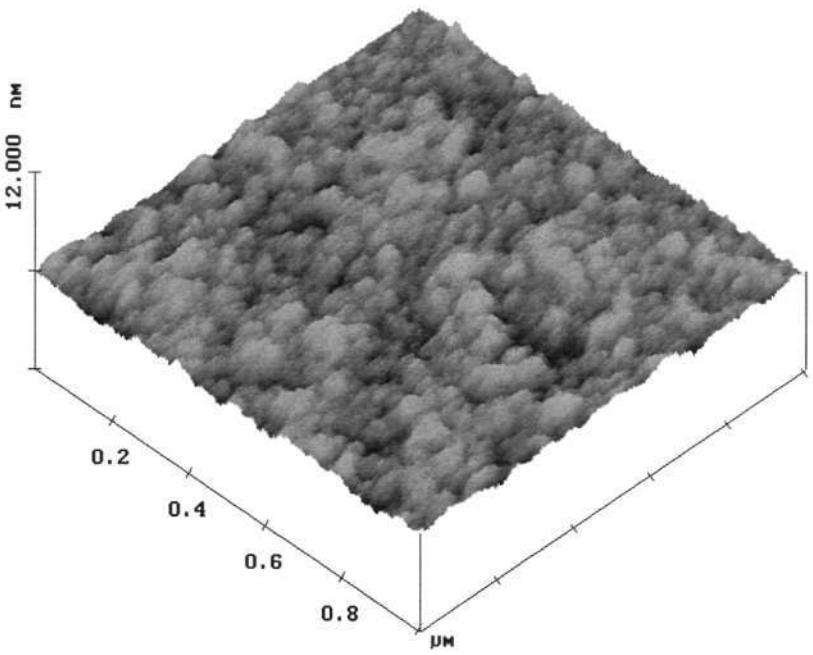

Figure 4.16 Surface morphology of polycyanurate thin film of cured polymer

4.4.2 Effect of Spin Speed

To study the influence of spin speed on the preparation of BACy thin films, the solution concentration and the spin time were fixed at 25 wt.% and 30 s respectively. A series of silicon substrates were coated at different spin speed varying from 500 rpm to 3000 rpm. The thicknesses of the coated films were then measured by using the Metricon prism coupler and the results are listed in Table 4.5. The results were then plotted against the spin speed as shown in Figure 4.17. All films were cured at 220 °C for 5 hours.

Table 4.5 Thicknesses of BACy thin films of different spin speeds

(Solution concentration: 25 wt.%, spin time: 30 s)

Spin speed (rpm)	500	1000	1500	2000	2500	3000
Film thickness (μm)	4.35	4.00	3.86	3.79	3.74	3.73

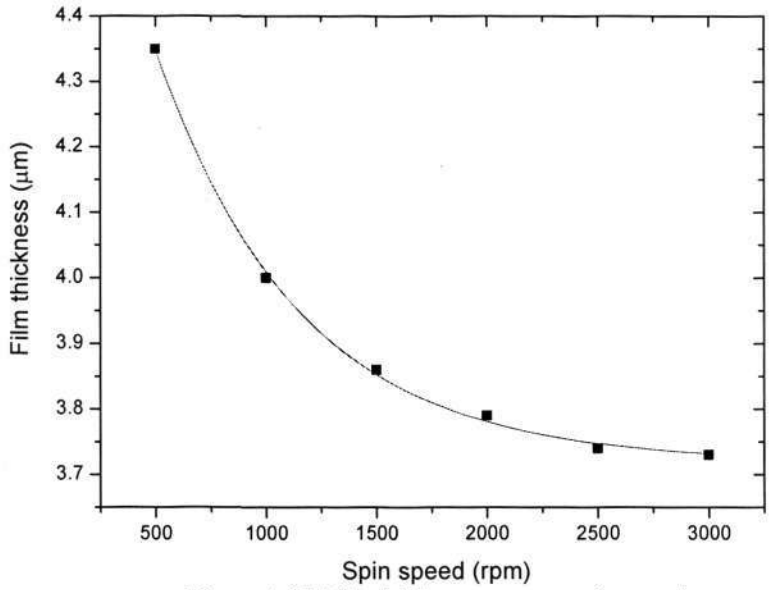

Figure 4.17 Film thickness versus spin speed
Solution concentration: 25 wt.%, spin time: 30 s

Figure 4.17 indicates that there is a nonlinear relationship between the film thickness and the spin speed at a fixed solution concentration and spin time. At spin speed lower than

2000 rpm, the film thickness decreases rapidly with the increase of spin speed. When the spin speed is higher than 2000 rpm, the variation of the film thickness is very little. It can be explained as follow. The final film thickness is the result of the balance of two forces, the centrifugal force and viscous force (Figure 4.18). The centrifugal force tries to spread the fluid onto the whole substrate and spins the excess amount of polymer solution off the edges of the substrate. On the contrary, the viscous force tries to cohere the whole fluid together. At lower spin speed, the centrifugal force is lower, the balance position of centrifugal force and viscous force is at a higher level away from the substrate, so more solution remains on the substrate, resulting in thicker film. With the increasing of spin speed, the increase of centrifugal force makes the balance position moving to nearer to substrate, and the solution above this position is spin off from the substrate resulting in a thinner film. At last, when the balance of two forces comes to an equilibrium position (Figure 4.18) (the maximum centrifugal force that can be reached to equilibrium with the viscous force), the film thickness will came to a stable value that no longer decreases. The equilibrium position depends on the adhesion between the prepolymer and the substrate.

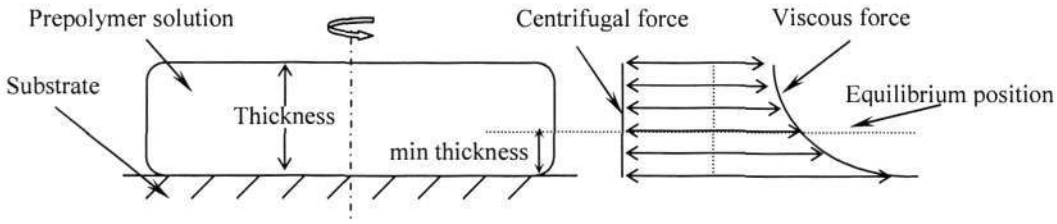

Figure 4.18 Sketch diagrams of centrifugal force and viscous force

Films of thickness varying from 3.7 μm to 4.3 μm can be obtained by controlling the spin speed at the fixed solution concentration and spin time. The controlled range is narrower than that by varying solution concentrations. It can be explained below. The minimum final film thickness is the result of the equilibrium of centrifugal force and viscous force. The solution of higher concentration has a relative higher intrinsic viscosity and therefore

a higher viscous force, hence more solution will stay on the surface of the substrate at the equilibrium stage of viscous force and centrifugal force, resulting in a thicker film than that of a solution of lower concentration. At fixed solution concentration, varying the spin speed cannot make the film thinner than the minimum value, and at a speed higher than 500 rpm, the upper value of the thickness is also limited, therefore, spin speed has a less influence on the thickness than that of solution concentration.

4.4.3 Effect of Spin Time

A series of prepolymer films were coated at different spin time varying from 5 s to 50 s while the other two processing parameters were fixed. The thicknesses of the coated films are listed in Table 4.6. The results are also plotted in Figure 4.19. All films were cured at 220 °C for 5 hours.

Table 4.6 Thicknesses of BACy thin films of different spin times

(Solution concentration: 25 wt.%, spin speed: 2500 rpm)

Spin time (s)	5	10	20	30	40	50
Film thickness (μm)	4.80	4.26	3.88	3.74	3.71	3.70

Figure 4.19 shows that there is also a nonlinear relationship between the film thickness and the spin time at fixed solution concentration and spin speed. At spin time shorter than 30 s, the film thickness decreases rapidly with the increase of spin time. When the time is longer than 30 s, the variation of the film thickness is very little. The phenomenon is very similar to that of the influence of spin speed. At spin time shorter than 30 s, the time is not sufficient to spin off all the exceed solution away from the substrate, resulting in thicker film. That is to say, the spin coating has been stopped before the centrifugal force and the viscous force reach the balance position, hence more solution stay on the substrate than that of balance position, resulting in thicker films. With increasing spin

time, the amount of the excess solution is reduced, resulting in decreased film thickness. When the spin time is sufficiently long for the centrifugal force and the viscous force to reach the balance position, the film thickness will no longer decrease and come to a stable value. In this case, 30 s is enough for preparing BACy spin coating films.

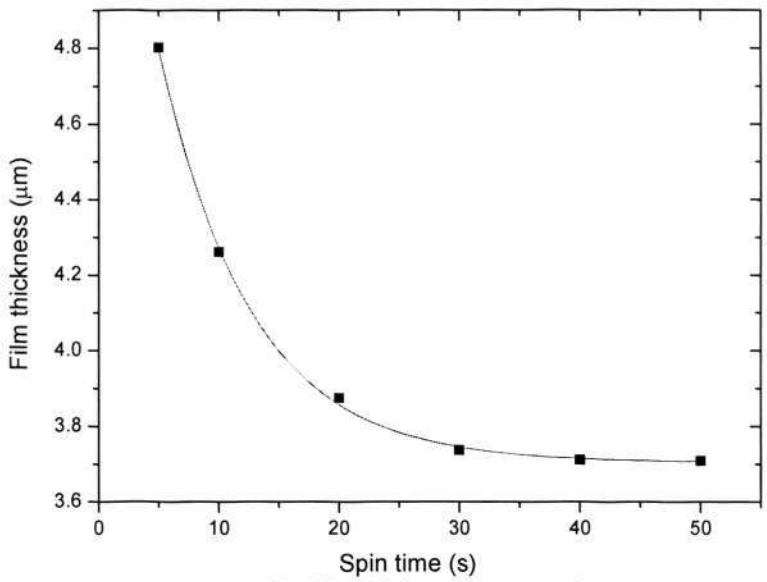

Figure 4.19 Film thickness versus spin time
Solution concentration: 25 wt.%, spin speed: 2500 rpm

Among the three main processing parameters of spin coating, the solution concentration is the dominant factor controlling the film thickness. Varying the spin speed or spin time also has affects on controlling the film thickness but to a less extent. In this case, films thickness can be controlled between submicron to about 5 μm. In this study, the solution concentration is between 5-25 wt.%, the spin speed is between 1000-3000 rpm and the spin time is between 15-40 s, which is appropriate to obtain polycyanurate thin films with desired thickness and surface smoothness.

4.5 Fourier-Transform Infrared (FTIR) Spectroscopy of Polycyanurate Thin Films

Infrared spectroscopy has been a very important tool for cyanate momoner indentification, measurement of conversion of polymer and indentification of hydrolysis products and impurities [100]. Figure 4.20 shows the FTIR spectra of BACy, BFCy and DFCy monomers between wavenumber 400 cm^{-1} to 4000 cm^{-1}. The test samples were polycyanurate thin films spin coated on silicon substrates. The assignments of important IR bands are summarized in Table 4.7.

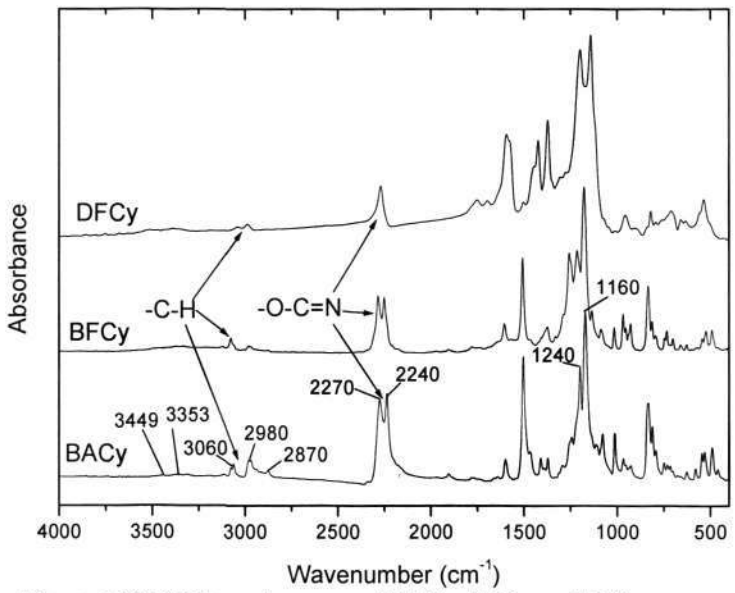

Figure 4.20 FTIR spectroscopy of BACy, BFCy and DFCy momoners

Table 4.7 Assignment of the main bands of FTIR spectra of cyanate ester monomer and polymer

Wavenumber (cm^{-1})	Assignment	Reference
3449, 3353	OH stretch	[27]
3060, 2980, 2870	CH stretch	[17]
2270, 2240	CN stretch	[17,51,56,99,100]
1240, 1160	C-O-C stretch	[99,100]

The cyanate ester monomer shows strong signature absorption at 2200 to 2300 cm^{-1} region, which are assigned to strong C ≡ N stretching vibration band. The strong absorption band at 1160-1240 cm^{-1} is attributed to the strong C-O-C stretching vibration [22]. Compare to aliphatic cyanate ester, the C-O-C band of aromatic cyanate ester is shifted to a relative higher wavenumber. The combination of the C ≡ N and C-O-C stretching band can be used to identify the cyanate ester functional group (-O-C ≡ N). This combination is instrumental in discriminating cyanates from isocyanates [100]. The C ≡ N stretching band in cyanate ester monomers is of considerable importance since it is frequency used to quantify the conversion to prepolymer and fully cured polymer [51,99]. Usually it is split into two, three or more fully or partially resolved bands [100] as shown in Figure 4.20 for BACy and BFCy monomers. It also can be observed that there is variation in both the position and degree of splitting of this band as the cyanate ester monomer structure varies. Some careful study has shown that the splitting is caused by a Fermi resonance between the 2240 cm^{-1} C ≡ N stretching and the first overtone of the 1160 cm^{-1} C-O-C asymmetric stretching mode [99]. During curing procedure, the C ≡ N stretching band decreases as shown in Figure 4.21 of an example of BFCy. Therefore, this band is of considerable importance since it can be used to quantify the curing conversion of prepolymer and fully cured polymer, and can be used to study the curing reaction kinetics.

when the C ≡ N stretching band decreases, triazine will be formed and peaks will appear at 1365 cm^{-1} and 1565 cm^{-1} which are caused by the triazine ring stretching vibration [99,103] as shown in Figure 4.22. Figure 4.22 shows the FTIR spectroscopy comparison of BACy monomer and fully cured polymer. The bands at 2870 cm^{-1}, 2980 cm^{-1} and 3060 cm^{-1} are assigned to CH vibration. Because the CH band remains nearly constant throughout the curing procedure, it severs well as a reference band in kinetics study of

polycyanurate. It is noted that there is a very weak absorption band at 3200-3500 cm^{-1}, which is not attributed to any part of the polycyanurate structure. It is believed to be the absorption of OH of the impurities resulted from the monomer synthesis and/or moisture. These impurities play a paradoxical role. On one hand, the curing of uncatalytic cyanate ester may need a very small amount of these impurities to start the reaction; on the other hand, excess amount of impurities would cause a dramatic decrease of the optical transparency in the cured polymer which has been discussed in Chapter two.

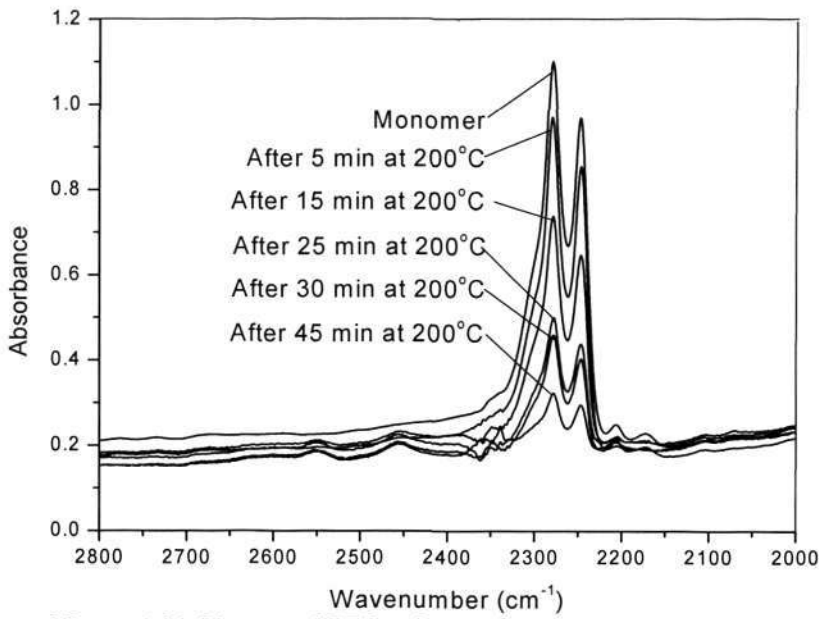

Figure 4.21 Change of BFCy -CN absorption peak with conversion

It should be noted that the conversion results measured by FTIR and DSC are agree well with each other as an example have been shown in Figure 4.8. BFCy monomer is cured at 200 °C for a period of time, and then the sample is divided into two parts, one part for FTIR measurement and the other part for DSC measurement. The good agreement between FTIR and DSC results make it convenient to select suitable conversion measuring technique during study.

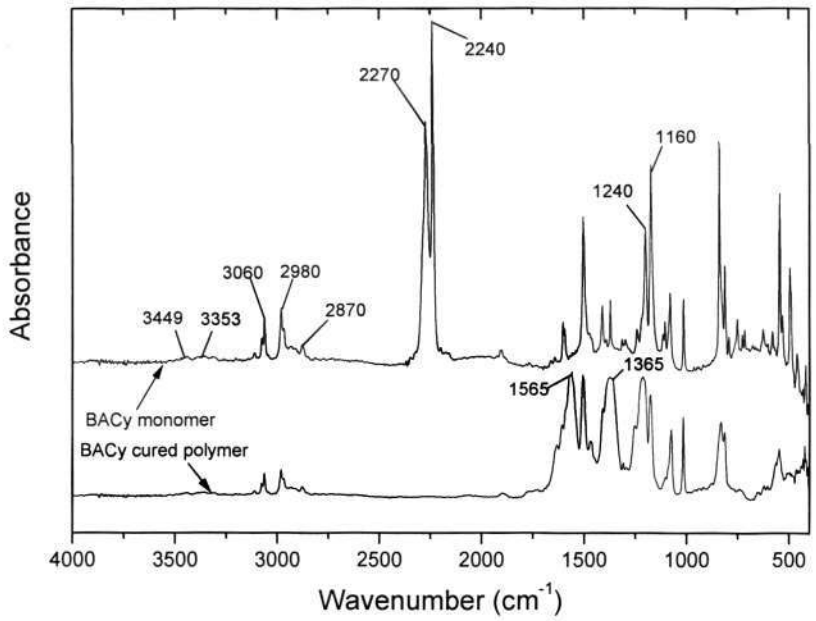

Figure 4.22 FTIR spectroscopy of BACy monomer and cured polymer

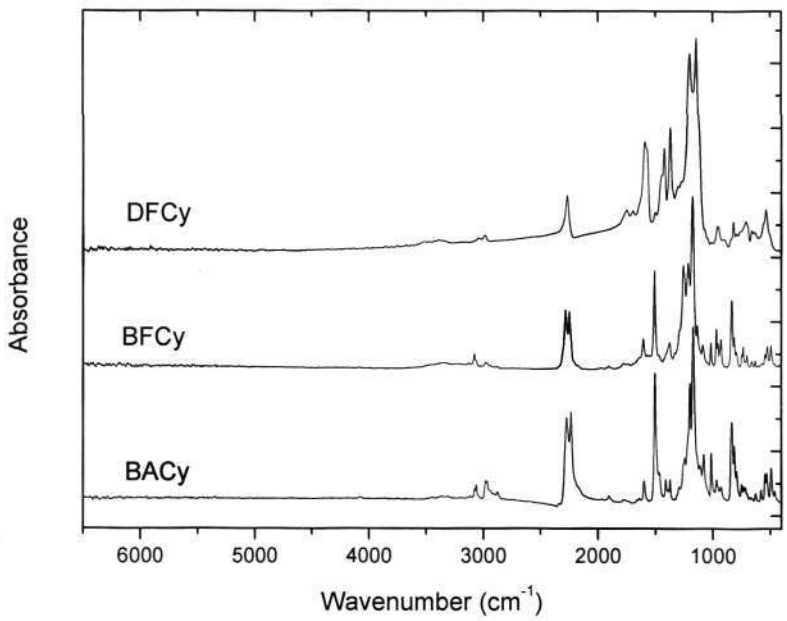

Figure 4.23 FTIR spectroscopy of BACy, BFCy and DFCy momoners

The FTIR results also show that there is not any absorption between the region 6500 cm^{-1} to 4000 cm^{-1} for all the cyanate ester monomers as shown in Figure 4.23. And there is also not any new absorption peak appears during the curing procedure in the wavenumber of

2000 cm^{-1} to 4000 cm^{-1}. That is to say, only the very small amount of impurities is suspected to trivially affect the optical transparency at telecommunication window of wavelength 1550 nm (wavenumber 6452 cm^{-1}). No other absorption tail and overtone are presented to influence the optical absorption loss. Therefore, FTIR results indicate that polycyanurate thin film is transparent in the region of about 1550 nm, which is favorable for fabrication waveguide or photonic devices working at this window.

4.6 Summary

Preparation of polycyanurate thin films consist of three steps, namely, prepolymerization, spin-coating and thermal curing. The study showed that prepolymerization is essential in three aspects for the preparation of polycyanurate thin films. (1) It prevents the crystallization of the cyanate ester monomers. (2) It prevents the evaporation of the cyanate ester monomers. (3) It provides appropriate viscosity to the precursor solution for the following spin-coating process. A basic consideration of the polymerization conditions for the preparation of polycyanurate thin films is that in order to minimize the evaporation of cyanate ester monomers, at the same time allow necessary solubility in the solvent, the degree of prepolymerization should be kept as high as possible but not exceed the gel point. In the present study, prepolymers with degree of prepolymerization between 44% and 47% were used for preparing optical quality polycyanurate thin films.

DSC study showed that most of the copolymerizations between different cyanate ester monomers with different compositions can be easily achieved. However, some BACy/DFCy copolymers such as 4:6 and 2:8 systems, showed an extra shoulder peak indicating the curing processing is not completely uniform. This may result in inhomogeneity in the cured copolymers. This in turn may influence the optical properties of the copolymers.

The study of the preparation of polycyanurate thin films by spin coating method demonstrated that the quality of the thin films is mainly influenced by three parameters, namely solution concentration, spin speed and spin time. Through adjusting the spin coating parameters, polycyanurate thin films with thickness varying from several microns to sub-microns only using a single-coating process could be obtained. SEM and AFM study of the prepared polycyanurate thin films showed that the films were optical smooth with surface roughness around 1 nm at 1 micron scale.

FTIR spectroscopy of cyanate ester monomers and polycyanurates showed that there is no absorption in the IR region of 6500 cm^{-1} to 2500 cm^{-1} before and after cured, which indicated that polycyanurates have a low optical loss at telecommunication wavelength 1550 nm (wavenumber 6452 cm^{-1}). The strong stretching vibration band of C≡N appears at 2200 cm^{-1} to 2300 cm^{-1}, which can be used to monitor the curing reaction of polycyanurates.

CHAPTER 5

DIELECTRIC PROPERTIES AND HETEROGENEITY OF POLYCYANURATE HOMOPOLYMERS AND COPOLYMERS

5.1 Introduction

There has been an increasing demand for low dielectric loss polymeric materials in design matrix resins for advanced electronic circuitry, radomes, microwave antennas, and composites for aircraft with low radar observability. Disadvantages of high-loss polymer systems include power loss via microwave reflection, power loss via energy absorption/dissipation, signal distortion through refraction and a decrease in power limited by destructive heat generation. A perfect dielectric insulating material absorbs no energy in an applied electromagnetic field. However, in practice, all dielectric insulating materials absorb electromagnetic field energy in dipoles and dissipate a fraction of this energy in the form of heat. There are some parameters can be used to describe the dielectric properties of a material. Among them, the most important ones are dielectric constant, loss factor and dissipation factor. Dielectric constant, also called permittivity, ε', is the property of a dielectric material which determines the amount of electrostatic energy that can be stored by the material when a given electromagnetic field is applied to it [146]. Actually, dielectric constant of a dielectric material is equal to the ratio of the

capacitance of a capacitor using the dielectric material to the capacitance of an identical capacitor using a vacuum (which has a dielectric constant of 1). Dielectric constant indicates the quality of a material to resist holding an electrical charge when placed between two conductors. ε' represents the amount of alignment of the dipoles to the electric field. Loss factor, ε'', is proportional to conductance and represents the energy required to align dipole. Dissipation factor, $\tan\delta$, is the tangent of the loss angle for a capacitor, a measure of stored electromagnetic energy converted to leakage current and ultimately to heat. The terms loss tangent and dissipation are used interchangeably and equal to $\varepsilon''/\varepsilon'$ [115].

Low dielectric constant and dissipation loss are great advantages of polycyanurate resins in many applications, not only for the traditional printed circuit board and aerospace composites matrix, but also for the novel optical applications. Owing to their unique symmetrical molecular structures, polycyanurate has inherently low dielectric constant and loss factor. Figure 5.1 (see Figure 2.11 in Chapter 2) shows the crosslink structure of BACy homopolymer as an example. The most important feature of polycyanurate network is that a high degree of polar symmetry tends to balance the pull of electrons, resulting in a short dipole moment and low energy storage in an electromagnetic field. Although polycyanurate contain an appreciable percentage of oxygen and nitrogen, their symmetrical arrangement and resulting weak polarity may explain the observed low dielectric constant and loss. The second characteristic of polycyanurate is the absence of strong hydrogen bonds; the absence of proton donor groups in polycyanurate molecular structure precludes the formation of strong hydrogen bonds and further supports the observed low dielectric loss properties [18]. Altering the chemical structure of the bisphenol backbone has produced a family of cyanate functional resins with even lower dielectric loss properties, opening more potential promising applications.

Although unmodified polycyanurate already have many attractive features, it still needs to be further modified in many cases. For example, if a predefined specific dielectric constant is required, while no single polycyanurate homopolymer can meet this requirement, therefore a polycyanurate copolymer or blend must to be developed to solve this problem. Copolymerization of different polycyanurate resins with different structures is of great interest because it does not change the unique symmetrical triazine structure of the polymer network; therefore, most of the properties contributed by this unique structure are expected to be maintained after the modification. A large variety of polycyanurate resins with different backbone structures and properties are commercial available, e.g., aromatic or aliphatic, monofunctional or multifunctional, and conjugate. It provides a new way to tailor the properties of resin formulations by copolymerizing different polycyanurates, which is favorable in modifying the dielectric and optical properties. The aim of this chapter is to understand the temperature and frequency effects on the dielectric properties of polycyanurate homopolymers and copolymers. This provides basic knowledge on the consideration for modification of the dielectric properties of such polymers. In this work, three kinds of polycyanurate resins were used. BACy is bisphenol A type which is the most commonly used polycyanurate resin for dielectric and aerospace composites matrix. BFCy is a fluorinated Bisphenol A cyanate ester, it has a lower dielectric constant and is expected to have good compatibility with BACy due to similarity in molecular structure and geometries. DFCy is a fluorinated aliphatic polycyanurate polymer, which was developed recently for photonics applications. Unlike most aromatic cyanate ester, it is not to be used as the matrix for high performance fiber reinforced composition, due to its significantly low T_g (about 92 ^{o}C). However, DFCy possesses the lowest dielectric constant (2.3-2.6) among the known polycyanurate resins. And it also has low refractive indices in the range 1.382-1.447,

optical loss about 0.21 dB/cm, which makes it very attractive in polymer photonic applications [27,41,42].

Understanding the heterogeneity in polymer blend system is very important, because it greatly influence the micro-morphology of the blend system and in turn influences the final properties of the blend. The heterogeneity of various polymer blend systems has been studied by many researchers mainly using thermal and mechanical analysis method such as DSC and DMA. As regard to polycyanurate blend or copolymer, because the components have the same functional group, -OCN, different polycyanurates react and are crosslinked together. The resulted polycyanurate copolymers are macroscopic homogeneous and the miscibility may not be detectable by using thermal analysis or mechanical analysis. However, because of the difference in the backbone structure there must be some heterogeneity in the polycyanurate copolymers. We use 'heterogeneity' to take place of 'miscibility' is because the polycyanurate copolymers show macro-miscible. The heterogeneity may not influence the finial mechanical properties of the copolymer, but it will have effects on the optical and dielectric properties of the systems.

Thus, it is important to know the heterogeneity of polycyanurate copolymer. In this study, dielectric analysis was used to characterize the temperature and frequency dependency of dielectric properties of polycyanurate copolymers. The Cole-Cole equation and a modified Gordon-Taylor equation were used to study the heterogeneity of the copolymer systems.

5.2 Dielectric Relaxation of Polycyanurate Homopolymers and Copolymers

For the solid polymer materials, there are two bulk effects that influence the dielectric property: molecular dipole orientation and ionic conductivity [128]. The dipole orientation in polymer comes from the motion of polar groups under electric field. Due to the cross-linking nature of the cured polymer, the molecular motions are hindered by the cross-linking network. When the dielectric measurement was taken under a low temperature, for example, below the glass transition temperature, the molecules lose their long-range segmental mobility. The dipolar relaxation due to the segmental movement and orientation with the electrical field cannot contribute to the dielectric response. Under this circumstance, the relaxation time to achieve a polar orientation can become very large. So for a glassy state polymer, the dipolar relaxation due to long-range molecular mobility does not dominate the material dielectric behavior. However, there exists local relaxation processes associated with the dipolar orientation of the side groups pending to the main polymer chain. These relaxation processes can contribute to the dielectric properties. Another effect, ionic conductivity, comes from the motion of ions under the electric field and is independent of applied frequency. Ionic conductivity is also related to the polymer mobility and increases dramatically with increasing temperature. Therefore, it usually dominates the dielectric properties at high temperature.

DEA was used to investigate the dielectric properties of polycyanurate homopolymers and copolymers from 75 °C to 300 °C at a heating rate of 5 °C/min. The frequency range used for measurement was from 1 to 10,000 Hz. The 3D plots of the relationship among dielectric properties, temperature, and log frequency of the polycyanurate systems are shown in Figures 5.2 to 5.4 for BACy, BFCy and DFCy homopolymer respectively. The behaviors of polycyanurate copolymers are generally between that of the two individual

components which compose the copolymer (not shown). In Figure 5.2 and 5.3, generally, a flat response of the dielectric constant and loss factor can be observed up to temperature around 250 °C in dielectric properties 3D plots at relatively lower frequencies. At higher frequencies, the flat response phenomenon can reach even higher temperature 300 °C. The loss factor response shows little more frequency and temperature dependency, but the values remain less than 0.03 at temperatures below the glass transition temperature at all frequencies for both BACy and BFCy homopolymers. The dielectric behavior of DFCy apparently shows something different. As seen in Figure 5.4, the dielectric constant and loss factor of DFCy increase with the increasing temperature first then decrease, followed by increase again. This is because the glass transition temperature of DFCy homopolymer is much lower than that of BACy and BFCy homopolymer. The glass transition temperatures of BACy, BFCy and DFCy homopolymers are 289 °C, 273 °C and 92 °C respectively. Below the glass transition region, the dielectric constant is low since the dipoles can not align with applied electric field since the molecules are rigid and frozen in place. Dielectric constant increases with the increasing temperature before glass transition temperature because the molecules gain mobility. The decrease in dielectric constant after the glass transition temperature is due to increased Brownian motion of the molecules with increasing temperature. This increased random motion tends to oppose the alignment of the molecules to the applied electric field. After the glass transition region, the dielectric constant increases again is due to the ionic conduction. The sample now has low enough viscosity that ionic impurities can migrate through the materials, which results in increasing in dielectric constant. In addition, the degradation of polymer also causes the increase in dielectric constant.

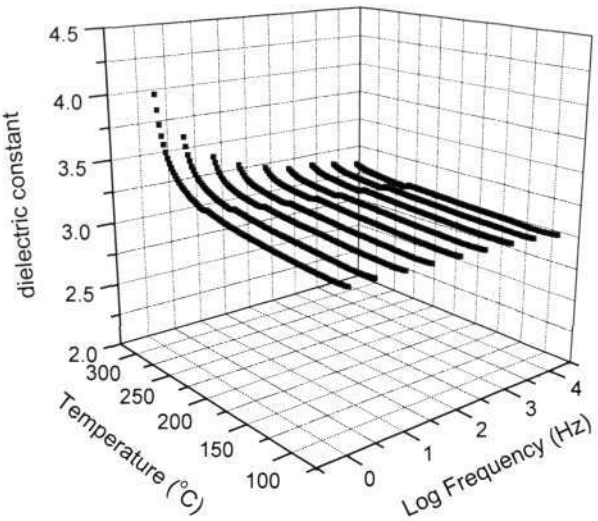

(a) Dielectric constant-Temperature-Log frequency

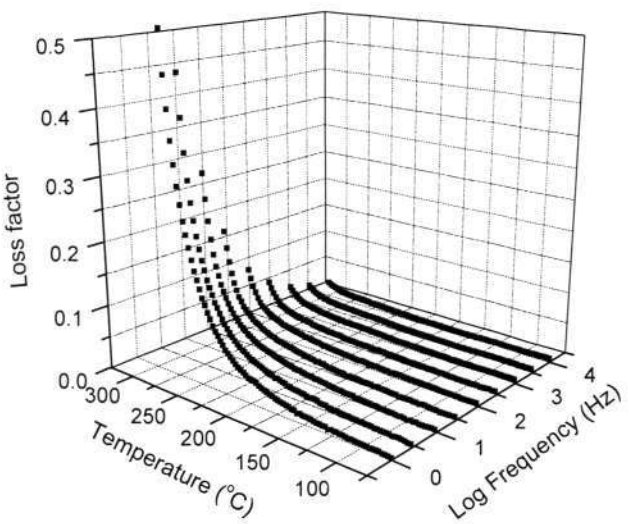

(b) Loss factor-Temperature-Log frequency

Figure 5.2 3D plot of dielectric properties-temperature-log frequency of BACy

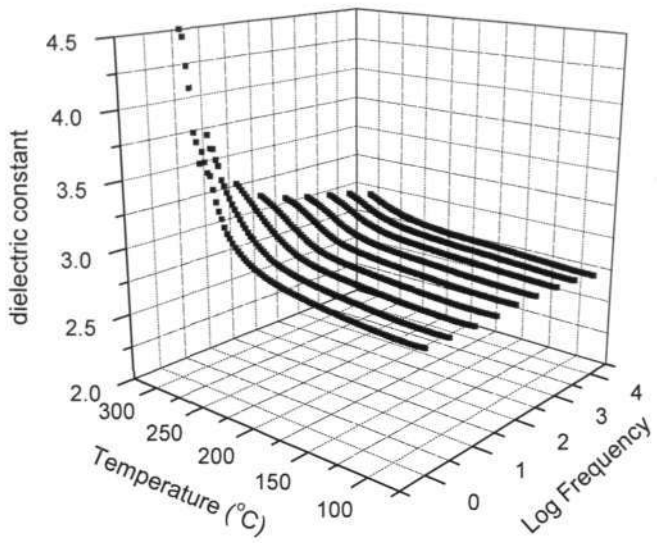

(a) Dielectric constant-Temperature-Log frequency

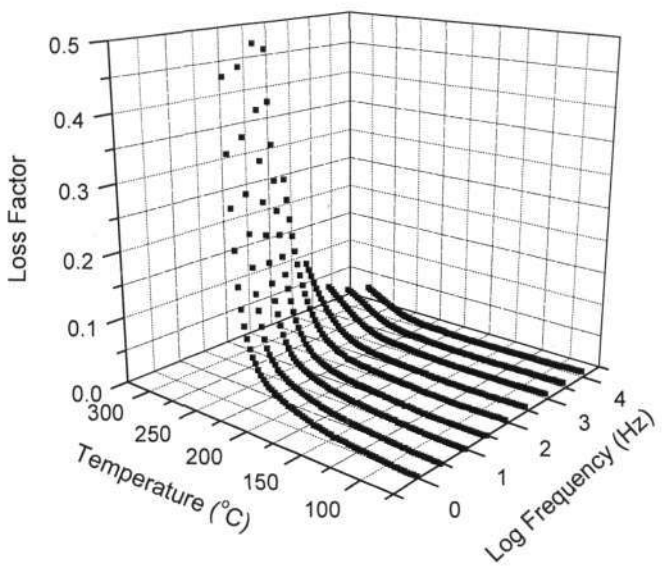

(b) Loss factor-Temperature-Log frequency

Figure 5.3 3D plot of dielectric properties-temperature-log frequency of BFCy

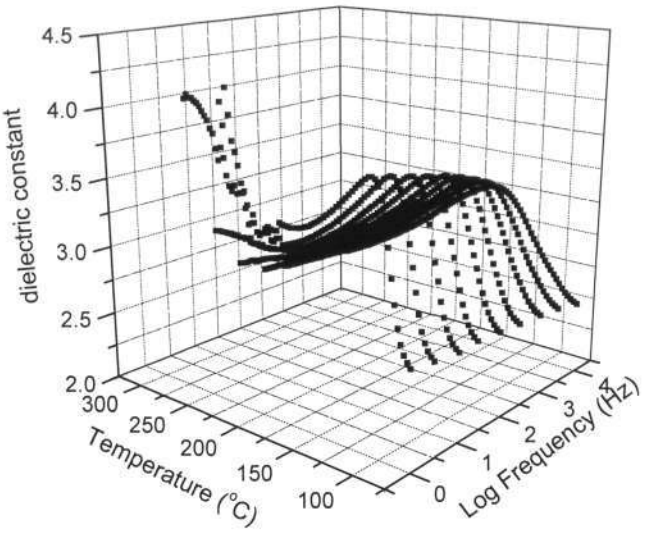

(a) Dielectric constant-Temperature-Log frequency

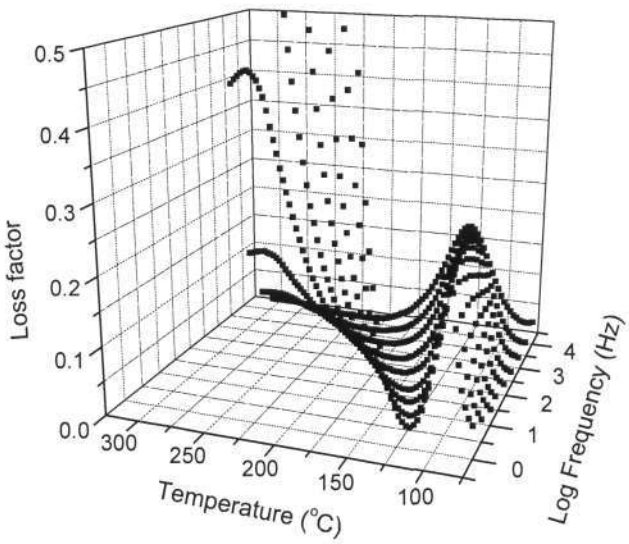

(b) Loss factor-Temperature-Log frequency

Figure 5.4 3D plot of dielectric properties-temperature-log frequency of DFCy

The characteristics of temperature and frequency dependence of the dielectric properties are very important factors to consider dielectric materials applications. The following sections focus on more detailed discussion of these two effects on the dielectric properties.

5.3 Temperature Dependency of Dielectric Properties

The plots of temperature dependence of the dielectric constant and the loss factor for the polycyanurates at several frequencies are displayed in Figures 5.5 to 5.7. As seen from Figure 5.5 and 5.6, the BACy and BFCy homopolymers and their copolymers all exhibit a similar behavior in the dielectric relaxation as shown by the change of the dielectric constant and loss factor with the temperature and frequency. The polycyanurate copolymers exhibit dielectric constant and loss factor intermediates between the two individual components. To illuminate, the dielectric constant and loss factor at 75 °C and 10,000 Hz of polycyanurate systems are listed in Table 5.1 as an example.

Table 5.1 Dielectric properties of polycyanurate systems at 75 °C and 10,000 Hz

Polycyanurate system	Dielectric constant	Loss factor
BACy	3.18	0.0024
BACy/BFCy(8:2)	3.14	0.0020
BACy/BFCy(5:5)	2.89	0.0017
BACy/BFCy(2:8)	2.83	0.0014
BFCy	2.78	0.0009
BACy	3.18	0.0024
BACy/DFCy(8:2)	2.95	0.0060
BACy/DFCy(5:5)	2.78	0.0092
BACy/DFCy(2:8)	2.64	0.0125
DFCy	2.55	0.0135

The dielectric constant and loss factor of BACy, BFCy and their copolymers show a small and gradual increase with temperature up to the glass transition temperature (in this Chapter, the glass transition temperature is defined as the onset of the relaxation transition temperature, for example, the glass transition temperatures of BACy, BFCy

and DFCy homopolymers are indicated as shown in Figure 5.5), while the dielectric behavior of DFCy homopolymer and its copolymers apparently exhibit something different as shown in Figure 5.7. This difference is attributed to that DFCy has much lower glass transition temperature than other two polycyanurates, which can be clearly observed from Figure 5.7 (e) and (f) and it makes the dielectric constant and loss factor peak appear at much lower temperature than that of BACy and BFCy homopolymer and copolymers. The dielectric properties of polymer depend on the orientation and relaxation of dipoles of polymers. Thus the polarity and mobility of dipoles in polymers play a dominant role on determining the dielectric properties. The dielectric behavior of polymers does not consider the complete long chain molecules as polarizable entities, but the component repeat units or segments. The predominant constraint on each segment is its covalent bonding to the rest of the molecular chain on either side, the strong intermolecular ordering and interaction of the segments along the chain. All these are significantly influenced by temperature. In the low-temperature range, polar groups of polymer are difficult to orient and relax in the applied electric field because of the frozen molecular chain segments in the glassy state. With increasing temperature, the chain-segment mobility increases, and polar groups begin to move in response to the applied electric field, which increase the orientation polarization and the dielectric constant of a polymer, as the temperature approaches the glass transition temperature, the dielectric constant increases dramatically as the dipoles attached rigidly to the polymer backbone gain sufficient mobility and become free to orient in an electric field [147,148].

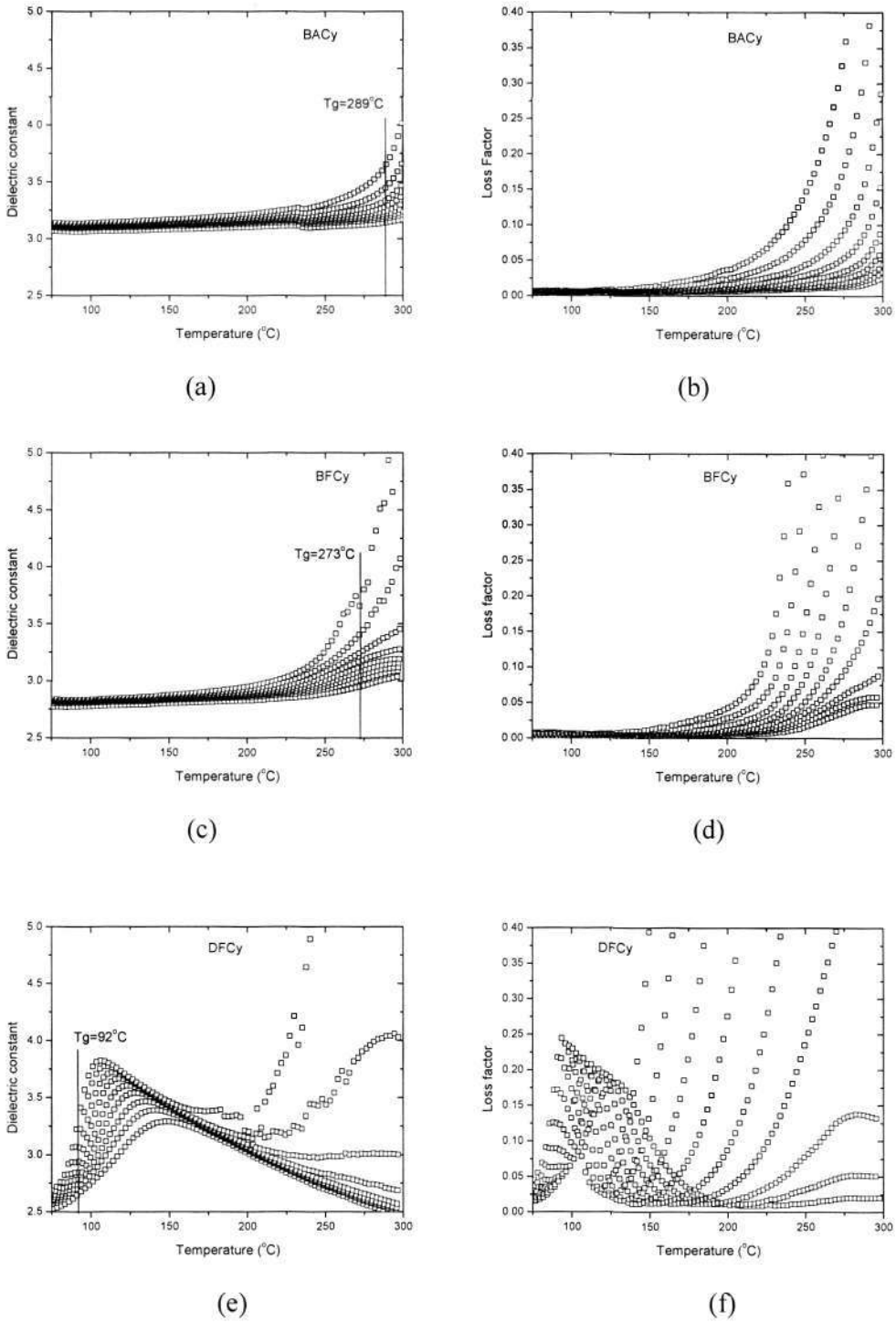

Figure 5.5 Temperature and frequency dependence of dielectric properties of BACy, BFCy and DFCy homopolymers
(For Figures 5.5 to 5.7, from top to bottom line, the frequency increases as 1,3,10,30,100,300,1000,3000,10000)

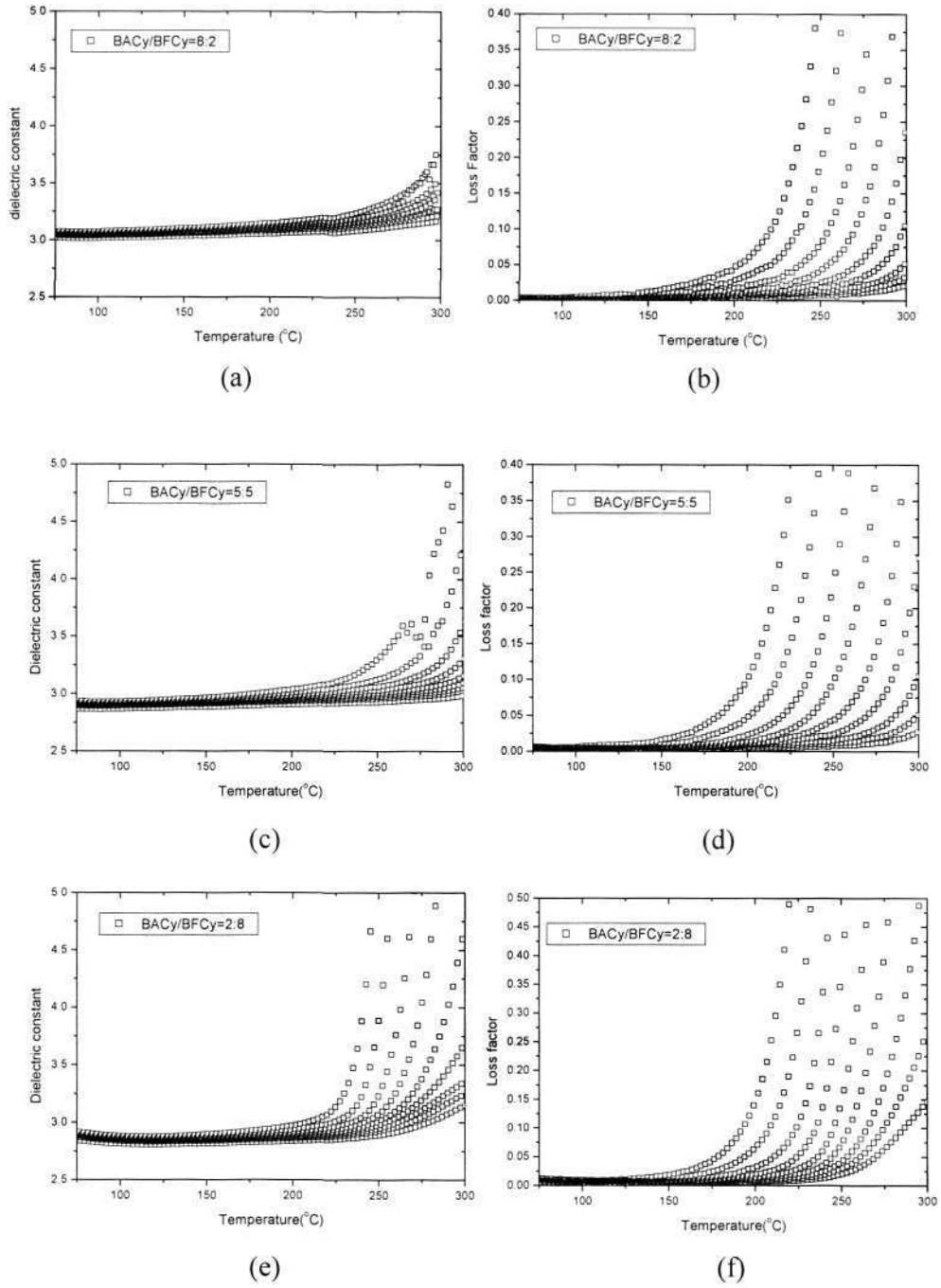

Figure 5.6 Temperature and frequency dependence of dielectric properties of BACy/BFCy (8:2, 5:5, and 2:8 in mole ratio) copolymers

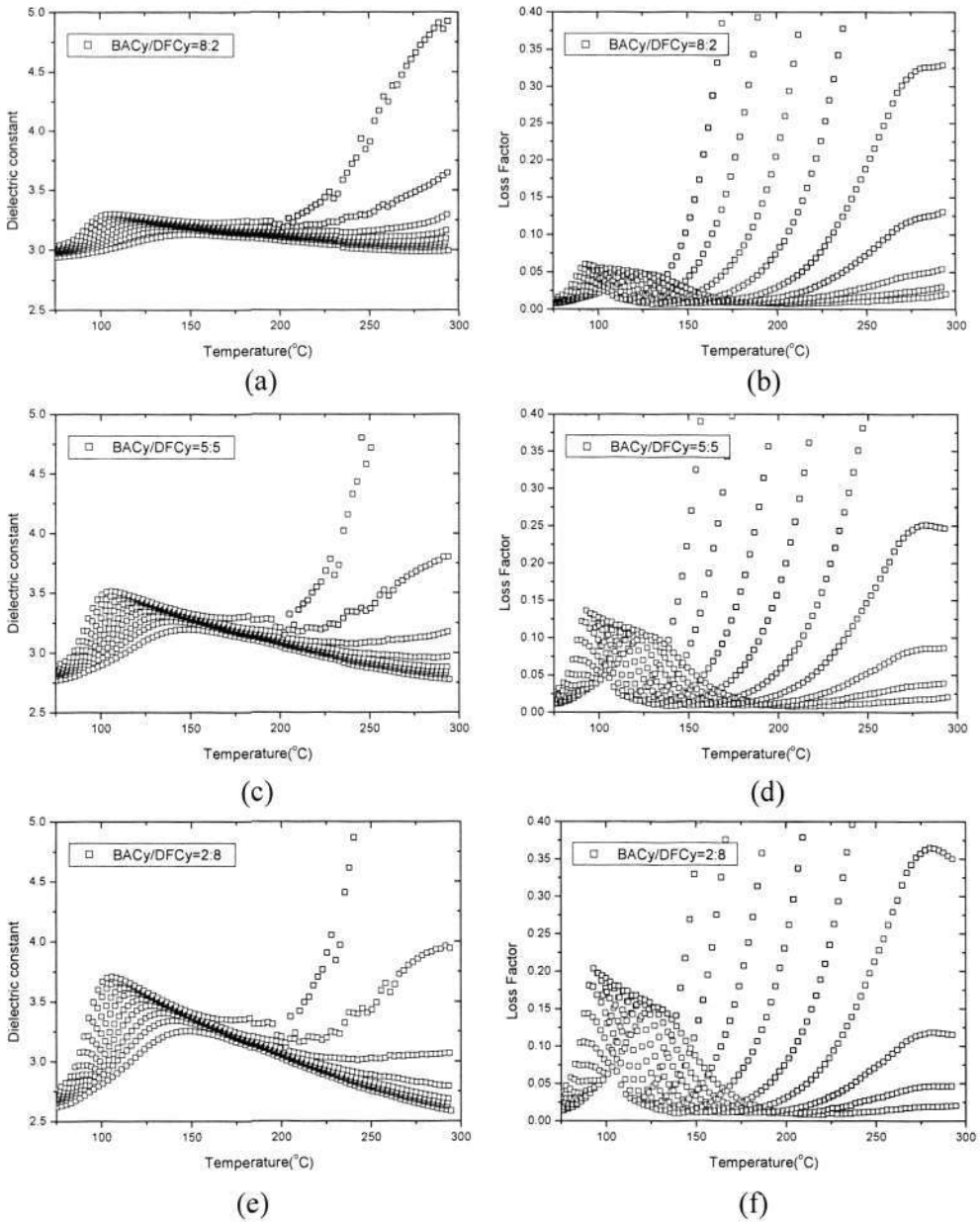

Figure 5.7 Temperature and frequency dependence of dielectric properties of BACy/DFCy (8:2, 5:5, and 2:8 in mole ratio) copolymers

After the onset of glass transition, the dielectric properties exhibit a much faster increasing trend with further increasing temperature. The observed stable dielectric constant of BACy and BFCy aromatic homopolymers and their copolymers could be attributed to the high glass transition temperature and stable structure at elevated temperature. Because DFCy is an aliphatic polymer and has much lower glass transition

temperature, it and its copolymers have relatively less stable dielectric properties response even at low temperature, showing high temperature dependency.

Figures 5.5 to 5.7 also show that the increasing trend of the dielectric constant and loss factor with temperature was first noted at 1 Hz, followed by 3, 10, 30, 100, 300, 1000, 3000, and 10,000 Hz, which indicated that dielectric analysis scanning at lower frequency produces better sensitivity to temperature effects. This phenomenon is because dipoles in the viscoelastic polymers have longer time to align according to the direction of the applied electric field at low frequency. Therefore, more dipole orientation polarization contributes to the dielectric constant and loss factor.

5.4 Frequency Dependence of Dielectric Properties

There are three components of molecular polarization, i.e., electronic polarization, atom polarization and dipole orientation polarization, which influence the dielectric properties of polymers. Electronic polarization is caused by a slight displacement of the electron of any atom in a polymer molecule relative to its positive nucleus. Atom polarization is the process of distorting the arrangement of atomic nuclei in a polymer molecule in an electric field. Both of them are very rapid electric field induced processes and respond at optical frequencies. The displacement resulting from these two polarizations is small because the applied electric field is usually very weak as compared with the intra-atomic field. Dipoles in a molecule have the tendency to be aligned in the applied electric field, and they give a net polarization in the field direction. This process is called dipole orientation polarization, which needs longer time than the electronic and atom polarizations, and can be observed at an electrical frequency range. Because this frequency range is similar to the working frequency range in most applications, the

dielectric constant and loss factor of polymer is mainly dependent on dipole orientation polarization in practice [148].

The frequency dependence of the dielectric constant and loss factor for polycyanurate homopolymers and copolymers is shown in Figures 5.8 and 5.9 respectively. As seen from Figure 5.8(a) the dielectric constant of the BACy homopolymer, BFCy homopolymer and their copolymers shows a slow downward linear response with slightly faster decrease in value at higher frequencies. As mentioned before, all three types of polarizations can respond to the applied electric field at low frequency. With increasing frequency, dipole orientation polarization may not happen because longer time is needed. The characteristic of the decreasing dielectric constant with increasing frequency could be explained by the decreasing dipole orientation polarization contributions to permittivity. As seen from Figure 5.8(b), the loss factor of the BACy homopolymer, BFCy homopolymer and their copolymers decreases rapidly at low frequencies and decreases slowly at high frequencies. This phenomenon also can be observed for other reported thermosetting polymers such as Bismaleimide system [15]. This is because at low frequencies the ionic conduction is the most prevalent mechanism and ionic conduction only introduces losses into a system. It was also noted that the values of loss factor of homopolymers and copolymers are near to each other at high frequencies. However, at low frequencies, their values are much different from each other and the values of the copolymers are not between the homopolymers of the individual components. This may be caused by the space charge polarization due to the heterogeneity of the copolymer systems.

Figure 5.9 show that the BACy/DFCy systems have different dielectric behavior from that of BACy/BFCy systems. The dielectric constant of DFCy homopolymer is highly

frequency dependent, for example, the dielectric constant of DFCy homopolymer changes from 3.41 to 2.65 when the frequency changes from 1 Hz to 10,000 Hz at 90°C, while the dielectric constant of BACy homopolymer only changes from 3.14 to 3.06. The dielectric constant of BACy/DFCy copolymers is between the homopolymers of the two individual components. DFCy is an aliphatic polycyanurate and has much lower glass transition temperature than BACy and BFCy. DFCy shows more frequency dependence, this can be understood as the polymer chain segments of DFCy is more mobile at the temperature and the dipoles are more easily aligned in response to the applied electric field. Therefore, more contributions of dipole orientation polarization added to the dielectric constant. With increasing BACy content, this effect becomes less significant and has the reduced frequency dependency of the dielectric constant. As seen from Figure 5.9(b), the loss factor of BACy/DFCy copolymers is between the BACy homopolymer and DFCy homopolyer.

Because the mobility of the chain segments of DFCy is high, resulting in high ionic conduction effect and contributing to observed high loss factor. When DFCy copolymerized with BACy, the mobility of DFCy is restrained by the aromatic BACy and this restrain is increase with the increasing BACy amount which makes the loss factor decrease gradually. It can also be seen from Figures 5.5 to 5.7 that the dielectric constant of all the systems studied shows less frequency dependence effects at lower temperature range and this is because the dipole orientation polarization is more restricted by the frozen molecular movement.

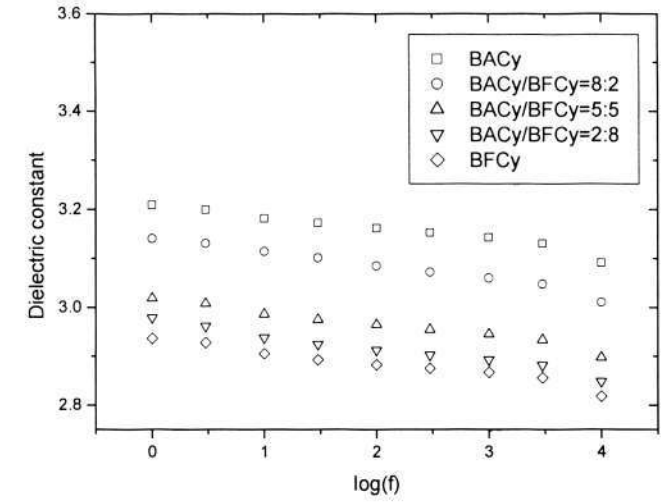

(a)

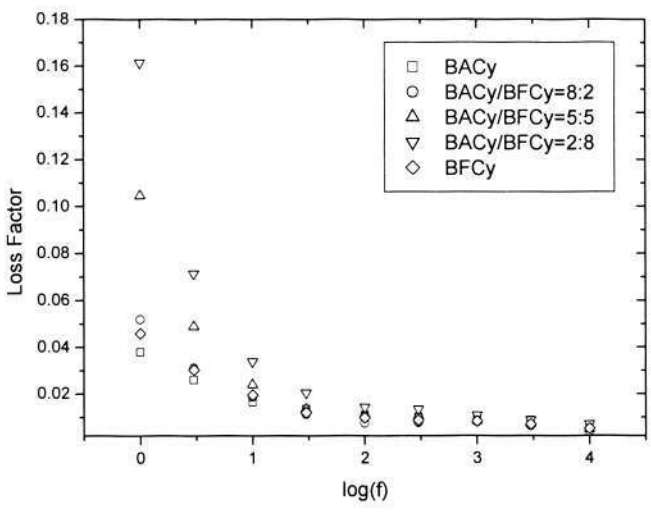

(b)

Figure 5.8 Relationships between dielectric properties and frequency of BACy, BFCy and their copolymers.
(Data obtained from Figures 5.5 and 5.6 at 200 °C)

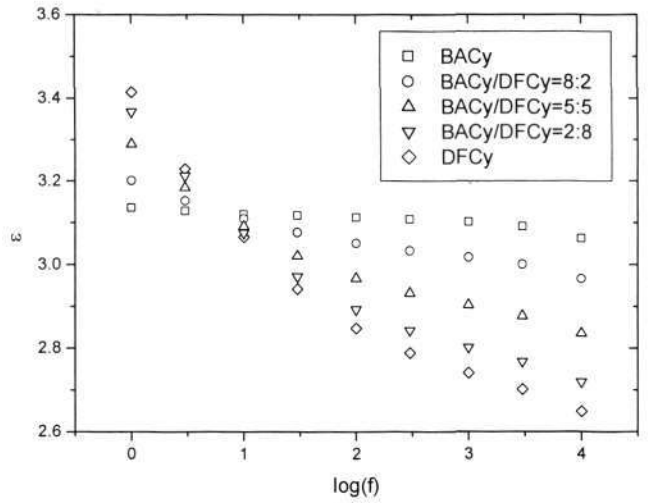

(a)

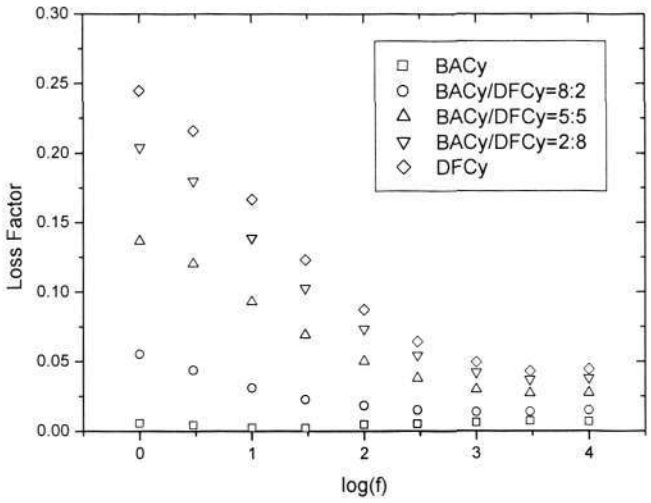

(b)

Figure 5.9 Relationships between dielectric properties and frequency of BACy, DFCy and their copolymers.
(Data obtained from Figures 5.5 and 5.7 at 90 °C)

5.5 Cole-Cole Plot and Heterogeneity of Polycyanurates

Dielectric spectroscopy yields valuable information about the molecular arrangement, intermolecular interactions and dynamics of the molecular reorientational motions in condensed matter. This method is very often used to study the molecular dynamics because of its wide frequency range and its ability to follow the reorientational movements of dipolar groups or whole molecules [149]. Typical relaxation response of a

polymeric material can not be described accurately with a 'single relaxation time' unlike that of most liquid material. This inability to be described by a single relaxation time is a result of its viscoelastic nature and is one of the characteristics that give polymers their unique properties [150]. The most simple relaxation model is that described by Debye via molecular modeling [151]. The time decaying function in the Debye model is described by the following exponential:

$$\Phi(t) = e^{-\frac{t}{\tau}} \qquad \text{(Equation 5.1)}$$

where $\Phi(t)$ is the decay function and τ is the single relaxation time, based upon this model, equations such as the one shown below may be derived to permit fitting of experimental data to evaluate the relaxation time.

$$\frac{\varepsilon^* - \varepsilon_\infty}{\varepsilon_s - \varepsilon_\infty} = \frac{1}{1 + i\omega t} \qquad \text{(Equation 5.2)}$$

where ε^* is the complex dielectric constant, ε_s and ε_∞ are the relaxed and unrelaxed dielectric constant respectively. In simply terms, ε_s and ε_∞ can be described as the dielectric constant at very low ($\omega \to 0$) and very high ($\omega \to \infty$) frequencies, respectively. Their difference ($\varepsilon_s - \varepsilon_\infty$) is directly related to the relaxation strength. The Debye model is far from being able to accurately describe the broad relaxation range of polymers. However, it forms the basis for other more accurate empirical for describing the relaxation distribution.

Advances in more accurately describing the relaxation distribution of polymers were made in the work of Cole and Cole [152]. These researchers described the response of a polymer in terms of multiple relaxation times, the time decaying function for a multiple relaxation model was assumed to be a linear summation of the time decaying function for a single relaxation model.

$$\Phi(t) = \sum_i A(\tau_i) e^{-\frac{t}{\tau_i}} \qquad \text{(Equation 5.3)}$$

where $A(\tau_i)$ is the fraction of a single relaxation time mechanism with relaxation time τ_i. Based upon this model, the following equation can be derived to permit fitting of experimental data.

$$\frac{\varepsilon^* - \varepsilon_\infty}{\varepsilon_s - \varepsilon_\infty} = \frac{1}{1 + (i\omega t_0)^{1-\alpha}} \qquad \text{(Equation 5.4)}$$

where τ_0 is considered as a central relaxation time about which all other relaxation times are distributed, and α is a fitting parameter with limits of $0 \le \alpha \le 1$. This equation reduces to the Debye expression for $\alpha = 0$, as can be seen by comparison with equation 5.2. As the deviation from a single relaxation time model becomes greater, $\alpha \to 1$, the dispersion becomes broader than that for a single relaxation time.

Electrical relaxation phenomena are usually analyzed in terms of the dielectric permittivity by the relaxation of the electric displacement vector, D, under the constraint of constant electric field, E. however, in practice it is convenient to concentrate on the relaxation of the electric field, E, under the constraint of a constant displacement vector, D. which leads to the inverse dielectric permittivity and the definition of electric modulus. An advantage of using the electric modulus to interpret bulk relaxation properties is that variations in the large values of permittivity and conductivity at low frequencies are minimized. In this way, issues, such as inconsistent electrode properties, space charge injection phenomena and absorbed impurity conduction effects, which appear to obscure relaxation in the permittivity presentation, can be resolved or even ignored [153,154]. Complex modulus, electric modulus or inverse complex permittivity, M*, is defined by the following equation:

$$M^* = \frac{1}{\varepsilon^*} = \frac{1}{\varepsilon' - j\varepsilon''} = \frac{\varepsilon'}{\varepsilon'^2 + \varepsilon''^2} + j\frac{\varepsilon''}{\varepsilon'^2 + \varepsilon''^2} = M' + jM'' \quad (j^2 = -1) \qquad \text{(Equation 5.5)}$$

where M' is the real the M'' is the imaginary electric modulus, and ε' the real and ε'' the imaginary permittivity. It is useful to adapt the above formalism to analyze the dielectric properties of polycyanurate and their copolymers.

Using M' and M'', the Debye equation can be rearranged as:

$$M^* = M_s M_\infty \frac{1 + j\omega\tau}{M_\infty + M_s j\omega\tau} \qquad \text{(Equation 5.6)}$$

where $M_s = 1/\varepsilon_s$ and $M_\infty = 1/\varepsilon_\infty$. Resolving the real and imaginary part of Equation 5.6, equation 5.7 and 5.8 are produced, which describe the electric field relaxation, in the frequency domain mode for a single relaxation time, in terms of electric modulus:

$$M' = M_\infty M_s \frac{(M_\infty + M_s)\omega^2\tau^2}{M_\infty{}^2 + M_s{}^2\omega^2\tau^2} \qquad \text{(Equation 5.7)}$$

$$M'' = M_\infty M_s \frac{(M_\infty - M_s)\omega\tau}{M_\infty{}^2 + M_s{}^2\omega^2\tau^2} \qquad \text{(Equation 5.8)}$$

the above equation are equivalent with Debye dispersion equation. Elimination of ωt between Equation 5.7 and 5.8 leads to the Debye Equation:

$$\left(M' - \frac{M_\infty + M_s}{2}\right)^2 + M''^2 = \left(\frac{M_\infty - M_s}{2}\right)^2 \qquad \text{(Equation 5.9)}$$

the coordinates of the centre of this semicircle are $M'' = 0$ and $M' = (M_\infty + M_s)/2$, and its radius is equal to $(M_\infty - M_s)/2$. Debye plot permits easy extrapolation of the results to the values of M_s and M_∞ even when few experimental points are available. This represents one of the main advantages of such a representation [155].

If experimental results form a Debye's semicircle, the effects responsible for dielectric relaxation can be described in terms of simply Debye's model with one relaxation time, which indicating a very pure and homogeneous system. Such a situation only can in fact

be observed for simple dielectric liquids. However, relaxation effects get much more complex in the case of strong intermolecular interactions, and also when a number of processes with different relaxation times are involved. Particularly large divergences from the simple mechanism of Debye are observed in the case of macromolecular and polymeric materials. For this reason we shall attempt a macroscopic description of relaxation effects in such systems. This leads Cole K. S. and Cole R. H. to suggest the following semi-empirical equation for dielectric relaxation in polymers [152]:

$$\left[M'-\frac{1}{2}(M_\infty+M_s)\right]^2+\left[M''+\frac{1}{2}(M_\infty-M_s)\tan\frac{\alpha\pi}{2}\right]^2=\left[\frac{1}{2}(M_\infty-M_s)\sec\frac{\alpha\pi}{2}\right]^2$$

(Equation 5.10)

where M_∞ stands for the value of M' when frequency $\omega\to\infty$ and M_s when $\omega\to 0$. α is the fitting parameter, when $\alpha=0$, Cole-Cole equation reduces to Debye equation. The radius of the semicircle is $r=\frac{1}{2}(M_\infty-M_s)\sec\frac{\alpha\pi}{2}$ and the centre lies below the x-axis, having co-ordinates $\frac{1}{2}(M_\infty+M_s)$ and $-\frac{1}{2}(M_\infty-M_s)\tan\frac{\alpha\pi}{2}$ for M' and M'' respectively. The experimental values of α increase with increasing number of the degrees of freedom of molecules, that is, for example, with increasing number of internal rotation axes in the molecules. The parameter α is a distribution constant describing the broadening of the relaxation area, while time τ is the mean relaxation time corresponding to the centre of the symmetric distribution of time constants [155]. In this study, the relationships between dielectric constant and loss factor are illustrated in a Cole-Cole plot. The values of α provides information on the heterogeneity of the polycyanurate system which may not be detectable by using other methods such as microscopy or thermal analysis [153].

Figure 5.10 shows the Cole-Cole plots of BACy and BFCy homopolymer and BACy/BFCy copolymers (2:8, 5:5 and 8:2 in mole ratio) at 300 °C. As seen from Figure 5.10, the experimental dielectric data points disperse on the semicircle and the circle-arc shape of the Cole-Cole plots is symmetrical, which indicates the relatively good homogeneity of BACy/BFCy copolymer systems [156]. The radii of the semicircles of the copolymers are between the individual component of BACy homopolymer and BFCy homopolymer. As have been described, the radio of the semicircles of a system is equals to $\frac{1}{2}(M_\infty - M_s)\sec\frac{\alpha\pi}{2}$, and its value is depends on the dielectric strength of the system and also the parameter α. Because the dielectric strength of the BACy and BFCy homopolymers are fixed, the differences in the radii of their copolymers can also indicate the homogeneity in certain degree. The experimental values of α were 0.184, 0.249, 0.258, 0.247 and 0.179 for BACy homopolymer, BACy/BFCy copolymers (8:2, 5:5, and 2:8 in mole ratio), and BFCy homopolymer, respectively. From the values of parameter α for different systems, it can be concluded that the dielectric relaxation of all the systems are close to Debye model, because the maximum values of α is less than 0.260. That is to say, all the BACy/BFCy polycyanurate systems have good homogeneity. The copolymer with mole ratio 5:5 has the maximum α values of 0.258, which means its heterogeneity is the highest among the BACy/BFCy polycyanurate copolymers. The good homogeneity of BACy/BFCy system is probably attributed to their same functional group, similar molecular structure and geometry.

Table 5.2 α values of Cole-Cole plot of polycyanurate copolymer systems

	1:0	2:8	5:5	8:2	0:1
BACy/BFCy	0.184	0.249	0.258	0.247	0.179
BACy/DFCy	0.184	0.183	0.305	0.279	0.192

The Cole-Cole plots of BACy homopolymer, DFCy homopolymer and BACy/DFCy copolymers (2:8, 5:5 and 8:2 in mole ratio) at 300 °C is shown in Figure 5.11. Different from Figure 5.10, the semicircle arcs in Figure 5.11 are not arranged regularly in evidence of the first intersection points on x axis are different, which indicate the homogeneity of BACy/DFCy copolymer is not as good as that of BACy/BFCy copolymer system. And the experimental values of parameter α were 0.184, 0.283, 0.305, 0.279 and 0.192 for BACy homopolymer, BACy/DFCy copolymers (8:2, 5:5, and 2:8 in mole ratio), and DFCy homopolymer, respectively. The α values are higher than that of the corresponding BACy/BFCy copolymer systems also further confirm that the homogeneity of BACy/DFCy copolymer is not as good as that of BACy/BFCy copolymer. This probably is because of the molecular structure difference in aromatic BACy and aliphatic DFCy. The DFCy homopolymer also has a higher α value than BACy and BFCy homopolymers. This may because the distortion of the relative long soft aliphatic chain in DFCy polycyanurate network increases the heterogeneity. It should be noted that for BACy/DFCy system, when mole ratio of the two components is equal to each other, the homogeneity is the worst, which is the same as BACy/BFCy system.

To study the temperature effects on the heterogeneity of the polycyanurate system. The Cole-Cole plots of BACy/BFCy=5:5 and BACy/DFCy=5:5 at three different temperatures are shown in Figure 5.12 (a) and (b), respectively. It can be seen from both Figure 5.12 (a) and (b) that all the experimental data points are distributed on one Cole-Cole semicircle. In the frequency range studied in this work, increasing temperature moves the data points towards the left side of the semicircle. An increase in temperature leads to a decrease in the value of M' in the low frequency range although this is less so at high frequencies. Increasing the temperature is equivalent to shifting the minimum

value of M'' to lower frequencies. Thus, the temperature has neglected influence on the homogeneity in certain temperature range.

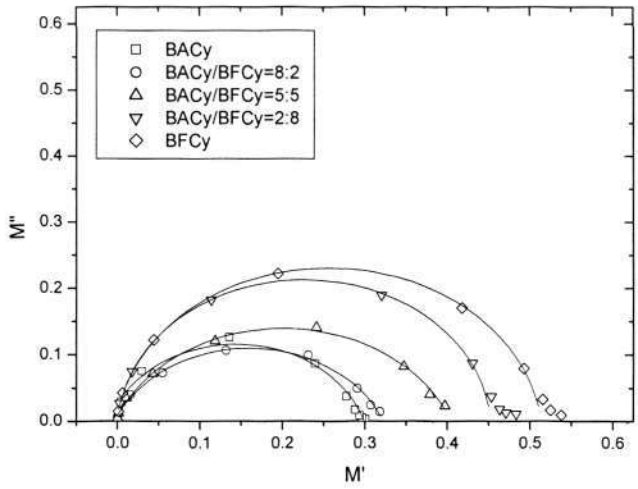

Figure 5.10 Cole-Cole plot of BACy homopolymer, BFCy homopolymer and BACy/BFCy copolymers (2:8, 5:5 and 8:2 in mole ratio) at 300 °C

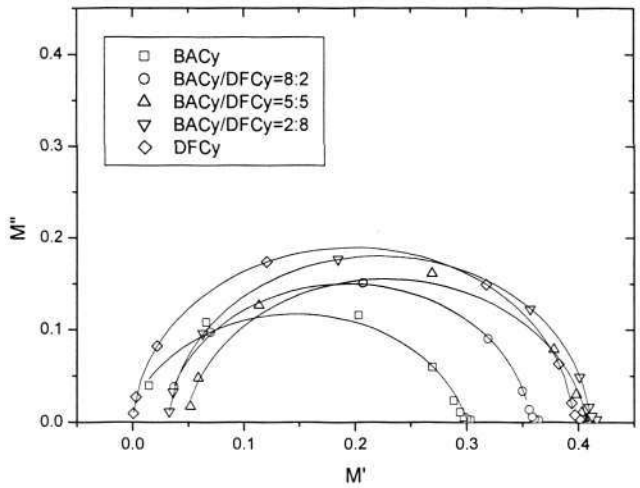

Figure 5.11 Cole-Cole plot of BACy homopolymer, DFCy homopolymer and BACy/DFCy copolymers (2:8, 5:5 and 8:2 in mole ratio) at 300 °C

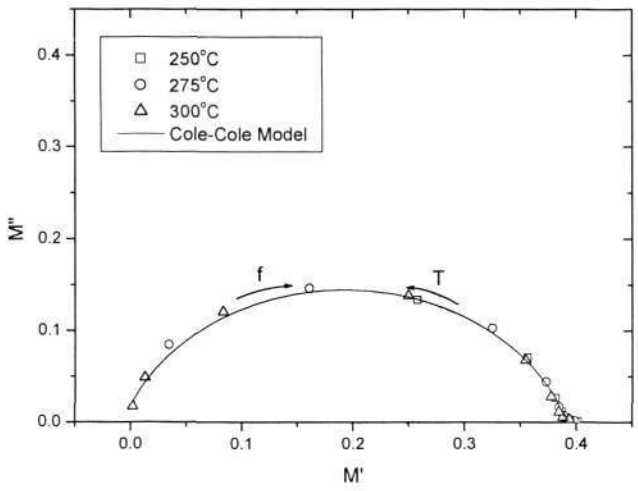

(a)

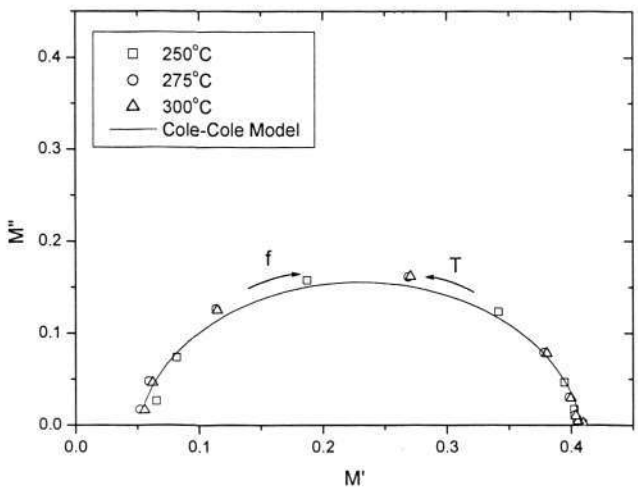

(b)

Figure 5.12 Cole-Cole plot of (a) BACy/BFCy (5:5) and (b) BACy/DFCy (5:5) copolymer at temperatures of 250 °C, 275 °C and 300 °C

5.7 Summary

Through the study on the temperature and frequency dependence of different polycyanurate homopolymers and copolymers, it can be concluded that the effect of temperature and frequency on dielectric properties in these polymers depend on their glass transition temperature. The dielectric properties of aromatic polycyanurates, including BACy homopolymer, BFCy homopolymer and BACy/BFCy copolymers,

show flat response to temperature up to 250 °C at all frequencies studied. The dielectric properties of aliphatic polycyanurate DFCy homopolymer and its copolymers show higher dependency on temperature and frequency, mainly because aliphatic DFCy homopolymer has much lower glass transition temperature than the aromatic counterparts.

Heterogeneity in multi-component polymeric systems has great influence on their properties and has been extensively studied both experimentally and theoretically. However, it is hard to study the heterogeneity of polycyanurate by traditional thermal and mechanical analysis methods, because polycyanurate copolymer shows macroscopically phase mixed structure and has a single glass transition temperature. In this study, the heterogeneity of polycyanurate homopolymers and copolymers can be quantified based on the DEA data and Cole-Cole equation. According to the values of the adjust parameter α in Cole-Cole equation, for all the polycyanurate systems studied in this work, the heterogeneity will reach maximum when the copolymer has 5:5 mole ratio. The values of parameter α can also reflect the difference in heterogeneity of different polycyanurate copolymers. Because BACy and BFCy both are aromatic and have very similar molecular structure and geometry, while DFCy is aliphatic and has a very different molecular structure, BACy/BFCy copolymers show better homogeneity than that of BACy/DFCy copolymers, which can be quantified from the α values.

CHAPTER 6

OPTICAL PROPERTIES OF POLYCYANURATE THIN FILMS

6.1 Introduction

In the present era of emerging technology, there is a great demand for new materials for the fabrication of optoelectronic devices, suitable for fast data processing and communication. Although a large number of inorganic materials are available for the fabrication of such devices, the technology that leads to the preparation of such inorganic based device is often cumbersome and expensive [103]. Polymers are expected to play an important role in the realization of integrated optical devices for application in the field of optical communications, optical data processing, electro-optic and thermo-optic switching devices, directional couplers, nonlinear optics etc [103,105]. The advantages of polymers for optic-electronic applications include their flexibility and feasibility of processing and fabricating, their compatibility with many substrate materials like glass, silicon and InP, and their good physical, chemical, mechanical and thermal properties. The optical and electrical properties of these polymer materials can be modified and adjusted to suit a particular application. Polymer optical components are also attractive due to their potentially lower production costs and lower power consumption.

One of the most important applications of the polymeric optoelectronic materials is for the fabrication of optical waveguides. The processing methods that are normally used to fabrication polymeric optical waveguides are vacuum deposition, spin coating, and dip coating. Polymeric systems offer the advantage of flexibility in fabrication of films of

optical quality that makes them suitable for integrated optical devices [103]. The preparation of light guiding films with polymers started in the 1970s. Conventional optical polymers including poly(methylmethacrylate) (PMMA), polystyrene (PS), polycarbonate (PC), polyurethane (PU) and epoxy resin (EP) are developed and commercialized. In the past twenty years, several major families of novel optical polymers have also been developed in academic and industrial laboratories. These polymers can be grouped into four major classes: deuterated and halogenated polyacrylates, fluorinated polyimides, perfluorocyclobutyl (PFCB) aryl ether polymers, and nonlinear optical polymers. Some of the commercial available optical polymers are given in Table 6.1 [105].

Polycyanurate resins are a class of high performance polymers, developed originally as matrix materials for printed circuit boards (PCB). This polymer shows a number of outstanding properties, for example high glass transition temperature, low loss, low dielectric constant good adhesion properties of different surface, excellent resistance against most common solvents and remarkable mechanical properties [1-3,27]. The refractive index tuning in a wide range covering the low, medium, high and super-high index contrast can be obtained by copolymerizing of different cyanate monomers. Moreover, the use of thermosetting resins permits low production cost of optical waveguides with well established procedures in semiconductor technology, such as photolithography and reactive ion etching (RIE). Polycyanurates have been reported as optical waveguide materials by HHI (Heinrich Hertz Institut) and IZM (Institut Zuverlassigkeitund Mikrointegration) [136,137]. More recently, polycyanurate thin films for optical waveguide application are reported by Bauer M et al [27-33]. Polycyanurate resins appear to be promising materials for integrated optics application.

Table 6.1 Characteristics of novel optical polymers developed globally by companies [105]

Company	Polymer type	Patterning techniques	Propagation loss, single-mode waveguide [dB/cm] (wavelength, [nm])	Other properties (wavelength, [nm])
Optical Crosslinks (formerly DuPont and Polymer Photonics)	Acrylate (Polyguide)	Diffusion	0.18 (800) 0.2 (1300) 0.6 (1550)	Laminated sheets Excimer-laser machinable
Corning (formerly AlliedSignal)	Acrylate	Photoexposure/ wet etch, RIE, laser ablation	0.02 (840) 0.3 (1300) 0.8 (1550)	Birefringence: 0.0002 (1550) Crosslinked, T_g: 25 °C Environmentally stable
	Halogenated acrylate	Photoexposure/ wet etch, RIE, laser ablation	0.01 (840) 0.06 (1300) 0.2 (1550)	Birefringence: 0.000001 (1550) Crosslinked, T_g: ~50 °C Environmentally stable
NTT	Halogenated acrylate	RIE	0.02 (830) 0.07 (1310) 1.7 (1550)	Birefringence: 0.000006 (1310) T_g: 110 °C
	Deuterated polysiloxane	RIE	0.17 (1310) 0.43 (1550)	Environmentally stable
	Fluorinated polyimide	RIE	TE:0.3, TM: 0.7 (1310)	PDL: 0.4 dB/cm (1310) Environmentally stable
Amoco	Fluorinated polyimide (Ultradel)	Photoexposure/ wet etch	0.4(1300) 1.0 (1550)	Birefringence: 0.025, crosslinked, thermally stable
General Electric	Polyetherimide (Ultem)	RIE, laser ablation	0.24 (830)	Thermally stable
Hitachi	Fluorinated polyimide	Photoexposure/ wet etch	TE: 0.5, TM: 0.6 (1300)	Birefringence: 0.009 (1300), PDL: 0.1 dB/cm (1300), T_g: 310 °C, thermally stable
Dow Chemical	Perfluorocyclobutane (XU 35121)	Photoexposure/ wet etch	0.25 (1300) 0.25 (1550)	T_g: 400 °C
	Benzocyclobutene (Cyclotene)	RIE	0.8 (1300) 1.5 (1550)	T_g: > 350 °C
Asahi Glass	Perfluorovinyl ether cyclopolymer (CYTOP)			n = 1.34 T_g: 108 °C
DuPont	Tetrafluoroethylene and perfluorovinyl ether copolymer (Teflon AF)			n = 1.31 (AF 1600) n = 1.29 (AF 2400)
JDS Uniphase (formerly Akzo Nobel)	Polycarbonate (BeamBox)	RIE	0.6 (1550)	Thermally stable
Telephotonics	(OASIC)	Photoexposure/ wet etch, RIE, laser ablation	< 0.01 (840) 0.03 (1300) 0.1 (1550)	Environmentally stable
Gemfire	(Gemfire)	Photoexposure/ wet etch	1.0 (1550)	Birefringence: 0.0002 (1550) Crosslinked
K-JIST	Fluorinated poly(arylene ether sulfide) (FPAESI)	RIE	TE: 0.42, TM: 0.4 (1550)	Birefringence: 0.0003 (1550), PDL: 0.02 dB/cm (1550), crosslinked, thermally stable
Redfern	Inorganic polymer glass (IPG)	RIE		Environmentally stable
Hoechst Celanese	PMMA copolymer (P2ANS)	Photobleaching	1.0 (1300)	NLO polymer
PacificWave	Polycarbonate with CLD-1 chromophore (PC-CLD-1)	RIE	1.8 (1550)	NLO polymer, r_{33} = 70 pm/V (1310), pigtail loss=1.5 dB/facet
Lumera	Polyurethane with FTC chromophore (PU-FTC)	RIE	2.0 (1330)	NLO polymer, r_{33} = 25 pm/V (1310), pigtail loss = 5 dB/facet
Ipitek	Poly(methylmethacrylate) with CLD-1 chromophore (PMMA-CLD-1)	RIE	5.0 (1300)	NLO polymer, r_{33} = 60 pm/V (1300), pigtail loss=3.5 dB/facet

One of the most crucial issues regarding the applicability of polymeric materials is the optical propagation loss at around 1550 nm [103]. The various factors contributing to optical loss in polymer waveguides can be divided into intrinsic loss (due to vibrational absorption, electronic transition absorption, and scattering) and extrinsic loss (due to impurities, dust, microcavities, and inhomogeneity). After optimum process conditions in waveguide fabrication have been achieved, the molecular vibrational absorption may be a major loss factor that can be reduced by modification [108].

If polymer is to serve as optical transmission media, the attenuation loss in the 1550 nm region must be low. To lower the optical loss in the critical region of 1550 nm it is strongly recommended to avoid absorbing molecular groups in the optical materials, especially OH and NH groups, which have strong absorption in 1550 nm region. The intrinsic optical advantage of polycyanurate is the absence of OH and NH groups, and even after the cyclotrimerization or curing none of these groups are present. But of course the polycyanurates contain CH groups. For polycyanurate BACy, the large part of overall optical loss is contributed by the fundamental and overtone absorption of CH group, especially aliphatic CH group. Therefore one way to reduce the optical loss of polycyanurate is to replace the hydrogen with fluorine [27,28,108]. The theoretically possible overtones of CF bond around 1550 nm are very weak and the overtone absorption in the region of interest is undetectable by conventional spectrometry. The CF bond can be introduced into the polycyanurate structure in different ways. One way is to replace the aliphatic H atoms by fluorine atoms in BACy, which produce BFCy. The other way is to incorporate fluoromethylene groups $-(CF_2)_m-$ in the main chain or side chains in polycyanurate, which produce DFCy. However this method generally decreases the glass transition temperature of polycyanurate. An additional advantage of fluorinated polycyanurate is that fluorinated polycyanurate not only have lower absorption but also show increased chemical stability and decreased water absorption [103].

For applications of polymer in optical devices, several requirements must be met. For example, the optical materials should be of as high transparency as possible at the applied wavelength. It should have a smooth surface, and be free of any microcracks or other defects, to reduce scattering of propagation light. For waveguide application, one of the important requirements is the tunable refractive index. Usually, a high refractive index contrast, Δn, is required between the core and cladding layers. It is also desirable that a

material should have a stable refractive index. Moreover, it is important for synthesis polymers with pre-defined indices and index contrasts.

For polycyanurate in optical waveguide applications, two approaches can be employed to tune the refractive index [27-33]. One way is through controlling the fluorine content in the polycyanurate copolymer to adjust the refractive index. This can be realized by copolymerizing BACy with fluorinated polycyanurate such as BFCy and DFCy. Because BFCy has low optical loss and lower refractive index around 1.54 and has similar structure to BACy. It is expected that a broader adjustable refractive index range of 1.54 to 1.61 can be achieved by changing the monomer ratio. Since this can be implemented without affecting to curing conversion in BACy/BFCy copolymer, the films are expected to maintain the excellent thermal stability and other properties. DFCy has an even lower refractive index of about 1.44, thus the BACy/DFCy copolymer is expected having a much broader tunable range of refractive index of 1.44 to 1.61. However, because of its aliphatic structure, DFCy has a much lower Tg than BACy and BFCy, which may limit the application of BACy/DFCy copolymers. Another useful approach to control the refractive index is to adjust the free volume of the modified polymer by using monofunctional polycyanurate (CPCy) to copolymerize with BACy. However, this approach may have some limitation. Firstly, because CPCy is monofunctional, it cannot form a crosslinked structure itself, hence its mole ratio should be kept below 0.5. In addition, CPCy reduces the crosslink density of BACy, which may cause a dramatic decrease in Tg of the copolymer and thus limit its high temperature application.

In this work, similar approaches as references [27-33] were used to tune the refractive index and reduce the optical loss of polycyanurate thin films. However, in the present study, discussions are focused on the more fundamental aspects, such as the structure-

optical properties relationship, the effect of conversion, copolymer composition, structure similarity and inhomogeneity on the refractive index and propagation loss of polycyanurate thin films, which provide fundamental understandings and basic knowledge for the design and fabrication of polycyanurate optical devices. In addition, experimental data are compared with the theoretically calculated refractive indices using a segment incremental model derived from Lorenz-Lorentz equation.

6.2 Measurement of Optical Properties by Prism Coupler

In integrated optics, thin dielectric films are usually used as planar waveguides. The important properties of optical thin films are refractive index (n), film thickness, birefringence and optical propagation loss. Normally the refractive index, film thickness and birefringence can be measured by prism coupler or ellipsometer. For the measurement of propagation loss, several techniques have been employed, including cutback method, prism coupling, photo-thermal deflection, Fabry-Perot interference method, intensity modulation using an acousto-optic modulator, photo-luminescence, optimized end-fire coupling, self-pumped phase conjugation, multisection single-pass technique and femtosecond pulses technique [157]. Among them, prism coupling technique is particularly useful, because it gives accurate measurement of all the four parameters, i.e., refractive index, film thickness, birefringence and propagation loss [158-161].

6.2.1 Measurement of Refractive Index and Film Thickness

The principal components of a prism coupler are illustrated in Figure 6.1. A laser beam strikes the base of a high refractive index prism and is reflected onto a photo detector as shown in Figure 6.1. The film to be measured is brought into contact with the prism base by means of a pneumatically operated coupling head, although there is still an air gap (typically less than 100-200 nm and caused by the roughness of the two surfaces) between

the sample and the prism. The angle of incidence, θ, of the laser beam can be varied by means of a rotary table upon which the prism, film, coupling head, and photo detector are mounted. At certain values of θ, called mode angles, photons violate the total internal reflection criterion, and tunnel from the base of the prism across the air gap and into the film and enter into optical propagation modes, causing a sharp drop in the intensity of light striking the photo detector. Figure 6.2 shows an example of the measurement of a BFCy polycyanurate thin film at wavelength of 632.8 nm.

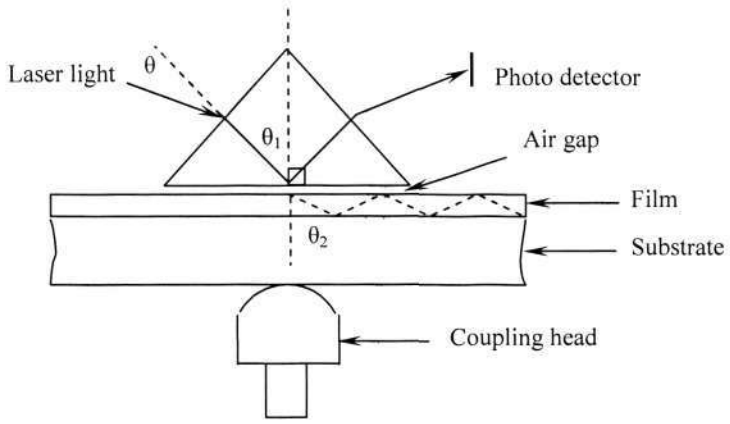

Figure 6.1 Schematic cross section through a prism film coupler

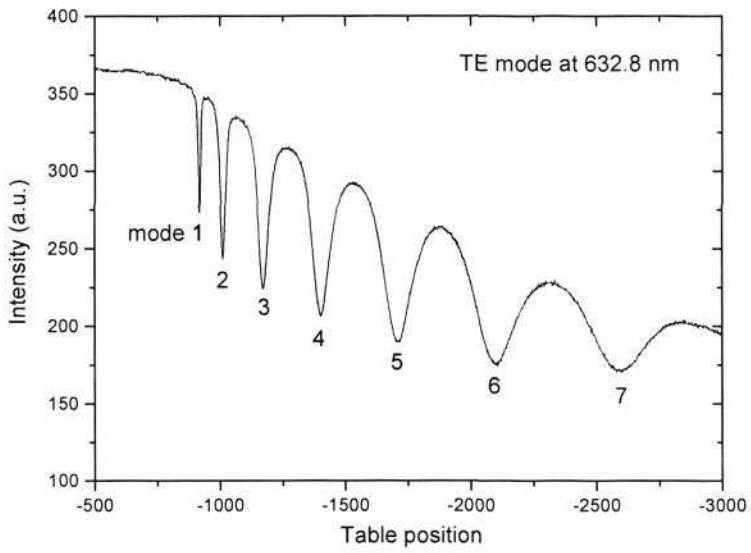

Figure 6.2 Measurement of TE (transverse electric) mode refractive index of BFCy polycyanurate thin film at 632.8 nm

The intensity striking the photo detector is plotted as a function of the table position, which is related to the angle θ. For a given substrate type, the angular location of the modes depends only on the film thickness and refractive index. Thus as soon as two mode angles are measured, the film thickness and index can be calculated by an appropriate computer algorithm. For the mth mode, the following eigenvalue equation [162], commonly referred to as the 'mode equation' applies:

$$\frac{2n\pi d\cos\theta_2}{\lambda} + \psi_{10} + \psi_{12} = (m-1)\pi \quad (m = 1, 2, 3\ldots) \qquad \text{(Equation 6.1)}$$

where λ is the wavelength, n is the film index, d is the film thickness, θ_2 is as defined in Figure 6.1, and ψ_{10} and ψ_{12} are the Fresnel phase shifts at the film-air and film-substrate interfaces. The above series of equations are complex transcendental equations which need to be solved numerically, but solution of the equations of two modes yields the thickness and refractive index of the film simultaneously.

It should be stressed that a pattern of minima similar to the one shown in Figure 6.2 is obtained regardless of whether the film is on a higher or lower index substrate. If the substrate is of lower index than the film, the modes maybe excited since total internal reflectation at the film substrate interface is possible. If the substrate index is higher than the film index, although total internal reflection at the film substrate interface and optical propagation in the film are not possible, the intensity minima will still be evident. Therefore the prism coupling technique provides an accurate measurement of both refractive index and film thickness regardless of the value of the refractive index of the substrate used.

The angle at which mode excitation occurs is related to the effective index, n_{eff}, through the following equation [29,104]:

$$n_{eff} = n_p \sin[\alpha + \sin^{-1}(\sin\theta / n_p)] \qquad \text{(Equation 6.2)}$$

where n_p is the refractive index of the prism material, α is the angle of the prism (in this case 60°) and θ is the incident angle. The incident angle could be measured up to an accuracy of 0.01°, hence the value of n_{eff} could be estimated to an accuracy of 1×10^{-4}. For a given series of mode indices, the index profile $n(x)$ can be easily estimated using WKB (Wentzel-Kramers-Brillouin) approximation [163]. The effective mode indices can also be expressed as a function of the mode order according to [29,104]:

$$n_{eff}^{\ 2} = n_{sur}^{\ 2} - \lambda^2 m^2 / 4d^2 \qquad \text{(Equation 6.3)}$$

where n_{sur} is the refractive index of the film surface, λ is the wavelength used, m is the mode order and d is the thickness of the film. The effective index n_{eff} is actually defined as below. Since each mode is characterized by a very well defined angle of incidence on the base of the prism, the effective index for light impinging at any angle θ_1 on the base of a prism with index n_p is simply defined as [164]:

$$n_{eff} = n_p \sin\theta_1 \qquad \text{(Equation 6.4)}$$

This is because the effective index for any ray of light is simply $n\sin\theta$ where n is the index of the medium in which the light is traveling and θ is the angle of incidence it makes on the boundary of the material as it is refracted into the next material. The plot of n_{eff} versus m^2 should be linear and gives the value of n_{sur} and d from the intercept and slop respectively. Figure 6.3 shows the plot of intensity versus effective index n_{eff} for a BFCy film on silicon substrate as an example. Table 6.2 summarized the table position and the effective index at each mode, and Figure 6.4 shows the plot of n_{eff} versus m^2.

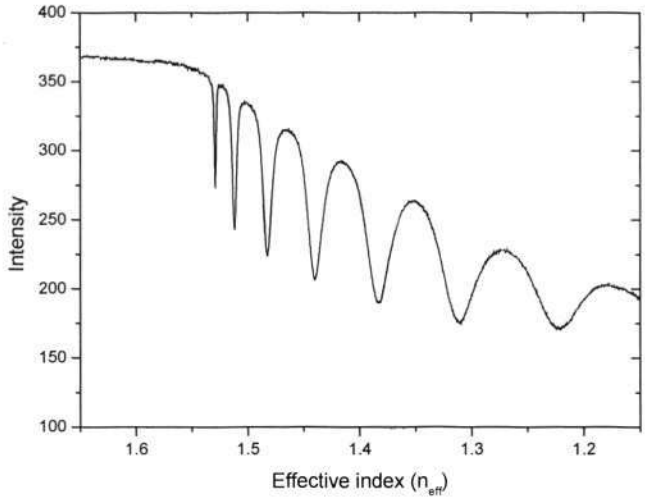

Figure 6.3 Intensity versus effective index of a BFCy film on silicon

Table 6.2 Measured table position and effective index of BFCy film on silicon

Mode number	Table position	Effective index
1	-918	1.5291
2	-1012	1.5120
3	-1172	1.4826
4	-1402	1.4402
5	-1710	1.3830
6	-2101	1.3109
7	-2597	1.2216

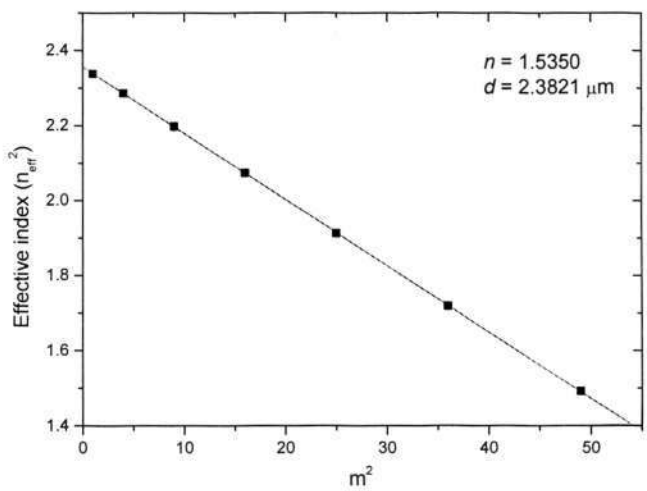

Figure 6.4 Effective index versus mode of a BFCy film on silicon

From equation 6.3, it can be deduced that for a film of a given thickness, the number of supporting modes will reduce when higher wavelength of incident light is used. An example is shown in Figure 6.5 when the wavelength of light is 1539 nm instead of 632.8 nm.

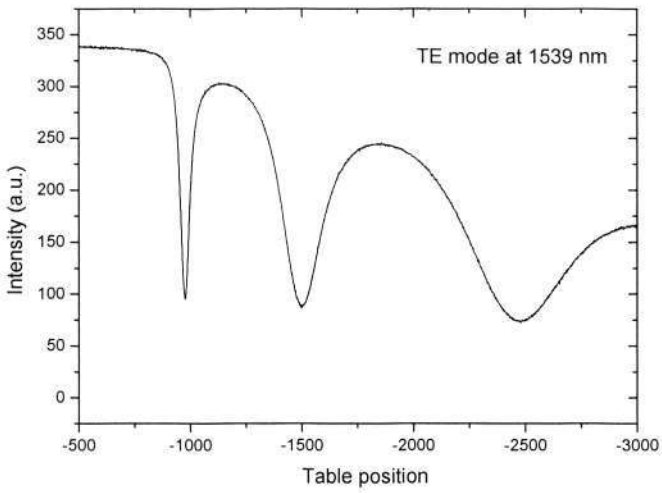

Figure 6.5 TE mode at 1539 nm of a BFCy film on silicon

Normally, the measurement of refractive index and film thickness uses TE (Transverse electric) modes [164]. In this case, the electric field vibrates vertically with respect to the optics module baseplate and hence the refractive index is measured in the plane of the film along this vertical direction. Moreover, rotation of the film about the coupling point permits measurement of refractive index along any arbitrary direction in the plane of the film. However, films also possess a second and independent set of optical propagation modes which can be excited by rotating the polarization state of the incoming laser beam by 90^{o} so that the magnetic field is transverse (the magnetic field vibrates vertically in the plane of the film). These modes, called TM (transverse magnetic) modes, can be used to calculate refractive index and thickness along a direction perpendicular to the plane of the film. Figure 6.6 shows the measurement of a BFCy film on silicon at TM mode at the wavelength of 632.8 nm.

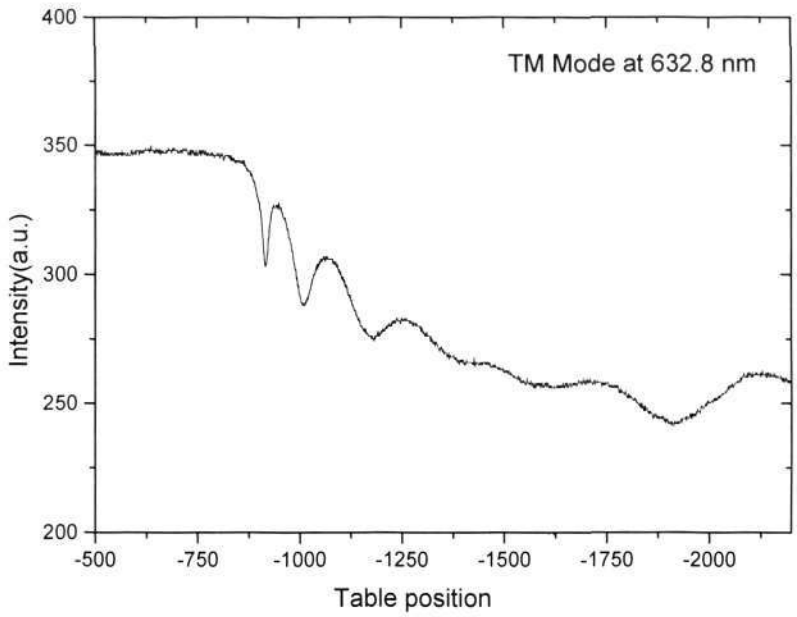

Figure 6.6 TM mode at 632.8 nm of a BFCy film on silicon

In this studying, silicon wafer was used as the substrate on which the polycyanurate thin films are spin coated. The reflectivity of a thin film at TM modes from a high index substrate drops to zero around the polarizing angle known as Brewster's angle [165,166] of the film-substrate interface. For a plane electromagnetic wavefront incidence on a plane boundary between two dielectric media having different refractive indices, the angle of incidence at which transmittance from one medium to the other is unity when the wavefront is linearly polarized with its electric vector parallel to the plane of incidence. Thus, for a certain range of angles, TM modes for low index films on high substrates are very difficult to observe. Although a TM mode may exist, it may be difficult to be detected. For multimode TM films, the first modes are usually visible, then one or more modes may not be visible, and one or more final modes may then be visible again. In other words, it is possible that middle modes may be missing. However, if continuous modes are chosen to be analyzed, correct results still can be obtained. Then the

birefringence can be calculated from $\Delta n = n_{TE} - n_{TM}$, in which Δn is the birefringence, n_{TE} and n_{TM} are the refractive indices at TE mode and TM mode respectively.

In comparison to other methods such as ellipsometer, the prism coupling technique has two important advantages [158]. It requires only the measurement of angles, which can be done conveniently and with high precision. Also if the film is thick enough to allow the observation of more than two modes of the same polarization, the method becomes a self-consistent one because the two unknowns n and d are then determined from more than two independent measurements. This improves the accuracy and greatly increases the reliability in the results.

6.2.2 Measurement of Propagation Loss

Accurate measurement of optical propagation loss in thin film waveguide is particularly important in the performance evaluation. Over the past few years, several techniques including the cutback method, prism coupling, photo-thermal deflection, Fabry-Perot interference method, intensity modulation using an acousto-optic modulator, photo-luminescence, optimized end-fire coupling, self-pumped phase conjugation, multisection single-pass technique and femtosecond pulses technique [157] have been employed for the evaluation of loss.

The measurement of scattered light from a guiding film has been widely used in the past because it is nondestructive and easy to measure [157,164,167-171]. Scattering loss measurement techniques involve the measurement of the propagated light scattered from the waveguide as a function of position. A decrease of scattered light along the light path can be obtained, which represents the intensity attenuation of light wave propagating inside the film. The losses measured therefore include the volume absorption and

scattering as well as the surface scattering. It is assumed that the light intensity scattered out of the waveguide is proportional to the intensity guided in it. By detecting the scattered light intensity, the propagation loss of a planar waveguide can be determined. The optical-fiber probe method measures loss of planar optical waveguides by measuring the exponential decay of light using a fiber probe scanning down the length of the propagation streak. The optical fiber method is identical in concept to the CCD camera approach for measuring the decay of the propagating streak, but offers an added advantage of insensitivity to the spatial nonuniformity of response which is common in CCD arrays. This method works well provided the guide has at least some slight scattering loss to provide a means of sampling the attenuated light intensity. An additional requirement is that scratches, particles, and abrupt thickness changes in the path of the propagating beam should be avoided so that the scattered light exhibits at least an approximate exponential decay versus distance along the guide. Finally, the guide must be planar with a top exposed in air [164].

When a guide mode was excited, a fiber probe scanned down the whole length of the propagation streak to detect the exponential decay of light. The intensity versus distance profile is obtained and an example is given in Figure 6.7. The propagation loss can be calculated from the following equation:

$$\phi = \frac{10}{L}\log\left(\frac{I_x}{I_y}\right) \qquad \text{(Equation 6.5)}$$

where ϕ is the propagation loss, I_x and I_y are the light intensities at arbitrary position x and y respectively (position x is nearer to the light source than position y), L is the distance between position x and y.

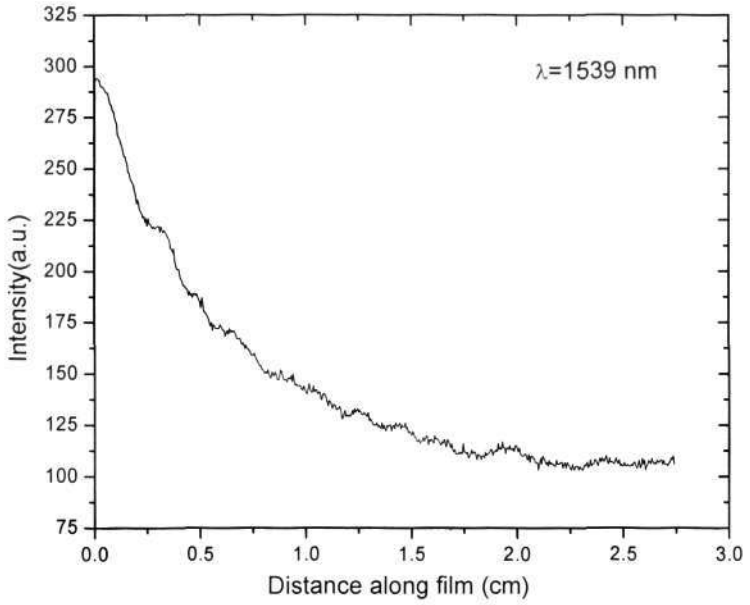

Figure 6.7 Measurement of optical propagation loss of a BFCy thin film on silicon dioxide

6.3 Refractive Indices of Polycyanurate Thin Films

6.3.1 Effect of Conversion on Refractive Index

The refractive indices and film thickness of BACy, BFCy and DFCy polycyanurate homopolymer thin films of different conversions were measured and the results are given in Table 6.3. The plots of refractive index and film thickness versus conversion are shown in Figures 6.8 and 6.9 respectively. In this study, the following procedures were used to ensure the comparability and consistency of the results. After the prepolymer thin film was spin coated on silicon substrate, the refractive index and film thickness was measured by a prism coupler, and the conversion of polycyanuate was measured by FTIR. Then the polycyanurate film was cured to a higher conversion and after that the refractive index, film thickness and conversion were measured again. Then the film was cured further followed by the measurement of the three parameters. This is repeated till the conversion reaches a stable value.

Table 6.3 Refractive indices, film thickness and conversion of polycyanurate homopolymer thin films

Polycyanurate	Conversion, α	Refractive index, n	n/n_{max} [1] (%)	Film thickness, d (μm)	d/d_0 [2] (%)
BACy	0.443	1.6051	99.282	2.1771	100
	0.523	1.6072	99.412	2.1518	98.84
	0.584	1.6088	99.511	2.1505	98.78
	0.603	1.6093	99.542	2.1494	98.73
	0.672	1.6103	99.604	2.1484	98.68
	0.718	1.6124	99.728	2.1474	98.64
	0.752	1.6143	99.852	2.1458	98.56
	0.814	1.6163	99.975	2.1446	98.51
	0.897	1.6166	99.994	2.1439	98.48
	0.953	1.6167	100	2.1438	98.47
BFCy	0.453	1.5376	99.245	2.3479	100
	0.513	1.5394	99.361	2.3266	99.09
	0.576	1.5408	99.451	2.3242	98.99
	0.623	1.5412	99.477	2.3228	98.93
	0.657	1.5428	99.580	2.3206	98.84
	0.725	1.5446	99.696	2.3195	98.79
	0.764	1.5473	99.871	2.3186	98.75
	0.797	1.5488	99.968	2.3171	98.69
	0.881	1.5492	99.994	2.3165	98.66
	0.938	1.5493	100	2.3164	98.66
DFCy	0.448	1.4291	98.524	2.3018	100
	0.518	1.4319	98.718	2.2786	98.99
	0.580	1.4347	98.911	2.2740	98.79
	0.613	1.4367	99.049	2.2690	98.68
	0.665	1.4382	99.152	2.2662	98.45
	0.722	1.4428	99.469	2.2631	98.32
	0.758	1.4464	99.717	2.2598	98.18
	0.806	1.4497	99.945	2.2584	98.11
	0.889	1.4501	99.972	2.2569	98.05
	0.946	1.4505	100	2.2565	98.03

(1): n/n_{max}, refractive index change; n, refractive index of polycyanurate at conversion α; n_{max}, refractive index of polycyanurate at maximum conversion.

(2): d/d_0, film thickness change; d, film thickness of polycyanurate at conversion α; d_0, initial film thickness.

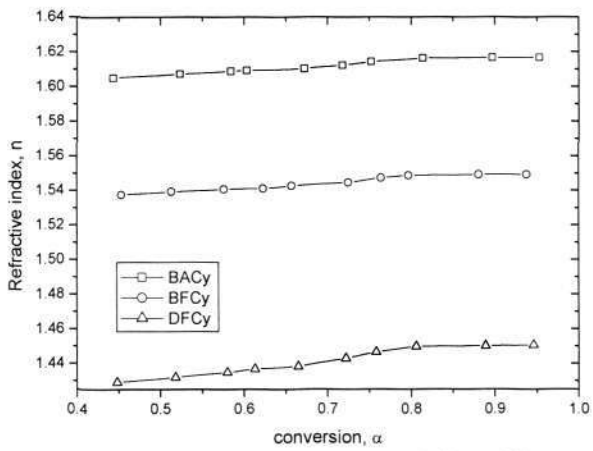

Figure 6.8 Refractive indices of polycyanurate thin films at different conversions

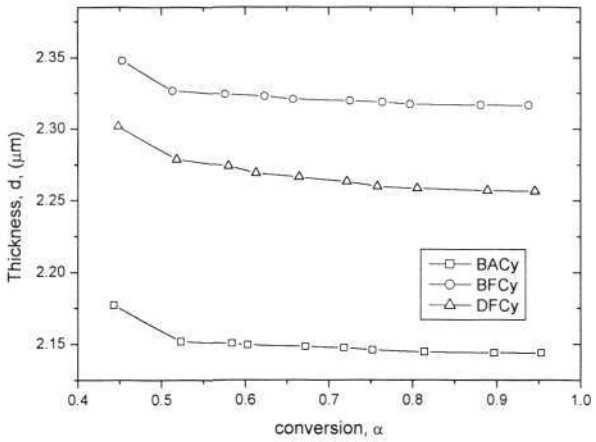

Figure 6.9 Film thickness of polycyanurate thin films at different conversions

From Figure 6.8, it can be seen that there is a consistent but gradual increase in the refractive index with conversion for all the three polycyanurate homopolymers. This is because the molecule packing density increases with conversion, resulting in increase of refractive index. At lower conversion, the increase of refractive index with conversion is faster than that at higher conversion. For example, the refractive index of BACy film increases from 1.6051 to 1.6103 ($\Delta n = 0.0052$) when the conversion increases from 0.443 to 0.672 ($\Delta\alpha = 0.229$), while the index increases from 1.6124 to 1.6167 ($\Delta n = 0.0043$) when the conversion increases from 0.718 to 0.953 ($\Delta\alpha = 0.235$). This can be clearly observed from the plot of the normalized refractive index versus conversion as shown in Figure 6.10, where the refractive index is normalized against the maximum value. After the conversion reaches 0.8, There is hardly increase in the refractive index, indicating that the polycyanurates have stable refractive indices at relatively higher conversion ($\alpha > 0.8$).

The index increments of the three polycyanurate homopolymers were found to be 0.0116, 0.0117 and 0.0214 for BACy, BFCy and DFCy thin films respectively. The DFCy homopolymer has a higher index increment than that of other two polycyanurates studied in this work. This is probably due to the flexible aliphatic structure of DFCy. After curing,

DFCy may form denser molecule packing than that of BACy and BFCy which have rigid aromatic structures.

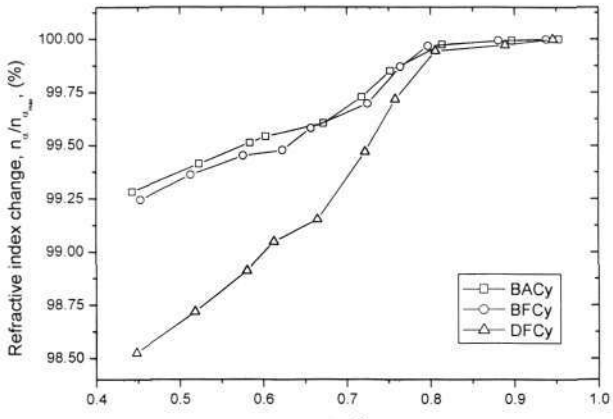

Figure 6.10 Refractive indices versus conversion of polycyanurate thin films

Figure 6.9 shows the thickness of the polycyanurate thin films at different conversions. For better clarity, normalized thickness against the initial thickness is plotted as a function of conversion in Figure 6.11. The thickness reductions of BACy, BFCy and DFCy are 1.93%, 1.34% and 1.53% respectively before and after curing. Similar to the index results, DFCy has a highest thickness change among the three polycyanurates, which also indicating DFCy has highest change in molecule packing density during curing. It also can be observed from Figure 6.11 that the thickness change curve of DFCy homopolymer is different from that of BACy and BFCy homopolymers. Comparing to BACy and BFCy, the film thickness of DFCy reaches a plateau at a higher conversion. This is attributed to the differences in the aromatic and aliphatic molecular structure of BACy, BFCy and DFCy. For aromatic BACy and BFCy, the steric effects of the rigid molecular chain hinder the molecule packing processing, result in slower decrease of film thickness after a moderate conversion.

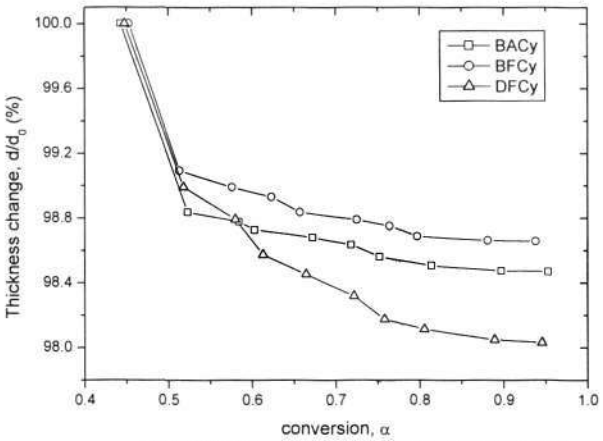

Figure 6.11 Film thickness change versus conversion of polycyanurate thin films

Another important effect seen in Figure 6.8 is that the molecular structure has great influence on the refractive index of polycyanurate. BACy homopolymer thin films have refractive indices around 1.61, BFCy homopolymer thin films have refractive indices around 1.54 and DFCy homopolymer thin films have refractive indices around 1.44. The large differences in refractive index indicate that it maybe possible to tune the refractive index of polycyanurate by copolymerization. This difference in refractive index may result from the difference in polymer structure particularly fluorine content. The fluorine contents of BACy, BFCy and DFCy polycyanurates are 0 wt.%, 29.5 wt.% and 55.3 wt.% respectively, according to their molecular formulas. The incorporation of fluorine atoms in the polymers can affect the refractive index in two ways simultaneously [105]. First, the increase in free volume, which often accompanies fluorine substitution, may decrease the refractive index attributed to the greater steric volume of fluorine relative to hydrogen, which may interfere with efficient chain packing. Second, the electronic polarizability is always lowered with fluorine substitution because of the smaller electronic polarization of C-F bond relative to C-H bond. The high content of fluorine is one of the reasons why DFCy homopolymer has a much lower refractive index than the other polycyanurate

polymers. Another feature contributing to raise the refractive index of BACy and BFCy is their high electronic polarizability resulting from conjugated aromatic structure.

By using the Lorenz-Lorentz equation and based on group contribution consideration, the theoretical refractive index of polycyanurate can be estimated. The Lorenz-Lorentz equation is given as follow [114]:

$$\frac{n^2-1}{n^2+2}\frac{M_G}{\rho} = R_L = \sum_{j=1}^{J} k_j R_j \qquad \text{(Equation 6.6)}$$

where n is the refractive index, M_G is the molecular weight of the repeating unit, ρ is the density (g/cm^3), R_L is the molar refraction (cm^3/mol), k_j is the number of increments of the substructure j in the repeating unit, R_j is the molar refraction increment of substructure j (cm^3/mol), and J is the total number of individual substructures. Using Equation 6.6, the theoretical refractive index of a polymer is given by:

$$n = \left[\frac{M_G/\rho + 2R_L}{M_G/\rho - R_L}\right]^{1/2} = \left[\frac{M_G/\rho + 2\sum_{j=1}^{J} k_j R_j}{M_G/\rho - \sum_{j=1}^{J} k_j R_j}\right]^{1/2} \qquad \text{(Equation 6.7)}$$

According to Equation 6.6 the molar refraction R_L can be regarded as a sum of refraction increments R_j, each corresponding to particular functional group within the polymer repeating unit. The repeating unit in polycyanurate crosslink network is illustrated in Figure 6.12. Table 6.4 shows the substructures of BACy, BFCy and DFCy and the calculation of theoretical refractive indices.

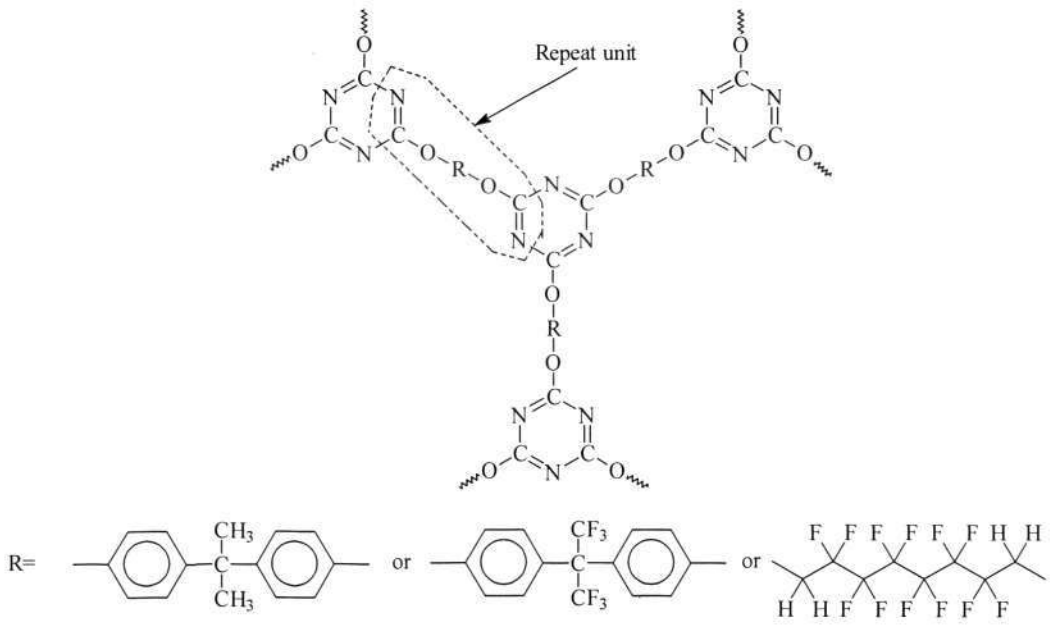

Figure 6.12 Illustration of repeat unit of polycyanurate for estimation of refractive index

Table 6.4 Substructures and calculation of theoretical refractive index of polycyanurates

polycyanurate	Substructure	R_j	k_j	k_jR_j	R_L	M_G/ρ	n*
BACy	CN	6.477	2	12.954	80.45	231.67	1.6112 (1.6167)
	O (ether)	1.625	2	3.250			
	p-C_6H_4 (arom)	25.235	2	50.470			
	CH_3	5.901	1	5.901			
	CCH_3	7.875	1	7.875			
BFCy	CN	6.477	2	12.954	80.946	257.85	1.5404 (1.5502)
	O (ether)	1.625	2	3.250			
	p-C_6H_4 (arom)	25.235	2	50.470			
	CF_3	6.149	1	6.149			
	CCF_3	8.123	1	8.123			
DFCy	CN	6.477	2	12.954	50.578	221.98	1.3730 (1.4505)
	O (ether)	1.625	2	3.250			
	CH_2	4.504	2	9.008			
	CF_2	5.061	6	30.366			

* Values in brackets are experimental results

The calculated theoretical refractive indices of BACy, BFCy and DFCy are 1.6112, 1.5404 and 1.3730 respectively, and the experimental values are 1.6167, 1.5493 and 1.4505 respectively. The predicted refractive index of DFCy is lower than the experimental value, which maybe due to its higher molecule packing density. Equation

6.6 and 6.7 are useful for predicting the refractive index of an unknown polymer and also useful for designing a polymer structure with specific refractive index.

6.3.2 Effect of Copolymerization on Refractive Index

Table 6.5 gives the experimental refractive indices at TE and TM mode, and the birefringence of BACy/BFCy, BACy/DFCy and BACy/CPCy copolymer thin films at wavelengths of 632.8 nm and 1539 nm. The plots of refractive index and birefringence versus BACy content of the polycyanurate thin films are shown in Figures 6.13 to 6.15.

Table 6.5 Refractive index of polycyanurate cured polymer thin films

	632.8 nm			1539 nm		
	n_{TE}	n_{TM}	Birefringence	n_{TE}	n_{TM}	birefringence
BACy:BFCy						
1:0	1.6167	1.6141	0.0026	1.5945	1.5934	0.0011
8:2	1.6079	1.6071	0.0008	1.5848	1.5846	0.0002
6:4	1.5929	1.5926	0.0003	1.5804	1.5765	0.0009
5:5	1.5893	1.5875	0.0018	1.5676	1.5667	0.0009
4:6	1.5785	1.5768	0.0027	1.5569	1.5565	0.0004
2:8	1.5669	1.5649	0.0020	1.5490	1.5456	0.0034
0:1	1.5502	1.5493	0.0009	1.5369	1.5331	0.0038
BACy:DFCy						
1:0	1.6167	1.6141	0.0026	1.5945	1.5934	0.0011
8:2	1.6094	1.6092	0.0002	1.5878	1.5876	0.0002
6:4	1.5675	1.5674	0.0001	1.5681	1.5672	0.0009
5:5	1.5464	1.5456	0.0008	1.5462	1.5458	0.0004
4:6	1.5385	1.5374	0.0011	1.5212	1.5208	0.0004
2:8	1.5178	1.5157	0.0021	1.5059	1.5037	0.0022
0:1	1.4508	2.4501	0.0007	1.4438	1.4435	0.0003
BACy:CPCy						
1:0	1.6167	1.6141	0.0026	1.5945	1.5934	0.0011
8:2	1.6077	1.6061	0.0016	1.5879	1.5866	0.0013
6:4	1.6005	1.5968	0.0019	1.5820	1.5813	0.0007
5:5	1.5947	1.5928	0.0019	1.5807	1.5797	0.0010

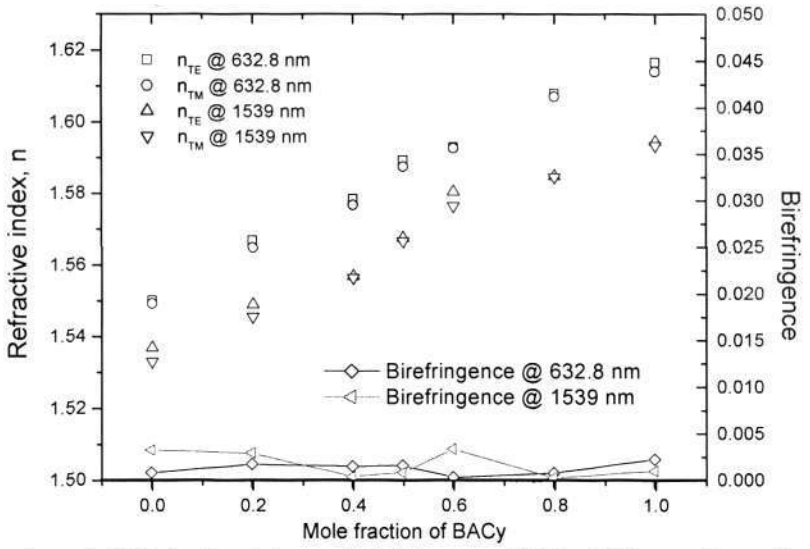

Figure 6.13 Refractive index and birefringence of BACy/BFCy copolymer films at wavelength 632.8 nm and 1539 nm

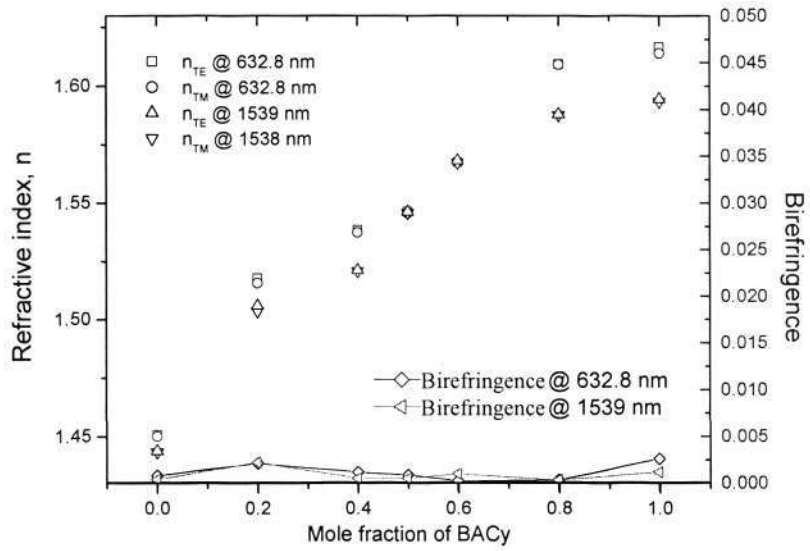

Figure 6.14 Refractive index and birefringence of BACy/DFCy copolymer films at wavelength 632.8 nm and 1539 nm

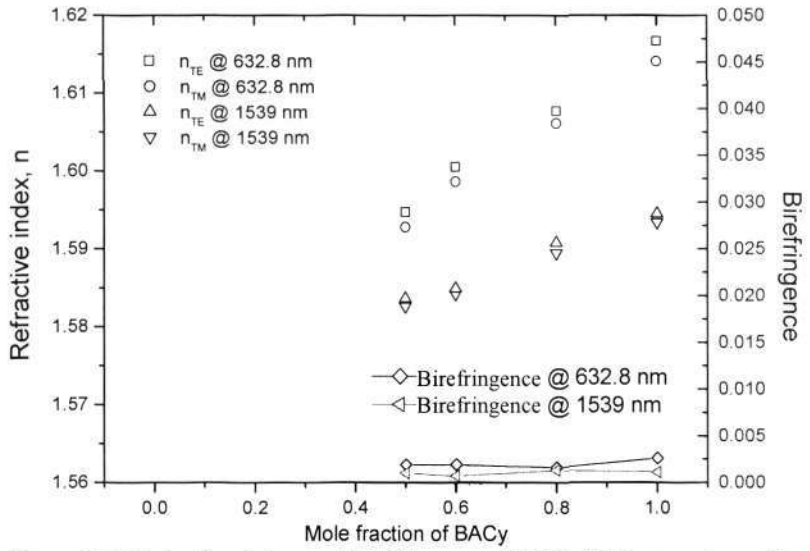

Figure 6.15 Refractive index and birefringence of BACy/CPCy copolymer films at wavelength 632.8 nm and 1539 nm

It can be seen from Figures 6.13 to 6.15 that a very broad and continuously adjustable range of refractive index, from 1.45 to 1.61 has been realized by controlling the composition of the polycyanurate copolymer systems. This adjustable range is very large in comparison to inorganic materials whose adjustable range is typically in the region around 0.02 [145]. The curves of BACy/DFCy show more deviation from linear relationship than BACy/BFCy and BACy/CPCy systems. In this case positive deviations were observed where the refractive indices of copolymers are slight higher than that predicted by the rule of mixture. As known, one of the effects influences the refractive index of a polymer is its free volume. The rule of mixture considers the free volume of a copolymer is simply the sum of the two components. This may not be always true, because there is interaction between the two components. For example, such interaction of the molecular chains or side groups of the two components may result in a reduced free volume of the copolymer and an increased refractive index. The interaction may also have effects on the intermolecular forces and dipole orientation polarization and/or electronic polarization, which in turn influences the refractive index.

To quantify the extent of interaction in different polycyanurate copolymer systems, the relationship between the refractive index and composition is curve fitted using Gordon-Taylor equation:

$$n_{AB} = \frac{kX_A n_A + X_B n_B}{kX_A + X_B} \quad (n_A > n_B) \qquad \text{(Equation 6.8)}$$

where n_{AB} is the refractive index of the polycyanurate binary copolymer, X_A and X_B are the molar fractions of the two individual components, respectively, n_A and n_B are the refractive indices of the polymer A and B, respectively, and k is an adjust parameter. k also can be regarded as the interaction parameter of homopolymer A and B. If there is no extra interaction between A and B in the copolymer, this is the case of rule of mixture, and the following equation should stand:

$$n_{AB} = X_A n_A + X_B n_B \qquad \text{(Equation 6.9)}$$

In fact the rule of mixture is a special case of Gordon-Taylor equation, in which the interaction parameter k equals to 1. If there is extra interaction between the two components, the value of k will not equal to 1. That is to say, the value of k can reflect the degree of interaction, which is related to their different molecular structures. This is interesting, because this similarity (difference in molecular structures) can be quantified by the value of the interaction parameter k. To study the effects of conversion on the interaction parameter k, the refractive indices of the polycyanurate prepolymers were also measured and analyzed. Table 6.6 shows the refractive index of polycyanurate cured prepolymer thin films

Figures 6.16 to 6.18 shows the Gordon-Taylor plot of the polycyanurate copolymer systems. Table 6.7 shows the k values of each polycyanurate copolymer systems at the two wavelength 632.8 nm and 1539 nm for both prepolymer and cured polymers.

Table 6.6 Refractive index of polycyanurate prepolymer thin films

	632.8 nm			1539 nm		
	n_{TE}	n_{TM}	Birefringence	n_{TE}	n_{TM}	Birefringence
BACy:BFCy						
1:0	1.6051	1.6025	0.0026	1.5839	1.5809	0.0030
8:2	1.5959	1.5950	0.0009	1.5775	1.5771	0.0004
6:4	1.5811	1.5810	0.0001	1.5640	1.5639	0.0001
5:5	1.5761	1.5758	0.0003	1.5600	1.5597	0.0003
4:6	1.5665	1.5644	0.0021	1.5505	1.5502	0.0003
2:8	1.5549	1.5548	0.0001	1.5394	1.5380	0.0014
0:1	1.5381	1.5376	0.0005	1.5271	1.5247	0.0024
BACy:DFCy						
1:0	1.6051	1.6025	0.0026	1.5839	1.5809	0.0030
8:2	1.5824	1.5798	0.0026	1.5761	1.5731	0.0030
6:4	1.5741	1.5735	0.0006	1.5397	1.5398	0.0001
5:5	1.5554	1.5546	0.0008	1.5314	1.5312	0.0002
4:6	1.5349	1.5323	0.0026	1.5168	1.5157	0.0011
2:8	1.4956	1.4922	0.0034	1.4671	1.4644	0.0027
0:1	1.4391	1.4368	0.0023	1.4163	1.4145	0.0018
BACy:CPCy						
1:0	1.6051	1.6025	0.0026	1.5839	1.5809	0.0030
8:2	1.5982	1.5962	0.0020	1.5770	1.5746	0.0024
6:4	1.5898	1.5883	0.0015	1.5686	1.5667	0.0019
5:5	1.5863	1.5849	0.0014	1.5641	1.5633	0.0018

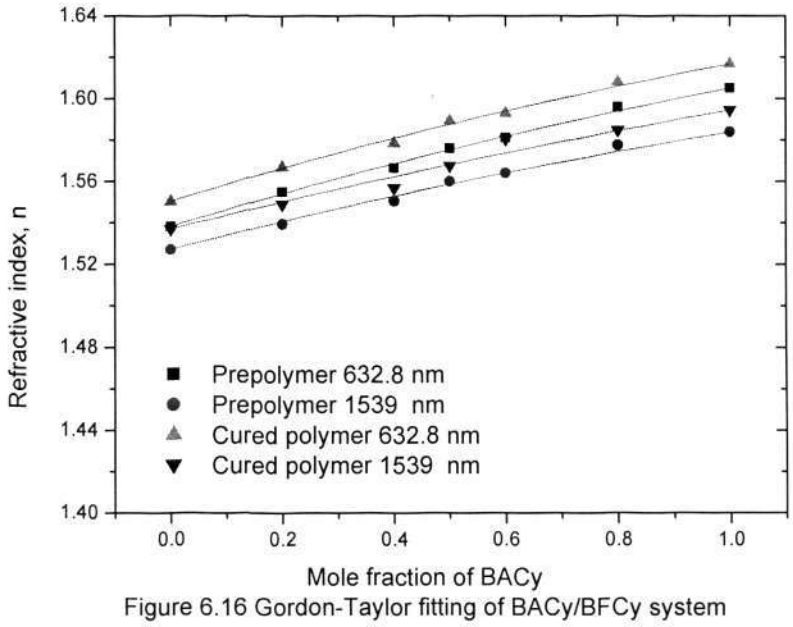

Figure 6.16 Gordon-Taylor fitting of BACy/BFCy system

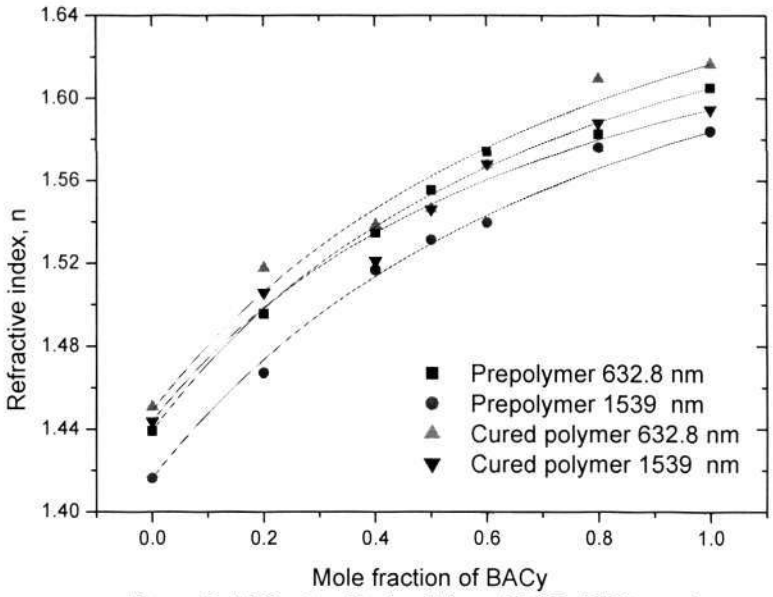

Figure 6.17 Gordon-Taylor fitting of BACy/DFCy system

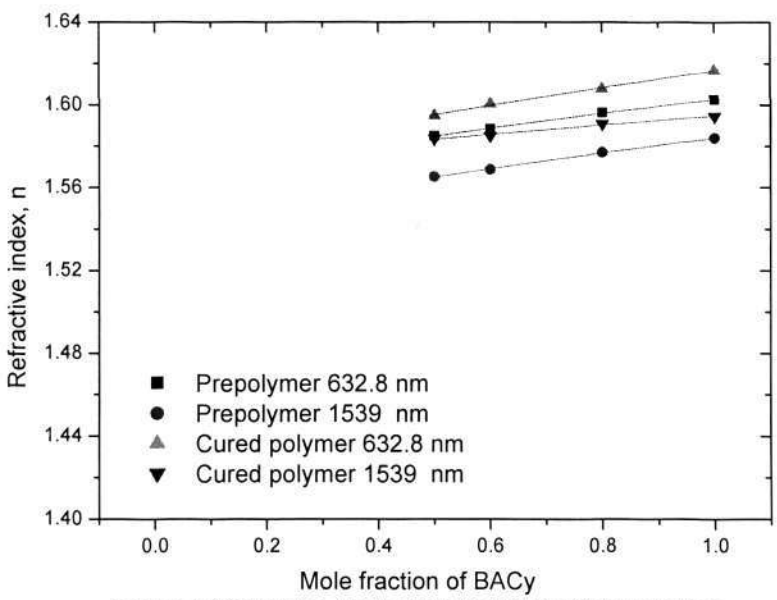

Figure 6.18 Gordon-Taylor fitting of BACy/CPCy system

Table 6.7 Summary of k values of Gordon-Taylor Equation

Polycyanurate system	632.8 nm		1539 nm	
	k	R^2	k	R^2
BACy/BFCy prepolymer	1.25	0.997	1.24	0.992
BACy/BFCy cured polymer	1.28	0.996	1.22	0.971
BACy/DFCy prepolymer	2.20	0.994	2.11	0.992
BACy/DFCy cured polymer	2.08	0.992	2.23	0.978
BACy/CPCy prepolymer	1.19	0.998	1.18	0.998
BACy/CPCy cured polymer	1.15	0.995	1.16	0.987

The refractive index data of poylcyanurate thin films shown in Figures 6.16 to 6.18 and Table 6.7 are of prepolymers and cured polymers at wavelength 632.8 nm and 1539 nm, thus for each polycyanurate copolymer system, there are four groups of data and four Gordon-Taylor fitting lines. From Figures 6.16 to 6.18, it can be seen that the Gordon-Taylor fitting lines for each series of copolymers are almost parallel in all the Figures, which means their k values are closer to each other as shown in Table 6.7. This means that the interactions between the components in the copolymers are not affected by the measuring wavelength. Also, no appreciable difference in k value was noted between the prepolymer and curd copolymer thin films.

However, the differences among the three polycyanurate copolymer systems can be clearly seen from Figures 6.16 to 6.18 and also from the k values in Table 6.7. The BACy/BFCy and BACy/CPCy polycyanurate copolymer systems show nearer linear relationship between the refractive index and the mole fraction of BACy, and their average k values are 1.25 and 1.17 respectively. The BACy/DFCy system shows large deviation from the rule of mixture and the average interaction parameter k value is 2.16. It can be concluded that the similarity of the three polycyanurate copolymer systems is in the order: BACy/CPCy > BACy/BFCy > BACy/DFCy. BACy and CPCy have very similar molecular structure, the only difference between them is that BACy is

difunctional and CPCy is monofunctional. Thus, BACy and CPCy have the highest similarity among the polycyanurate systems studied in this work. BFCy also has similar molecular structure and physical geometry to BACy. On the contrary, DFCy has very different molecular structure comparing to BACy, which cause the largest deviation from the rule of mixture among the polycyanurate systems studied in this work. It should be pointed out that the "interaction" discussed here is in the context of the variation of refractive index within the copolymer components. This interaction refers to the possible change in molecular packing and/or intermolecular forces. Understanding this is helpful in modification of the optical properties of polycyanurate and fabrication of optical devices.

6.4 Birefringence of Polycyanurate Thin Films

Birefringence, also called double refraction, occurs when an optical materials in the path of a light beam causes the beam to be split into two polarization components which travel at different velocities [172,173]. Birefringence is measured as the difference of refractive indices of the two polarization components traveling through the material.

$$\Delta n = n_{TE} - n_{TM} \qquad \text{(Equation 6.10)}$$

where Δn is the birefringence, n_{TE} and n_{TM} are the refractive indices at transverse electric mode and magnetic mode respectively. Birefringence indicates the optical anisotropy of a material. Birefringence is an intrinsic property of many optical materials, and may also be induced by external forces applied to the materials. Induced birefringence may be temporary, as when a material is stimulated by an external field. Residual birefringence may occur when, for example, a material experiences thermal stress during processing or thermal treatment. Polymers are typically spin coated onto

substrates where the spin coating and curing processes may leads to a molecular ordering, resulting in in-plane and out-of-plane optical anisotropy for the thin polymer films [174].

For applications in optical communication, it is desirable that an optical material has birefringence as low as possible (ideally $< 5\times10^{-5}$) [103]. Higher birefringence will increase the polarization dependent loss. The polarization dependent loss requirement demands that the channel wavelength shift between TE and TM polarized light should be minimized. For example, a birefringence of $\Delta n = 0.001$ will give channel shift of the order of ~1 nm, which may not be acceptable for some devices [175].

In this study, the birefringence of all the polycyanurate thin films is in the range of 0.0001-0.0030, which is acceptable for optical waveguide applications. It also can be seen from Figures 6.16 to 6.18 that there is no clear regular relationship between the birefringence and the composition for the polycyanurate thin films. Our explanation is as below. As have been mentioned, birefringence of a material is affected by many complicated factors. The birefringence of the polycyanurate not only depends on the composition of the copolymers but also considerably depends on many other factors, such as the nature of the substrate, stress in the film, morphology of the film. Unlike silica glass, whose birefringence is directly and solely the result of stress formed in processing, the birefringence of polymer materials comes mainly from the preferred orientation of rigid groups and polymer chains, although the orientation may be induced by stress during the formation of the final polymer thin films. Stress induced birefringence is associated with bending, twisting, and generally deforming polymers [103]. Studies have also shown that the substrate plays and important role in inducing birefringence of thermally cured films, because of the mismatching of thermal expansion coefficients of the polymer and the substrate. Polycyanurate thin film has higher birefringence on silicon

substrate than on polymer substrates [27]. We believe that the birefringence of polycyanurate thin films can be further reduced after the processing is optimized and proper substrate is used.

6.5 Propagation Loss of Polycyanurate Thin Films

Table 6.8 shows the optical propagation loss of polycyanurate prepolymer and the cured polymer thin films measured by prism coupler at wavelength 1539 nm. Figure 6.19 shows the propagation loss versus composition of the cured polycyanurate films.

Table 6.8 Propagation loss of polycyanurate prepolymer and cured polymer thin films

Mole ratio	Prepolymer (dB/cm)			Cured polymer (dB/cm)		
	BFCy/BACy	DFCy/BACy	CPCy/BACy	BFCy/BACy	DFCy/BACy	CPCy/BACy
0:1	1.65	1.65	1.65	1.82	1.82	1.82
2:8	1.54	1.57	1.62	1.72	1.74	1.79
4:6	1.42	1.46	1.60	1.59	1.64	1.76
5:5	1.36	1.38	1.59	1.53	1.56	1.75
6:4	1.29	1.29	--	1.45	1.47	--
8:2	1.14	1.09	--	1.29	1.28	--
1:0	1.01	0.86	--	1.13	1.07	--

It can be seen from Table 6.8 that curing process seems to have caused an increase in the optical propagation loss. For example, the propagation loss of BACy, BFCy and DFCy films are of 1.62 dB/cm, 1.01 dB/cm and 0.86 dB/cm respectively, while the cured thin films have optical loss of 1.82 dB/cm, 1.14 dB/cm and 1.07 dB/cm respectively. The reason for this is not completely clear. However, the increase in propagation loss is only about 10% which is not very significant. The propagation losses of BACy and BFCy homopolymers are higher than the reported values [27,28], which is probably due to different processing conditions. For example, the films were cured in air while the samples reported in the literature were cured in nitrogen.

It is understandable that the fluorinated polycyanurate thin films, including the aromatic and aliphatic, have much lower propagation loss than the non-fluorinated polycyanurate films as shown in Figure 6.19. The loss of their copolymer films is between that of the two individual components of the polycyanurate copolymer. However, it is quite unexpected that the difference between the propagation loss of the two fluorinated polycyanurate thin films (BFCy and DFCy) are very small (only 0.06 dB/cm for cured polymer films), although the aliphatic DFCy has a much higher fluorine content (55.3%) than BFCy (29.5%). This probably because that the DFCy monomer also contains CH bonds which lead to higher propagation loss. Although BFCy also contains CH bonds, they are of aromatic CH bonds but not aliphatic. It is known that aliphatic CH bonds cause relative higher propagation loss compared to aromatic CH bonds which has been discussed in the literature review in Chapter 2.

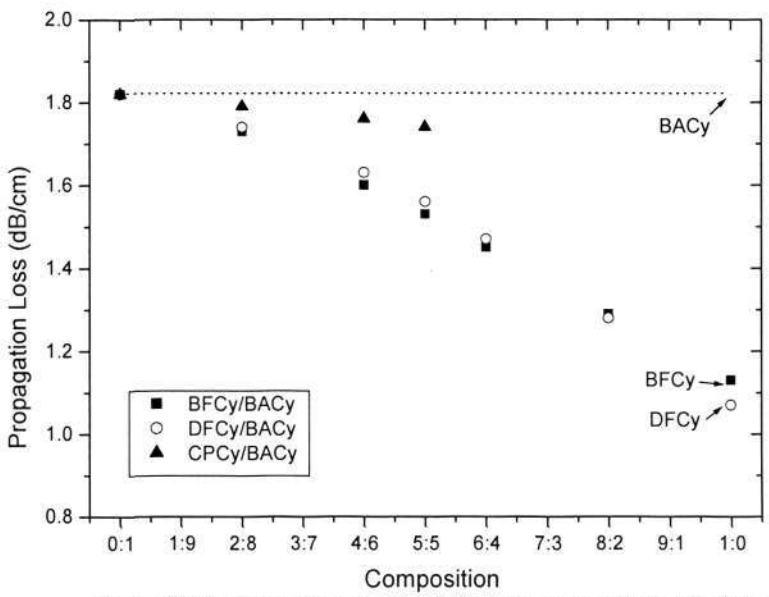

Figure 6.19 Propagation Loss of cured polycyanurate thin films

It can also be seen from Figure 6.19 that the relationship between the optical propagation loss and composition for all the polycyanurate thin films deviates from linearity. Further

analysis of this deviation $\Delta\phi$ as exemplified in Figure 6.20 for the BACy/DFCy system, shows that $\Delta\phi$ is dependent on compositions.

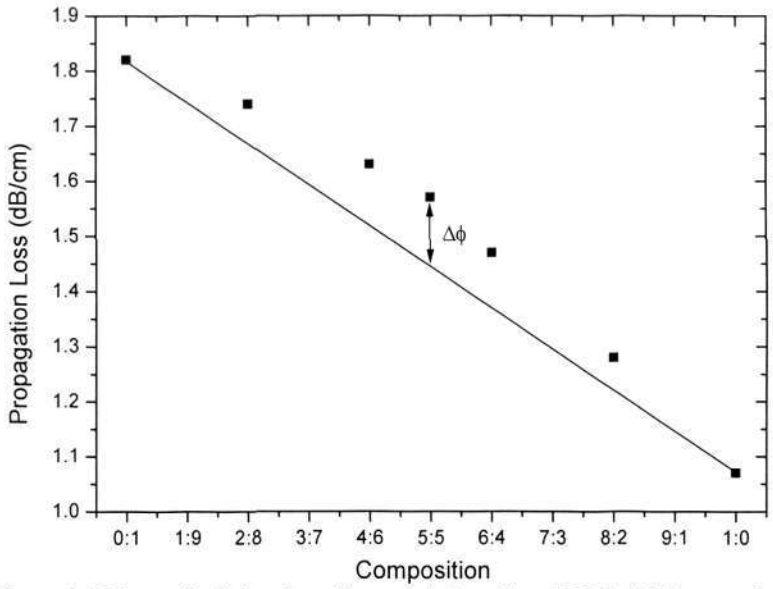

Figure 6.20 Loss deviation from linear relationship of BACy/DFCy cured polymer

The propagation loss deviations ($\Delta\phi$) for the BACy/BFCy and BACy/DFCy copolymers are shown in Figure 6.21.

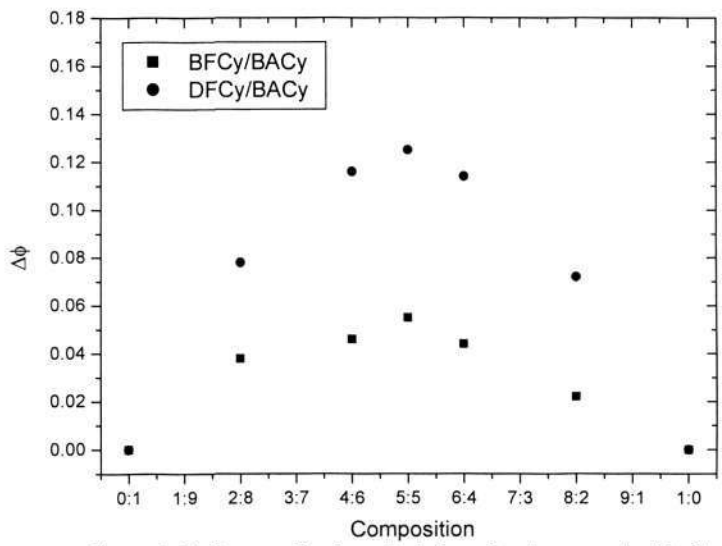

Figure 6.21 Propagation loss deviation of polycyanurate thin films

It can be seen from Figure 6.21 that $\Delta\phi$ changes with composition and reaches the highest value at 5:5 for all the copolymer systems. For a given composition, BACy/DFCy has a higher deviation among the two copolymer systems. For example, at composition 4:6, $\Delta\phi$ values are 0.12 dB/cm and 0.05 dB/cm for BACy/DFCy and BACy/BFCy respectively. It is believed that this deviation is caused by the inhomogeneity due to copolymerization. For a given copolymer, the inhomogeneity increases with the increase of mole fraction of one component and reaches maximum before decreases again when this component becomes the major consistent. For different copolymer systems, the inhomogeneity is strongly affected by the differences of the two components in the copolymer. It is easy to understand the inhomogeneities of the BACy/DFCy copolymers are higher than those of BACy/BFCy, in terms of their differences in molecular structures and geometries. This discussion is consistent with the dielectric analysis explained in Chapter 5. This is also supported by the DSC study which was discussed in Chapter 4. Most BACy/DFCy and BACy/BFCy copolymer of different composition showed a single reaction peak, while some BACy/DFCy copolymers showed an extra shoulder reaction peaks indicating the curing processing is not completely uniform which resulted in inhomogeneity in the cured copolymers.

6.6 Summary

We optimized various waveguide parameters, such as refractive index, thickness of the film, propagation loss and absorption spectra of polycyanurate thin films. The characterization of polycyanurate thin films revealed that the material exhibits unique properties and is promising for use in optical waveguide and integrated optical devices.

The study on the conversion effects on the refractive index shows that the refractive index of polycyanurate homopolymer thin films increases with the increase of curing conversion and reaches a stable value at conversion > 0.8, while the film thickness decreases with the increase of conversion and also reaches a stable value at conversion > 0.8. For both refractive index and film thickness, the aromatic polycyanuate (BACy and BFCy) change slower than aliphatic polycyanurate (DFCy) which may due to their different molecular packing density resulted from different steric effects.

The theoretical refractive indices of BACy, BFCy and DFCy homopolymers were calculated using a segment incremental model derived from Lorenz-Lorentz equation. The theoretical values have reasonable agreement with the experimental data.

The refractive index of the polycyanurate thin films can be controlled in a broad range of 1.44-1.61 by copolymerizing of four cyanate ester monomers, BACy, BFCy, DFCy and CPCy. The effect of composition on the refractive index can be described by the Gordon-Taylor type equation. And the interaction parameter k indicates and quantifies the similarity of different polycyanurate in the copolymer systems. The similarities of the polycyanurate copolymers are in the order: BACy/CPCy > BACy/BFCy > BACy/DFCy.

The propagation loss of the polycyanurate thin films is between 0.86-1.82 dB/cm. The inhomogeneity of the polycyanurate copolymers has strong effects on the propagation loss. For a given copolymer, inhomogeneity changes with composition and reaches the highest value at 5:5 for all the copolymer systems. For a given composition, the inhomogeneities of BACy/DFCy copolymers are higher than those of BACy/BFCy copolymers.

CHAPTER 7

THERMAL AND MECHANICAL PROPERTIES OF POLYCYANURATE THIN FILMS

7.1 Introduction

In the last two decades, polycyanurate resins have attracted a lot of research attention in the high performance composites and dielectric materials field. Polycyanurate resins have received considerable attention owing to their highly desirable chemical, physical, dielectric, thermal and mechanical properties [1-5]. New interests in optical waveguide and photonic applications have also evolved recently and they are expected to enthuse researchers for a long period of time in future [27-33]. Generally, for the applications of polymeric materials in universal passive waveguide devices, not only are the tunable refractive index and low optical propagation loss of great importance, but other properties such as high thermal stability and good mechanical properties are also necessary [103]. Characterization of different properties is important to evaluate the performance of the materials. In this thesis, various techniques were used to characterize the thermal, mechanical, optical and dielectric properties of polycyanurate resins and their thin films. Important properties such as the dielectric relaxation, refractive index and optical propagation loss have been measured and discussed in the previous chapters. In this Chapter, the thermal and mechanical properties of polycyanurates and their thin films will be discussed.

The glass transition temperature is an important thermal property of thermosetting polymers. The glass transition temperature of a copolymer or polymer blend can be calculated from values of the pure components. Various empirical or theoretical formulae were suguested and extensively used in practice [176-181]. Among them the Couchman equation is most frequently and universally used, which is based on classical thermodynamics consideration. For modelling the glass transition temperature versus conversion of homopolymer, the polymer can be assumed to be a random mixture of monomer and fully cured polymer, and then similar considersation as copolymer or blend systems can then be taken [93-97]. For study the composition and conversion effects on the glass transition temperature of polycyanurate copolymer, we suggest that it can be treated as a four-component system based on the thermodynamics consideration. In this Chapter, similar derivation procedures as original presented by Couchman [177] is applied to study the composition and conversion effects on the glass transition temperature of polycyanurate copolymer. Conversion dependence of the glass transition temperature of polycyanurate homopolymer is also discussed. This is not only important for prediction of the glass transition temperature of the polycyanurate copolymers, but also helpful in understanding the interaction between polycyanurates with different backbone structures and also essential to study the cure phenomena.

Characterization of mechanical properties of polymer thin films at surface or subsurface is important [182-184]. Fakirov et al. [184] found that there was a linear correlation between the hardness and the glass transition temperature for a number of polyolefine type amorphous polymers. Polycyanurate thin films have been widely used in adhesive and dielectric applications [34-38], and also promising in photonic applications [27-33]. However, the mechanical properties of polycyanurate thin films have not been reported so far. In this work, the nanoindentation technique, which provides an effective method to

study the deformation of thin films, was used to determine the hardness and modulus of polycyanurate homopolymer and copolymer thin films. Based on the experimental data and theoretical derivation, linear relationship was also found between the hardness and the glass transition temperature of polycyanurate thin films. However, the slope and the intercept are different from what Fakirov et al. reported, which is probably due to the differences in their chemical structures.

The thermal expansion of polymer materials is one of the important thermal-mechanical properties for many applications such as electronic devices and optical components. Thermal expansion of the cured polycyanurate homopolymers and copolymers are studied using TMA techniques.

7.2 Glass Transition Temperature of Polycyanurates

The glass transition temperature, Tg, is one of the most important material parameters of a polymer. Glass transition temperature can be treated as an endothermic transition of second order. The thermodynamic functions, entropy, enthalpy, and volume, are continuous at the glass transition temperature, but the first derivatives of these functions undergo discontinuities at the glass transition temperatures. Glass transition temperature marks the temperature boundary of significant changes in the viscoelastic, dilatometric, enthalpic properties of all glass-forming materials [97]. There are various techniques for determining the values of glass transition temperatures such as differential scanning calorimetry (DSC), thermomechanical, or dynamic mechanical analysis. In this work, DSC was utilized for the measurement of glass transition temperature and curing conversion of polycyanurate homopolymers and copolymers. Figure 7.1 shows the DSC curves of partial cured BACy samples. The conversion measurement followed the method

described in Chapter 3. Same procedures are used for both polycyanurate homopolymers and copolymers.

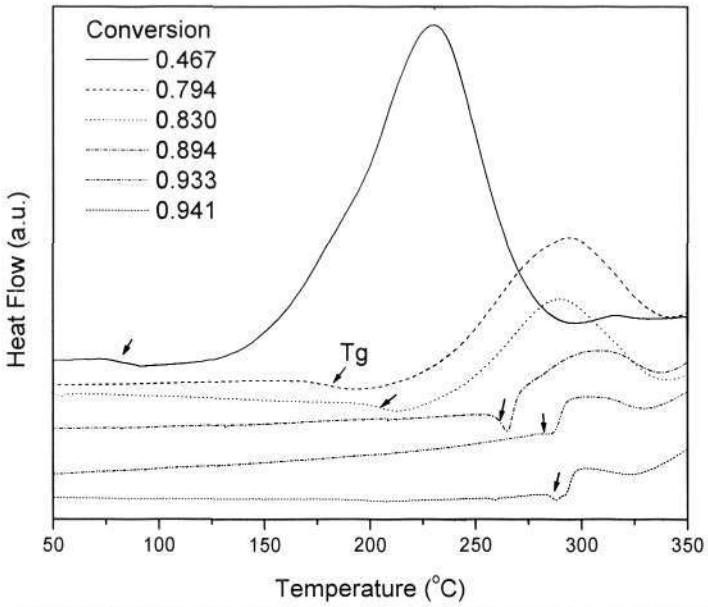

Figure 7.1 DSC measurement of Tg of BACy partial cured sample (the arrows indicating the glass transition temperatures)

For a fully cured polycyanurate, it is difficult to measure its Tg using normal DSC, because of the high crosslink density nature of thermosetting resin, the Tg relaxation transition may not be sensitive to normal DSC. MDSC is a more accurate method to measure the Tg of this type of materials, since it can separate the reversing and non-reversing heat flow from the total heal flow. This provides an increased sensitivity. Thus in this work MDSC was used to determine the Tg of fully cured polycyanurate samples, an example of MDSC measurement is shown in Figure 7.2.

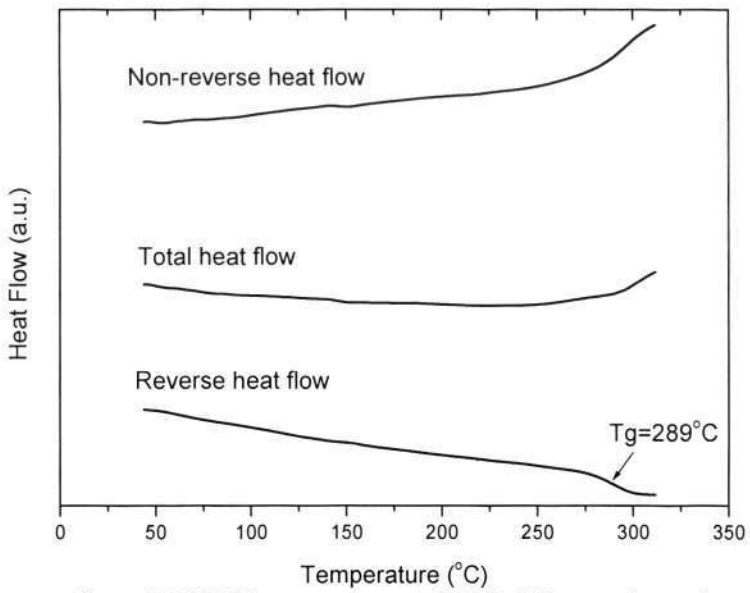

Figure 7.2 MDSC measurement of BACy fully cured sample

7.2.1 Effect of Composition on Glass Transition Temperature

Based on basic thermodynamic consideration, the dependency of glass transition temperature on composition can be derived [177]. Consider a copolymer from monomers A and B, the respective molar fractions of the two components in the system are denoted as X_A and X_B and the molar entropies of the pure components are designated in turn as S_A and S_B. The molar entropy, S, of the copolymer may be written generally as:

$$S = X_A S_A + X_B S_B + \Delta S \qquad \text{(Equation 7.1)}$$

where ΔS is the excess entropy of mixing which includes any and all excess entropy changes associated with mixing the two components. At a given temperature T, the entropies of the two components are related to their entropies at their respective glass transition temperature Tg, i.e., $S_A^{Tg_A}$ at Tg_A and $S_B^{Tg_B}$ at Tg_B. The following equation may be constructed from basic thermodynamic definitions:

$$S = X_A\left(S_A^{Tg_A} + \int_{Tg_A}^{T} Cp_A \ln T\right) + X_B\left(S_B^{Tg_B} + \int_{Tg_B}^{T} Cp_B \ln T\right) + \Delta S \qquad \text{(Equation 7.2)}$$

where Cp_A and Cp_B are the specific heat capacities at constant pressure of components A and B respectively. The glass transition temperature of the mixed system, Tg, is defined by the requirement that S in the glassy state is equal to S in the liquid/rubbery state [98].

$$S^l = S^g \qquad \text{(Equation 7.3)}$$

where the superscripts l and g denote the liquid/rubbery state and glassy state respectively. Incorporate Equation 7.2 in Equation 7.3:

$$X_A\left(S_A^{Tg_A,g} + \int_{Tg_A}^{Tg} Cp_A^g \ln T\right) + X_B\left(S_B^{Tg_B,g} + \int_{Tg_B}^{Tg} Cp_B^g \ln T\right) + \Delta S^g = X_A\left(S_A^{Tg_A,l} + \int_{Tg_A}^{Tg} Cp_A^l \ln T\right) + X_B\left(S_B^{Tg_B,l} + \int_{Tg_B}^{Tg} Cp_B^l \ln T\right) + \Delta S^l \qquad \text{(Equation 7.4)}$$

the choice of pure component reference states at Tg_A and Tg_B provides the indentities that $S_A^{Tg_A,g} = S_A^{Tg_A,l}$ and $S_B^{Tg_B,g} = S_B^{Tg_B,l}$. Further, the excess mixing entropy is continuous with respect to temperature at the glass transition temperature, $\Delta S^g = \Delta S^l$. After simplifying and regrouping, equation 7.4 becomes:

$$X_A\left(\int_{Tg_A}^{Tg} \Delta Cp_A \ln T\right) + X_B\left(\int_{Tg_B}^{Tg} \Delta Cp_B \ln T\right) = 0 \qquad \text{(Equation 7.5)}$$

where $\Delta Cp_A = Cp_A^l - Cp_A^g$ and $\Delta Cp_B = Cp_B^l - Cp_B^g$, respectively. Assuming [93]:

$$\Delta Cp(T) = \Delta Cp^{Tg} \times \frac{Tg}{T} \qquad \text{(Equation 7.6)}$$

solving Equation 7.5 can arrive:

$$Tg = \frac{X_A \Delta Cp_A Tg_A + X_B \Delta Cp_B Tg_B}{X_A \Delta Cp_A + X_B \Delta Cp_B} \qquad \text{(Equation 7.7)}$$

taking $k = \Delta Cp_B / \Delta Cp_A$ can obtain:

$$Tg = \frac{X_A Tg_A + kX_B Tg_B}{X_A + kX_B} \qquad \text{(Equation 7.8)}$$

Equation 7.8 was first derived by Couchman [177] and modified by Pascault and Williams [94]. It has the identical mathematical form as the Gordon-Taylor Equation

which are oringinal derived by Gordon and Taylor using volumetric arguments to predict the value of glass transition temperature of a linear random copolymer with repeat units A and B versus mole fraction of A and B [181]. The difference with Equation 7.8 and the Gordon-Taylor equation is that the parameter k in Gordon-Taylor is equal to $\Delta\alpha_A / \Delta\alpha_B$, where $\Delta\alpha_A$ and $\Delta\alpha_B$ are the differences in the thermal expansion coefficient between the liquid/rubbery state and the glassy state for polymer A and B respectively.

The relationship between glass transition temperature and conversion was derived by using general thermodynamic arguments, e.g., by equating the entropy of the liquid with the entropy of the glass at the glass transition. Information on structural features of the molecular architecture versus conversion are not necessary to utilize this equation. For example, the crosslink density, molecular weight, and the conversion at gelation are not used in the equation. Accordingly, this equation is general in its scope, capable of fitting glass transition temperature versus conversion for a wide variety of thermosetting structures [98].

For copolymer or binary miscible polymer blend, the dependence of glass transition temperature on composition also can be presented by two other well known empirical equations, Fox equation and the equation based on rule of mixture [179]:

$$\frac{1}{Tg} = \frac{X_A}{Tg_A} + \frac{X_B}{Tg_B} \quad \text{(Fox equation)} \qquad \text{(Equation 7.9)}$$

$$Tg = X_A Tg_A + X_B Tg_B \quad \text{(Rule of mixture)} \qquad \text{(Equation 7.10)}$$

In these two equations the interaction between components is not considered which may not suitable in our case.

Figures 7.3 to 7.5 show the MDSC measured results of glass transition temperatures of cured polycyanurate homopolymer and copolymer samples.

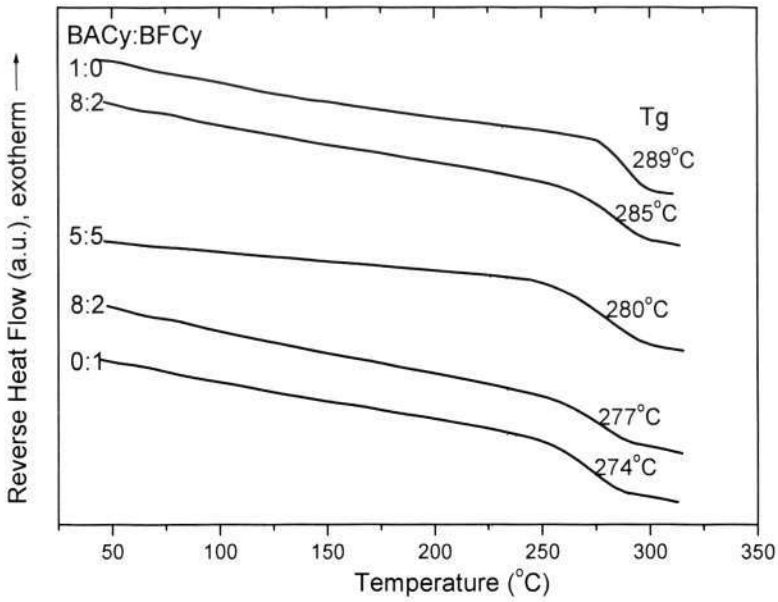

Figure 7.3 MDSC measurement of glass transition temperature of BACy/BFCy

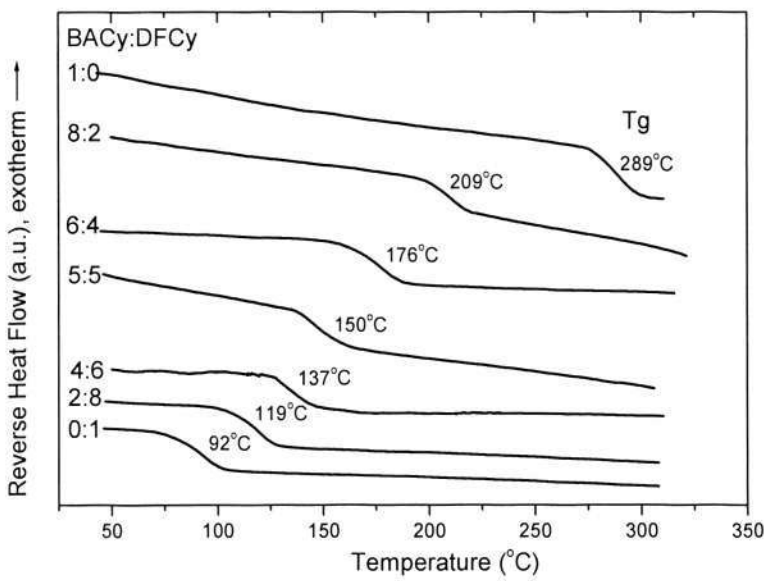

Figure 7.4 MDSC measurement of glass transition temperature of BACy/DFCy

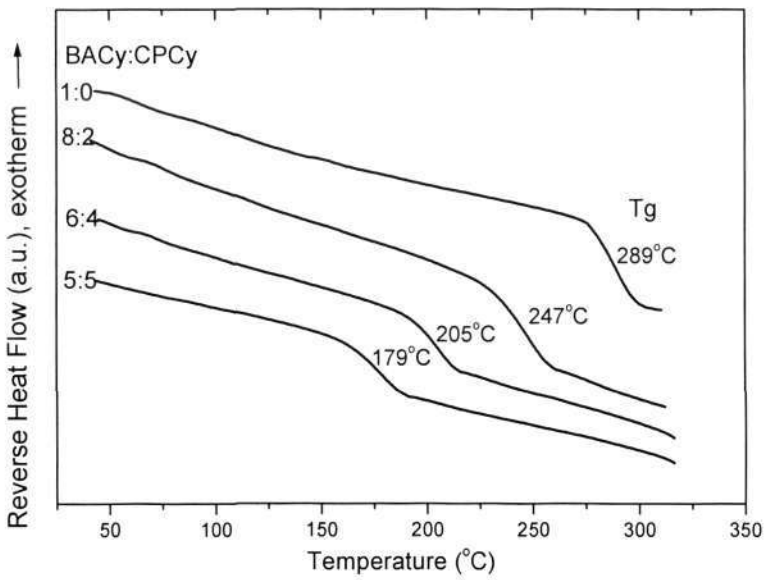

Figure 7.5 MDSC measurement of glass transition temperature of BACy/CPCy

It can be seen from Figure 7.3 to 7.5 that the glass transition temperature of the copolymer is between the two individual homopolymer components and dependent on the composition. DFCy and CPCy reduce the glass transtion temperature of BACy dramtically after copolymerization as expected. DFCy reduces the glass transition temperature of BACy because it introduces flexible aliphatic units into the copolymer, while CPCy reduces the glass transition temperature of BACy because it reduces the crosslinking density of BACy after copolymerization.

Figures 7.6 to 7.8 plot the experimentally data of glass transition temperatures versus conversion. For each copolymer series, the data were fitted using the least squares method to Equation 7.8 to yield the parameter k. The curves of Fox equation and rule of mixture are also shown in Figures 7.6 to 7.8 for comparison.

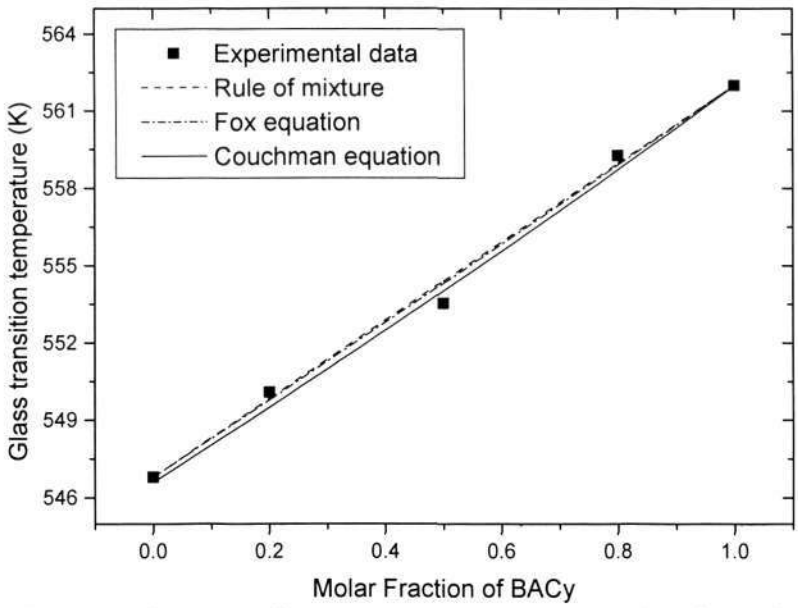

Figure 7.6 Glass transition temperature versus composition for BACy/BFCy

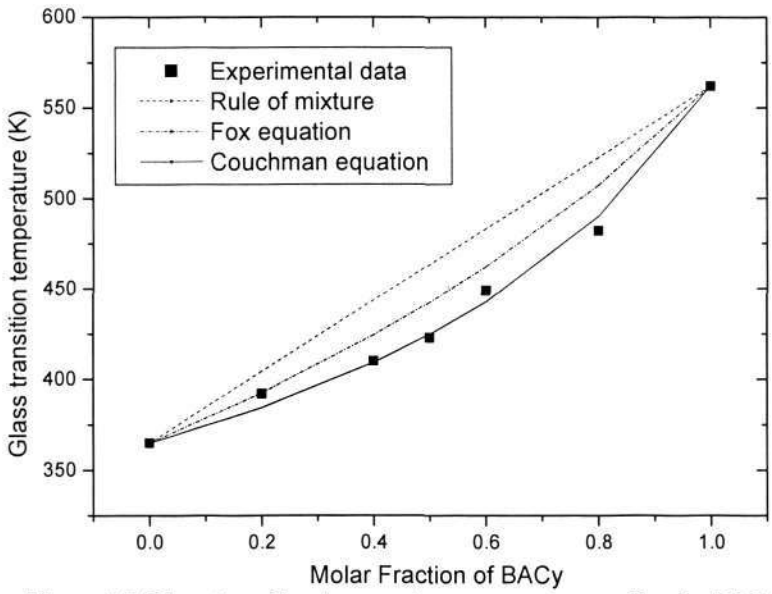

Figure 7.7 Glass transition temperature versus composition for BACy/DFCy

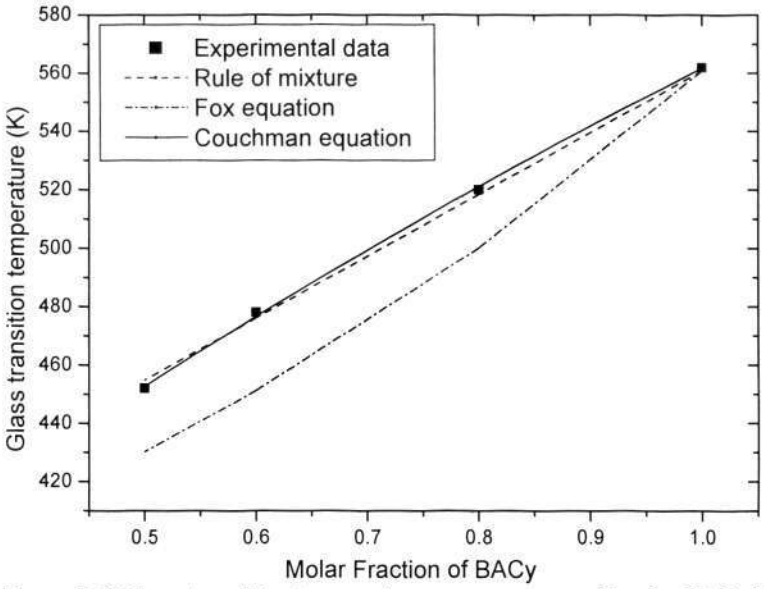

Figure 7.8 Glass transition temperature versus composition for BACy/CPCy (Note: the Tg of CPCy is obtained by a linearly extrapolating the data to molar fraction of BACy equal to zero)

From Figures 7.6 to 7.8, it can be observed that apparently the fittings of the dependence of glass transition temperature on composition for the polycyanurate copolymer systems are different. BACy/BFCy system can be fitted by all the three equations, BACy/CPCy system can be fitted by both the Couchman equation and the rule of mixture, while BACy/DFCy can only be fitted by Couchman equation. With proper k values, Couchman Equation fits the data of all the three polycyanurate copolymer systems very well. The obtained interaction parameter k values are 0.79, 0.44 and 0.93 for BACy/BFCy, BACy/DFCy and BACy/CPCy polycyanurate systems respectively. Therefore Couchman Equation can be effectively used to predict the glass transition temperature of a polycyanurate copolymer.

The glass transition temperature of a glassy material is mainly influenced by two factors, i.e., the intensity of the interaction force among molecules and the flexibity of the main chain [119]. For a copolymer, the relationship between the glass transition temperarure

and the composition may fall into four cases [119]. (1) When the two monomers A and B have similar properties, there may be a linear relationship between the glass transition temperature and the composition. As shown in Figure 7.9 curve A. (2) When the two monomers A and B have little different properties, the glass transition temperature of the copolymer may be slight lower than that predicted by the linear relationship. As shown in Figure 7.9 curve B. (3) When the two monomers A and B have large different properties, the glass transition temperature of the copolymer may be lower than those of both homopolymer A and B. As shown in Figure 7.9 curve C. (4) When the two components A and B have synergistic effect after copolymerization, the glass transition temperature of the copolymer may be higher than that predicted by the linear relationship. As shown in Figure 7.9 curve D. For example, if hydrogen bonds can be formed between the two components, or if strong interaction can be generated among the strong polarized groups, which will decrease the mobility of the molecular chain and result in higher glass transition temperature.

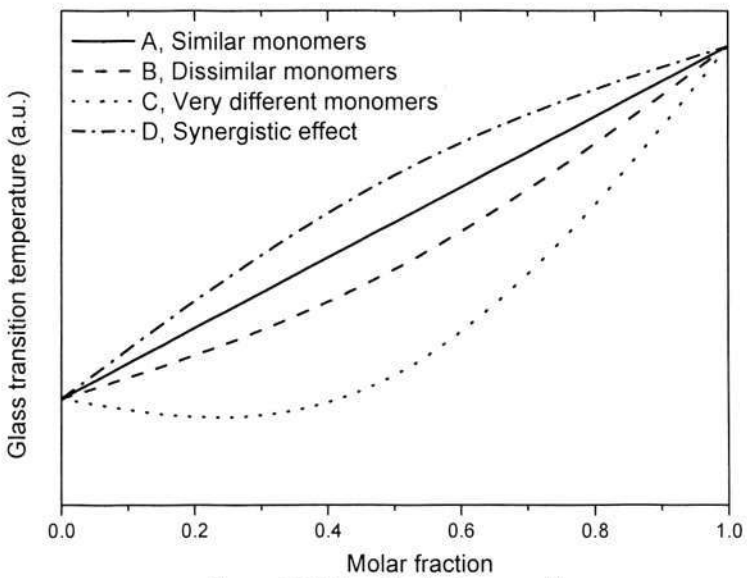

Figure 7.9 The effect of composition on the glass transition temperature of copolymers

It can be found from Figures 7.6 to 7.8 that the relationship between the glass transition temperature and molar fraction for BACy/BFCy and BACy/CPCy can be classified to the case (1), while that for BACy/DFCy copolymer system can be classified to the case (2). The differences of deviation from linear relationship also can be quantified in terms of the k values of Couchman Equation. CPCy and BFCy have similar backbone structure to BACy. The flexibity of the main chain and intensity of the intermolecular interaction forces should not change significantly by the copolymerization and therefore there is a linear dependency of glass transition temperature on composition. For BACy/DFCy copolymers, the two monomers BACy and DFCy have different backbone structures as shown in Figure 3.1 in Chapter 3. DFCy has a more flexible aliphatic structure, while BACy has a rigid and aromatic structure. In the BACy/DFCy copolymer, the entire crosslinking network contains both flexible aliphatic chains and rigid aromatic chains, although there is no phase boundary between the two parts as illustrated in Figure 7.10. After copolymerization, it is possible that the rigid networks become more flexible in the copolymer than in the homopolymer which has a different molecular 'environment'. Hence Tg of BACy/DFCy copolymer has the largest deviation from linear relationship with composition.

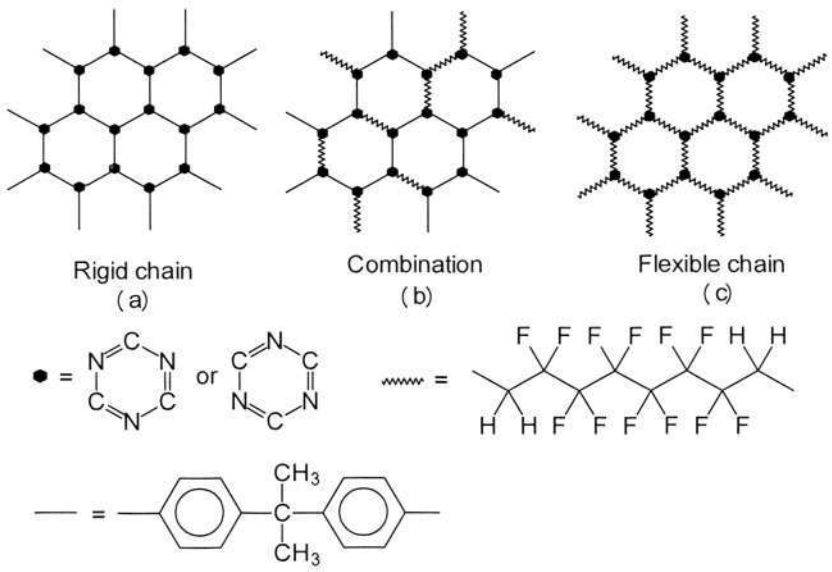

Figure 7.10 Schematic illustration of rigid and flexible chain crosslinking network of polycyanurates

7.2.2 Effect of Conversion on Glass Transition Temperature

The relationship between the glass transition temperature and the conversion for thermosetting polymer is important in quantitative analysis of cure phenomena of thermosetting resins [98]. Consider a thermosetting polymer that has an arbitrary fractional conversion α. This partially cured polymer is assumed to be a random mixture of unreacted part with a concentration of $(1-\alpha)$ and an associated glass transition temperature $Tg = Tg_0$, and reacted part with a concentration of α and an associated glass transition temperature $Tg = Tg_\infty$. Based on the consideration of basic thermodynamic definitions similar to the binary copolymer systems discussed above, the relationship between the glass transition temperature and the fractional conversion can be expressed in Dibenedetto Equation [93,94]:

$$Tg = \frac{(1-\alpha)Tg_0 + \lambda\alpha Tg_\infty}{(1-\alpha)+\lambda\alpha} \qquad \text{(Equation 7.11)}$$

where $\lambda = \Delta Cp_\infty / \Delta Cp_0$, ΔCp_∞ and ΔCp_0 are the specific heat capacities at constant pressure at $\alpha = 1$ and $\alpha = 0$, respectively.

Figures 7.11 to 7.13 shows the experimental data and the Dibenedetto equation model for the three polycyanurate homopolymers studied in this work.

The Dibenedetto equation fits the experimental data very well. The obtained values of λ are 0.23, 0.14 and 0.17 for BACy, BFCy and DFCy homopolymer respectively. Tg_∞ obtained from the best fitting of the curves are 359 °C, 342 °C and 97 °C for BACy, BFCy and DFCy homopolymers with 100% conversion respectively, which is reasonable. The Dibenedetto equation predicts the $Tg \sim \alpha$ relationship well and it is the basis for studying the curing kinectics of polycyanurates.

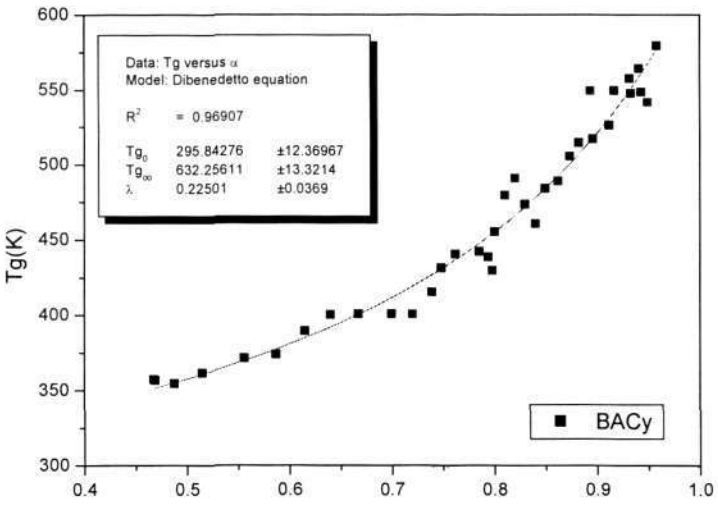

Figure 7.11 Tg versus α for BACy

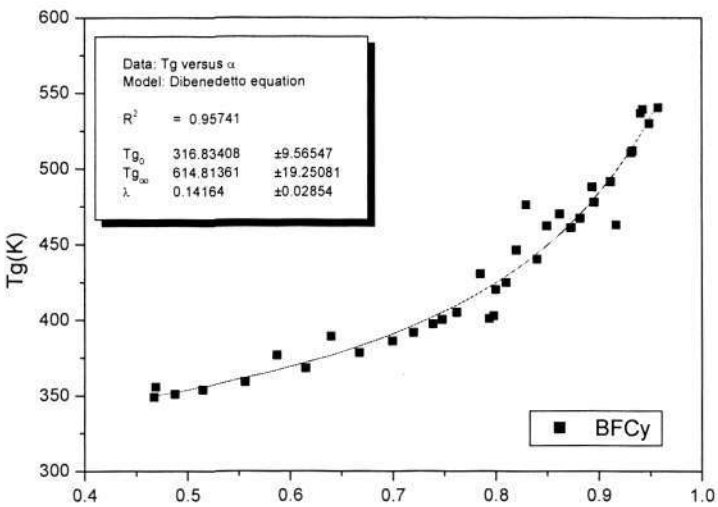

Figure 7.12 Tg versus α for BFCy

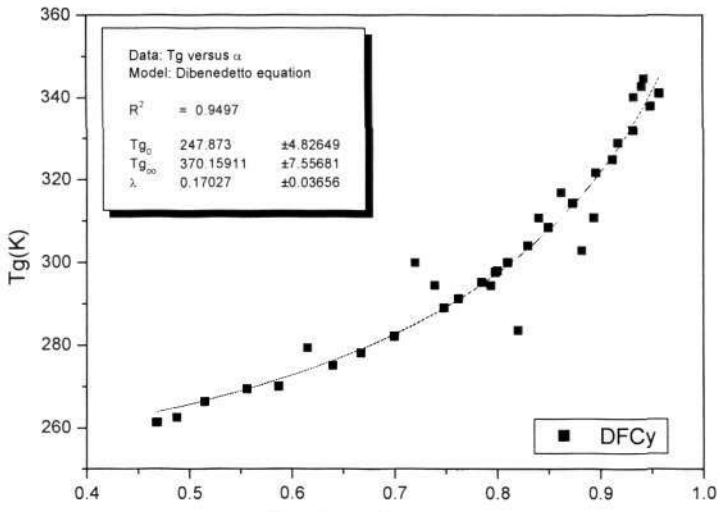

Figure 7.13 Tg versus α for DFCy

7.2.3 Modeling the Tg-α Relationship of Polycyanurate Copolymer

We have discussed the dependence of glass transition temperature on the fractional conversion of polycyanurate homopolymer and the composition of polycyanurate copolymers. It is also important to analyze the Tg-α relationship in polycyanurate copolymers. For a polycyanurate copolymer, the fractional conversion is defined as the same as homopolymer:

$$\alpha = \frac{[OCN]_{reacted}}{[OCN]_{reacted} + [OCN]_{un-reacted}} \qquad \text{(Equation 7.12)}$$

Consider a polycyanurate copolymer with an arbitrary conversion α. Assume it was copolymerized from cyanate ester A and B with molar fraction of X_A and X_B respectively, $X_A + X_B = 1$. The polycyanurate copolymer can be regarded as a four-component mixture, i.e., unreacted A with concentration $X_1 = X_A(1-\alpha)$, reacted A with concentration $X_2 = X_A\alpha$, unreacted B with concentration $X_3 = X_B(1-\alpha)$, and reacted B with concentration $X_4 = X_B\alpha$. Similar to the binary system, the mixed system molar entropy, S, can thus be written as:

$$S = \Delta S + \sum_{i=1}^{4} X_i S_i \qquad \text{(Equation 7.13)}$$

Based on the basic thermodynamic definition arguments similar to the binary system, Equation 7.14 can be finally arrived:

$$\sum_{i=1}^{4} X_i Tg_i \Delta Cp_i \int_{Tg_i}^{Tg} \frac{1}{T^2} dT = 0 \qquad \text{(Equation 7.14)}$$

Solving Equation 7.14 can obtain:

$$Tg = \frac{\sum_{i=1}^{4} X_i \Delta Cp_i Tg_i}{\sum_{i=1}^{4} X_i \Delta Cp_i} \qquad \text{(Equation 7.15)}$$

substitude $X_1 = X_A(1-\alpha)$, $X_2 = X_A\alpha$, $X_3 = X_B(1-\alpha)$ and $X_4 = X_B\alpha$ into Equation 7.15:

$$Tg = \frac{X_A(1-\alpha)\Delta Cp_{A,0}Tg_{A,0} + X_A\alpha\Delta Cp_{A,\infty}Tg_{A,\infty} + X_B(1-\alpha)\Delta Cp_{B,0}Tg_{B,0} + X_B\alpha\Delta Cp_{B,\infty}Tg_{B,\infty}}{X_A(1-\alpha)\Delta Cp_{A,0} + X_A\alpha\Delta Cp_{A,\infty} + X_B(1-\alpha)\Delta Cp_{B,0} + X_B\alpha\Delta Cp_{B,\infty}}$$

(Equation 7.16)

re-arranging Equation 7.16,

$$Tg = \frac{(1-\alpha)\dfrac{X_A\Delta Cp_{A,0}Tg_{A,0} + X_B\Delta Cp_{B,0}Tg_{B,0}}{X_A\Delta Cp_{A,0} + X_B\Delta Cp_{B,0}} + \alpha\dfrac{X_A\Delta Cp_{A,\infty}Tg_{A,\infty} + X_B\Delta Cp_{B,\infty}Tg_{B,\infty}}{X_A\Delta Cp_{A,0} + X_B\Delta Cp_{B,0}}}{(1-\alpha) + \alpha\dfrac{X_A\Delta Cp_{A,\infty} + X_B\Delta Cp_{B,\infty}}{X_A\Delta Cp_{A,0} + X_B\Delta Cp_{B,0}}}$$

(Equation 7.17)

Equation 7.17 can be simplified to Equation 7.18,

$$Tg = \frac{(1-\alpha)Tg_{AB,0} + \alpha\lambda_{AB}Tg_{AB,\infty}}{1-\alpha+\alpha\lambda_{AB}} \qquad \text{(Equation 7.18)}$$

where:

$$Tg_{AB,0} = \frac{X_A\Delta Cp_{A,0}Tg_{A,0} + X_B\Delta Cp_{B,0}Tg_{B,0}}{X_A\Delta Cp_{A,0} + X_B\Delta Cp_{B,0}} \qquad \text{(Equation 7.19)}$$

$$Tg_{AB,\infty} = \frac{X_A \Delta Cp_{A,\infty} Tg_{A,\infty} + X_B \Delta Cp_{B,\infty} Tg_{B,\infty}}{X_A \Delta Cp_{A,\infty} + X_B \Delta Cp_{B,\infty}} \qquad \text{(Equation 7.20)}$$

$$\lambda_{AB} = \frac{X_A \Delta Cp_{A,\infty} + X_B \Delta Cp_{B,\infty}}{X_A \Delta Cp_{A,0} + X_B \Delta Cp_{B,0}} \qquad \text{(Equation 7.21)}$$

where $Tg_{AB,0}$ and $Tg_{AB,\infty}$ are the glass transition temperature of the monomer mixture and the fully cured polycyanurate copolymer respectively. λ_{AB} is the interaction parameter. Figures 7.14 and 7.15 shows the Tg- α relationship of BACy/BFCy=50/50 and BACy/DFCy=50/50 copolymers. The fitting results using equation 7.18 are displayed in the insets of the Figures. The obtained values of λ_{AB} are 0.18 and 0.20 for BACy/BFCy and BACy/DFCy copolymer systems respectively. The obtained Tg_{∞} of BACy/BFCy and BACy/DFCy copolymers are 347°C and 180°C respectively which is between those of the homopolymers of the indivudual components.

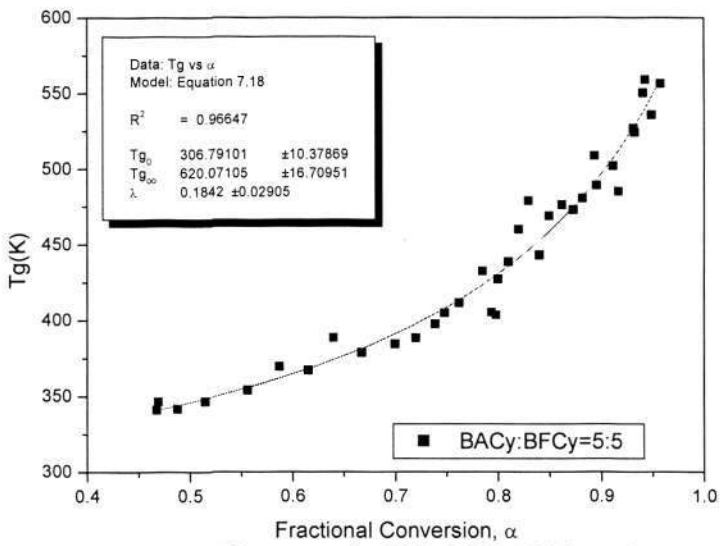

Figure 7.14 Tg versus α for BACy/BFCy=50/50 copolymer

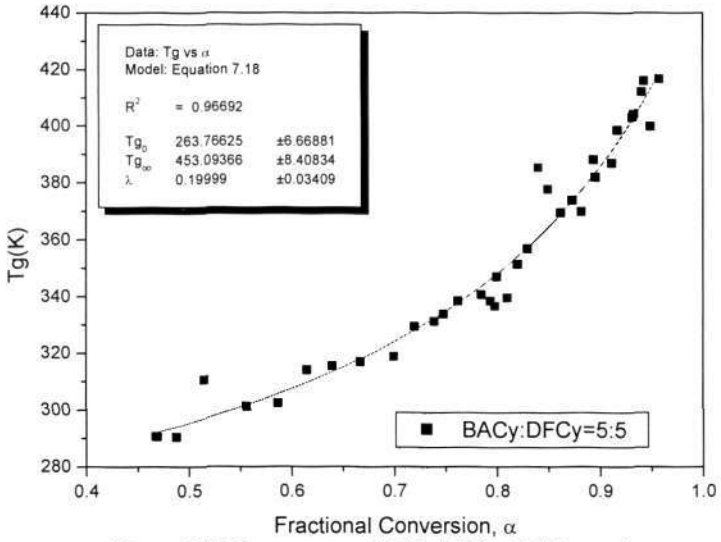

Figure 7.15 Tg versus α of BACy/DFCy=50/50 copolymer

More generally, Equation 7.15 can be expanded to an n-component system, which is:

$$Tg = \frac{\sum_{i=1}^{n} X_i \Delta Cp_i Tg_i}{\sum_{i=1}^{n} X_i \Delta Cp_i} \qquad \text{(Equation 7.22)}$$

Thus, the glass transition temperature can be predicted. The advantage of Equation 7.18 or Equation 7.22 is that the glass transition temperature can be calculated from those of the pure monomers and homopolymers of the individual components, without knowing the glass transition temperature of the co-monomer and fully cured copolymers. Understanding this is helpful in designing a copolymer with a given glass transition temperature.

7.3 Mechanical Properties of Polycyanurate Thin Films

Mechanical properties of dielectric and optical thin films are important in the integration process. For spin coated thin films on substrate, it is impossible to detach the films from the substrate to measure the mechanical properties of the 'free standing' films.

Characterization of mechanical properties of thin film at surface or subsurface using a nanoindentation technique has been developed and widely used during the last decade [182-194]. The method uses a diamond pyramid that penetrates the surface of a specimen on application of a given load at a constant rate for a given time [184]. The measurement is a localized, microscopic test with the materials surrounding the indentation sites remaining uncreeped during the experiments [182].

A typical experimental load-depth curve is shown in Figure 7.16. As the load is increased, the indenter sinks into the material due to both elastic and plastic deformation. Then the load is held constant, the indenter continues to sink into the material due to time-dependent deformation (creep). When the indenter is unloaded, the material recovers by a process that is primarily elastic [186].

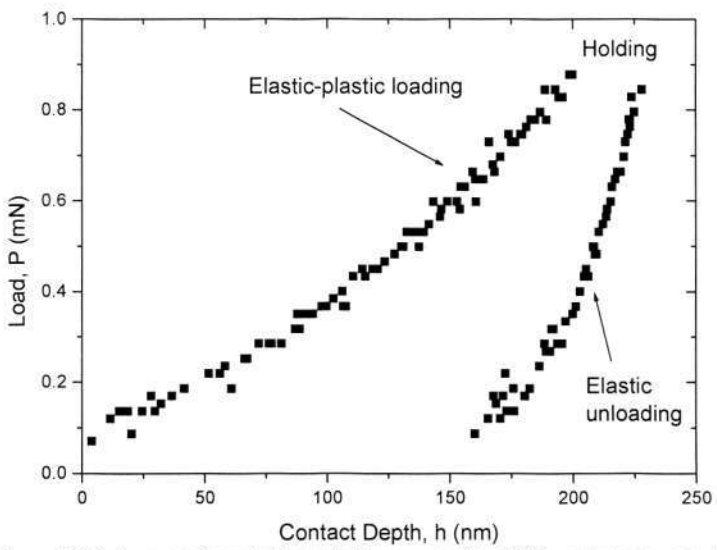

Figure 7.16 An experimental indentation curve of a BACy polycyanurate thin film

In a standard indentation, the penetration depth of a calibrated diamond probe is measured as a function of the applied load during a load-unload cycle. On unloading, the elastic component of the displacement starts to recover producing a sloped rather than horizontal unloading curve. It is from this slope that the elastic properties can be derived. The

hardness and modulus are derived from the residual depth of the unloading curve [186-188]. The reduced modulus is given by [188]:

$$E_r = \frac{1}{2}\frac{dP}{dh}\frac{\sqrt{\pi}}{\sqrt{A}} \qquad \text{(Equation 7.23)}$$

where E_r is the reduced modulus, A is the contact area which is dependent on the contact depth and the shape of the indenter. P is the load and h is the indentation depth.

The elastic modulus can be obtained by the following equation [194]:

$$\frac{1}{E_r} = \frac{1-v_i^2}{E_i} + \frac{1-v^2}{E} \qquad \text{(Equation 7.24)}$$

where E_i and v_i are the elastic modulus and Poisson's ratio of the indenter materials which are 1140 GPa and 0.07 respectively [194], E and v are the elastic modulus and Poisson's ratio of the indented material respectively, where v is assumed to be 0.35. Then the elastic modulus of the indented material can be calculated from Equation 7.24.

The hardness of the sample is given by [188]:

$$H = \frac{P_{\max}}{A} \qquad \text{(Equation 7.25)}$$

where H is the hardness, A is the contact area, and $P_{\max}$ is the maximum load, which is corresponding to the 'holding" in Figure 7.16.

Polycyanurate homopolymer thin films with different conversions are measured by nanoindentator. Figure 7.17 shows the hardness as a function of conversion of the three polycyanurate homopolymer thin films.

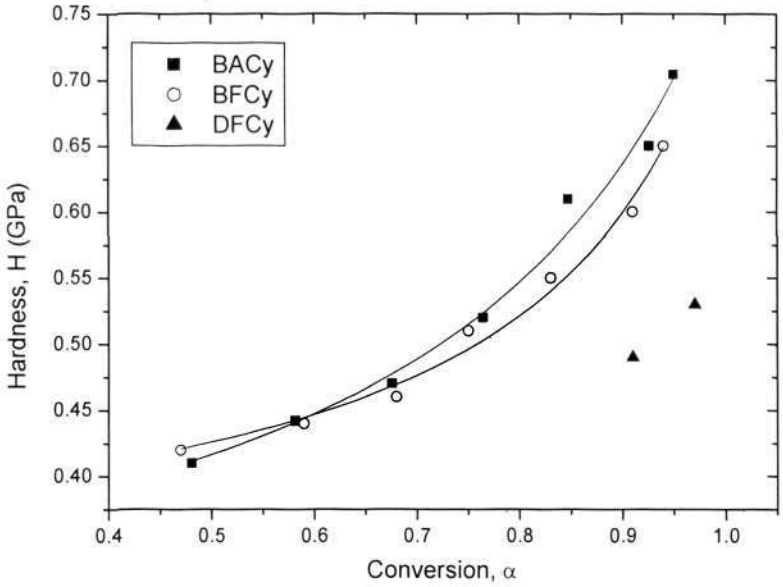

Figure 7.17 Hardness as a function of conversion of polycyanurate homopolymers

From Figure 7.17 it can be clearly observed that the hardness of the polycyanurate film increases gradually with the increase of the fractional conversion of the polymer. At the same conversion, the aromatic polycyanurates namely BACy and BFCy have similar hardness and which is higher than the aliphatic DFCy polycyanurate films. This is due to the rigid aromatic structure of BACy and BFCy and the flexible aliphatic structure of DFCy. It is noted that the hardness of DFCy thin films with lower conversion cannot be measured at room temperature, because their glass transition temperature are too low. Therefore only two data of DFCy thin films are shown in Figure 7.17. The hardness of aromatic polycyanurate thin films are close to those reported polyimide thin films of 0.60-0.75 GPa [183] and higher than those amorphous thermoplastic polymers [184].

It is also noted that the trend of the hardness versus conversion is similar to the relationship between the glass transition temperature and the conversion. And further analysis also shows that the dependency of hardness of polycyanurate thin film on conversion can be described by the following equation which is similar to the Dibenedetto equation:

$$H_\alpha = \frac{(1-\alpha)H_0 + \lambda\alpha H_\infty}{1-\alpha+\lambda\alpha} \qquad \text{(Equation 7.26)}$$

where α is the fractional conversion of polycyanurate, H_α is the hardness of the polycyanurate film at conversion α, H_0 and H_∞ are the hardness of polycyanurate thin films at conversion $\alpha = 0$ and $\alpha = 1$ respectively. λ is an fitting parameter. The obtained values of λ are 0.22 and 0.15 for BACy and BFCy polycyanurate homopolymer thin films respectively.

Rearrange the Dibenedetto equation (Equation 7.11) and Equation 7.26, can arrive Equations 7.27 and 7.28 respectively:

$$\frac{1-\alpha}{\alpha} = \lambda_{Tg}\frac{Tg_\infty - Tg_\alpha}{Tg_\alpha - Tg_0} \qquad \text{(Equation 7.27)}$$

$$\frac{1-\alpha}{\alpha} = \lambda_H \frac{H_\infty - H_\alpha}{H_\alpha - H_0} \qquad \text{(Equation 7.28)}$$

Where λ_{Tg} and λ_H are the fitting parameters for Dibenedetto Equation and Equation 7.26 respectively. In this study, the experimental data showed $\lambda_{Tg} \approx \lambda_H$.

Compare Equations 7.27 and 7.28, we have:

$$\frac{Tg_\infty - Tg_\alpha}{Tg_\alpha - Tg_0} = \frac{H_\infty - H_\alpha}{H_\alpha - H_0} \qquad \text{(Equation 7.29)}$$

Regrouping Equation 7.29 can obtain:

$$Tg_\alpha = \frac{H_\infty - H_\alpha}{H_\infty - H_0}Tg_0 + \frac{H_\alpha - H_0}{H_\infty - H_0}Tg_\infty \qquad \text{(Equation 7.30)}$$

or,

$$H_\alpha = \frac{Tg_\infty - Tg_\alpha}{Tg_\infty - Tg_0}H_0 + \frac{Tg_\alpha - Tg_0}{Tg_\infty - Tg_0}H_\infty \qquad \text{(Equation 7.31)}$$

Equation 7.30 or 7.31 is of important because it established a relationship between the hardness and the curing extent of a thermosetting polymer. The curing extent of a thermosetting polymer infuluences its properties greatly. Up to now, there is no reported study on the relationship between the modulus or hardness and the glass transition temperature of thermosetting polymers.

Equation 7.30 or 7.31 also can be wrote as:

$$H_\alpha = \frac{H_\infty - H_0}{Tg_\infty - Tg_0} Tg_\alpha + \frac{Tg_\infty H_0 - Tg_0 H_\infty}{Tg_\infty - Tg_0} \qquad \text{(Equation 7.32)}$$

Equation 7.32 predicts a linear relationship between the hardness and glass transition temperature. The slope of the curve equals to $(H_\infty - H_0)/(Tg_\infty - Tg_0)$ and the intercept at Y axis equals to $(Tg_\infty H_0 - Tg_0 H_\infty)/(Tg_\infty - Tg_0)$. Figure 7.18 shows the plots of hardness as a function of glass transition temperature for the polycyanurate homopolymer thin films of BACy and BFCy.

It can be seen from Figure 7.18 that the correlation between hardness and glass transition temperature of BACy and BFCy can be described in a same linear relationship, while DFCy disobeys this linear relationship. Equation 7.32 can be simplified as:

$$H = kTg + C \qquad \text{(Equation 7.33)}$$

Where $k = (H_\infty - H_0)/(Tg_\infty - Tg_0)$ and $C = (Tg_\infty H_0 - Tg_0 H_\infty)/(Tg_\infty - Tg_0)$. For BACy and BFCy, C =-35MPa and k =1.29 MPa/K from linear curve fitting of the experimental data.

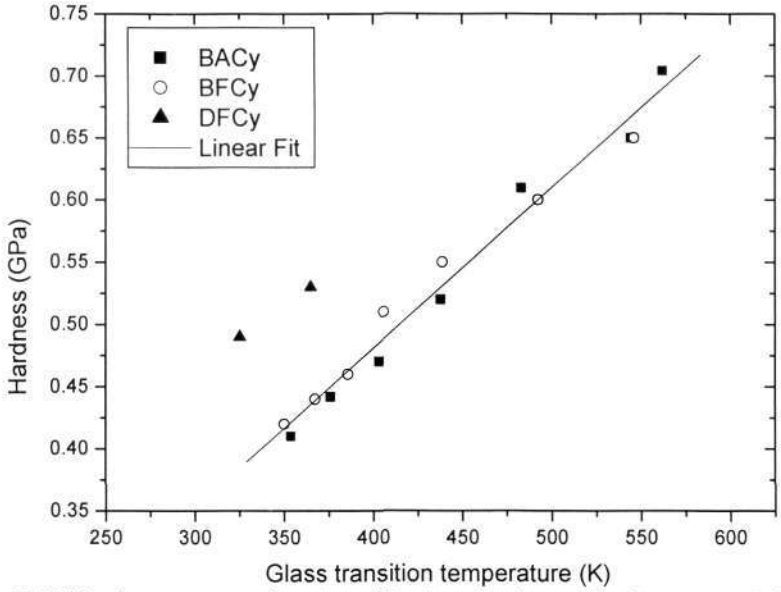

Figure 7.18 Hardness versus glass transition temperatures of polycyanyurate homopolymers

Fakirov et al also reported that there is a linear relationship between the hardness and glass transition temperature based on the analysis of the nanoindentation data of a series of different amorphous thermoplastic polymer thin films [184]. They established an empirical equation same as Equation 7.32, where C=-571 MPa and k=1.97 MPa/K in their case regardless of the structure of the polymer, however, the physical meaning of the parameters k and C are very ambiguous. In the present study, Equations 7.30 to 7.33 are semi-empirical formula, in which the parameters have clear physical meaning.

Comparing our study and those reported [182-184,194], it becomes clear the only those polymers possessing similar molecular structures can be described in a single linear relationship. That is to say, the parameters k and C are dependent on the chemical structures. Thermosetting polymers seems to have different k and C values from amorphous thermoplastic polymer. Polymers containing more aromatic structures also appear to have different k and C values from polymers containing mainly aliphatic groups. This is necessary for better understanding. However, it would be very challenging

to develop a universal model to describe the relationship between the hardness and glass transition temperature including all polymers, because the large difference in chemical structures among different polymers. In fact, Fakirov et al also mentioned that certain polymers such as polycarbonate and polyarylate, in which the benzene rings dominate in the main chain structures, do not fit into the linear relationship between the hardness and glass transition temperature observed for aliphatic thermoplastics [184]. In our opinion, these aromatic thermoplastics may follow another linear relationship with a different set of k and C values. In this study, it is noted that the data from DFCy cannot be fitted together with those from BACy and DFCy (see Figure 7.18) because of their large difference in chemical structures. Thus, a universal model would have to incorporate parameters that reflect the chemical structures of the polymers and this requires extensive further work.

In this study, the composition effect on the hardness of the polycyanurate copolymer thin films is also investigated. Figure 7.19 shows the hardness as a function of composition of polycyanurate copolymer thin films. A simple linear relationship between the hardness and the mass fraction of BACy was found for BACy/BFCy and BACy/DFCy copolymer systems. Which agrees well with the additivity law of hardness for muticomponent systems [172].

$$H = \sum_i H_i \varphi_i \qquad \text{(Equation 7.33)}$$

where H is the hardness of the material, H_i is and hardness of component i, and φ_i is the mass fraction of component i.

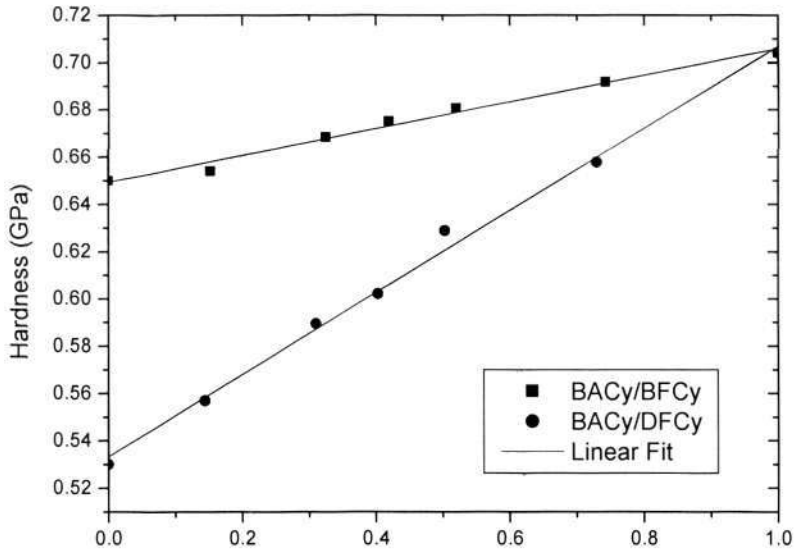

Figure 7.19 Hardness as a function of composition

An almost linear relationship of hardness and elastic modulus is observed as shown in Figure 7.20. The elastic modulus of polycyanurate thin films are higher than that of the bulk materials [17], which is probably due to their thin film nature.

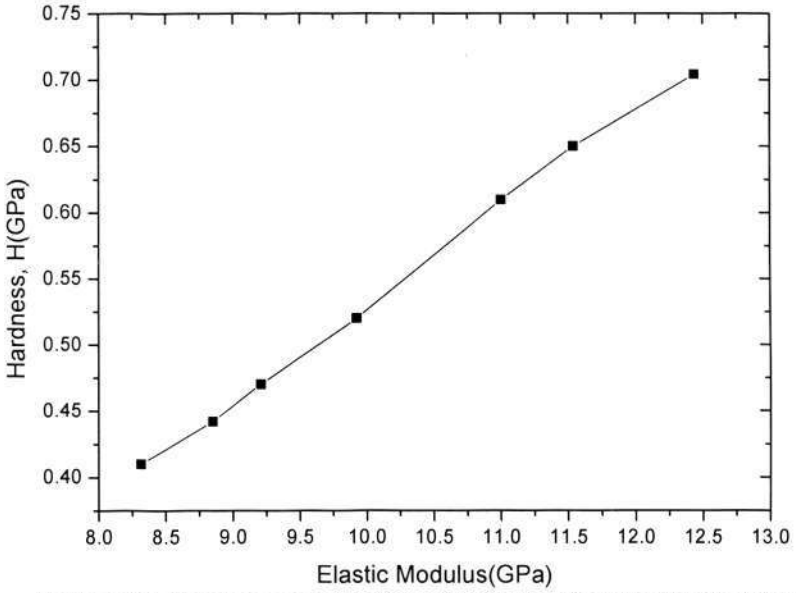

Figure 7.20 Hardness as a function of modulus of polycyanurate thin films

7.4 Thermal Expansion of Polycyanurate

The thermal expansion of polymer materials is one of the most important properties for many applications such as electronic devices and optical components. Dimension stability can be a critical issue in the design of components subjected to temperature variations. Coefficient of thermal expansion (CTE) mismatch between two levels of materials can cause thermal fatigue failures in their interconnections. Therefore, matching the CTE of polymers to that of chips or other components is a subject of interest [195]. Normally the chips are made from inorganic materials such as silicon, which has lower CTE than most of the polymeric materials, therefore searching polymer with low CTE is one of the major approaches for the modification of dimension stability.

CTE of polycyanurate polymer was measured by using TMA. A typical measured curve is shown in Figure 7.21, the sample is fully cured BACy homopolymer.

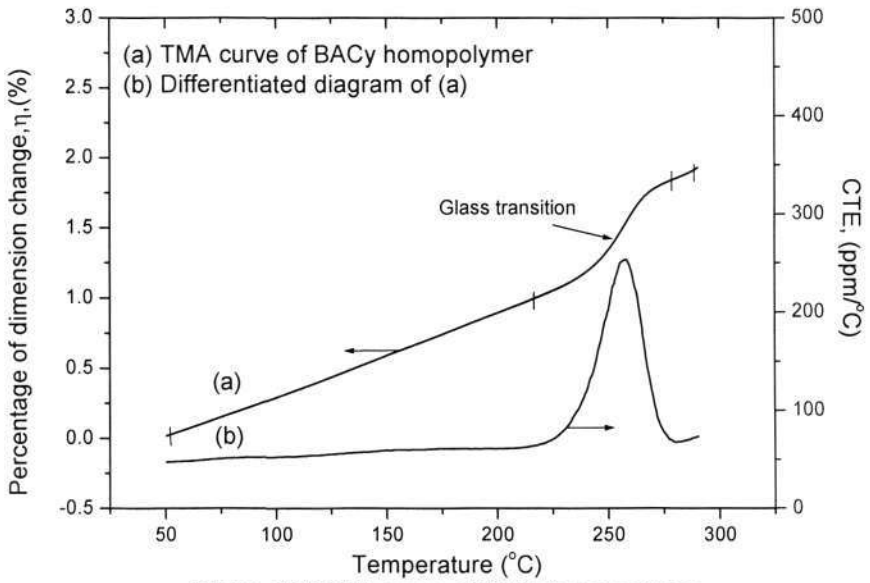

Figure 7.21 TMA curve of BACy homopolymer

Curve (a) is the percentage of dimension change as a function of temperature, with the increase of the temperature, the thermal-mechanical behaviors of the polycyanurate can

be divided into three regions, namely, below the glass transition (room temperature to 200 °C), glass transition (200 °C to 265 °C), and above the glass transition (temperature above 265 °C). Below the glass transition, the polymer is in glassy state, the mobility of molecular chains is very low, and therefore, the CTE is relatively low. The CTE values in this region are of importance, since most high temperature-resistant thermosetting resins used below their glass transition temperatures (T_g). It can be seen from curve (b) in Figure 7.21 that the CTE values of BACy homopolymer in the temperature range from 50 °C to 200 °C keep nearly constant with an average of 61.2 ppm/°C. This value is similar to other higher performance thermosetting resin systems such as multifunctional epoxy and modified BMI systems [128].

Above the glass transition region, the polymer is in rubbery state, which has a higher CTE than that of below the glass transition. In this study, the CTE values of BACy homopolymer vary from 102.8 ppm/°C to 125.7 ppm/°C in the temperature range from 265 °C to 300 °C. Normally, thermosetting resins are not used above the glass transition.

In the glass transition region, the molecular chains gain more heat energy, and their mobility increases, leading to an abrupt change in the CTE value. Glass transition temperature (T_g), which is an extremely important thermal stability parameter for polymers, can be easily determined by TMA (the glass transition temperature of BACy homopolymer was indicated in Figure 7.21). The peak temperature is 257.3 ^{o}C which is agree well with the previous reported glass transition values of BACy homopolymer [2,3]. It should be noted that the glass transition temperarure measured by TMA is lower than that measured by MDSC method, which is due to their different measuring principles; however, both of them are acceptable in literatures.

The CTE values of BACy, BFCy and DFCy polycyanurate homopolymers are 61.2 ppm/°C, 68.7 ppm/°C and 124.3 ppm/°C respectively. The CTE values of the copolymers are between those of the homopolymers of the two individual components. BACy and BFCy homopolymers have similar CTE values, while DFCy homopolymer has relative higher CTE values, which is probably due to their differences in molecular structures. BACy and BFCy have aromatic backbone structures, the molecular chain mobilities of which are restrained and less sensitive response to the external force. DFCy has flexible aliphatic backbone structure which results in relatively higher CTE than that of BACy and BFCy. The CTE values of polycyanurates are not match well with silicon, which is commonly used as substrate material in waveguide and photonic application [27-33]. This may be solved by introducing nanoparticles into polycyanurate systems.

7.5 Summary

Based on the basic thermodynamic consideration, the dependency of glass transition temperature on the composition and conversion are investigated. Studies show that the composition and molecular backbone structure will affect the glass transtion temperature of the polycyanurate copolymer to some extent. A Dibenedetto equation is used to model the relationship between the glass transition temperature and the conversion. The relationship among the glass transition temperature, composition and conversion of the polycyanurate copolymer was also established, which is useful to predict the glass transtion temperature of the polycyanurate copolymers at any given conversion and composition from the pure homopolymer components.

Nanoindentation study of the polycyanurate thin films reveal that the relationship between the hardness and conversion is similar to that of the glass transition temperature between the conversion, because the factors which influence the glass transition

temperature and hardness are almost the same. A linear relationship between the hardness and glass transition temperature is established. It is found that the chemical structure will have a strong effect on the slope and intercept of the linear relationship. Only those polymers contain similar main chain structures can be described in a same linear relationship.

TMA study shows that the CTE values of polycyanurate homopolymer and copolymer thin films are between 61.2 ppm to 124.3 ppm, which still need to be further reduced to match the CTE of the silicon substrate.

CHAPTER 8

CURING STUDY OF POLYCYANUATES

PART I. VARIABLE REACTION ORDER

KINETICS MODEL FOR

ALIPHATIC CYANATE ESTER

8.1 Introduction

Thermosetting resins play an important role in industry because of their flexibility in tailoring desired ultimate properties. To understand and control the curing process to design suitable processing parameters and achieve optimum properties, it is imperative to study the kinetic aspects of its cure reaction, as they drive the complex changes in morphology and structure of the polymer during its processing operations.

Many studies have been conducted on the curing reaction kinetics of thermosetting resins such as epoxy, bismaleimides and polycyanurate [77-87] employing various techniques, experimental procedures and data analysis methods. Among them, isothermal Differential Scanning Calorimetry technique is most frequently used. A variety of kinetic models have been developed to relate the chemical reaction rate to time, temperature, and curing conversion. In general, the kinetics models of thermosetting resins fall into two main types: nth order model and autocatalytic model. For an nth order kinetics model, the following equation stands [70]:

$$\frac{d\alpha}{dt} = k(1-\alpha)^n \qquad \text{(Equation 8.1)}$$

Where α is the curing conversion, n is the reaction order which is a constant independent of temperature and conversion, $d\alpha/dt$ is the reaction rate, and k is the apparent rate constant. The reaction rate constant k is temperature dependent and given by Arrhenius relationship:

$$k = Ae^{-\frac{E}{RT}} \qquad \text{(Equation 8.2)}$$

where E is the activation energy, R is the gas constant (8.314 J/K), T is absolute temperature, and A is the pre-exponential or frequency factor. From Equation 8.1, two characteristics can be derived for the curing reaction with nth order. One is that the reaction rate is maximum at the beginning of the curing reaction (α=0), and the other is that the relationship between $\ln(d\alpha/dt)$ and $\ln(1-\alpha)$ must be linear, the slope of the linear curve is equal to the reaction order n and the intercept is equal to $\ln k$.

The efficiency of the nth order kinetics model has been postulated by some researchers [65-67]. However, this model can only be applied to the earlier stage of the curing reaction of thermosetting, because in general, thermosetting materials exhibit the vitrification phenomenon, which greatly reduces the reaction rate before complete conversion is achieved. After vitrification, the cure process exhibits a diffusion controlled mechanism and as a consequence, the experimental conversion and conversion rate are much lower than those predicted by the above kinetics equation [60,61,73]. Therefore the above nth order model do not satisfy the observed reduced reaction rate condition at the later reaction stage of the cure where the reaction becomes very slow before a complete conversion is achieved. Understanding the diffusion phenomenon of thermosetting reaction is important for achieving optimum properties of the cured resin. For curing of high performance resins such as cyanate ester and bismaleimide, it is important to have a

working equation to describe the entire curing process in order to obtain the optimum properties of the cured resin.

To characterize the entire curing of thermosetting reaction system, a two-step plateau kinetics model was proposed [98], which treats the kinetics model as composed of two simply nth order models:

$$\frac{d\alpha}{dt} = k_1(1-\alpha)^{n_1} \qquad (\alpha < \alpha_{onset})$$

$$\frac{d\alpha}{dt} = k_2(\alpha_{\max} - \alpha)^{n_2} \qquad (\alpha \geq \alpha_{onset}) \qquad \text{(Equation 8.3)}$$

where k_1 and k_2 are the rate constants in chemical controlled and diffusion controlled regions respectively, n_1 and n_2 are reaction orders. $\alpha_{\max}$ is the maximum or plateau conversion and α_{onset} is the onset conversion where the reaction shifts from chemical controlled to diffusion controlled. An advantage of this model is its simplicity in presentation. However, there may be some inconsistence in the region where the reaction changes from a chemical controlled to diffusion controlled processing. In addition, the chemical or physical meanings of certain parameters such as k_2 and n_2 are not clearly defined.

Another model was proposed using more fundamental approach, by considering the overall reaction rate constant to be composed of two components, one associated with the diffusion controlled reaction step and another with the chemical controlled reaction step [74,83]. This model is in the same form of Equation 8.1. However, the overall reaction rate constant was defined as:

$$\frac{1}{k} = \frac{1}{k_T} + \frac{1}{k_D} \qquad \text{(Equation 8.4)}$$

where k is the overall rate constant, k_T is the rate constant of chemical controlled region and described by Arrhenius relationship, k_D is the diffusion rate constant. k_T is a function of curing temperature (T), while k and k_D are functions of conversion (α) and curing temperature (T). The preceding equation shows that the overall rate constant is governed at one extreme by the Arrhenius rate constant when $k_T << k_D$ (prior to vitrification), and at the other extreme by the diffusion rate constant when $k_D << k_T$ (after vitrification) [54].

The diffusion rate constant can be described as a function of glass transition temperature by a WLF-type equation [84]:

$$\log \frac{k_D}{k_{D-onset}} = \frac{C_1[Tg_{onset} - Tg(\alpha)]}{C_2 + |Tg_{onset} - Tg(\alpha)|} \qquad \text{(Equation 8.5)}$$

where C_1 and C_2 are fitting parameters, $k_{D-onset}$ is an adjustable parameter, Tg_{onset} is the glass transition temperature at the onset conversion of diffusion control. $Tg(\alpha)$ is the glass transition temperature at the conversion α.

It should be pointed out that even in the chemical controlled region, the kinetics model with a fixed reaction order may not be suitable for thermosetting curing systems according to our study. Because the fixed reaction order kinetics model is based on the assumption that the functional groups have equal reactivity during the entire curing process. This assumption can be accepted for reaction systems with low molecular weight, but for curing of thermosetting resins, this assumption may not be accurate, because the reactivity of the functional groups decreases with the increase of curing conversion due to increasing viscosity. The increase in the viscosity decreases the mobility and accessibility of the reactive functional group and result in decreasing the reactivity. In this work, we

take account of this effect and a kinetics model with variable reaction order *n* was proposed.

The cure kinetics of cyanate ester has attracted much research attention. Cyanate ester resins cure via a cyclotrimerization to form a polycyanurate network with a high degree of efficiency, as shown in Figure 8.1. To understand and control the curing processing of this new generation thermosetting resin to design suitable processing parameters and achieve optimum properties, it is imperative to study the kinetic aspects of its cure reaction, as they drive the complex changes in morphology and structure of the polymer during its processing operations.

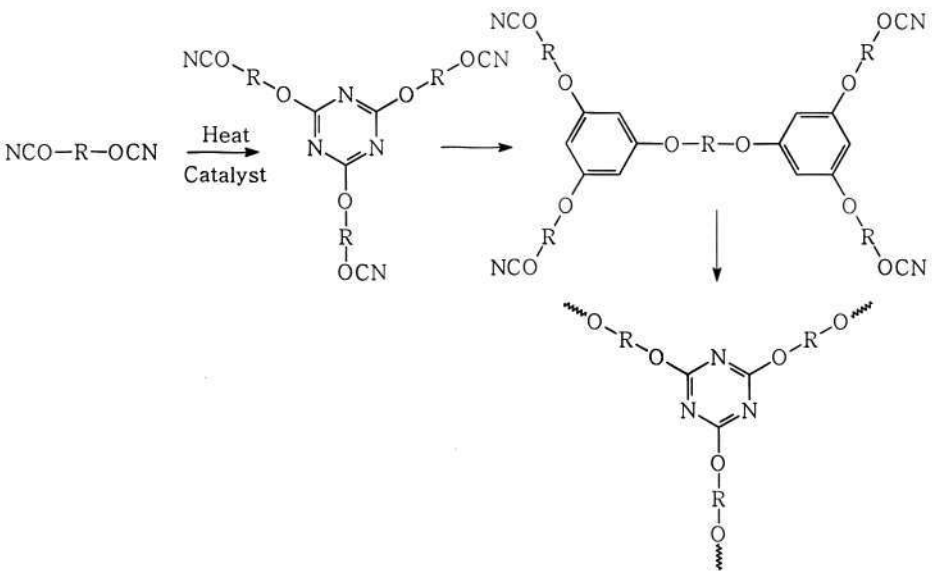

Figure 8.1 Polycyclotrimerization reaction of cyanate ester to form triazine network

In this study, the kinetics of DFCy cyanate ester was investigated in detail. DSC was used to obtain the reaction kinetics data. New models were developed to accurately describe the curing reactions in both the chemical and diffusion controlled regions for the isothermal measurement.

8.2 Variable '*n*' Kinetics Model for Chemical Controlled Region

Figure 8.2 shows the experimental curves of conversion (α) versus curing time (t) of DFCy at isothermal curing temperatures from 140 to 190 °C at interval 10 °C.

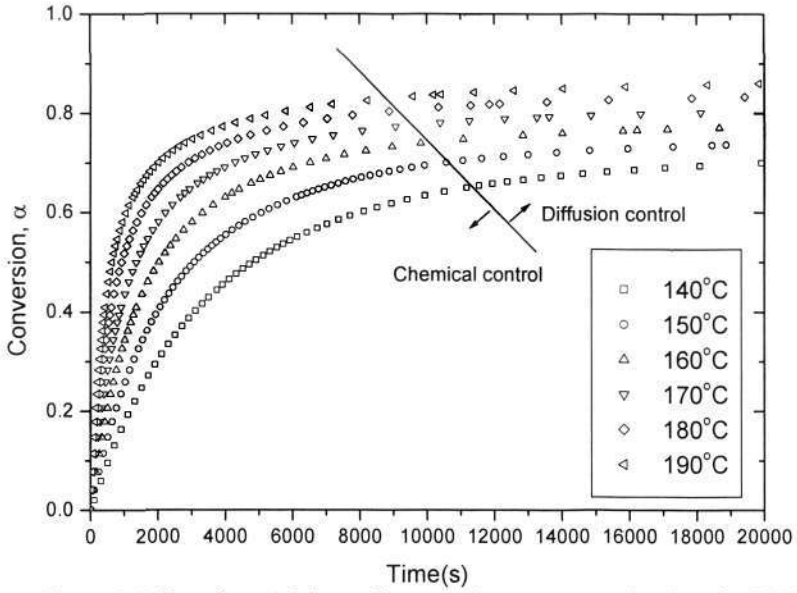

Figure 8.2 Experimental data of conversion versus curing time for DFCy

It can be observed from Figure 8.2 that the reaction rate ($d\alpha/dt$) of the cyanate ester reaction is initially rapid and then slows down experiencing a transition from a chemical controlled to a diffusion-controlled mechanism. Finally the conversion reaches a plateau towards maximum conversion (α_{max}). The plateau conversion can be empirically expressed as [6]:

$$\alpha_{max} = p_1\left(\frac{1}{T_1} - \frac{1}{T}\right) \qquad \text{(Equation 8.6)}$$

where p_1 is a fitting parameter, T is the curing temperature, T_1 is the theoretical critical temperature below which no cure reaction could occur ($\alpha_{max} = 0$). An approximate transition from the chemical control to diffusion control was marked by an indicative line in Figure 8.2. It can also be seen that the onset conversion, α_{onset}, at which the reaction

becomes dominated by diffusion, increases with increasing curing temperature, as does the maximum or plateau conversion.

Using a similar approach reported earlier [82], in this present study, the relationship between the onset conversion and the curing temperature is established:

$$\alpha_{onset} = p_2(\frac{1}{T_2} - \frac{1}{T}) \qquad \text{(Equation 8.7)}$$

where p_2 is a fitting parameter, T is the curing temperature, T_2 is the hypothetical critical temperature below which no chemical controlled reaction could occur ($\alpha_{onset} = 0$) when $T = T_2$. In Equations 8.6 and 8.7, the upper bound of $\alpha_{\max}$ and α_{onset} is unity. The parameters p_1, p_2, T_1, and T_2 can be obtained from curve fitting of $\alpha_{\max}$ and α_{onset} versus curing temperature T, as shown in Figure 8.3 (p_1=601.5 K, p_2=664.8 K, T_1=278.6 K, and T_2=293.0 K). In this study, the conversions at 20,000 second were taken approximately as the $\alpha_{\max}$. The values of α_{onset} are obtained by comparing the experimental data and our variable 'n' kinetics model shown in Figure 8.9, which are estimated as the points where the experimental data deviate significantly from the proposed model due to onset of the diffusion controlled mechanism. This will be discussed in detail later.

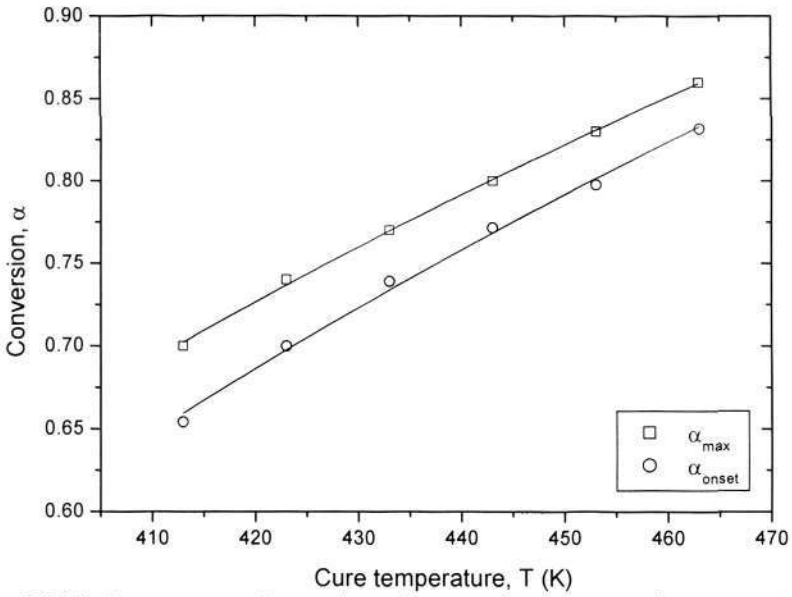

Figure 8.3 Maximum conversion and onset conversion versus curing temperatures for DFCy

In order to identify the reaction kinetics of DFCy being whether n th order or autocatalytic model, the reaction rate, $d\alpha / dt$, versus curing time, t, of DFCy at different isothermal curing temperatures 140-190 °C is plotted in Figure 8.4.

Figure 8.4 shows that the reaction rate ($d\alpha / dt$) is maximum at begin of the reaction ($t = 0$). The kinetics resembles the n th order reaction kinetics. Hence the plot of $\ln(d\alpha / dt)$ versus $\ln(1-\alpha)$ should be linear with the slope equal to the reaction order n.

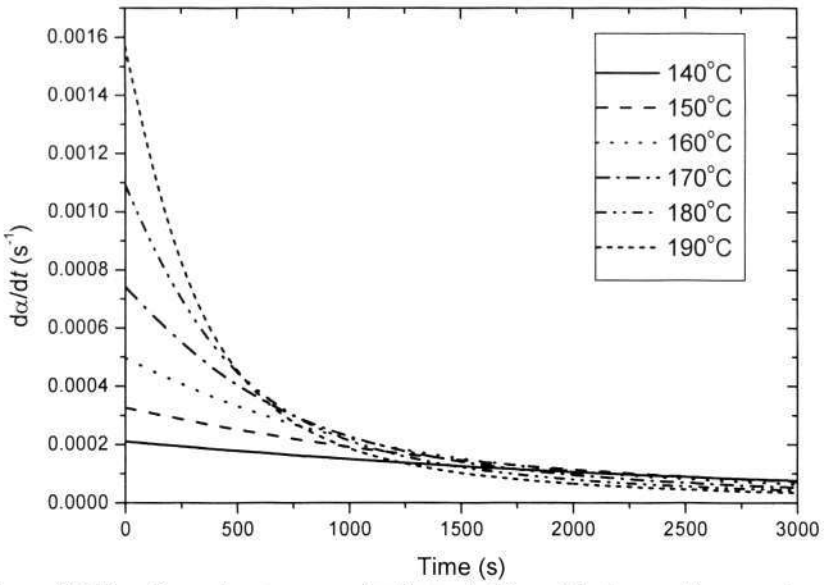

Figure 8.4 Reaction rate versus curing time at different isothermal temperatures for DFCy

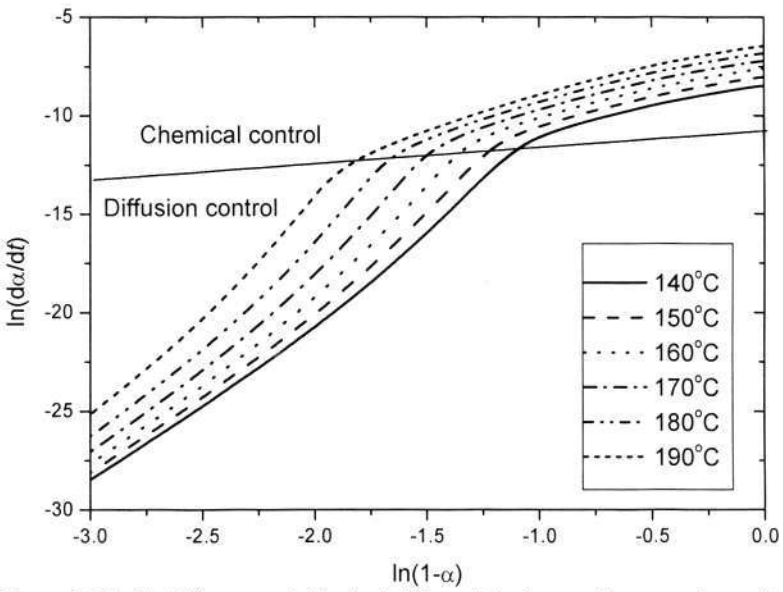

Figure 8.5 ln(dα/dt) versus ln(1-α) at different isothermal temperatures for DFCy

Figure 8.5 shows the plots of $\ln(d\alpha/dt)$ against $\ln(1-\alpha)$ for DFCy. However, it can be seen that the relationship between $\ln(d\alpha/dt)$ and $\ln(1-\alpha)$ is approximately linear at the initial reaction stage ($\alpha \leq 0.35$) at the isothermal curing temperatures studied in this work,

then it deviates considerably from linear relationship at higher conversions. The abrupt change in slope seen in Figure 8.5 indicates the reaction mechanism shifts from chemical controlled to diffusion controlled. The shift is marked at an onset conversion of α_{onset} which increases with increasing temperature. Their relationship can be described by Equation 8.7. In a normal nth order kinetics model, the 'n' values are obtained from the linear fitting of $\ln(d\alpha/dt)$ against $\ln(1-\alpha)$ at different reaction temperatures. However, the linear relationship assumption is only valid at initial stage of reaction ($\alpha \leq 0.35$). Therefore, considerably large errors are expected in this fixed 'n' nth order kinetics model at moderate and high conversion regions. Fixed 'n' kinetics model may be useful as a simplistic approximation for processing control of thermosetting polymers, but it is inaccurate and cannot provide insight understanding of the fundamentals in curing reactions. In fact, in the chemical controlled region, it can be seen from Figure 8.5 that the relationship between $\ln(d\alpha/dt)$ versus $\ln(1-\alpha)$ deviates significantly from linear relationship. Based on this observation, a variable 'n' kinetics model is proposed in this study.

In this study, we assume a conversion dependent reaction order n and the kinetics model for the chemical controlled region is modified as:

$$\frac{d\alpha}{dt} = k(1-\alpha)^{n(\alpha)}, \quad [n(\alpha) = q_1 + q_2 \ln(1-\alpha)] \qquad \text{(Equation 8.8)}$$

where the reaction order is not a constant, but a function of conversion $n = n(\alpha)$. q_1 and q_2 are fitting parameters.

To further illustrate this variable 'n' model, an enlarged plot of $\ln(d\alpha/dt)$ versus $\ln(1-\alpha)$ in the chemical controlled region at 140°C is shown in Figure 8.6 as an example.

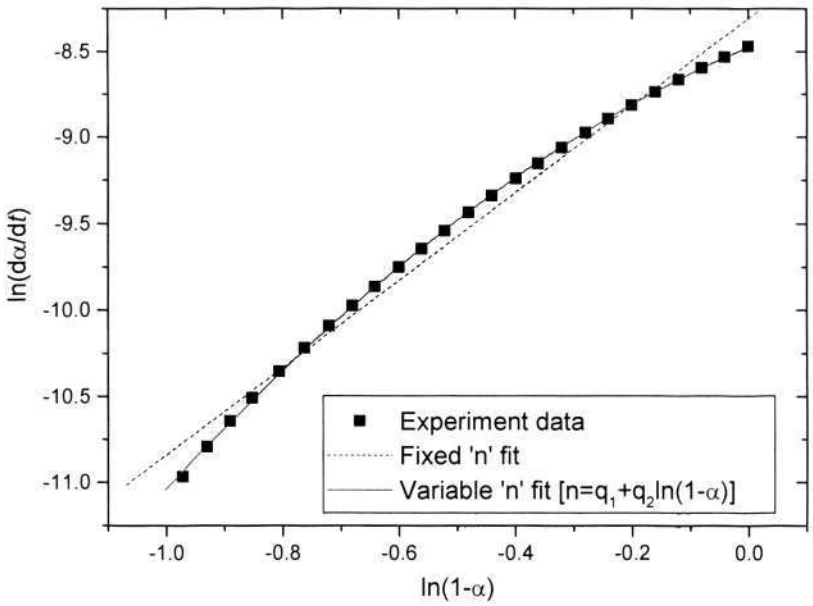

Figure 8.6 ln(dα/d*t*) as a function of ln(1-α) Isothermal at 140 °C

It can be seen that using the variable '*n*' kinetics model resulted in much better fitting to the experimental data than the fixed '*n*' model. The reaction order, *n*, actually did not keep constant during the curing process at the isothermal temperatures studied. At the initial stage of the reaction, the reaction order is the lowest. With the increase of the curing conversion or reaction time, the reaction order also increases.

The rate constant *k* is temperature dependent and given by Arrhenius relationship. According to Arrhenius Equation (Equation 8.2), the activate energy *E* and frequency factor *A* can be obtained by plotting ln(*k*) against $1/T$ as shown in Figure 8.7. The obtained *E* and frequency factor A for DFCy were 67248 J/mol and 63704 s^{-1} respectively.

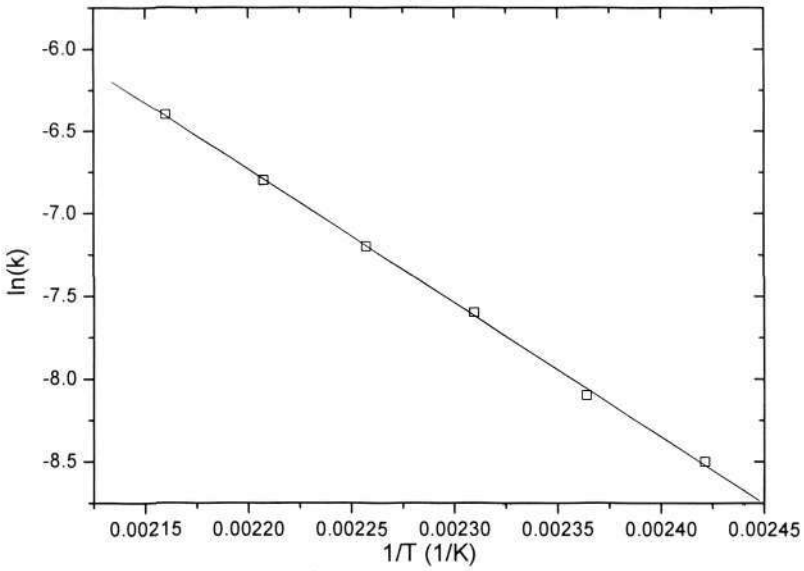

Figure 8.7 Arrhenius plot of the rate constants in chemical controlled region and diffusion controlled region as a function of 1/T

Equation 8.8 was used to fit the experimental data of $\ln(d\alpha/dt)$ versus $\ln(1-\alpha)$ for each isothermal temperature studied (The fit for data obtained at 140 ^{o}C was shown in Figure 8.6 as an example). It can be observed that the conversion predicted by the variable 'n' kinetics model is closer to the experimental data in comparison to fixed 'n' model. It can be clearly seen from Figure 8.8 (a), (b) and (c) that the variable 'n' model is notably better in the chemical controlled region and has almost perfect fitting to the experimental data at early stage of the curing reaction.

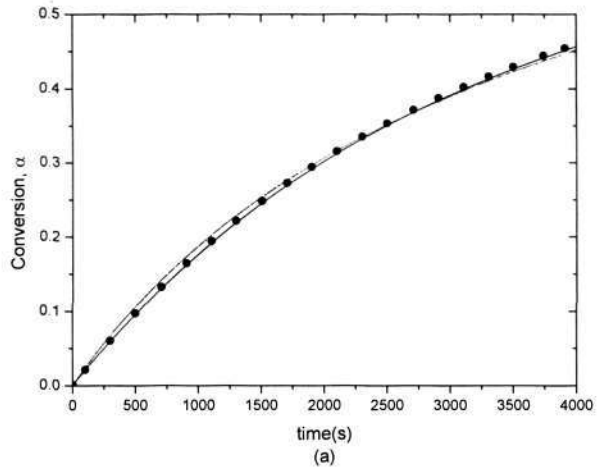

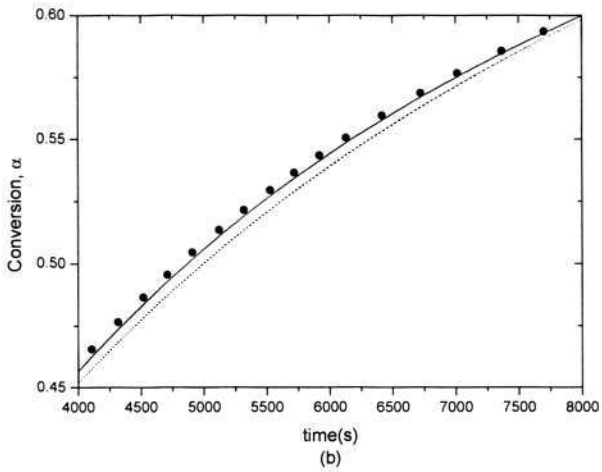

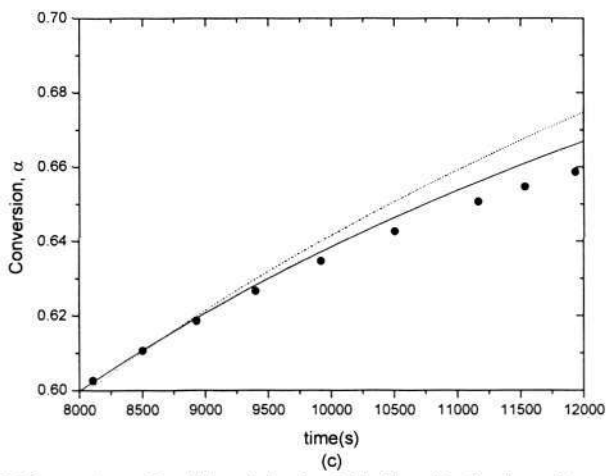

Figure 8.8 Comparison of fixed 'n' model and variable 'n' model at isothermal temperature 140°C
● Experiment data · Fixed 'n' model —·— Variable 'n' model, $n=q_1+q_2*\ln(1-\alpha)$

Figure 8.9 shows the comparison of experiment $\alpha \sim t$ data versus that predicted by the variable 'n' reaction kinetics model for DFCy.

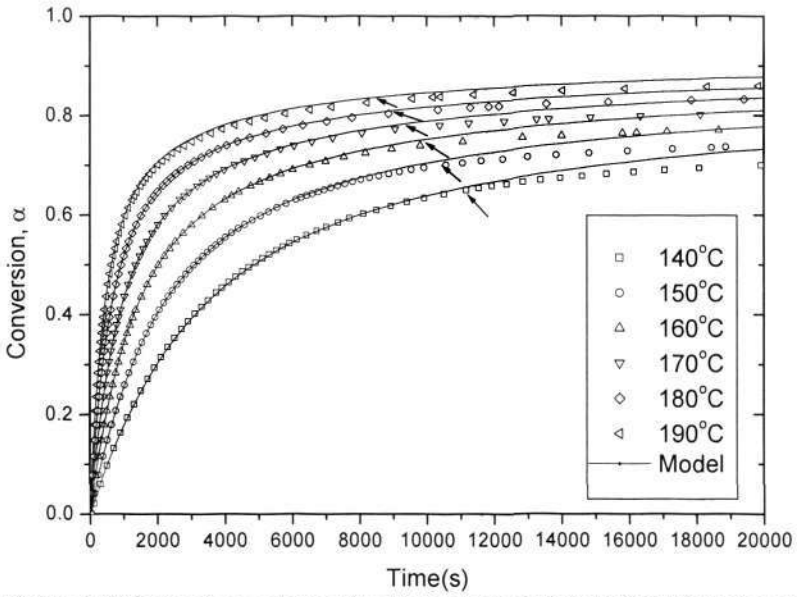

Figure 8.9 Comparison of experimental data versus variable 'n' kinetics model in chemical controlled region
(Arrows indicating the deviation from chemical controlled to diffusion controlled mechanism)

In Figure 8.9, the experimental data obtained at different isothermal temperatures all agree well with the variable 'n' kinetics model prediction throughout the chemical controlled region ($\alpha < \alpha_{onset}$). The experimental data then deviate from the model at certain conversion as expected. For different isothermal temperatures, the values of α_{onset} are also different. It can be seen that, the higher the isothermal temperature, the higher the onset conversion. This agrees well with Equation 8.7 and Figure 8.3 discussed earlier.

When $\alpha > \alpha_{onset}$, the reaction mechanism shifts from chemical controlled to diffusion controlled. Thus the model based on Equation 8.11 is not applicable. The reaction system shows viscoelastic behavior and the reaction rate becomes much slower than that in the chemical controlled region. The rate constant in the diffusion controlled region can be described in terms of the well-known WLF equation.

8.3 Variable '*n*' - WLF Kinetics Model

In this study, a new kinetics model, which combines the variable 'n' kinetics model and the WLF equation, is proposed for the entire conversion range of the curing reaction. A similar approach adapted by Simon and Gillham [83] is used, i.e.:

$$\frac{1}{k} = \frac{1}{k_T} + \frac{1}{k_D} \qquad \text{(Equation 8.4)}$$

In practice, k_T can be obtained by fitting the experimental data at the early curing stage ($\alpha < \alpha_{onset}$). The overall rate constant k can be determined from the following equation:

$$k = \frac{d\alpha / dt}{(1-\alpha)^n} \qquad \text{(Equation 8.9)}$$

Then the diffusion rate constant k_D can be obtained from Equation 8.4. However, a kinetics model is proposed using the variable 'n' approach in this study, where $n = n(\alpha) = q_1 + q_2 \ln(1-\alpha)$ as described in Equation 8.11. In this case:

$$k = \frac{d\alpha / dt}{(1-\alpha)^{q_1 + q_2 \ln(1-\alpha)}} \qquad \text{(Equation 8.10)}$$

The experimental overall rate constant as a function of conversion at an isothermal curing temperature of 140 °C is shown in Figure 8.10 as an example. It can be seen that in the chemical controlled region, $k \approx k_T$. Then there is a region that both chemical control and diffusion control take effect, i.e., k_T is comparable to k_D. At the later curing stage, the reaction is dominated by diffusion controlled mechanism, $k \approx k_D$.

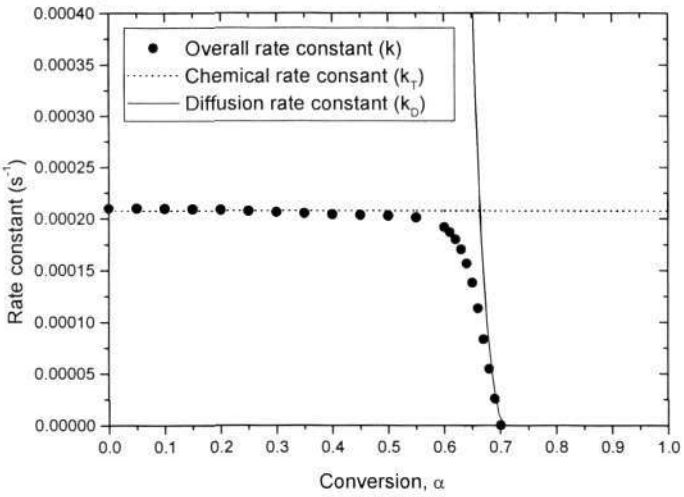

Figure 8.10 Relationship between overall rate constant and α at 140 °C for DFCy

The diffusion rate constant is expected to be inversely proportional to the relaxation time of the polymer segments. It was suggested that the temperature dependence of k_D can be described by WLF equation [83,84]:

$$\log \frac{k_D}{k_{D-onset}} = \frac{C_1[Tg_{onset} - Tg(\alpha)]}{C_2 + |Tg_{onset} - Tg(\alpha)|} \qquad \text{(Equation 8.5)}$$

Since the relationship between k_D and conversion has been established, once the correlation between glass transition temperature, Tg and conversion is established, the diffusion rate constant k_D can be expressed explicitly as a function of temperature and conversion. Then the unknown parameters in Equation 8.5 can be obtained accordingly. The measured Tg of DFCy as a function of conversion is given in Figure 8.11 (also seen Figure 7.13 in Chapter 7). The experimental curve was fitted using Dibenedetto equation [93,94]:

$$Tg(\alpha) = \frac{(1-\alpha)Tg_0 + \lambda\alpha Tg_\infty}{1-\alpha+\lambda\alpha} \qquad \text{(Equation 8.11)}$$

where α is the conversion. Tg_0 is the theoretical glass transition temperature of the polymer at very low conversion. Tg_∞ is the glass transition temperature of the fully cured

polymer, λ is a fitting parameter. Both Tg_0 and Tg_∞ are obtained by curve fitting of the experimental data using the Dibenedetto equation.

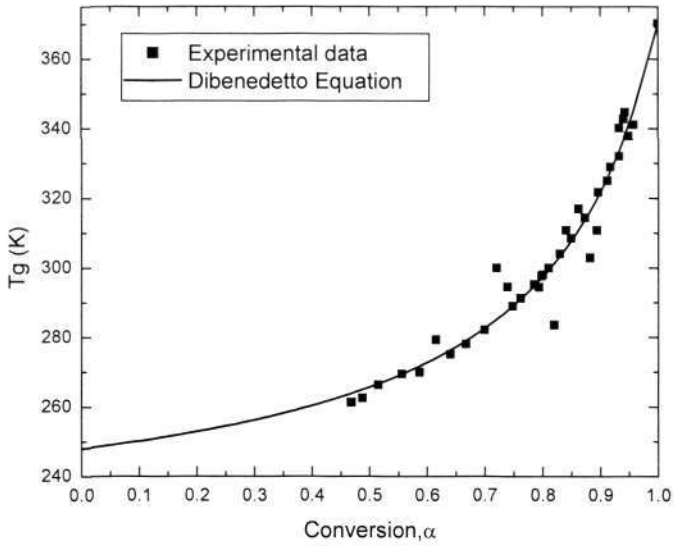

Figure 8.11 Tg versus conversion for DFCy

Once the relationship between conversion and glass transition temperature is established, the parameters in Equation 8.5 can be obtained by plotting the logarithm of diffusion rate constant k_D versus $(Tg_{onset} - Tg)/(C_2 + |Tg_{onset} - Tg|)$. The fitting constant C_2 is accepted as the WLF universal constant, 51.6. The obtained parameters for the variable 'n' - WLF kinetics model were listed in Table 8.1. The comparison of experimental data versus those calculated from the model is shown in Figure 8.12. It can be seen that the variable 'n' - WLF type kinetics model describes the curing behavior very well. Excellent agreement between experimental data and model is observed for the entire conversion range at different isothermal temperatures, including both chemical controlled and diffusion controlled regions.

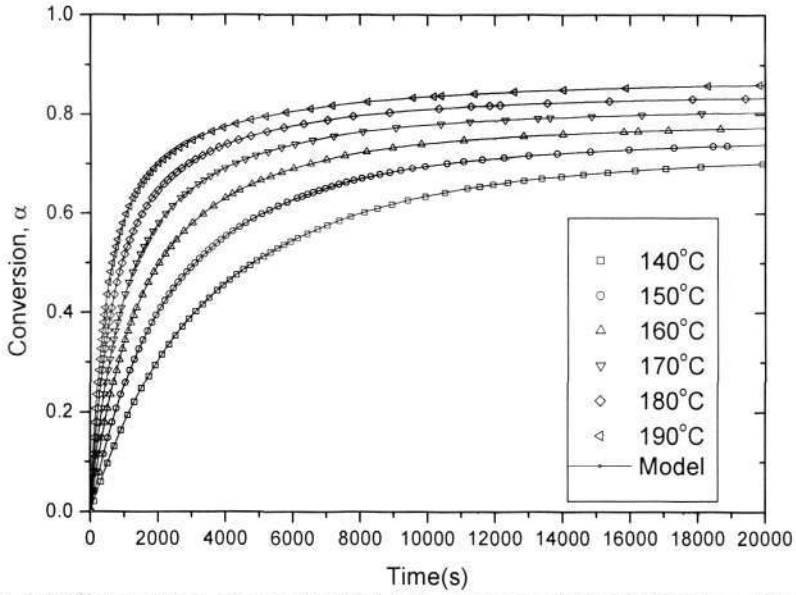

Figure 8.12 Comparison of experimental data versus variable '*n*' WLF type kinetics model

Summary, the equations used in the variable 'n' - WLF kinetics model are listed below.

Table 8.1 list the kinetics parameters for DFCy.

$$\frac{d\alpha}{dt} = k(1-\alpha)^{q_1+q_2\ln(1-\alpha)}$$

$$\frac{1}{k} = \frac{1}{k_T} + \frac{1}{k_D}$$

$$k_T = Ae^{-\frac{E}{RT}}$$

$$\log\frac{k_D}{k_{D-onset}} = \frac{C_1[Tg_{onset} - Tg(\alpha)]}{C_2 + |Tg_{onset} - Tg(\alpha)|}$$

$$\alpha_{onset} = p_2\left(\frac{1}{T_2} - \frac{1}{T}\right)$$

$$Tg(\alpha) = \frac{(1-\alpha)Tg_0 + \lambda\alpha Tg_\infty}{1-\alpha+\lambda\alpha}$$

Table 8.1 Parameters of variable 'n' kinetics model for DFCy

A=63704 s^{-1}	E=67248 J/mol	q_1=1.5	q_2=-1.0
Tg_0=247.9 K	Tg_∞=370.2 K	$\lambda = 0.17$	$p_2 = 664.8$ K
C_1=8.16 K	C_2=51.6 K	$k_{D-onset}$=2.24×10^{-3} s^{-1}	$T_2 = 278.6$ K

8.4 Summary

The kinetics study of the aliphatic cyanate ester DFCy indicates that the reaction follows nth order kinetics model in the chemical controlled region and approaches a plateau conversion at certain curing temperature, which is less than complete conversion. The diffusion limitation occurs at certain onset conversion, and this onset conversion increases with the increasing of isothermal curing temperature. The study found that the reaction order 'n' is not a constant throughout the whole reaction time. A conversion dependent reaction order was proposed, based on which a new kinetics model, which combines the variable 'n' kinetics model and WLF equation, was established to describe both the chemical and diffusion controlled regions. For the temperature range studied (140-190 ^{o}C), the new variable 'n' kinetics model predict the experimental data with much better accuracy. Our preliminary study also showed that the variable 'n' kinetics model is also suitable for the curing of other thermosettings such as BMI/DBA system. Therefore, the variable 'n' WLF kinetics model should be useful for other thermosetting systems which follow the nth order kinetics in general.

CHAPTER 9

CURING STUDY OF POLYCYANUATES PART II. MODELLING THE CURING KINETICS OF UNCATALYZED AROMATIC CYANATE ESTER

9.1 Introduction

n th order model cannot describe the progress of complex reactions of some thermosetting resin systems, in which several reactions may occur simultaneously during the cure process [78-81,88-92]. For example, Equation 8.1 predicts the maximum of reaction rate at $t = 0$, which is not the case for certain thermosetting resins, for example, epoxy/amine curing system [81]. The following autocatalytic kinetics model represents adequately these curing reaction systems and first proposed by Kamal et al based on curing of epoxy resins [88,89].

$$\frac{d\alpha}{dt} = k_1(1-\alpha)^n + k_2\alpha^m(1-\alpha)^n \qquad \text{(Equation 9.1)}$$

where k_1 and k_2 are rate constants following Arrhenius temperature dependency. m and n are reaction orders that are constants independent of temperature and conversion. This autocatalytic kinetics equation has been widely used in the literature to represent the curing of a range of thermosetting resins such as epoxy [78-81,88-92].

Unlike the nth order kinetics model, which has maximum reaction rate at $t = 0$ or $\alpha = 0$, it can be derived from Equation 9.1 that an autocatalytic kinetics model predicts

maximum reaction rate ($d\alpha/dt$) at some intermediate conversion ($\alpha > 0$). At the point of maximum reaction rate, $d(d\alpha/dt)/d\alpha = 0$, hence the following equation can be derived from Equation 9.1:

$$\left(\alpha^m - \frac{m}{m+n}\alpha^{m-1}\right)\Big|_{\frac{d\alpha}{dt}=\left(\frac{d\alpha}{dt}\right)_{max}} = -\frac{n}{m+n}\frac{k_1}{k_2} \qquad \text{(Equation 9.2)}$$

Usually $k_1 << k_2$, then we have:

$$\alpha_{peak} = \alpha\Big|_{\frac{d\alpha}{dt}=\left(\frac{d\alpha}{dt}\right)_{max}} \approx \frac{m}{m+n} \qquad \text{(Equation 9.3)}$$

For a typical autocatalytic reaction, α_{peak}, the conversion at which reaction rate reaches its maximum value is around 0.3~0.4 [68].

In general, thermosetting polymers exhibit gelation and vitrification phenomenon, which greatly reduces the reaction rate. After vitrification, the cure process becomes diffusion controlled and as a consequence, the experimental conversion and reaction rate are much lower than those predicted by the model [60,61,73]. The phenomenon occurs in thermosetting curing systems regardless whether the reaction follows an nth order or autocatalytic curing kinetics model. Therefore the above kinetics models cannot describe the observed reduced reaction rate at the later stage of cure where the reaction becomes very slow. Understanding this diffusion controlled phenomenon of thermosetting reactions is important in order to achieve optimum properties of the cured resins. For curing of high performance resins such as cyanate ester and bismaleimide, it is important to have a working model which describes the entire curing process.

To take into account both the chemical and diffusion controlled regions the curing kinetics, a model was proposed by considering the overall reaction rate constant to be composed of two components, one associated with the diffusion controlled reaction step

and another with the chemical controlled reaction step [74,83]. The overall reaction rate constant was defined as:

$$\frac{1}{k} = \frac{1}{k_T} + \frac{1}{k_D} \qquad \text{(Equation 9.4)}$$

where k is the overall rate constant, k_T is the rate constant in the chemical controlled region and described by Arrhenius relationship, k_D is the diffusion rate constant. k_T is a function of curing temperature (T), while k and k_D are functions of conversion (α) and curing temperature (T). The preceding equation shows that the overall rate constant is governed at one extreme by the Arrhenius rate constant when $k_T << k_D$ (prior to vitrification), and at the other extreme by the diffusion rate constant when $k_D << k_T$ (after vitrification) [54].

In Chapter 8, we have discussed the nth order reaction kinetics of aliphatic polycyanurate DFCy, and a variable 'n' kinetics model was proposed, which provided much better prediction of the experimental data than that of normal nth order kinetics model. In this Chapter, we will more focus on the autocatalytic curing kinetics model based on the study of curing reaction of aromatic polycyanurate BACy.

Polycyanurate resins belong to an important class of high performance thermosetting resins and have been used as low dielectric materials in aerospace composites, printed circuit boards and electronic adhesives [1-5]. More recently, polycyanurate resins have found new applications in thin films [34-38], nano-composites [39,40] and optical waveguides [27-33]. The curing kinetics of cyanate ester has attracted much research attention. Normally, to reduce the curing temperature and enhance the reaction rates of cyanate ester, usually a metal catalyst is used in practical curing schedules [1]. Curing kinetics of catalyzed cyanate ester systems have been reported and different techniques,

such as DSC [52,53], FTIR [56], and DEA (Dielectric analysis) [59] have been employed to monitor the curing reaction. A general agreement is that, the cure reaction of cyanate ester is dominanted by chemical control at lower conversions and diffusion control at higher conversions. In the chemical controlled region, the curing kinetics may follow either an nth order or an autocatalytic model depending on the presence of catalysts and the structures of the monomers.

Although the catalyzed cyanate ester systems are often used in composites applications, the uncatalyzed systems are important for dielectric or photonic applications, because the use of metal catalysts increases the dielectric or optical loss of the polymer. However, very few studies were reported on the curing kinetics of uncatalyzed aromatic cyanate esters [55,91], furthermore, these studies only discussed the curing in the chemical controlled region.

In the present study, the cure reaction of uncatalyzed BACy was monitored and investigated by isothermal DSC. A new kinetics model, which takes into account both the chemical and diffusion controlled regions, was established to describe the entire conversion range for the curing reaction of BACy. The study also found that the reaction orders are temperature dependent rather than constants. The new kinetic model also takes this phenomenon into consideration.

9.2 Temperature Dependent Reaction Orders in Autocatalytic Curing Kinetics

The isothermal curing kinetics of BACy was investigated at several curing temperatures from 180 °C to 260 °C at a 20 °C interval. Figure 9.1 shows the experimental conversion (α) versus curing time (t) of BACy at different isothermal curing temperatures.

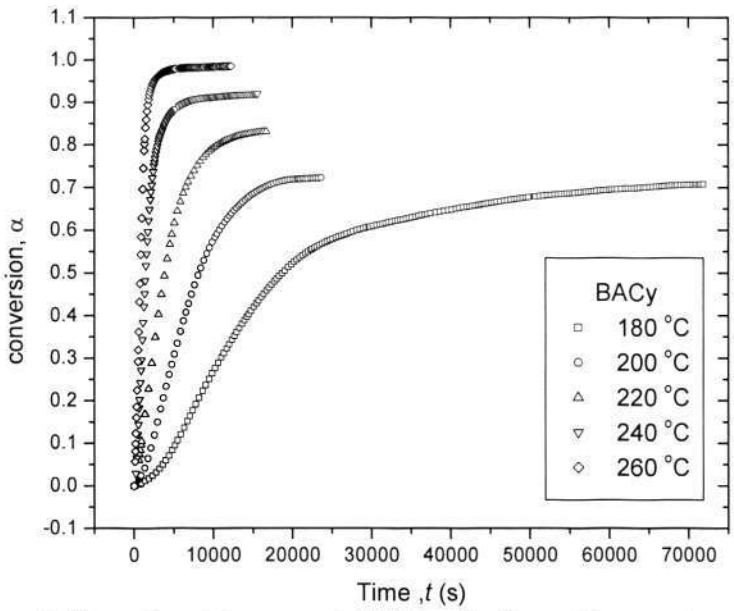

Figure 9.1 Experimental α versus t of BACy at isothermal temperatures 180-260°C

Figure 9.1 shows that the increase of conversion with curing time of cyanate is initially slow, then becomes rapid, and then slows down further before the conversion finally reaches a plateau towards maximum conversion. The plot of $\alpha \sim t$ shows a 'S' shape which is the characteristic feature of autocatalytic kinetics and different from those of the reactions following the n th order kinetics model. This is particular notable in $\alpha \sim t$ curves of lower curing temperatures. Usually, there is a trace amount of phenol impurities in aromatic cyanate ester monomers, which resulted from the synthesis process. These phenol impurities act as the catalyst for the initialization of the cyclotrimerization of cyanate esters. Because the phenol concentration is very low, the reaction rate is also very

low, until enough amount of reaction intermediates are generated, which can autocatalyze the reaction or accelerate the reaction rate [1-2].

Another important phenomenon is the diffusion at the later curing stage. At the early stage of the curing reaction, the concentration of the functional group is higher and the mobility of the molecules is not constrained, so the reaction rate is not affected by the diffusion. During the curing processing of cyanate ester resin, the viscosity of the reaction system increases with time due to the increase of molecular weight. The mobility of the reactive group is constrained and the reaction becomes diffusion controlled because of the very high viscosity in the matrix. Finally, the molecular weight and the viscosity become infinitely high such that no further cure may occur, and a plateau conversion is reached. At this point, only limited further reaction can be observed, unless the cure temperature is raised to increase the mobility of the molecular chains.

As mentioned earlier, the reaction behavior of thermosetting resin may follow two different types of kinetics models, namely nth order model and autocatalytic model. To predict the curing kinetics of BACy, the relationship between the reaction rate versus curing time or conversion were obtained by differentiate the $\alpha \sim t$ experimental curves which lead to the $d\alpha/dt \sim t$ plots $d\alpha/dt \sim \alpha$ plots in Figures 9.2 and 9.3 respectively. If the reaction can be described by an nth order kinetics model, the reaction rate should be the highest at the beginning of the curing reaction ($\alpha = 0$ or $t = 0$). If the reaction follows an autocatalytic model, however, the reaction rate reaches its maximum value at a certain intermediate conversion. It can be observed in Figures 9.2 and 9.3 that the maximum reaction rate does occur at an intermediate conversion, and this conversion, α_{peak}, increases with the increasing curing temperature. Therefore the reaction of BACy follows an autocatalytic kinetics model. The autocatalytic model can be represented by

Equation 9.3. The kinetics parameters k_1, k_2, m and n can be obtained by curve fitting of the experimental $d\alpha/dt \sim \alpha$ curves, as shown in Figure 9.3 using Equation 9.3. The kinetic parameters obtained from the curve fitting are given in Table 9.1.

Table 9.1 Curing kinetics parameters for BACy

T (K)	k_1 (s^{-1})	k_2 (s^{-1})	m	n	$\frac{m}{m+n}$	α_{peak} *	R^2
453	6.6×10^{-6}	3.3×10^{-4}	0.93	3.63	0.20	0.16	0.9693
473	2.0×10^{-5}	5.4×10^{-4}	0.88	2.80	0.24	0.18	0.9807
493	4.0×10^{-5}	9.1×10^{-4}	0.84	2.30	0.26	0.23	0.9620
513	1.0×10^{-4}	1.9×10^{-3}	0.86	1.86	0.31	0.29	0.9806
533	2.9×10^{-4}	2.7×10^{-3}	0.91	1.21	0.43	0.42	0.9845

* α_{peak} : experimental conversion of peak reaction rate

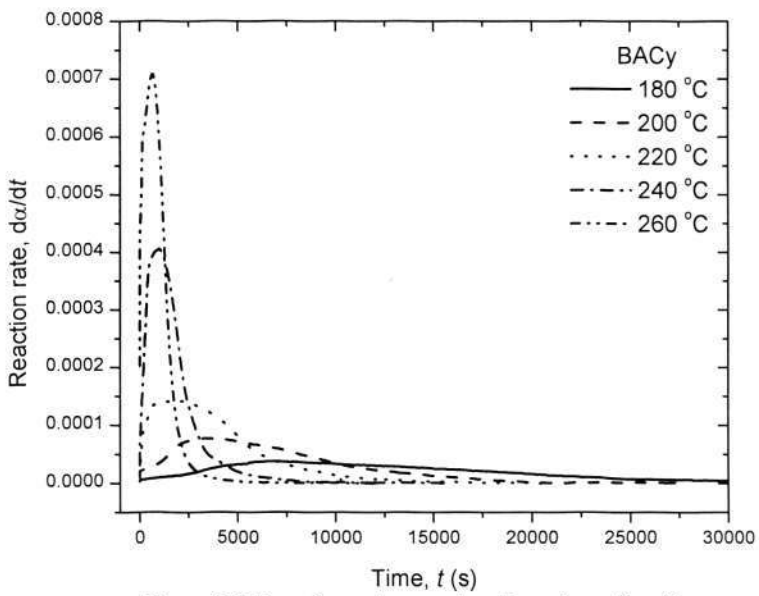

Figure 9.2 Reaction rate as a function of reaction time of BACy at different isothermal temperatures

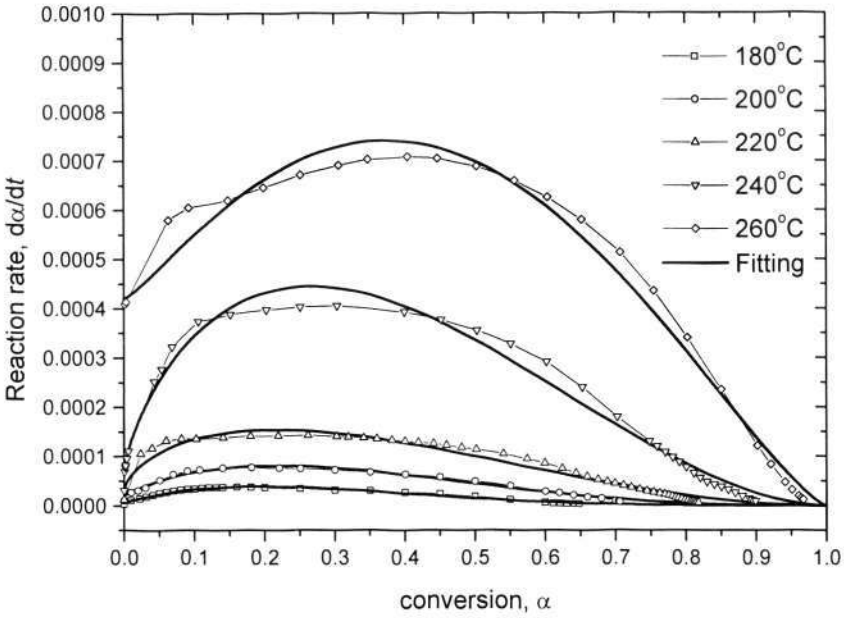

Figure 9.3 Reaction rate as a function of conversion of BACy at different isothermal temperatures

It can be seen from Figure 9.3 and Table 9.1 that the conversions, where the reaction rates reach maximum values increase with the increase of curing temperature. This is different from some other previous reported thermosetting curing systems [55,73-75], in which the maximum reaction rate occurs at almost the same conversion in all the curing temperature range. The reason for this difference is not completely clear, but it is probably originated from the competition between the autocatalytic and non-autocatalytic reaction which may be material dependent.

It is worth pointing out that the reaction orders m and n may not always be temperature independent constants [78-81]. The plots of reaction orders m and n versus curing temperature of BACy are shown in Figure 9.4.

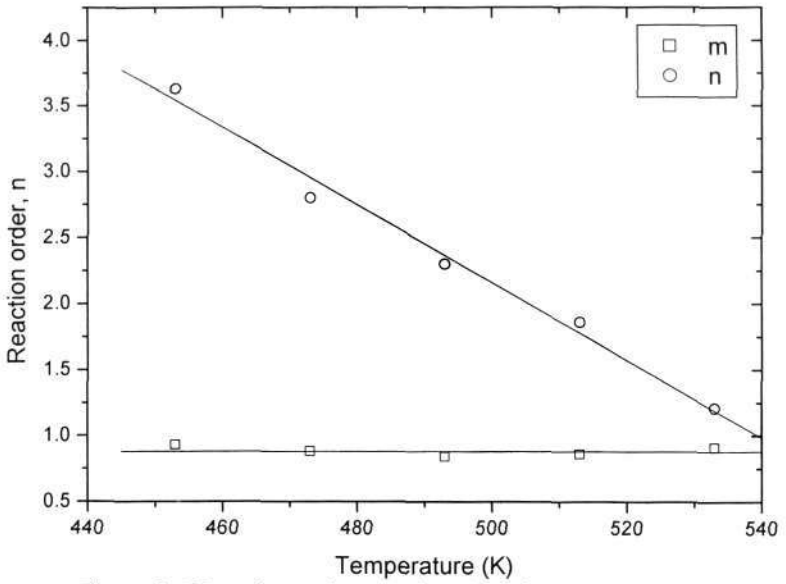

Figure 9.4 Reaction order as a function of temperature for BACy

It is interesting that a linear relationship between the reaction order n and temperature was observed in Figure 9.4. Although the reaction order m can be approximately regarded as a constant in this particular case, both m and n can be expressed by:

$$n(T) = n_0 + p_0 T \qquad \text{(Equation 9.5a)}$$

$$m(T) = m_0 + q_0 T \qquad \text{(Equation 9.5b)}$$

where T is the curing temperature, m_0, q_0, n_0 and p_0 are fitting parameters, in this work, $m_0 = 0.88$, $q_0 = 0$, $n_0 = 16.86$ and p_0=-0.0294 K^{-1}.

Actually most of the reported work on autocatalytic curing kinetics of thermosetting resins showed different reaction orders for different curing temperatures [78-81], but normally an average was taken as the reaction order for calculation and very few comments on the change of reaction order can be found in literatures. A very recent report discussed the linear relationship between m, n and T in aromatic amine cured epoxy resin [87].

Although further studies are necessary in order to have more clear understanding on the temperature dependency of reaction orders m and n, the fact that the reaction orders may vary with temperature is certain. Thus the reaction kinetics of uncatalyzed BACy cannot be simply described by Equation 9.1 even in the chemical controlled region. In the present discussion on curing kinetics, we would like to take more rigorous treatment. By considering the effect of temperature on the reaction orders, a more generic equation is obtained,

$$\frac{d\alpha}{dt} = (k_1 + k_2\alpha^{m_0+q_0T})(1-\alpha)^{n_0+p_0T} \qquad \text{(Equation 9.6)}$$

where reaction orders m and n are temperature dependent and expressed in Equation 9.5, although for BACy $q_0 = 0$.

The activation energies (E_1 and E_2) can be obtained by Arrenius plots of $\ln(k_1)$ and $\ln(k_2)$ versus $1/T$ as shown in Figure 9.5, which give $E_1 = 94{,}957\ J/mol$, $E_2 = 52{,}120\ J/mol$, A_1=510,936 s^{-1} and A_2=327 s^{-1}.

If the parameters k_1, k_2 m_0, q_0, n_0 and p_0 in Equation 9.6 are known, the theoretical prediction of α versus t can be obtained by integration:

$$t = \int_0^{\alpha} \frac{d\alpha}{(k_1 + k_2\alpha^{m_0+q_0T})(1-\alpha)^{n_0+p_0T}} \qquad \text{(Equation 9.7)}$$

The comparison of theoretical prediction and experimental curves of α versus t is shown in Figure 9.6.

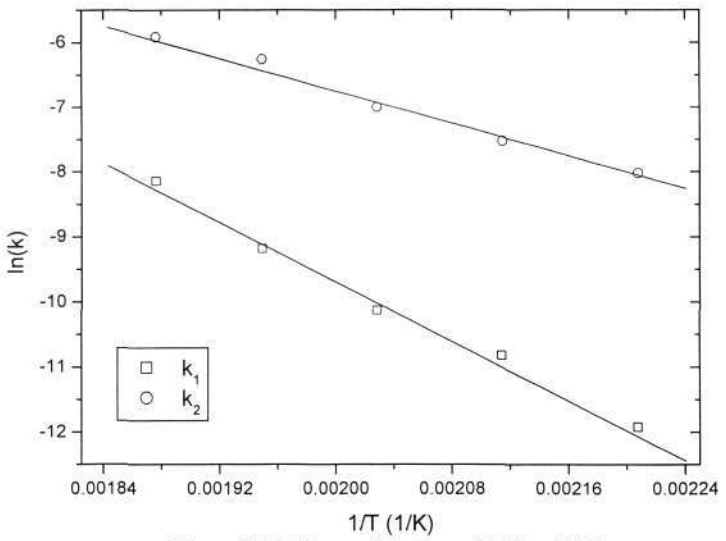

Figure 9.5 ln(k) as a function of 1/T for BACy

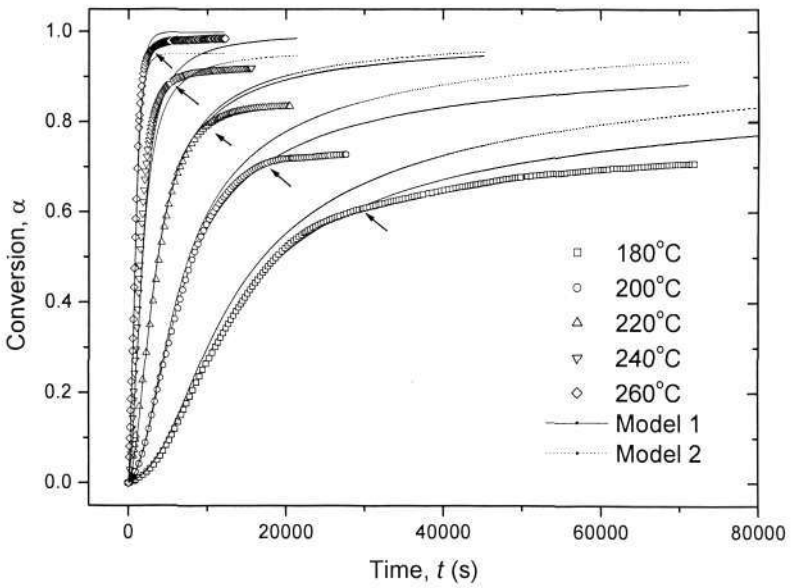

Figure 9.6 Comparison of model prediction and experimental curves of α~t
Model 1: temperature dependent reaction orders. Model 2: fixed reaction orders
(arrows indicating the onset deviation from chemical control to diffusion control)

It can be seen from Figure 9.6 that Equation 9.6 involving temperature dependent reaction order gives much more accurate prediction than Equation 9.3 using the average reaction order. Equation 9.8 can be fitted with the experimental data very well in the chemical controlled region. It eventually deviate from experimental at higher conversions due to the onset of diffusion controlled kinetics. As a consequence, the experimental conversion

and reaction rate are generally lower than those predicted by Equation 9.6. It can also be observed that the α_{onset}, at which the reaction kinetics shifts from chemical controlled to diffusion controlled is dependent on the curing temperature. α_{onset} increases with increasing temperatures, and can be empirically expressed as:

$$\alpha_{onset} = p_1(\frac{1}{T_1} - \frac{1}{T}) \qquad \text{(Equation 9.8)}$$

where p_1 is a fitting constant, T is the curing temperature, and T_1 is the hypothetical critical temperature below which no chemical controlled reaction could occur (i.e., $\alpha_{onset} = 0$ when $T = T_1$). p_1 and T_1 can be obtained from curve fitting, as shown in Figure 9.7.

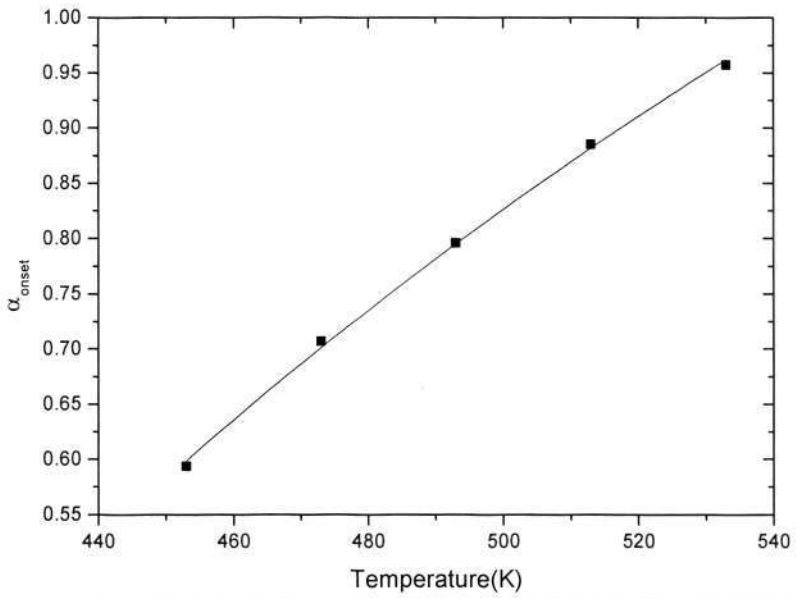

Figure 9.7 Onset conversion as a function of temperature for BACy

Most of the reported studies on the curing of thermosetting resins with an autocatalytic kinetics model have only limited within the chemical controlled region. However, it is also important to be able to predict the diffusion controlled curing reaction. In order to derive a kinetics model to describe the entire curing conversion range of BACy including the chemical controlled and diffusion controlled regions, a simple generic expression is used:

$$\frac{d\alpha}{dt} = k(1-\alpha)^{n_0+p_0T} \qquad \text{(Equation 9.9)}$$

Note that Equation 9.9 has a similar form as Equation 8.1. However, in this case, k is the overall rate constant given by Equation 9.4, which is dependent on temperature, conversion and reaction order. Hence, the overall rate constant k can be determined from the experimental data by using the following equation:

$$k = \frac{d\alpha / dt}{(1-\alpha)^{n_0+p_0T}} \qquad \text{(Equation 9.10)}$$

The rate constant in the chemical controlled region k_T is given by:

$$k_T = k_1 + k_2\alpha^{m_0+q_0T} \quad (\alpha < \alpha_{onset}) \qquad \text{(Equation 9.11)}$$

Then the diffusion rate constant k_D can be calculated using Equation 9.4. The relationship between k (determined experimentally) and α^m at isothermal temperature 220 °C is shown in Figure 9.8 as an example. It can be seen that in the chemical controlled region, $k \approx k_T = k_1 + k_2\alpha^m$, which follows the solid line. Then there is a region that both chemical control and diffusion control take effect, i.e., the value of k_T is comparable to k_D. At the later curing stage, the reaction is dominated by diffusion controlled kinetics, $k \approx k_D$.

k_D is expected to be inversely proportional to the relaxation time of the polymer chain segments, and can be described by the WLF equation [7, 8]:

$$\log\frac{k_D}{k_{D-onset}} = \frac{C_1[Tg_{onset} - Tg(\alpha)]}{C_2 + |Tg_{onset} - Tg(\alpha)|} \qquad \text{(Equation 9.12)}$$

where C_1 and C_2 are fitting parameters, $k_{D-onset}$ and Tg_{onset} are the diffusion rate constant and the glass transition temperature at α_{onset} respectively. $Tg(\alpha)$ is the glass transition temperature at conversion α.

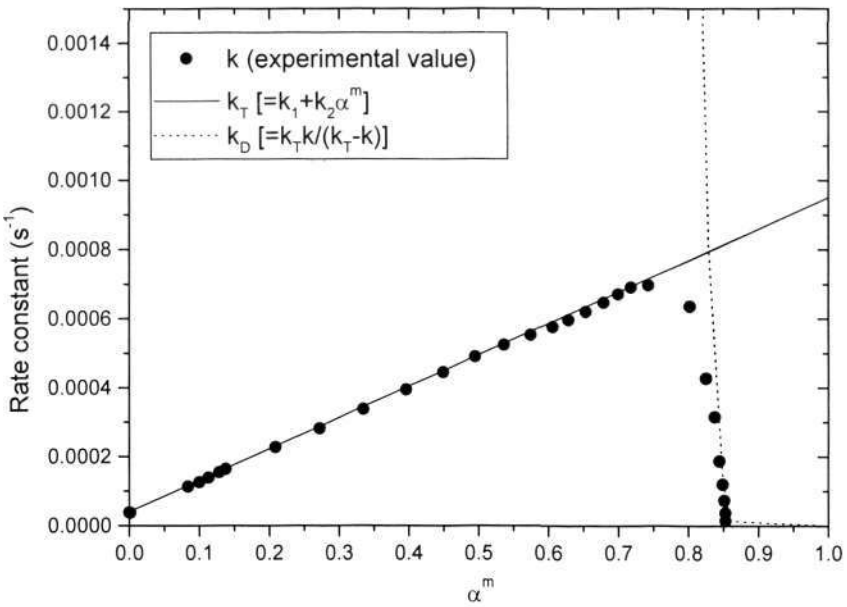

Figure 9.8 Relationship between overall rate constant and α^m at 220 °C for BACy

Equation 9.12 established the relationship between k_D and the glass transition temperature. Once the correlation between the glass transition temperature and conversion $Tg(\alpha)$ is established, k_D can be expressed explicitly as a function conversion. Also the unknown parameters in Equation 9.12 can be obtained by curve fitting accordingly. The constant C_2 is accepted as the WLF universal constant, 51.6 as suggested [98]. $k_{D-onset}$ and C_1 can be obtained by plotting $\log k_D$ versus $[Tg(\alpha_{onset}) - Tg(\alpha)]/[C_2 + |Tg(\alpha_{onset}) - Tg(\alpha)|]$.

Therefore, to apply this WLF-type equation to a diffusion controlled kinetics model, it is necessary to establish a relationship between the glass transition temperature, Tg, and the conversion, α. Figure 9.9 shows the measured Tg of BACy as a function of conversion (also see Figure 7.11 in Chapter 7). The experimental curve can be fitted using the Dibenedetto equation [93,94]:

$$Tg(\alpha) = \frac{(1-\alpha)Tg_0 + \lambda\alpha Tg_\infty}{1-\alpha+\lambda\alpha} \qquad \text{(Equation 9.13)}$$

where α is the conversion. Tg_0 is the theoretical glass transition temperature of the polymer at very low conversion. Tg_∞ is the glass transition temperature of the fully cured polymer, λ is a fitting parameter. Both Tg_0 and Tg_∞ are obtained by curve fitting of the experimental data using Equation 9.13.

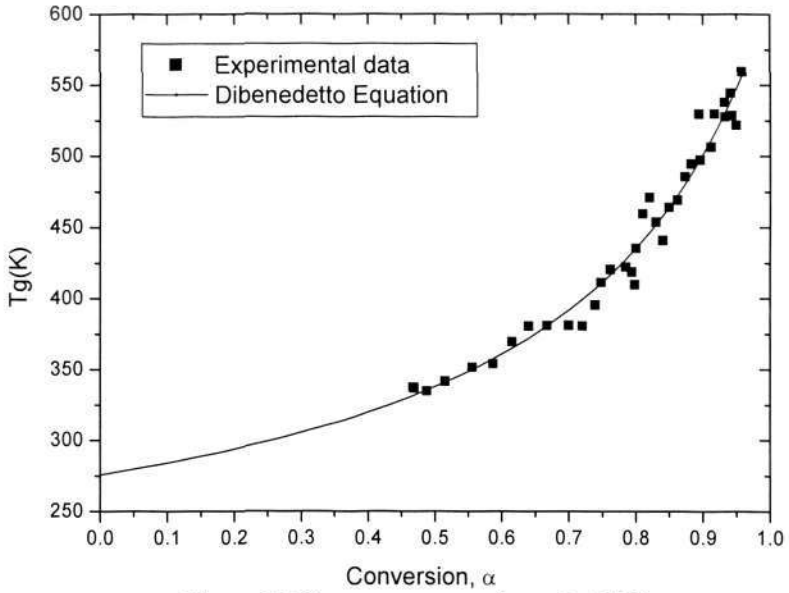

Figure 9.9 Tg versus conversion α for BACy

Thus, the relationship between k_D and α can be established from Equation 9.12, and then a new kinetics model is established. The equations used in this new kinetics model are listed below and the obtained values of parameters are listed in Table 9.2.

$$d\alpha / dt = k(1-\alpha)^{n(T)}$$

$$n(T) = n_0 + p_0 T$$

$$1/k = 1/k_T + 1/k_D$$

$$k_T = k_1 + k_2 \alpha^{m(T)}$$

$$m(T) = m_0 + q_0 T$$

$$k_{1,2} = A_{1,2} EXP(-E_{1,2} / RT)$$

$$\log \frac{k_D}{k_{D-onset}} = \frac{C_1[Tg(\alpha_{onset}) - Tg(\alpha)]}{C_2 + |Tg(\alpha_{onset}) - Tg(\alpha)|}$$

$$\alpha_{onset} = p_1(1/T_1 - 1/T)$$

$$Tg(\alpha) = \frac{(1-\alpha)Tg_0 + \lambda\alpha Tg_\infty}{1-\alpha+\lambda\alpha} \qquad \text{(Equations 9.14)}$$

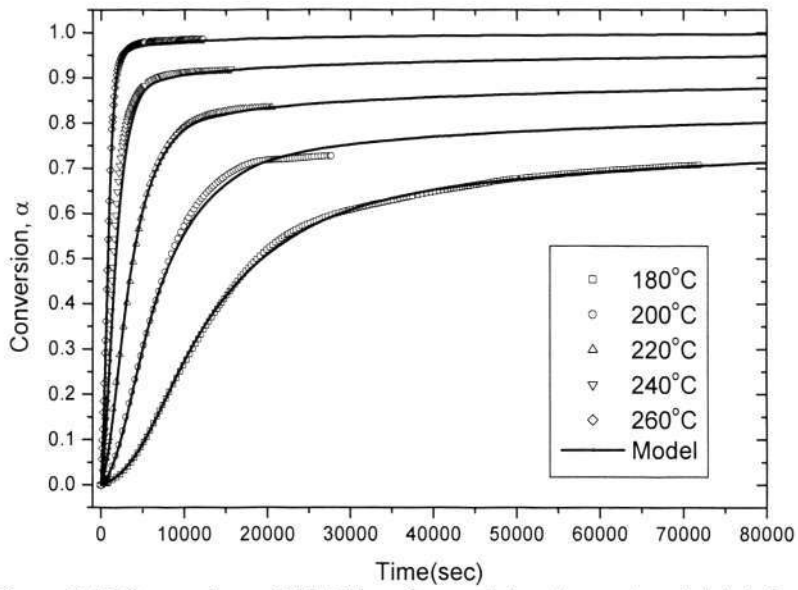

Figure 9.10 Comparison of WLF kinectics model and experimental data for BACy

Table 9.2 Parameters for WLF-type kinetics model of BACy

A_1=508897 s^{-1}	E_1=94957 J/mol	A_2=326 s^{-1}	E_2=52120 J/mol
m_0=0.88	$q_0 = 0$	n_0=16.86	p_0=-0.0294 K^{-1}
$k_{D-onset}$=9.33×10^{-4} s^{-1}	C_1=2.54 K	C_2=51.6 K	
p_1=1096 K	T_1=363 K		
Tg_0=295.8 K	Tg_∞=632.3 K	λ=0.225	

The comparison of experimental data versus WLF type kinetics model is shown in Figure 9.10. The WLF type kinetics model describes the curing behavior well for BACy. Good agreement between experimental data and the kinetics model prediction is obtained.

9.3 Summary

Curing study of uncatalyzed BACy was conducted using isothermal DSC. The study revealed that the reaction of uncatalyzed BACy follows an autocatalytic kinetics model in the chemical controlled region. The reaction becomes diffusion controlled after certain onset conversion, and this onset conversion increases with increasing isothermal curing temperature. WLF equation was used to describe the reaction diffusion rate constant. A new kinetics model, which takes into account both the chemical and diffusion controlled regions, was established to describe the entire conversion range for the curing reaction of BACy.

An important contribution of this new model is that it considers the variation of the reaction orders m and n with curing temperature. Such variation can be substantial in thermoset resins but has usually been overlooked in literature as far as the modeling of curing is concerned. By considering the temperature dependency of the reaction orders, the new kinetics model predicts the experimental data of BACy more accurately. Therefore, this new model should be used for accurate modeling of curing reactions of thermosets following autocatalytic kinetics.

CHAPTER 10

CONCLUSIONS AND FUTURE WORK

10.1 Conclusions

In this study, several modified polycyanurates have been prepared by copolymerization of four cyanate ester monomers with different backbone structures: 2,2'-bis(4-cyanatophenyl)iso-propylidene (BACy), 2,2-bis(4-cyanatophenyl)-1,1,1,3,3,3-hexafluoropropane (BFCy), 2,2,3,3,4,4,5,5,6,6,7,7-dodecafluorooctanediol dicyanate ester (DFCy) and 4-phenylphenol cyanate ester (CPCy). The prepared polycyanurate copolymers are BACy/BFCy, BACy/DFCy and BACy/CPCy with different molar ratios from 0:1 to 1:0. Thin films of polycyanurate homopolymers and copolymers have also been prepared by appropriate prepolymerization and spin-coating followed by thermal curing.

The factors influencing the preparation of polycyanurate thin films were studied and optimized. The dielectric, optical, thermal, mechanical properties and surface morphology of the polycyanurate resins and their thin films were systematically investigated. The curing kinetics of the polycyanurates were also studied in detail, and two new models were established for the curing reactions of aliphatic DFCy and aromatic BACy respectively. Detailed conclusions have been provided at the end of each chapter. Main conclusions of this study are as follows.

Preparation and characterizations of polycyanurate thin films

Preparation of polycyanurate thin films consist of three steps, namely, prepolymerization, spin-coating and thermal curing. The study showed that prepolymerization is essential in three aspects for the preparation of polycyanurate thin films. (1) It prevents the crystallization of the cyanate ester monomers. (2) It prevents the evaporation of the cyanate ester monomers. (3) It provides appropriate viscosity to the precursor solution for the following spin-coating process. A basic consideration of the polymerization conditions for the preparation of polycyanurate thin films is that in order to minimize the evaporation of cyanate ester monomers, at the same time allow necessary solubility in the solvent, the degree of prepolymerization should be kept as high as possible but not exceed the gel point. In the present study, prepolymers with degree of prepolymerization between 44% and 47% were used for preparing optical quality polycyanurate thin films.

The study of the preparation of polycyanurate thin films by the spin coating method demonstrated that the quality of the thin films is mainly influenced by three parameters, namely solution concentration, spin speed and spin time. Through adjusting the spin coating parameters, polycyanurate thin films with thicknesses varying from several microns to sub-microns only using a single-coating process could be obtained. AFM study of the prepared polycyanurate thin films showed that the films were optical smooth with surface roughness around 1 nm at 1 micron scale.

FTIR spectroscopy of cyanate ester monomers and polycyanurates showed that there is no absorption in the IR region of 6500 cm^{-1} to 2500 cm^{-1} before and after cured, which indicated that polycyanurates have a low optical loss at telecommunication wavelength 1550 nm (wavenumber 6452 cm^{-1}). The strong stretching vibration band of C≡N appears

at 2200 cm^{-1} to 2300 cm^{-1}, which can be used to monitor the curing reaction of polycyanurates.

Dielectric properties and heterogeneity of polycyanurates

The dielectric properties of polycyanurate homopolymers and copolymers are analyzed using the Cole-Cole plot. For the first time, the tiny heterogeneity of the polymer/polymer system was quantified in terms of the values of the adjust parameter α in the Cole-Cole equation. Such a tiny heterogeneity has great influence on the optical and/or dielectric properties of the polymer, and hardly can be detected by traditional thermal and mechanical analysis methods, because the polycyanurate copolymer shows macroscopically phase mixed structure. Different polycyanurate homopolymers and copolymers have different values of α, which reflect the differences in heterogeneities of different polycyanurate systems. For a polycyanurate copolymer with given components, the heterogeneity reaches the maximum when the composition reaches the maximum, i.e., 5:5. While for different polycyanurate copolymers with a given composition, the BACy/DFCy has higher heterogeneity than that of BACy/BFCy copolymer. This is probably because that BACy and BFCy both are aromatic and have very similar molecular structure and geometry, while DFCy is aliphatic and has a very different molecular structure, therefore BACy/BFCy copolymers show better homogeneity than that of BACy/DFCy copolymers, which can be quantified from the values of α.

Optical properties of polycyanurate thin films

The film thickness, refractive index and optical loss of the polycyanurate thin films were characterized using a prism coupler technique. The theoretical refractive indices of BACy, BFCy and DFCy homopolymers were calculated using a segment incremental model

derived from Lorenz-Lorentz equation. The theoretical values have reasonable agreement with the experimental data.

The refractive index of the polycyanurate thin films can be adjusted in a broad range between 1.44 and 1.61 by copolymerizing of four cyanate ester monomers, i.e., BACy, BFCy, DFCy and CPCy with different compositions. The relationship between the refractive index and the composition deviates from linear relationship and can be described by the Gordon-Taylor type equation ($k \neq 1$). And the interaction parameter k indicates and quantifies the similarity of different polycyanurate in the copolymer systems. The similarities of the polycyanurate copolymers are in the order: BACy/CPCy > BACy/BFCy > BACy/DFCy.

The propagation loss of the polycyanurate thin films is between 0.86-1.82 dB/cm. The heterogeneity of the polycyanurate copolymers has strong effects on the propagation loss. Higher heterogeneity results in higher propagation loss. For a given copolymer, heterogeneity changes with composition and reaches the highest value at 5:5 for all the copolymer systems. For a given composition, the heterogeneities of BACy/DFCy copolymers are higher than those of BACy/BFCy copolymers.

Thermal and mechanical properties

Based on the basic thermodynamic consideration, the dependency of glass transition temperature on the compisition and conversion are inverstigated. Study shows that the composition and molecular backbone structure will affect the glass transtion temperature of the polycyanurate copolymer to some extent. A Dibenedetto equation is used to model the relationship between the glass transition temperature and the conversion. The relationship among the glass transition temperature, composition and conversion of the polycyanurate copolymer was also established, which is useful to predict the glass

transtion temperature of the polycyanurate copolymers at any given conversion and composition from the pure homopolymer components.

Nanoindentation study of the polycyanurate thin films reveal that the relationship between the hardness and conversion is similar to that of the glass transition temperature between the conversion, because the factors which influence the glass transition temperature and hardness are almost the same. A linear relationship between the hardness and glass transition temperature is established. It is found that the chemical structure will have a strong effect on the slop and intercept of the linear relationship. Only those polymers contain similar main chain structures can be described in a same linear relationship.

Curing kinetics of polycyanurates

The kinetics study of the aliphatic cyanate ester DFCy indicate that the reaction follows n th order kinetics model in the chemical controlled region and approaches a plateau conversion at certain curing temperature, which is less than complete conversion. The diffusion limitation occurs at certain conversion, and this onset conversion increases with the increasing of isothermal curing temperature. The study found that the reaction order 'n' might not keep constant throughout the whole reaction time, because the viscosity of the reaction system hinders the mobility and reactivity of the functional group. A conversion dependent reaction order was accepted in this study. A new kinetics model, which combing the variable 'n' kinetics models and WLF equation, was established to describe the entire curing range of DFCy. For the temperature range we studied (140-190 ^{o}C), the new kinetics models predict the experimental data reasonably well. Our preliminary study also showed that the variable 'n' kinetics model is also suitable for the curing of other thermosettings such as BMI/DBA system.

The study revealed that the reaction of uncatalyzed BACy follows an autocatalytic kinetics model in the chemical controlled region. The reaction becomes diffusion controlled after certain onset conversion, and this onset conversion increases with the increasing of isothermal curing temperature. WLF equation was used to describe the reaction rate constant in the diffusion controlled region. A new kinetics model, which takes into account both the chemical and diffusion controlled regions, was established to describe the entire conversion range for the curing reaction of BACy. The study found that the reaction orders are dependent on the curing temperatures. By considering the temperature dependency of the reaction orders, the new autocatalytic kinetics predicted the experimental data of BACy more accurately. This new model should be used for accurate modeling of curing reactions of thermosets following autocatalytic kinetics.

10.2 Future Work

Based on the fundamental understanding and the learned studying methodology on the prepolymerization, preparation of thin film, characterizations, and curing reaction kinetics of polycyanurate resins, some meaningful studies to further understand the fundamentals in addition to some remained work mentioned in this thesis are recommended as the future work.

Preparation of ultra-thin polycyanurate thin film by evaporation method

Since the cyanate ester monomer will undergo evaporation upon heating, it provides another approach to preparation polycyanurate thin film by evaporation method. By using this method, polycyanurate thin film can be directly thermally deposited and cured at the surface of the substrate from the vapor of cyanate ester monomer. The experimental time is expected to be reduced and the film thickness may be controlled by multi depositions. Obvious advantages of the evaporated polycyanurate thin film is that it has a high purity

and expected to have low surface roughness than that of spin coated film. The method can prepare ultra-thin polymer films of few nano-meters. The morphology, chemical structure, and thermal stability of the films are also worth studying.

UV or electron-beam curing of cyanate ester

With added photocatalyst, cyanate ester may be cured by UV irradiation or by electron beam, or at least the curing temperature can be reduced considerably after the irradiation. This is interesting because it provides a way to obtain patternable polycyanurate thin films. Figure 10.1 displays a schematic diagram of the fabrication process.

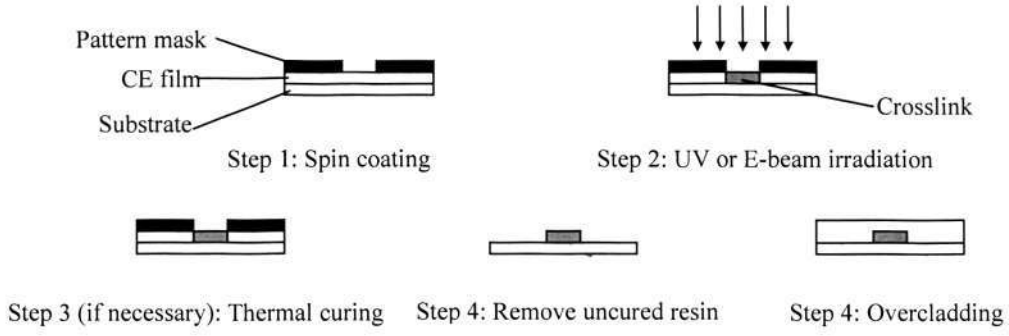

Figure 10.1 Fabrication process of patternable polycyanurate thin film

First, cyanate ester with added photocatalyst is spin coated onto silicon substrate. Then is the UV or electron beam irradiation, and the exposed resin will be crosslinked or the curing temperature of the exposed resin is considerably reduced. If necessary, the film is heated at a relatively low temperature so that the exposed resin can be crosslinked while the unexposed resin can not be cured. Then the uncured resin is dissolved and removed from the substrate. Finally, the overcladding layer was formed over the patterned polycyanurate film by spin coating and curing.

Fabrication of polycyanurate planar waveguide devices

Polycyanurate thin films have various desirable properties for waveguide applications. For example, low dielectric constant and loss factor, good adhesion on different substrates,

excellent resistance against most common solvents, high glass transition temperature and remarkable mechanical properties. Furthermore, their properties can be further adjusted and improved by changing the backbone structure and by blending or copolymerizing with other polycyanurate resins or other thermosetting and thermoplastic polymer systems according to the specific requirements. Using UV or electron beam curing process, polycyanurate thin film waveguide devices can be easily fabricated. Then the performance of the devices can be evaluated.

REFERENCES

[1] Hamerton, I. (Ed.) (1994). *Chemistry and technology of cyanate ester resins*. Glassgow: Chapman and Hall.

[2] Nair, C. P. R., Dona, M., & Ninan, K.N. (2001). Cyanate ester resins, recent developments. *Advanced in Polymer Science*, 155, 1-99.

[3] Hamerton, I., & Hay, J. N. (1998). Recent developments in the chemistry of cyanate esters. *Polymer International*, 47, 465-473.

[4] Graver, R. B. (1986). Cyanate esters – high performance resins. In: Seymour, R. B. & Kirshenbaum, G. S. (Eds.), *High performance polymers: their origin and development.* Elsevier Science Publishing Co., Inc.

[5] Galy, J., Gerard, J. F. & Pascault, J. P. (1991). Reactivity of cyanate-ester resins and characterization polycyanurate networks. In Abadie, M. J. M. & Sillion, B. (Ed.), Polyimides and other high-temperature polymers. Netherlands: Elsevier Science Publishers.

[6] Hwang, J. W., Park, S. D., Cho, K, Kim, J. K., Park, C. E., & Oh, T. S. (1997). Toughening of cyanate ester resins with cyanated polysulfones. *Polymer*, 38, 1835-1843.

[7] Takao, I., Takanori, M., & Masao, T. (1999). Toughening of cyanate ester resin by N-phenylmaleimide styrene copolymers. *Journal of Applied Polymer Science*, 74, 2931-2939.

[8] Harismendy, I., Delrio, M., Eceiza, A., Gavalda, J., Gómez, C. M., & mondragon, I. (2000). Morphology and thermal behavior of dicyanate ester-polyetherimide semi-IPNS cured at different conditions. *Journal of Applied Polymer Science*, 76, 1037-1047.

[9] Kim, B. S. (1997). Effect of cyanate ester on the cure behavior and thermal stability of epoxy resin. *Journal of Applied Polymer Science*, 65, 85-90.

[10] Nair, C. P. R., & Francis, T. (1999). Blends of bisphenol A-based cyanate ester and bismaleimide: Cure and thermal characteristics. *Journal of Applied Polymer Science*, 74 (14), 3365-3375.

[11] Karad, S. K., Jones, F. R., & Attwood, D. (2002). Moisture absorption by cyanate ester modified epoxy resin matrices. Part 1. Effect of spiking parameters. *Polymer*, 43(19), 5209-5218.

[12] Karad, S. K., Jones, F. R., & Attwood, D. (2002). Moisture absorption by cyanate ester modified epoxy resin matrices. Part II. The reverse thermal effect. *Polymer*, 43(21), 5643-5649.

[13] Guo, B. C., Fu, W. W., Jia, D. M. (2002). Cure behaviour and structure of dicyanate-epoxy novolac blends. *Polymer Composites*, 10 (3), 237-248.

[14] Martin, M. D., Ormaetxea, M., Harismendy, I. (1999). Cure chemo-rheology of mixtures based on epoxy resins and ester cyanates. *Europe Polymer Journal*, 35 (1), 57-68.

[15] Fan, J., Hu, X., & Yue, C. Y. (2001). Interpenetrating polymer networks based on modified cyanate ester resin. *Plastic Rubber Composites*, 30 (10), 448-454.

[16] Hu, X., Fan, J., & Yue, C. Y. (2001). Rheological study of crosslinking and gelation in bismaleimide/cyanate ester interpenetrating polymer network. *Journal of Applied Polymer Science*, 80 (13), 2437-2445.

[17] Fan Jing (2001). Synthesis and Characterization of high performance resins based on bismaleimide-cyanate ester interpenetrating network. Unpublished Ph.D thesis of Nanyang Technological University, Singapore.

[18] Fan, J., Hu, X. & Yue, C. Y. (2003). Dielectric properties of self-catalytic interpenetrating polymer network based on modified bismaleimide and cyanate ester resins. *Journal of Polymer Science: Part B: Polymer Physics*, 41, 1123-1134.

[19] Hamerton, I., Herman, H., Mudhar, A. K. (2002). Multivariate analysis of spectra of cyanate ester/bismaleimide blends and correlations with properties. *Polymer*, 43 (11), 3381-3386.

[20] Papathomas, K. I., & Wang, D. W. (1992). Triazine networks modified with monofunctional reactive cyanate ester monomers. *Journal of Applied Polymer Science*, 44, 1267-1274.

[21] Arnold, C. (1992). Siloxane-modified cyanate ester resins for space applications, *37th International SAMPE Symposium Exhibition*, pp. 128-36.

[22] Speak, S. C., Sitt, H. & Fuse, R. H. (1991). Novel cyanate ester based products for high performance radome applications, *36th International SAMPE Symposium*, pp. 336~347.

[23] Alman, G., Mackenzie, P., Malhotra, V., & Maskell, R. (1990). Toughened cyanate for aerospace applications, *35th International SAMPE Symposium*, pp. 408~418.

[24] Lefebvre, P. (1991), moisture resistant and toughened cyanate systems for aerospace applications in Europe. *Composites in Manufacturing*, January 7-10, California.

[25] Bogan, G. W. (1988). Unique polyaromatic cyanate ester for low dielectric printed circuit boards, *SAMPE Journal*, 24,19-24.

[26] Ising, S. J. (1991). Moisture resistant cyanate formulations for PCB, *5th International SAMPE Electronics Conference*, pp. 288-99.

[27] Dreyer, C., Bauer, M., Bauer, J., Keil, N., Yao, H., & Zawadzki, C. (2002). Reduction of the optical loss and optimization of polycyanurate thermosets used in integrated optics. *Microsystem Technologies*, 7, 229-238.

[28] Dreyer, C., Schneider, J. (2003). New reactive polymeric systems for use as waveguide materials in integrated optics. *Macromol. Symp.*, 199, 307-319.

[29] Sharma, S. K., Misra, S. C. K. & Tripathi, K. N. (2003). Polycyanurate thin film optical waveguide for integrated optics applications. *Journal of Nonlinear Optical Physics & Materials*, 12, 1-5.

[30] Bauer, M. (1998). Plastic optical components. United States Patent 5780159.

[31] Bauer, M. (2004). Waveguide systems or structures or parts thereof, containing polycyanate copolymers prepared from polyfunctional cyanates and fluorinated monocyanates. United States Patent 6716958.

[32] Bauer, M. (2004). Temperature insensitive optical waveguide device. United States Patent 6757469.

[33] Bauer, M. (2005). Optical waveguides derived from a combination of poly(perfluorocyclobutanes) and polymeric cyanates. United States Patent 6853790.

[34] Possart, W., & Dieckhoff, S. (1999). Adhesion mechanisms in a cyanurate prepolymer on silicon and on aluminium. *International Journal of Adhesion & Adhesives*, 19, 425-434.

[35] Gesang, T., Höper, R., Dieckhoff, S., Schlett, V., Possart W., & Hennemann, O. D. (1995). Organic film formation investigated by atomic force microscopy on the nanometre scale. *Thin Solid Films*, 264, 194-204.

[36] Günster, J., Dieckhoff, S., & Souda, R. (1998). The absorption of 2,4,6-triphenyl-1,3,5-triazine on Si(111) 7×7 studied by STM. *Thin Solid Films*, 325, 24-29.

[37] Dieckhoff, S., Schlett, V., Possart W., & Hennemann, O. D. (1995). XPS studies of thin polycyanurate films on silicon wafers. *Fresenius' Journal of Analytical Chemistry*, 353, 278-281.

[38] Pozdnyakov, O. F., Possart, W., Redkov, B. P., Valeske B., Pozdnyakov, A. O., & Moiseeva, M. M. (2000). Polycyanurate thin film deposition on metal via thermal cyclotrimerisation from the monomer vapor phase. *Thin Solid Films*, 366, 1-3.

[39] Sabyasachi, G., Derrick, D., Kelvin, J., Gary, P., & Richard, V. (2003). Mechanical properties of intercalated cyanate ester-layered silicate nanocomposites. Polymer, 44, 1315-1319.

[40] Alexander, B. M., & Jeffrey, W. G. (2003). Characterization of polymer-layered silicate (clay) nanocomposites by transmission electron microscopy and X-ray diffraction: a comparative study. *Journal of Applied Polymer Science*, 87, 1329-1338.

[41] Snow, A. W., Buckley, L. J., & Armistead, J. P. (1999). $NCOCH_2(CF_2)_6CH_2OCN$ cyanate ester resin. A detailed study. *Journal of Polymer Science: Part A: Polymer Chemistry*, 37, 135-150.

[42] Snow, A. W., & Buckley, L. J. (1997). Fluoromethylene cyanate ester resins. Synthesis, characterization, and fluoromethylene chain length effects. *Macromolecules*, 30(3), 394-405.

[43] Barton, J. M., Chaplin, A., Hamerton, I., & Howlin, B. J. (1999). A new synthetic route for the preparation of alkenyl functionalized aryl cyanate ester monomers. *Polymer*, 40, 5421–5427.

[44] Abed, J. C., Mercier, R., & McGrath, J. E. (1997). Synthesis and characterization of new phosphorus and other heteroatom containing aryl cyanate ester monomers and networks. *Journal of Polymer Science: Part A: Polymer Chemistry,* 35(6), 977-987.

[45] Maya, E. M., Snow, A. W., & Buckley, L. J. (2002). Oligodimethylsiloxane linked cyanate ester resins. *Macromolecules*, 35, 460-466.

[46] Werner, M. & Jörg, G. Z. (1996). Liquid crystalline thermosets through cyclotrimerization of diaromatic dicyanates. *Macromolecules*, 29, 1105-1109.

[47] Körner, H., Shiota, A., & Ober, C. K. (1997). Mixtures of liquid-crystalline and amorphous dicyanurates: unusual curing behavior and mechanical properties. *Chemical Materials*, 9, 1588-1597.

[48] Kern, W., Cifrain, M., Schroder, R. (1998). Polymers with pendant cyanate ester groups: Synthesis, thermal curing and photocrosslinking. *Europe Polymer Journal*, 34(7), 987-995.

[49] Nair, C. P. R., Mathew, D., & Ninan, K. N. (2001). Imido-phenolic-triazine network polymers derived from maleimide-functional novolac. *Europe Polymer Journal*, 37(2), 315-321.

[50] Kasehagen, L. J. & Christopher, W. M. (1997). Structure development in cyanate ester polymerization, Polymer International, 44, 237-247.

[51] Liu, H. P., & George, G. A. (1996). Mechanism and kinetics of polymerization of a dicyanate ester resin photocatalyzed by an organometallic compound. *Polymer*, 37, 3675-3682.

[52] Mathew, D., Nair, C. P. R., Krishnan, K. (1999). Catalysis of the cure reaction of bisphenol A dicyanate. A DSC study. *Journal of Polymer Science: Part A: Polymer Chemistry*, 37 (8), 1103-1114.

[53] Isabel, H., Clara, M. G., Marcos, D. R. & Mondragon, I. (2000). Cure monitoring of catalysed cyanate ester resins. *Polymer International*, 49, 735-742.

[54] Chen, Y. T. & Macosko, C. W. (1996). Kinetics and rheology characterization during curing of dicyanates. *Journal of Applied Polymer Science*, 62, 567-576.

[55] Chen, C. C., Don, T. M., Lin, T. H. & Cheng, L. P. (2004). A kinetic study on the autocatalytic cure reaction of a cyanate ester resin. *Journal of Applied Polymer Science*, 92, 3067-3079.

[56] Bartolomeo, P., Chailan, J. F., & Vernet, J. L. (2001). Curing of cyanate ester resin: a novel approach based on FTIR spectroscopy and comparison with other techniques. *European Polymer Journal*, 37, 659-670.

[57] Liu, H. P., & George, G. A. (2000). Determination of thermal cure kinetics of thin films of photocatalysed dicyanate ester by FTIR emission spectroscopy. *Polymer International*, 49, 1505-1512.

[58] Xu, Y. Z. E., & Sung, C. S. P. (2002). UV, luminescence, and FTIR characterization of cure reaction in bisphenol A dicyanate ester resin. *Macromolecules*, 35, 9044-9048.

[59] Bartolomeo, P., Chailan, J. F., & Vernet, J. L. (2001). On the use of WLF equation to study resin curing by dielectric spectroscopy. *Polymer*, 42, 4385-4392.

[60] Deng, Y. & Martin, G. C. (1996). Effect of diffusional limitations on the gelation of cyanate ester resins. *Journal of Applied Polymer Science*, 64, 115-125.

[61] Deng, Y. & Martin, G. C. (1995). Diffusion phenomena during cyanate resin cure. *Polymer*, 37, 3593-3601.

[62] Bauer, J., & Bauer, M. (2002). Cyanate ester based resin systems for snap-cure applications. *Microsystem Technology*, 8(1), 58-62.

[63] GrenierLoustalot, M. F., Lartigau, C., Metras, F. (1996). Mechanism of thermal polymerization of cyanate ester systems: Chromatographic and spectroscopic studies. *Journal of Polymer Science: Part A: Polymer Chemistry*, 34 (14), 2955-2966.

[64] GrenierLoustalot, M. F., & Lartigau, C. (1997). Molten state reactivity of difunctional cyanates: thermal and spectroscopic studies by liquid and solid CP-MAS ^{13}C-NMR. *Journal of Polymer Science: Part A: Polymer chemistry*, 35, 1245-1254.

[65] Lin, K. F., & Shyu, J. Y. (2001). Early cure behavior of a liquid dicyanate ester resin. *Journal of Polymer Science: Part A: Polymer Chemistry*, 39, 3085-3092.

[66] Liu, H. P., & George, G. A. (1997). Study on the gelation of photocatalszed dicyanate ester resins. *Polymer*, 38, 2997-3002.

[67] Liu, H. P., & George, G. A. (2000). Determination of thermal cure kinetics of thin films of photocatalysed dicyanate ester by FTIR emission spectroscopy. *Polymer International*, 49, 1505-1512.

[68] Yousefi, A., Lafleur., P. G. & Gauvin, R. (1997). Kinetic studies of thermoset cure reactions: a review. *Polymer Composites*, 18 (2), 157-168.

[69] TA instruments manual. A review of DSC kinetics methods.

[70] Turi, E. A. (Ed.) (1981). Thermal characterization of polymeric materials. New York: Academic Press.

[71] He, Y. (2001). DSC and DEA studies of underfill curing kinetics. *Thermochimica Acta*, 367-368, 101-106.

[72] Maazouz, A., Texier, C., Taha, M. & Alglave, H. (1998). Chemo-rheological study of a dicyanate ester for the simulation of the resin-transfer molding process. *Composites Science and Technology*, 58, 627-632.

[73] Christopher, W. W., Wayne, D. C. & Andy, A. G. (1997). Chemico-diffusion kinetics of model epoxy-amine resins. *Polymer*, 38, 3251-3261.

[74] Goodwin, A. A. (1993). The curing kinetics of a modified bismaleimide, *Polymer International*, 32, 87-92.

[75] Boey, F. Y. C. & Qiang, W. (2000). Experimental modeling of the cure kinetics of an epoxy-hexaanhydro-4-methylphthalicanhydride (MHHPA) system, *Polymer*, 41, 2081-2094.

[76] Boey, F. Y C., Song, X. L, Yue, C. Y. & Zhao, Q. (2000). Modeling the curing kinetics for a modified bismalemide resin, *Journal of Polymer Science, Part A: Polymer Chemistry*, 38, 907-913.

[77] Lars, A. (1991). Processing science for high performance thermoset composites, *SAMPE Journal*, 27, 27-36.

[78] Xie, H. F., Liu, B. H., (2005). Cure kinetics study of carbon nanofibers/epoxy composites by isothermal DSC. *Journal of Applied Polymer Science*, 96, 329-335.

[79] Guo, Z. S., (2005). Cure kinetics of T700/BMI prepreg used for advanced thermoset composite. *Journal of Applied Polymer Science*, 97, 2238-2241.

[80] Coasta, M. L., (2005). Influence of aromatic amine hardeners in the cure kinetics of an epoxy resin used in advanced composites. *Materials Research*, 8, 65-70.

[81] Macan J., (2004). Study of cure kinetics of epoxy-silica organic-inorganic hybrid materials. *Thermochimica Acta*, 414, 219-225.

[82] Batch, G. L. & Macosko, C. W. (1992). Kinetic-model for cross-linking free-radical polymerization including diffusion limitations. *Journal of Applied Polymer Science*, 44, 1711-1729.

[83] Gillham, J. K. (1986). Formation and properties of thermosetting and high Tg polymeric materials, *Polymer Engineering and Science*, 26, 1429-1433.

[84] Kim, D. H. & Kim, S. C. (1989). Vitrification effect during the reaction injection molding (RIM) process of epoxy resin. *Polymer Engineering and Science*, 29, 456-462.

[85] Senen, P. A., Arturo, L.Q., Mercedes, P. P., Montserrat, V. & Pilar, P. (1998). Autoaccelaration and inhibition: free volume. epoxy-amine kinetics. *Journal of Polymer Science: Part A: Polymer Chemistry*, 36, 1001-1016.

[86] Han, S. Yoon, H. G., Suh, K. S., Kim, W. G. & Moon, T. J. (1999). Cure kinetics of biphenyl epoxy-phenol novolac resin system using triphenylphosphine as catalyst. *Journal of Polymer Science: Part A: Polymer Chemistry*, 37, 713-720.

[87] Michelle, L. C., Luiz, C. P. & Mirabel, C. R. (2005). Influence of aromatic amine hardeners in the cure kinetics of an epoxy resin used in advanced composites, *Materials Research*, 8, 65-70.

[88] Kamal, M. R. & Sourour, S. (1973). Kinetics and thermal characterization of thermoset cure. *Polymer Engineering and Science*, 13, 59-64.

[89] Kamal, M. R. (1974). Thermoset characterization for moldability analysis, *Polymer Engineering and Science*, 14, 231-239.

[90] Simon, S. L. & Gillham, J. K. (1993). Cure kinetics of a thermosetting liquid dicyanate ester monomer/high- Tg polycyanurate material. *Journal of Applied Polymer Science*, 47, 461-485.

[91] Georjon, O., Galy, J. & Pascault, J. P. (1993). Isothermal curing of an uncatalyzed dicyanate ester monomer:kinetics and modeling. *Journal of Applied Polymer Science*, 49, 1441-1452.

[92] Kenny, J. M. (1994). Determination of autocatalytic kinetic model parameters describing thermoset cure. *Journal of Applied Polymer Science*, 51, 761-764.

[93] Dibenedetto, A. T. (1987). Prediction of the glass transition temperature of polymers: a model based on the principle of corresponding states. *Journal of Polymer Science: Part B: Polymer Physics*, 25, 1949-1969.

[94] Pascault, J. P. & Williams, R. J. J. (1990). Glass transition temperature versus conversion relationships for thermosetting polymers. *Journal of Polymer Science: Part B: Polymer Physics,* 28, 85-95.

[95] Hale, A., Macosko, C. W. & Bair, H. E. (1991). Glass transition temperature as a function of conversion in thermosetting polymers, *Macromolecules*, 24(9), 2610-2621.

[96] Bauer, M. & Gnauck, R. (1987). *Acta Polymer*, 38, 658.

[97] Venditti, R. A. & Gillham, J. K. (1997). A relationship between the glass transition temperature (Tg) and fractional conversion for thermosetting systems. *Journal of Applied Polymer Science*, 64, 3-14.

[98] Chen, Y. T. & Macosko, C. W. (1996). Kinetics and rheology characterization during curing of dicyanates. *Journal of Applied Polymer Science*, 62, 567-576.

[99] Hamerton, I. (1994). Introduction to cyanate ester resins. In: Hamerton, I. (Ed.), *Chemistry and technology of cyanate ester resins* (pp. 1-5). Glassgow: Chapman and Hall.

[100] Snow, A. W. (1994). The synthesis, manufacture and characterization of cyanate ester monomers. In Hamerton, I. (Ed.), *Chemistry and technology of cyanate ester resins* (pp. 7-57). Glasgow: Chapman and Hall.

[101] Simon, S. L., & Gillham, J. K. (1994). Cyanate ester/polycyanurate systems: structure-property relationships. In Hamerton, I. (Ed.), *Chemistry and technology of cyanate ester resins* (pp. 87-111). Glasgow: Chapman and Hall.

[102] Shimp, D. A. (1994). Technologically driven applications for cyanate ester resins. In Hamerton, I. (Ed.), *Chemistry and technology of cyanate ester resins* (pp. 282-328). Glasgow: Chapman and Hall.

[103] Zhou, M. (2002). Low-loss polymeric materials for passive waveguide components in fiber optical telecommunication. *Optical Engineering*, 41, 1631-1643.

[104] Gupta, M., Sharma, V. K., Kapoor, A. & Tripathi, K. N. (1997). Fabrication and characterization of polycarbonate thin film optical waveguides. *Journal of Optics*, 28, 37-40.

[105] Ma, H., Jen, A. K. Y., & Dalton, L. R. (2002). Polymer-based optical waveguides: materials, processing and devices. *Advanced Materials*. 14, 1339-1365.

[106] Bader, M. A., Keeler, H. M., & Marowsky, G. (1998). Polymer-based waveguides and optical switching. *Optical Materials*, 9, 334-341.

[107] Rojo, G., & Agulló-López, F. (2000). Optical waveguiding in novel phosphazene polymer films. *Polymer Bulletin*, 45, 145-150.

[108] Lawrence, A. H. (Ed.). (1992). *Polymers for lightwave and integrated optics*. Marcel dekker, Inc. 4.

[109] Groh, W. (1988). Overtone absorption in macromolecules for polymer optical fibers. *Macromolecule Chemistry*, 189, 2861-2874.

[110] Liang, J., & Toussare, E. (1998). Low loss, low refractive index influorinated self-corsslinking polymer waveguides for optical applications. *Optical Materials*, 9, 230-235.

[111] Kim, J. P., & Lee, W. Y. (2001). Fluorinated poly(arylene ether sulfide) for polymeric optical waveguide devices, *Macromolecules*, 34, 7817-7821.

[112] Claire, P., Sonia, V., & Anders, H. (1999). Low-loss passive optical waveguides based on photosensitive poly(pentafluorostyrene-co-glycidyl methacrylate). *Macromolecules*, 32, 2903-2909.

[113] Kowalczyk, T. C., Kosc, T., & Singer, K. D. (1994). Loss mechanisms in polyimide waveguides. *Journal of Applied Physics*, 76, 2505-2508.

[114] Groh, W. & Zimmermann, A. (1991). What is the lowest refractive index of an organic polymer?. *Macromolecules*, 24, 6660-6663.

[115] Shimp, D. A., & Chin, B. (1994). Electrical properties of cyanate ester resins and their significance for applications. In Hamerton, I. (Ed.), *Chemistry and technology of cyanate ester resins* (pp. 230-257). Glasgow: Chapman and Hall.

[116] Sperling, L.H. (Ed.) (1986). *Introduction to physical polymer science* (pp.254-257). New York: John wiley & Sons.

[117] Cowie, J. M. G. (Ed.) (1991). *Polymers: chemistry and physics of modern materials* (pp.205). Glasgow: Bell and Bain Ltd..

[118] Narayan, R. & Duda, J. L. (2001). A modified free-volume model: correlation of ion-conduction in stroungly associating polymeric materials. *Journal of Membrane Science*, 191, 13-20.

[119] Lan, L. W. (Ed.) (1993). *Polymer physics* (pp.78-81). Xi'an: Northwestern Polytechnical University.

[120] Tsai, M. H. & Whang, W. T. (2001). Low dielctric polyimide/poly(silsesquioxane)-like nannocomposite material. *Polymer*, 42, 4197-4207.

[121] Park, J. M. & Rhee, S. W. (2002). Remote plasma-enhanced chemical vapor deposition of nanoporous low-dielectric constant SiCOH films using vinyltrimethylsilane. *Journal of the Electrochemical Society*. 149,92-97.

[122] Alegaonkar, P. S., Mandale, A. B., Sainkar, S. R., & Bhoraskar, V. N. (2002). Refractive index and dielectric constant of the boron and fluorine diffused polyimide. *Nuclear Instruments and Methods in Physics Research B*, 94, 281-288.

[123] Liu, W. C., Yang, C. C., Chen, W. C., Dai, B. T., & Tsai, M. S. (2002). The structural transformation and properties of spin-on poly(sisesquioxane) films by thermal curing. *Journal of Non-Crystalline Solids*. 311, 233-240.

[124] Liang, G. Z. & Gu, A. J. (1997). Toughening bismaleimide resins by N-allyl aromatic amine. *Polymer Journal*, 29, 553-556.

[125] Stenzenberger, H. D., & Konig, P. (1991). BMI/bis(allylphenoxyphthalimide)-copolymers: a new family of resins for advanced composites with improved thermal oxidative stability, *36th International SAMPE Symposium*, April 15-18.

[126] Liang, G. Z., Gu, A. J. & Lan, L. W. (1996). Modification of BMI with allyl compounds. *Journal of Advanced Materials*, 27, 61-64.

[127] Chaudhari, M. A. & King, J. J. (1985). A new bismaleimides resin system for high performance composite. *Conference of Fabricating Composites*, June 11-13.

[128] Hamerton, I. (1994). Properties of unreinforced cyanate ester matrix resins. In Hamerton, I. (Ed.), *Chemistry and technology of cyanate ester resins* (pp. 1-5). London: Blackie Acadamic and Professional.

[129] Ramirez, M. L., Walters, R., & Lyon, R. E. (2002). Thermal decomposition of cyanate ester resins. *Polymer Degradation Stability*, 78 (1), 73-82.

[130] Ramirez, M. L., Walters, R., Savitski, E. P, & Lyon, R. E. (2001). Thermal decomposition of cyanate ester reisns, Final report of U.S. department of Transportation of Federal Aviation Administration.

[131] Hay, J. N. (1994). Processing and cure schedules for cyanate ester resins. In Hamerton, I. (Ed.), *Chemistry and technology of cyanate ester resins* (pp. 151-192). London: Blackie Acadamic and Professional.

[132] Stroh, R. & Gerber, H. (1960). *Angew. Chem.*, 72, 1000.

[133] Weirauch, K. K., Gemeinhardt, P. G. & Baron, A. L. (1976). Soc. Plast. Eng., Technical paper, 22, 317.

[134] Mcconnell, V, P. (1992). *Advanced Composites*, May/June issue, p. 28.

[135] Shimp, D. A. (1994). Technologically driven applications for cyanate ester resins. In Hamerton, I. (Ed.), *Chemistry and technology of cyanate ester resins* (pp. 282-328). London: Blackie Acadamic and Professional.

[136] http://itisdom.itri.org.tw/ITISPub/infoshare.nsf/0/4277b4f32537ec7e48256dd400347435?OpenDocument

[137] http://www.pb.izm.fhg.de/epc/010_activities/020_materials_techn/064_polymercyanurate/

[138] Birnie. D. (1999). *Coating quality and spin coating* [On-line]. Available: http://www.mse.arizona.edu/faculty/birnie/Coatings/index.htm.

[139] Birnie. D. (1999). *Applications of spin coating* [On-line]. Available: http://www.mse.arizona.edu/faculty/birnie/Coatings/AppAreas.htm.

[140] Birnie. D. (1999). *The key stages in spin coating* [On-line]. Available: http://www.mse.arizona.edu/faculty/birnie/Coatings/KeyStages.htm.

[141] Birnie. D. (1999). *Fluid flow effects important for spin coating* [On-line]. Available: http://www.mse.arizona.edu/faculty/birnie/Coatings/FluidFlo.htm.

[142] Boey, F. Y. C., & Qiang, W. (2000). Experimental modeling of the cure kinetics of an epoxy-hexaanhydro-4-methylphthalicanhydride (MHHPA) system. Polymer, 41, 2081-2094.

[143] Snow, A. W. & Gtiffith, J. R. (1980), *Journal of Fluorine Chemistry*, 15, 471

[144] Cercena, J. L. & Huang, S. J. (1984), *Polymer Preprints*, 25, 114

[145] Que, W. X., Zhou, Y., Lam, Y. L., Chan, Y. C., & Kam, C. H. (2001). Preparation and characterizations of $SiO_2/TiO_2/\gamma$-glycidoxypropyltrimethoxysilane composite materials for optical waveguides. *Applied Physics A: Materials Science and Processing*, 73, 171-176.

[146] Sun, Y. Y., Zhang, Z. Q. & Wong, C. P. (2005). Influence of interphase and moisture on the dielectric spectroscopy of epoxy/silica composites. *Polymer*, 46, 2297-2305.

[147] Ku, C. C., & Liepins, R. (1987). *Electrical properties of polymers: Chemical Principles*, Hanser Publishers.

[148] Fan. J. (2002). Synthesis and characterization of high performance resins based on bismaleimide-cyanate ester interpenetrating network. Ph.D. Thesis, Nanyang Technological University.

[149] Jan, J. Charistian, L., Grzegorz, C. & Danuta, B. (1998). Dielectric relaxation processes in the namatogen 4-cyanophenyl 4-n-heptylbenzoate. *Liquid Crystals*, 24, 689-694.

[150] Kwan, K. S. J. (1998). The role of penetrant structure on the transport and mechanical porperties of a thermoset adhesive, Ph.D. thesis, kman@vt.edu

[151] Debye, P. (Ed.) (1929) *Polar Molecules*, Dover, New York.

[152] Cole, K. S. & Cole, R. S. (1941). *Journal of Chemical Physics*, 9, 341-351.

[153] Tsangaris, G. M., Psarras, G. C., & Kouloumbi (1998). Electric modulus and interfacial polarization in composite polymeric systems. *Journal of Materials Science*, 33, 2027-2037.

[154] Yu, S. Z., Hing, P., & Hu, X. (2000). Dielectric properties of polyctyrene-aluminum-nitride composites. *Journal of Applied Physics*, 88, 398-404

[155] Bozena, H. & Jerzy, M. (Ed.) (1986). Electrets, Warszawa: Pwn-Polish Scientific Publishers

[156] Hsiue, G. H., Lee, R. H., Jeng, R. J. & Chang, C. S. (1996). Dielectric study of ferroelectric side-chain liquid crystalline polysiloxanes with broad temperature ranges of the chiral smectic C phase 1. Structure dependence of dielectric relaxation. *Journal of Polymer Science: Part B: Polymer Physics*, 34, 555-563.

[157] Rao, S. V., Moutzouris, K., Ebrahimzadeh, M., Rossi, A. D., Gintz, G., Calligaro, M., Ortiz, V. & Berger, V. (2003). Influence of scattering and two-photon absorption on the optical loss in GaAs-Al_2O_3 nonlinear waveguides measured using femtosecond pulses.

[158] Ulrich, R. & Torge, R. (1973). Measurement of thin film parameters with prism coupler, *Applied Optics*, 12, 2901-2908.

[159] Tien, P. K. (1971). Light waves in thin films and integrated optics, *Applied Optics*, 10, 2395-2413.

[160] Monneret, S., Huguet-Chantome, P. & Flory, F. (2000). M-lines technique: prism coupling measurement and discussion of accuracy for homogeneous waveguides. *Journal of Optics: A: Pure Applied Optics*, No.2, 188-195.

[161] http://www.metricon.com/basic.htm#anchor1875481

[162] http://www.cobalt.chem.ucalgary.ca/ziegler/educmat/chm386/rudiment/mathbas/eigen.htm

[163] http://www.du.edu/~jcalvert/phys/wkb.htm

[164] http://www.metricon.com/

[165] http://www.cyto.purdue.edu/flowcyt/educate/ee520/tsld037.htm

[166] http://www.atis.org/tg2k/_brewster_s_angle.html

[167] Strasser, T. A. & Gupta, M. C. (1992). Optical loss measurement of low-loss thin-film waveguides by photographic analysis. *Applied Optics*, 31, 2041-2046.

[168] Hensler, D. H., Cuthbert, J. D., Martin, R. J. & Tien, P. K. (1971). Optical propagation in sheet and pattern generated films of Ta_2O_5. *Applied Optics*, 10, 1037-1042.

[169] Himel, M. D. & Gibson, U. J. (1986). Measurement of planar waveguide losses using a coherent fiber bundle. *Applied Optics*, 25, 4413-4416.

[170] Itzkovitz, M., Croitoru, N., Hardy, A., Griffel, G. & Ruschin, S. (1985). Guided-wave method for measuring optical parameters in moderately lossy thin films, 125,193-198.

[171] Okamura, Y., Yoshinaka, S. & Yamamoto, S. (1983). Measuring mode propagation losses of integrated optical waveguides: a simple method. *Applied Optics*, 22, 3892-3894.

[172] http://en.wikipedia.org/wiki/Refractive_index

[173] http://www.exicor.com/literature/tutorial.aspx

[174] Agan, S., Ay, F., Kocabas, A. & Aydinli, A. (2005). Stress effects in prism coupling measurements of thin polymer films. *Applied physics A*, 80, 341-345.

[175] Janz, S., Cheben, P., Dayan, H. & Deakos, R. (2003). Measurement of birefringence in thin-film waveguides by rayleigh scattering. *Optics letters*, 28, 1778-1780.

[176] Lu, X. Y. & Weiss, R. A. (1992). Relationship between the glass transition temperature and the interaction parameter of miscible binary polymer blends. *Macromolecules*, 25, 3242-3246.

[177] Couchman, P. R. & Karasz. (1977). A classical thermodynamic discussion of the effect of composition on glass-transition temperatures. *Macromolecules*, 11, 117-119

[178] Lu, X. Y. & Weiss, R. A. (1991). Development of miscible blend of polyamide-6 and manganese sulfonated polystyrene using specific interactions. Macromolecules, 24, 4381-4385

[179] An, L. J., He, D. Y., (1997). Effects of molecular weiht and interaction parameter on the glass transition temperature of polystyrene mixtures and its blends with polystyrene/poly(2,6-dimenthyl-p-phenylene oxide). *Eur. Polym. J.*, 33, 1523-1528

[180] Yang, J., An, L. J. & Xu, T. (2001). The glass transition temperatures of PS/PPO blends: couchman volume-based equation and its verification. *Polymer*, 42, 7887-7892.

[181] Gordon, M. & Taylor, J. S. (1952). J. Chem. Phys., 2, 493-513

[182] Yang, S., Zhang, Y. W. & Zeng, K. Y. (2004). Analysis of nanoindentation creep for polymeric materials. Journal of Applied Physics, 95, 3655-3666

[183] Lee, C., Kwon, J., Park, S., Sundar, S., Min, B. & Han, H. (2004). Nanoindentation studies of polyimide thin films with various internal linkages in the diamine component, Journal of Polymer Science: Part B: Polymer Physics, 42, 861-870.

[184] Fakirov, S., Calleja, F. J. B. & krumova, M. (1999). On the relationship between microhardness and glass transition temperature of some amorphous polymers. Journal of Polymer Science: Part B: Polymer Physics, 37, 1413-1419.

[185] http://www.mee-inc.com/nano.html

[186] http://www.nanoindentation.cornell.edu/Model/Nanoindentation-Model.htm

[187] http://www.bfrl.nist.gov/nanoscience/DSI.htm

[188] www.lot-oriel.com/pdf_uk/all/mm_nanotest_br.pdf

[189] F., Benitez, E. Martinez, M. Galan, J. Serrat & J. Esteve (2001), Mechanical properties of plasma deposited polymer coatings, *Surface and coatings Technology*, 125, 383-387.

[190] F. Benitez, E. Martinez, J. Esteve (2002), improvement of hardness in plasma polymerized hexamethyldisiloxane coatings by silica like surface modification, *Thin Solid films*, 377-378, 109-114

[191] Yu, S. Z. (2004). Fabrication and characterization of mesoporous dielectric materials for ulsi interconnect applications. Ph.D. Thesis, Nanyang Technological University

[192] Yu, S. Z., Wong, T. K. S., Pita, K. and Hu, X. (2002). Synthesis of organically modified mesoporous silica as a low dielectric constant intermetal dielectric, J. Vac. Sci. Technol. B., 20, *2036-2042*

[193] Yu, S. Z., Wong, T. K. S., Hu, X. & Pita, K. (2003). The comparison of thermal and dielectric properties of silsesquioxane films cured in nitrogen and in air, *Chemical Physics Letters*.

[194] Yu, S. Z. (2004). Fabrication and characterization of mesoporous dielectric materials for unsi interconnect applications. Ph.D thesis, Nanyang Technological University, Singapore

[195] Rinde, J. A. (1970). Poisson's ratio for rigid plastic foams, *J. Applied Polymer Science*, 14, 1913-1926.